Novel Insights in Structure and Mechanism of *Escherichia coli* Transketolase

Dissertation

for the award of the degree

„Doctor rerum naturalium“

of the Georg-August-Universität Göttingen

within the doctoral program Biomolecules: Structure-Function-Dynamics

of the Georg-August-University School of Science (GAUSS)

submitted by

Fabian Nikolaus Rabe von Pappenheim

from Stuttgart, Germany

Göttingen 2017

Members of the Thesis Advisory Committee

Prof. Dr. Kai Tittmann	Department of Molecular Enzymology
	Georg-August University Göttingen
Dr. Manfred Konrad	Research Group Enzyme Biochemistry
(Second referee)	Max Planck Institute for Biophysical Chemistry Göttingen
Dr. Vladimir Pena	Department of Macromolecular Crystallography
	Max Planck Institute for Biophysical Chemistry Göttingen

Members of the Examination Board

Prof. Dr. Ralf Ficner	Department of Molecular Structural Biology
(First referee)	Georg-August University Göttingen
Prof. Dr. Ricardo Mata	Department of Computational Chemistry and Biochemistry
	Georg-August University Göttingen
Prof. Dr. Franc Meyer	Institute for Inorganic Chemistry
	Georg-August University Göttingen
Dr. Fabian Commichau	Department of General Microbiology
	Georg-August University Göttingen

Date of oral examination: 23.05.2017

Hereby I declare that I prepared the thesis at hand titled „Novel Insights in Structure and Mechanism of *Escherichia coli* Transketolase“ independently and with no sources and aids other than quoted. This thesis has not been submitted elsewhere.

Göttingen, 30.03.2017

Fabian Nikolaus Rabe von Pappenheim

Contents

List of Tables

List of Figures

Abbreviations

ADP	atomic displacement parameter
AP	4′-aminopyrimidine
APH$^+$	4′-aminopyrimidinium
Arg	arginine
BSA	Bovine serum albumin
CV	column volume
Da	dalton
Daf	*Desulfovibrio africanus*
DCPIP	2,6-dichlorphenolindophenol
DHAP	dihydroxyacetone phosphate
DMSO	dimethyl sulfoxide
DTE	dithioerythritol
E4P	erythrose 4-phosphate
E. coli	*Escherichia coli*
EDTA	ethylenediaminetetraacetic acid
F6P	fructose 6-phosphate
FAD	flavin adenine dinucleotide
FMN	flavin mononucleotide
FBP	fructose-1,6-bisphosphate aldolase
G3P	glycerol 3-phosphate
Ga3P	glyceraldehyde 3-phosphate
GDH	α-glycerophosphate dehydrogenase from rabbit muscle
Glu	glutamic acid
His	histidine
hs	*Homo sapiens*
HPA	β-hydroxypyruvate
Ile	isoleucine
IP	1′,4′-iminopyrimidine

Lp	*Lactobacillus plantarum*
Leu	leucine
MALS	multi angle light scattering
MAP	methylacetylphosphonate
MES	2-(*N*-morpholino)ethanesulfonic acid
MWCO	Molecular weight cut-off
NADH	nicotinamide adenine dinucleotide (reduced form)
PAGE	polyacrylamide gel electrophoresis
PCR	polymerase chain reaction
PDHC	pyruvate dehydrogenase complex
PEG	polyethylene glycol
XFPK	xylulose/fructose phosphoketolase
PMSF	phenylmethanesulfonylfluoride
POX	pyruvate oxidase
***Lp*POX**	*Lactobacillus plantarum* pyruvate oxidase
Phe	phenylalanine
R5P	ribose 5-phosphate
Ru5P	ribulose 5-phosphate
Sc	*Saccharomyces cerevisae*
S7P	sedoheptulose 7-phosphate
SDS	sodium dodecyl sulfate
Ser	serine
TEMED	N,N,N',N'-Tetramethylethylenediamine
ThDP	thiamine diphosphate
AcThDP	acetyl-thiamine diphosphate
DHEThDP	dihydroxyethyl-thiamine diphosphate
HEThDP	hydroxyethyl-thiamine diphosphate
LThDP	lactyl-thiamine diphosphate
MeOThDP	2'-methoxythiamine diphosphate

PLThDP	phosphonolactyl-thiamine diphosphate
THF	tetrahydrofuran
Thr	threonine
TIM	triosephosphate isomerase
TK	transketolase
***Ec*TK**	*Escherichia coli* transketolase
***h*TK**	*Homo sapiens* transketolase
***Sc*TK**	*Saccharoymces cerevisae* transketolase
Tris	tris-(hydroxymethyl)-aminomethan
Tyr	tyrosine
VDW	van-der-Waals
X5P	xylulose 5-phosphate

Acknowledgments

First and foremost, I would like to deeply thank Prof. Dr. Kai Tittmann for giving me the opportunity and time to work on this thesis for the last years. Without his supervision and fruitful input this thesis would have been impossible. Furthermore, he performed the NMR- and quench-flow experiments of this work. During his absence, Prof. Dr. Ralf Ficner took over the duty as first referee, for which I am deeply thankful.

Further, I am thankful to Dr. Manfred Konrad, who agreed to take up the responsibility of being the second referee for this work, and who provided meaningful input. In the same breath, I want to thank Dr. Vladimir Pena, who took over the duty of being the third thesis advisory committee member from Prof. Dr. Ulf Diederichsen and greatly contributed to this thesis by discussion in the thesis advisory committee meetings.

I am thankful to Prof. Dr. Ricardo Mata, Prof. Dr. Franc Meyer and Dr. Fabian Commichau, who all agreed to be part of my examination board.

Dr. Danilo Meyer, Dr. Kathrin Schröder-Tittmann and Dr. Florian Brodhun were my designated go-to persons during the differing stages of my scientific development, and for all their patience and input I am deeply grateful.

I would like to thank Dr. Piotr Neumann, Dr. Ashwin Chari and Dr. Gleb Bourenkov. All of them provided great input regarding all aspects of X-ray crystallography, be it the theoretical or practical nature. Further, I would like to thank the staff of the beamlines P13 and P14 of the Deutsches Elektronensynchrotron, as well as the staff of the European Synchrotron Radiation Facility.

I want to thank Prof. Dr. Ralf Ficner and Prof. Dr. Ivo Feussner for the generous access to their facilities and devices. Additionally, I would like to thank Dr. Achim Dickmanns, Dr. Ellen Hornung and Dr. Thomas Monecke for sharing their experience whenever needed, as well as Johannes Arens for performing the MALS-assay.

Furthermore, I want to thank Prof. Dr. Tadhg Begley for providing the 2'-methoxythiamine diphosphate.

I am thankful to Gerd Mader, Malte Bürsing and Daniel Weinrich for providing their technical expertise and support, and to Christoph Mader, Dr. Guido Kriete and Benjamin Köster who took care of any IT-troubles.

I am very grateful to all recent and former colleagues of the Department of Molecular Enzymology for the years of pleasant working atmosphere, discussions and fun. I am especially thankful to Dr. Viktor Sautner who always was a great source of input, and Lisa-Marie Funk, who provided the kinetic data for *Lp*POX$_{WT}$. In addition, I would like to thank all of them for proofreading this thesis.

I would like to thank Jan Brunken and Stephan Requardt, the bachelor students who contributed to this thesis by their hard work, and hopefully learned a thing or two in their time.

Further, I would like to thank the DFG Research Group 1296, by which funding for this work was provided. They provided a fruitful scientific environment. Here, I am especially thankful to Prof. Dr. Georg Sprenger, who provided great input.

In addition, I want to thank the Göttingen Graduate School for Neuroscience, Biophysics and Molecular Bioscience for providing a great environment for graduate students by their extensive program for advanced training and social interaction. I am especially thankful to the office team, who eased the administrative work by a far margin and were always helpful.

Finally, I want to mention my family and friends, for supporting me and putting up with me during this ever-growing number of years.

1 Introduction

1.1 Thiamine

Thiamine is vitamin B_1, precursor to thiamine diphosphate, a vital cofactor in a wide variety of enzymes in all domains of life, both in primary as well as in secondary metabolism. Thus, it is highly important and deficiency of thiamine results in severe, adverse conditions.

1.1.1 A History of Thiamine

The first evidence for its existence, and concomitantly, its importance for human health was discovered in the late nineteenth century. The Japanese navy surgeon Takaki Kanehiro was able to reduce the incidence of *beriberi*, a disease nowadays known to be caused by thiamine deficiency, on a Japanese warship from 61 % to below 10 %. He achieved this by increasing the meat and whole grain content in a virtually white-rice only diet. However, he falsely attributed this effect to the increased uptake of nitrogen (Takaki, 1906; Bay, 2012).

In the following years, Dutch scientists in what is now Indonesia narrowed down the cause of *beriberi*. The Nobel prize awardee Eijkman discovered that brown rice, opposed to white rice, protected fowls from a disease similar to *beriberi*, but initially attributed this to an adverse effect of the white rice itself (Eijkman, 1897).

Upon his departure, his coworkers continued where he stopped. Vorderman used the prison population of the Dutch East Indies to compare the health of prisoners fed with mainly brown rice to those fed with white rice. Amongst nearly 300,000 inmates, he found that the propensity to develop *beriberi* was 300-fold higher in the population fed with white rice (Vorderman, 1897).

While Eijkman argued that polished rice contains a toxin against which the bran supplies a protective agent, his coworker Grijns came to the correct conclusion that the bran contains a compound essential for metabolism, now named the antineuric vitamin, or anitneurin. This assumption was further supported by the finding that mung bean

consumption helps in *beriberi* prevention and alleviates the disease (Hulshoff-Pol, 1902; Grijns, 1901).

In 1926, thiamine was isolated from rice hulls for the first time, and was proven to protect against polyneuritis (Jansen and Donath, 1926). In 1936, Williams and Cline reported the composition and synthesis of thiamine for the first time (Williams and Cline, 1936). The first isolation of thiamine diphosphate was performed in 1932. At this time, its identity was not understood, and it was termed co-carboxylase (Auhagen, 1932). It was characterized as the pyrophosphate of thiamine five years later, one year after the chemical composition of thiamine itself was revealed (Lohmann and Schuster, 1937).

1.1.2 Thiamine in Physiology

1.1.2.1 Thiamine Metabolism and Derivatives

Thiamine-dependent enzymes occur in all classical domains of life. However, animals lack the capability of *de novo*-synthesis of thiamine. They are dependent on external sources of thiamine (Fitzpatrick and Thore, 2014). In general, biosynthesis in bacteria, plants and fungi follows the same path. Thiazole phosphate and hydroxymethyl pyrimidine pyrophosphate are synthesized by separate pathways and then conjoined by a thiamine phosphate synthase, yielding thiamine monophosphate (Backstrom *et al.*, 1995; Jurgenson *et al.*, 2009). This compound is phosphorylated by thiamine monophosphate kinase, yielding thiamine diphosphate (Nishino, 1972).

In humans, absorption occurs in the small intestine. Interestingly, only the non-phosphorylated form is taken up. While plants contain this form, in animal tissue it is mainly present as pyrophosphate. Therefore, thiamine released from consumed animal tissue is dephosphorylated by thiamine pyrophosphatase prior to uptake. Absorption is mainly achieved by diffusion, but at low concentrations it requires active transport by pH- or sodium dependent transporters (Laforenza *et al.*, 1997; Dudeja *et al.*, 2003). The active form, the pyrophosphate is then generated by thiamine pyrophosphate kinase (Nosaka *et al.*, 1993).

While thiamine diphosphate (ThDP) is the predominant thiamine species in cells, there are also mono- and triphosphate derivatives (ThMP, ThTP). For the monophosphate, no role except as intermediate in the synthesis of ThDP was determined as of today (Lonsdale, 2006). The triphosphate has been controversially discussed for many years. Since its discovery in 1948, different functions were ascribed to this compound. It seems to have some importance in neurophysiology, as its presence increases permeability of neuronal membranes for chloride and was shown to activate an anion channel in mouse neuroblastoma (Bettendorff *et al.*, 1994; Bettendorff *et al.*, 1993). Additionally, a function in cell signaling was proposed, based on the finding that ThTP phosphorylates rapsyn in the electric organ of the electric ray *Torpedo marmorata*, as well as unidentified targets in rat and mouse brains (Nghiêm *et al.*, 2000). Despite the progress in identifying these functions, the physiological importance of ThTP and its biosynthesis remain not fully understood (Bettendorff *et al.*, 2014). In addition, adenosine derivatives of ThDP and ThTP were discovered in recent years, (Bettendorff *et al.*, 2007; Frédérich *et al.*, 2009). Their function is not yet understood. Adenosine ThTP is possibly involved in signaling related to metabolic stress, mainly carbon starvation and electron transport chain malfunction (Gigliobianco *et al.*, 2010).

1.1.2.2 The Pathology of Thiamine Diphosphate Deficiency

Deficiency of ThDP is the result of various, independent issues. Failure to consume adequate amounts of thiamine-containing food, thiamine transporter defects, either mitochondrial or in the gut, or thiamine pyrophosphate kinase malfunction share the same outcome, a systemic incapacity to supply the organism with adequate amounts of ThDP.

The effects of thiamine deficiency are manifold. It is the cause for *beriberi*, thiamine-responsive megaloblastic anaemia (Neufeld *et al.*, 2001), Amish microcephaly (Siu *et al.*, 2010) and Wernicke-Korsakoff syndrome (Guerrini *et al.*, 2005). All these are, at least partially, characterized by neurodegeneration, leading to multiple adverse effects, e.g. ataxia, memory impairment, acidosis and dysautonomia.

1.1.3 The Catalytic Properties of Thiamine and Related Compounds

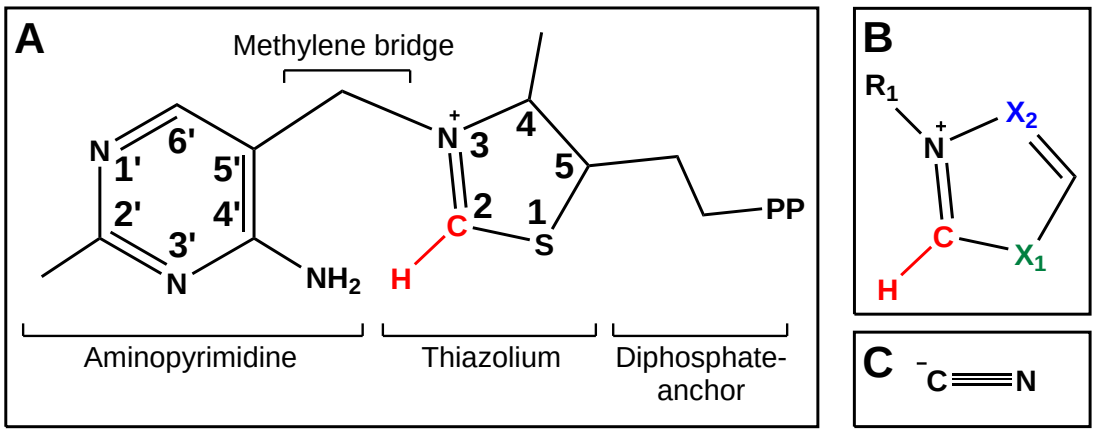

Figure 1. General structure of thiamine diphosphate (A), the catalytically related N-heterocyclic carbenes (B) and cyanide (C). In A and B the reactive carbon atom and the abstractable hydrogen are displayed in red. X_1 (green) can be either a sulfur or nitrogen atom, X_2 (blue) can be nitrogen or carbon.

For nearly 20 years after the identification of ThDP it remained unclear which moiety of it is the catalytically active site, disproved candidates being the amino-function of the aminopyrimidine ring or the methylene bridge linking it to the thiazolium (Kluger and Tittmann, 2008). By investigation of the deuterium exchange rates at different sites it became clear that the thiazolium ring, the C2 atom to be exact, must be the reactive part. It was inferred that the active species is the deprotonated carbanion form, in high similarity to the cyanide anion, capable of catalyzing similar reactions. In both cases, the negative charge at the carbon is stabilized by an adjacent nitrogen, as shown in figure 1 (Breslow, 1957; Breslow and Appayee, 2013). Thiazolium salts were the first described N-heterocyclic carbenes (NHCs), a large group of organocatalysts. Structurally, they are formed by a five-membered ring, in which the characteristic reactive carbon is flanked by a positively charged nitrogen on the one side and a sulfur (i.e in thiamine) or nitrogen atom on the other side (Fig. 1B) (Flanigan *et al.*, 2015). They are often used in the breaking and forming of carbon-carbon bonds, as it was initially described for the benzoin condensation, which mirrors the reactivity of ThDP-dependent enzymes *in vivo* (Ugai *et al.*, 1943; Breslow, 1958).

As the reactive site of the thiazolium is the C2 atom, it has to be deprotonated first.

However, the pK_A of the C2 is around 18 in aqueous solution, and deprotonation only occurs with a rate of $3x10^{-3}\,s^{-1}$ at pH 7.0 (Washabaugh and Jencks, 1988; Kern *et al.*, 1997). This makes activation of thiazoles, or NHCs in general, dependent on the presence of bases for deprotonation. Activated NHCs are potent Lewis bases and exhibit a nucleophile C2 ylid/carbene, prone to attack electrophilic carbon atoms (e.g. carbonyl atoms in aldehydes and ketones) (Maji *et al.*, 2011). Subsequent to formation of a covalent substrate-NHC adduct, an enamine in resonance with an carbanion is formed (Fig. 3).

This intermediate is commonly called Breslow intermediate, named after Ronald Breslow, who described it in 1958. As the electronegativity of the C2α atom is inverted by this reaction, it is commonly called *umpolung* (Seebach, 1979). The negative charge of the C2α-carbanion makes it a potent nucleophile. While aldehydes are the primary acceptor molecules for ThDP-dependent carboligations *in vivo*, NHCs, including thiazoles, have been used for carboligation with aldehydes, ketones and ketimines in solution (Hachisu *et al.*, 2003; Enders *et al.*, 2010; Li *et al.*, 2007; Sun *et al.*, 2013). The increased acceptor diversity is owed to the fact that electron withdrawing groups can be more easily deployed without the steric confines of an enzyme environment. This makes them interesting candidates for reactions of biotechnological relevance.

1.2 Thiamine Diphosphate Dependent Enzymes

1.2.1 Catalytic Features

1.2.1.1 Properties and Activation of the Cofactor

Naturally, the behavior of ThDP-dependent enzymes differs in many aspects from that of NHCs in solution, even though the basic principles are very similar. This begins with the fact that NHCs are a very diverse family with a wide variety of chemical makeups and substituents, while there are virtually no catalytically competitive analogs of ThDP *in vivo*. The most obvious difference is the absence of an external, solvent originating base for activation of the C2-atom. Early studies using thiamine analogs (e.g. N3'-pyridyl-ThDP and 4'-OH-ThDP) showed that the 4'- and the 1'-amine of the pyridine

ring are of special catalytic importance as removal or substitution of these positions resulted in nearly complete loss of enzymatic activity. They obtained evidence pointing towards the adoption of the so called V-conformation of ThDP in the enzyme, opposed to the relaxed F-conformation observed for ThDP *in crystallo* or ThDP in thiamine pyrophosphokinase (Schellenberger, 1967; Pletcher *et al.*, 1972; Jordan and Patel, 2003). In the V-conformation, C2 and N4' are in close proximity to each other (Fig. 2), strongly hinting towards a cocatalytic functionality of the N4' *in vivo*. They concluded that the aminopyrimidine moiety is most probably involved in the activation of the cofactor and acts as an acid-base catalyst for some of the protonation/deprotonation steps taking place during catalysis (Schellenberger, 1990).The importance of these positions was verified with the advent of new NMR-techniques allowing the observation of the H/D-exchange rate at the C2. These experiments showed a decrease in the exchange rates of enzyme bound 4'-desamino-ThDP and N3'-pyridyl-ThDP below those of ThDP in solution (Kern *et al.*, 1997).

As the aminopyrimidine itself is not prone to abstract a proton, it has to be primed for this purpose. This task is performed by a glutamate residue conserved in virtually all ThDP-dependent enzymes. In its protonated form it interacts with the N1' of the aminopyrimidine, which abstracts the proton. This results in the formation of a 4'-aminopyrimidinium species. After deprotonation of this species by the solvent, the 1',4'-iminopyrimidine is now primed to abstract the proton at the C2 of the thiazolium. This process results in formation of the reactive ylidene species at the C2 (Fig. 2B)(Kern *et al.*, 1997). There is only one known exception to this mechanism, glyoxylate carboligase, in which the glutamate is replaced by a valine, which is necessary for fine-tuning of the reaction (Kaplun *et al.*, 2008; Nemeria *et al.*, 2012).

The deprotonation of the C2 by the Glu-N1'-N4' proton-relay is however not the only factor impacting the accelerated activation of ThDP in enzymes. Elegant studies on the polarity of the active site in yeast pyruvate decarboxylase, in which the fluorescence of the ThDP analog thiochrome diphosphate bound to the enzyme was compared to that in solvents of different dielectric constants (ε_r), showed an ε_r of 13-15 for the active site,

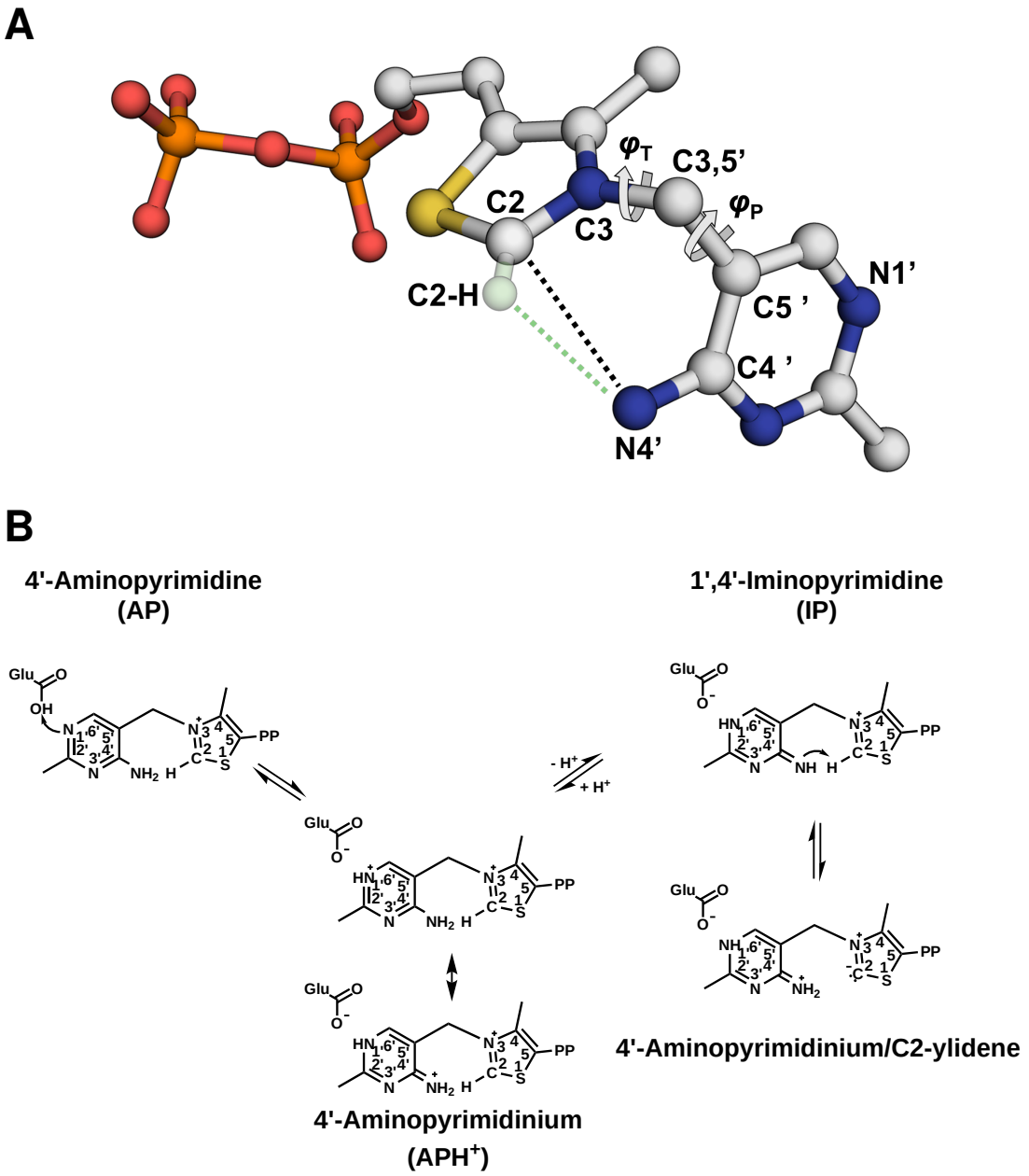

Figure 2. (A) Geometry of the V-Conformation of enzyme bound thiamine diphosphate. The ThDP backbone is shown in opaque colors, the C2-H in transparent green. φ_T denotes the torsion angle C2-C3-C3,5'-C5', φ_P the torsion angle C3-C3,5'-C5'-C4' (PDB:1QGD). **(B) Activation of thiamine diphosphate.** The activation of the C2 is performed by the Glu-N1'-N4' proton-relay. The respective states of the ThDP are named. Adapted from Kluger and Tittmann, 2008.

compared to 80 for water. As the thiazole ring is positively charged in the protonated state and formally neutral in the activated state, the low dielectric constant of the active site may significantly contribute to the pK_A suppression (Jordan *et al.*, 1999). This effect

is even more pronounced in the glyoxylate carboligase, probably partially compensating the absence of the conserved glutamate (Kaplun *et al.*, 2008; Shaanan and Chipman, 2009).

As of today it is not clear in which magnitude the activation takes place in the enzyme in the ground state, as no accumulation of deprotonated thiamine was observed in the pyruvate decarboxylase from *Saccharomyces cerevisae* (*Sc*) (Kern *et al.*, 1997). It is thought to be triggered by substrate binding, as evidenced by recent studies on pyruvate oxidase of *Lactobacillus plantarum* (*Lp*), which showed accumulation of a carbene species at the C2 in presence of phosphate, which mimics the negative charge of the substrate pyruvate, but is not able to form a covalent intermediate (Meyer *et al.*, 2013). The ylide component of the assumed active ylidene was not yet observed, however. Furthermore, it is not understood if ylide or carbene is the reactive species.

One remarkably useful feature of ThDP is the fact that each of the three different species of the aminopyrimidine-ring as shown in figure 2 is distinct in its spectral properties, as was shown by spectroscopic studies using synthetic analogues for the respective states. As certain states along the reaction trajectory can be associated with the population of distinct tautomers, this is a useful tool in kinetic investigations on ThDP-dependent enzymes (Nemeria *et al.*, 2004; Nemeria *et al.*, 2007).

1.2.1.2 Reactivity

In addition to their highly similar activation mechanism, the donor reactions resulting in formation of the Breslow intermediate are alike along the family of ThDP-dependent enzymes (Fig. 3). Upon encounter, a carbonyl-harboring substrate is nucleophilically attacked by the activated C2. By internal acid-base catalysis, most probably by the N4', the carbonyl oxygen is reduced and a covalent, tetrahedral intermediate is formed. Subsequently, one substituent of the C2α is removed, either in a decarboxylation reaction or once again by acid-base catalysis, forming the Breslow intermediate.

From there on, the pathways diverge depending on the second substrate. There are

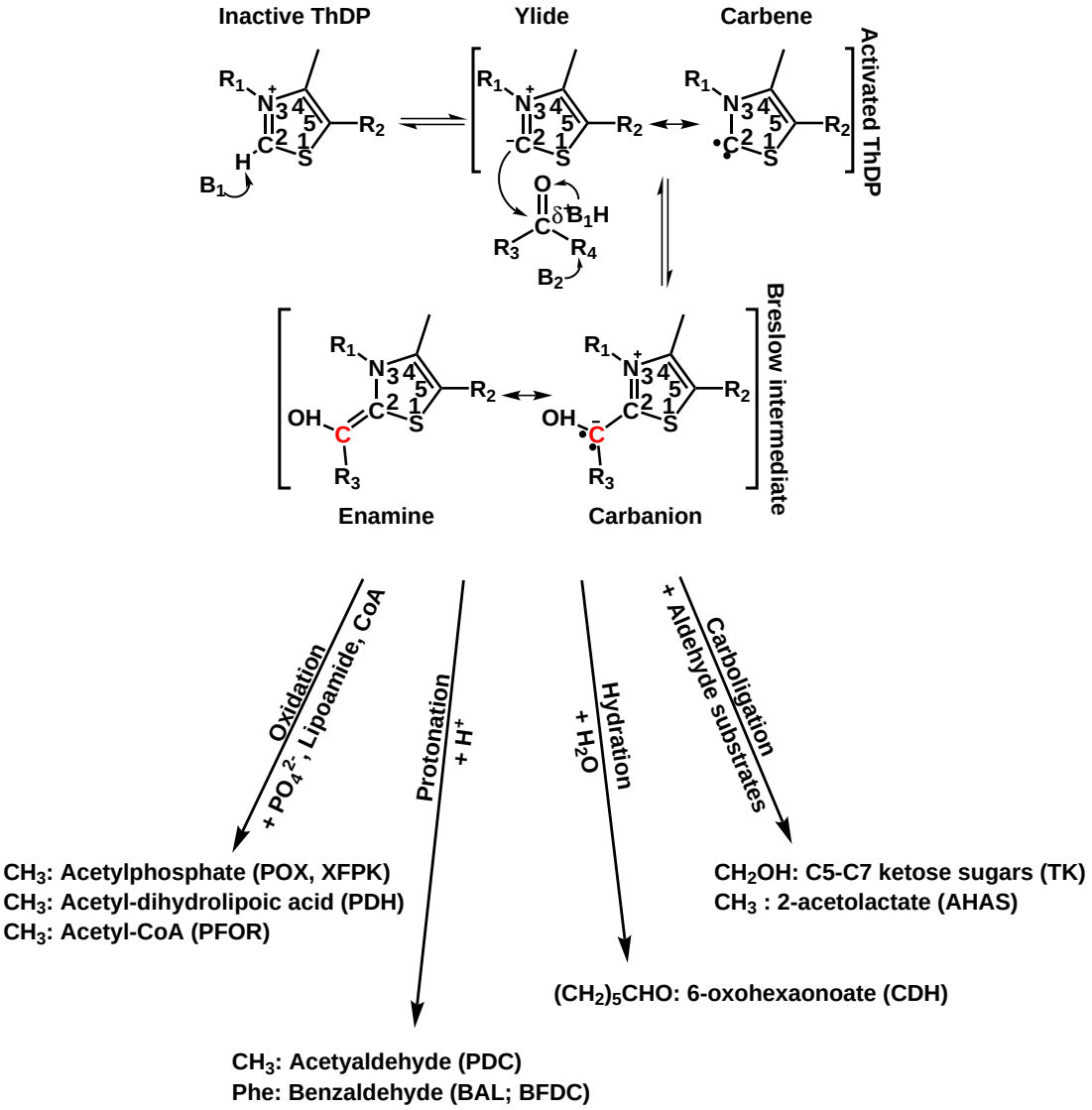

Figure 3. Shared reaction steps of ThDP-dependent enzymes and pathway divergence. The C2-H is abstracted by a base, forming the activated ylidene species. This species attacks an electrophilic carbon atom, and by base-assisted rearrangement and bond cleavage forms the Breslow intermediate. R_1 denounces the aminopyrimidine moiety in ThDP, R_2 the pyrophosphate anchor in ThDP, R_3 and R_4 denote the substituents neighboring the carbonyl function. The multiple pathways diverging from the Breslow intermediate are shown below, indicating common substrates and the different products according to the identity of R_3, as well as the catalyzing enzymes. The C2α is denoted in red.

at least 18 different ThDP-dependent enzymes described, belonging to the enzyme classes of oxidases, transferases, hydrolases and lyases.

Oxidases catalyze the oxidation of their substrate using electron acceptors such as phosphate (e.g. pyruvate oxidase (POX)), lipoamide (e.g. pyruvate dehydrogenase (PDH))

or coenzyme A (e.g. pyruvate:ferredoxin oxidoreductase (PFOR)). They often employ additional cofactors such as flavin adenine dinucleotide (FAD) or iron-sulfur clusters. The transferases commonly employ aldehyde-containing acceptor substrates, linking the C2α of the Breslow intermediate to the acceptors carbonyl atom (e.g. transketolase (TK), acetohydroxyacid synthase (AHAS)). However, there are exceptions, for example acetoin dehydrogenase, which uses CoA as an acceptor substrate and reduces NAD^+ to NADH. Cyclohexane-1,2-Hydrolase is the only known ThDP-dependent hydrolase, in so far unique as it does not cleave off any part of the product after formation of the covalent adduct, by virtue of its circularity (Steinbach *et al.*, 2011; Steinbach *et al.*, 2012). The final group are the lyases. They cleave their respective substrates, often decarboxylating it (e.g. pyruvate decarboxylase (PDC), benzaldehyde lyase (BAL)). However, some of them still use acceptor substrates, such as phosphate (e.g. xylulose/fructose phosphoketolase (XFPK)). They, as well as the transferases, are of special biotechnological interest as they frequently display a relatively broad substrate spectrum and can be modified to accept uncommon compounds (Müller *et al.*, 2013).

One common question is how this broad reaction and substrate specificity is modulated. The most obvious answer is by variations in the active site, which enable access for substrates of varying sizes and properties, and modify the stereo- and enantioselectivities (Hailes *et al.*, 2013; Westphal *et al.*, 2014; Wechsler *et al.*, 2015; Affaticati *et al.*, 2016).

Recent research revealed an additional possibility to control the reaction pathway, which was disregarded for a long time. As shown in figure 3, the shared intermediate in ThDP-dependent enzymes is assumed to exist as the enamine and carbanion tautomers, while formation of a keto-form was assumed to cause breaking of aromaticity of the thiazolium ring. As such, it was regarded as thermodynamically unfavorable (Breslow, 1958). However, in the last decade evidence accumulated supporting the existence of this intermediate. In solution studies of NHCs revealed a ketone species to be the thermodynamic minimum of the reaction of 1,3,4-triphenyl-4,5- dihydro-1*H*-1,2,4-triazol-5-ylidene with propionic aldehyde in tetrahydrofuran (Fig. 4A)(Berkessel *et al.*,

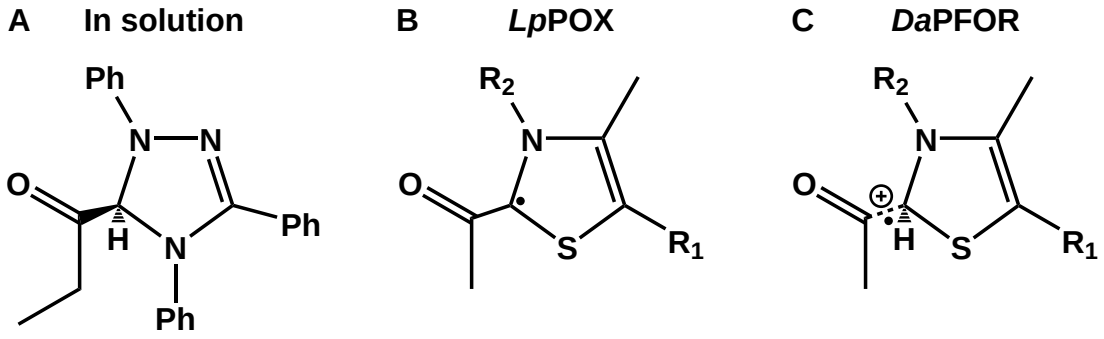

Figure 4. Putative ketone-intermediates in NHCs and ThDP-dependent enzymes. **(A)** The intermediate generated using 1,3,4-triphenyl-4,5- dihydro-1*H*-1,2,4-triazol-5-ylidene and propionic acid in THF (Berkessel *et al.*, 2010). **(B)** The putative radical species derived from the intermediate observed *in crystallo* of *Lp*POX (Meyer *et al.*, 2012). **(C)** The σ/n cationic radical of *Daf*PFOR, observed *in crystallo* (Amara *et al.*, 2007).

2010). Additionally, and in the context of biological systems much more substantial, a similar intermediate was observed in two different ThDP-dependent enzymes. In pyruvate:ferredoxin oxidoreductase (PFOR), a stable σ/n cationic radical was captured *in crystallo*. The structure showed significant distortion of the thiazolium ring, indicating loss of aromaticity, as well as generation of a keto-function at the C2α, albeit the character of the radical *in vivo* is subject to discussion, as spectroscopic studies point towards a π-type radical (Fig. 4C)(Chabriere, 2001; Cavazza *et al.*, 2006; Amara *et al.*, 2007).

In pyruvate oxidase, a tetrahedral, covalent hydroxyethyl-ThDP intermediate was observed, where the C2α-Oα bond showed at least partial double bond character. While this specific intermediate would be incompetent in the native reaction, it suggests the presence of an acetyl radical species, where the radical is localized at the C2, opposed to the precedent model employing a hydroxyethyl-radical, with radical-localization at the C2α. It is suggested that the second substrate phosphate nucleophilically attacks the radical intermediate at the C2α. In the old model it would attack an electron rich center, whereas in the new model it would attack a carbonyl carbon (Fig. 4B)(Meyer *et al.*, 2012). All these results suggest that ThDP-dependent enzymes employing nucleophilic or electron rich substrates are capable of forming intermediates with an electrophilic C2α. As the formation of this intermediate would be detrimental in enzymes catalyzing carboligations, ThDP-dependent enzymes seem to have the capability to stabilize the

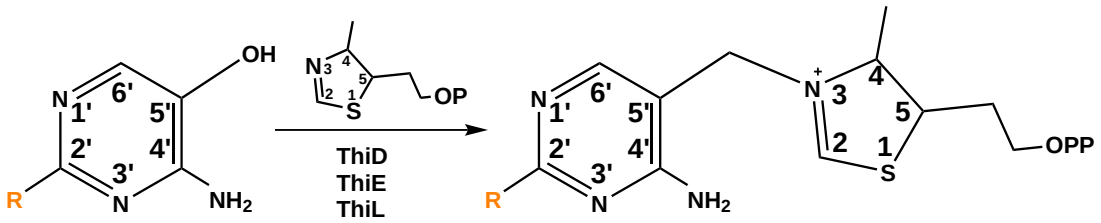

Figure 5. Synthesis of ThDP and MeOThDP in *E. coli*. Hydroxymethylpyrimidin (HMP, R: Me) or bacimethrin (R: OMe) are transformed into ThDP (R: Me) or MeOThDP (R: OMe) by the native *E. coli* thiamine synthesis machinery. The HMP-P kinase ThiD transforms the pyrimidine-moiety into the respective pyrophosphate derivative, the thiamine phosphate synthase ThiE links it to the 4-methyl,5-hydroxyethyl thiazole phosphate moiety and the thiamine phosphate kinase ThiL phosphorylates the joint molecule to yield ThDP (adapted from Reddick *et al.*, 2001)

.

respective intermediate by virtue of their active site.

As stated before, until today, no derivatives of ThDP with a similar effectivity were discovered, as all investigated substitutions at different positions of ThDP resulted in a severe loss of activity in the respective model enzymes (Schellenberger and Winter, 1960; Schellenberger *et al.*, 1966a; Schellenberger *et al.*, 1966b; Schellenberger, 1967; Schellenberger *et al.*, 1967). This immutable character of ThDP is exploited by the bacterial species *Bacillus megaterium*, *Streptomyces albus* and *Clostridium botulinum* (Tanaka *et al.*, 1962; Drautz *et al.*, 1987; Cooper *et al.*, 2014). These produce a compound called bacimethrin (Fig. 5), which was shown to be an inhibitor for bacterial growth. It was shown that the toxicity does not stem from an inhibition of the ThDP biosynthesis pathway, as bacimethrin is incorporated at an up to 6-fold elevated rate compared to the natural precursor hydroxymethylpyrimidin, forming 2'-methoxythiamine diphosphate. In the same study, *E. coli* transketolase, deoxy-D-xylulose-5-phosphate synthase (DXPS) and α-ketoglutarate dehydrogenase (KGDH) were identified as major inhibition targets *in vivo* by the produced methoxythiamine (Reddick *et al.*, 2001). This was later supported by *in vitro* studies for DXPS, while the ThDP containing E1 component of the KGDH-complex proved to be resistant against MeOThDP, opposed to E1 of the pyruvate dehydrogenase complex, which showed a loss of activity of around 90 % (Nemeria *et al.*, 2016). As of now, the mode of action by which this reduction in activity is achieved is unknown.

1.2.2 Structure

Even though ThDP-dependent enzymes catalyze a wide range of reactions, in all domains of life with large evolutionary distances, they all share some common, highly important features. As mentioned before, virtually all of them employ a glutamate residue to increase the rate of thiamine activation via an intramolecular proton-relay. A further shared feature is the ThDP binding motif, $GDGX_{24\text{-}27}N$. The aspartate and asparagine residue coordinate the bivalent metal cation which is obligate for cofactor binding. The fold of the pyrophosphate binding pocket is also conserved, in an $\alpha/\beta/\alpha$ sandwich. The domain responsible for binding of the pyrophosphate was termed PP domain, the one responsible for binding of the pyridine ring PYR domain (Hawkins *et al.*, 1989, Muller *et al.*, 1993). In many ThDP-dependent enzymes there is a third domain present, adapted to the individual needs of the respective enzyme.

While the overall structure of the PP and PYR domain is pretty much conserved, their arrangement is not. There exist nine super-families of ThDP-dependent enzymes, in all of which the order of the domains is different, as well as the binding mode for ThDP. This is exemplified in figure 6, where the architecture of a functional dimer is shown, using transketolase as representative for the TK family, and pyruvate oxidase as example for the decarboxylase (DC) family. In transketolase, moving from N-terminus to C-terminus, the PP domain is the first domain, the PYR domain follows and at the C-terminus is the C-terminal domain of unknown function, which could potentially be involved in regulation as it contains a nucleotide binding fold (Schenk *et al.*, 1997). In pyruvate oxidase, the PYR domain comes first, followed by the TH3 domain which is required for FAD binding, with the PP domain being located at the C-terminus. While both DC and TK super-families are of the inter-monomer type, meaning two monomers are required to form an active site, there are also families of the intra-monomer type, where the active site is formed by the domains of one monomer alone, for example in deoxy-D-xylulose-5-phosphate synthase (Vogel and Pleiss, 2014).

In addition to the shared macro-structural features like domain architecture and arrangement, there is one strictly conserved water molecule in hydrogen-bonding distance to

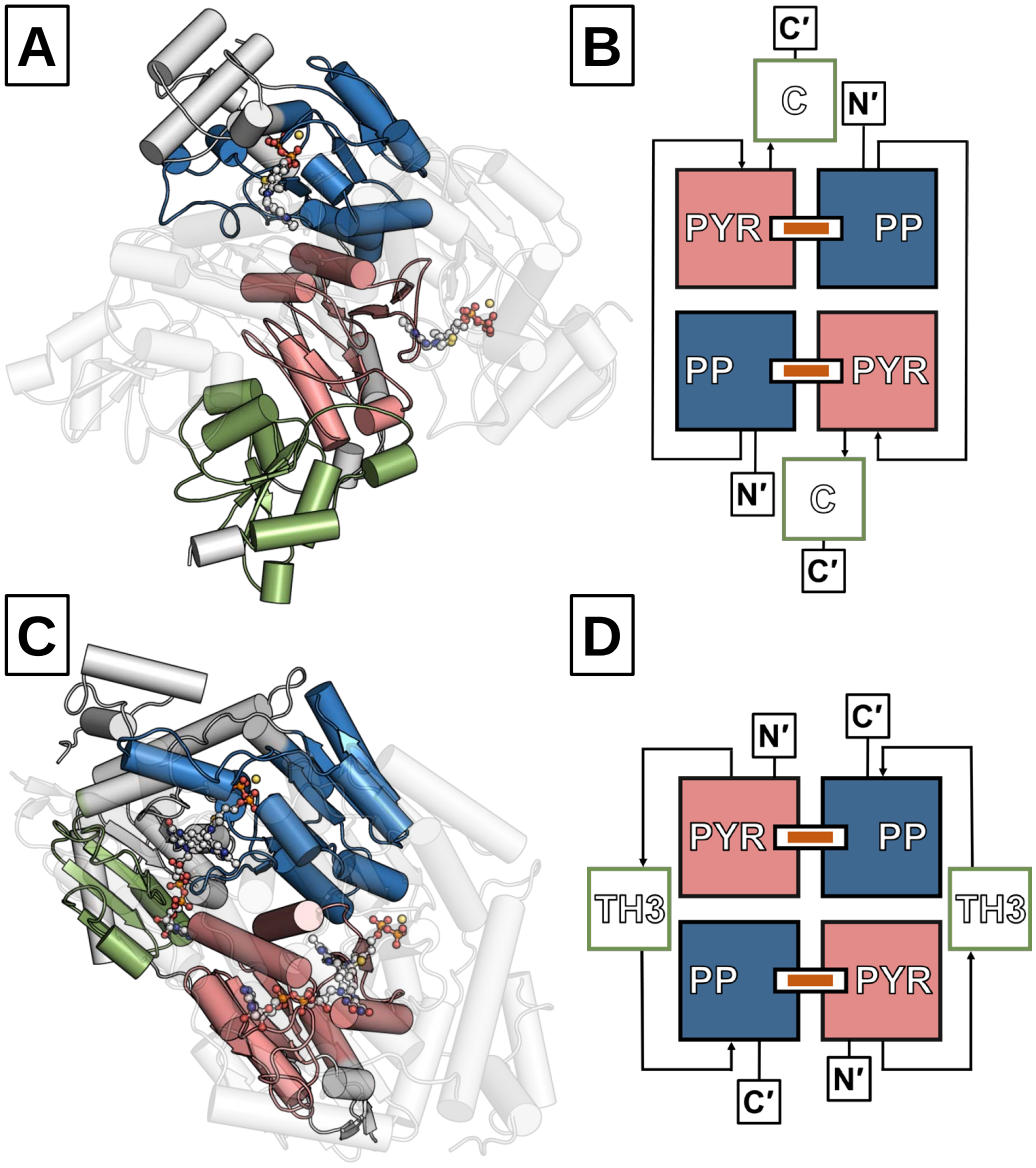

Figure 6. Domain architecture of *Ec*TK (top) and *Lp*POX (bottom). The PYR domain is displayed in rose, the PP domain in blue. The C-terminal TK domain is denoted C, the FAD-binding domain of *Lp*POX TH3. N' and C' denote the N- and C-terminus respectively. The domain architectures were adapted from Vogel and Pleiss, 2014.

the activating glutamate, also present in the glutamate-lacking glyoxylate carboligase. This water may act as a control for the pK_A of the glutamate, or as proton source in activation or active site communication. The glutamate is often further flanked by an additional acid-base catalyst, mostly amino acids (e.g. glutamate or histidine), but sometimes water.

1.2.3 Transketolase

Transketolase is an enzyme present in all domains of life. It is part of the non-oxidative pentose phosphate pathway, which is central in generation of precursors for many metabolic processes. It generates ribose 5-phosphate, which is required for the generation of nucleotides, erythrose 4-phosphate, which is necessary for the biosynthesis of aromatic amino acids, as well as reducing equivalents in form of NADPH for anabolic processes. In photosynthetically active organisms, it is also responsible for the transfer of two-carbon units from fructose 6-phosphate or sedoheptulose 7-phosphate to the glyceraldehyde 3-phosphate moieties yielded by the CO_2 fixation. It generates xylulose 5-phosphate (X5P) and ribose 5-phosphate (R5P) in the process, which are in turn used for the generation of ribulose 5-phosphate (Ru5P), required for further fixation cycles. Thus, it is indispensable in almost all organisms. The general function is the transfer of a dihydroxyethyl unit from a donor ketose to an acceptor aldose, employing a narrow range of both donor and acceptor molecules *in vivo* (Fig. 8B).

As shown in figure 6, thiamine binding is performed by the PP domain of one monomer and the PYR domain of the other monomer of the functional dimer. Furthermore, the residues constituting an individual active site are provided by both monomers of the functional dimer (Fig. 7), making dimerization obligate.

The active site of transketolase is located closely to the surface, connected by a single channel to the solvent. This channel contains multiple, highly conserved polar residues and is by virtue of two arginines positively charged. Thus, it important for binding of the phosphate group of the substrate sugars. This explains the significant preference for phosphorylated substrates, as the sugar itself is only involved in half of the possible interactions with the protein in the neutral core of the active site. In total, eight amino acids form hydrogen bonds with the sugar phosphate in the docking site. Serine 385, histidine 461 as well as the arginines 358 and 520 interact with the phosphate moiety, while aspartate 469 and histidine 473 form strong hydrogen bonds with the C4-OH. The histidines 26 and 261 interact weakly with the C3- and C2-OH.

In close proximity to the cofactor there are five conserved histidines (His_{473} is substituted

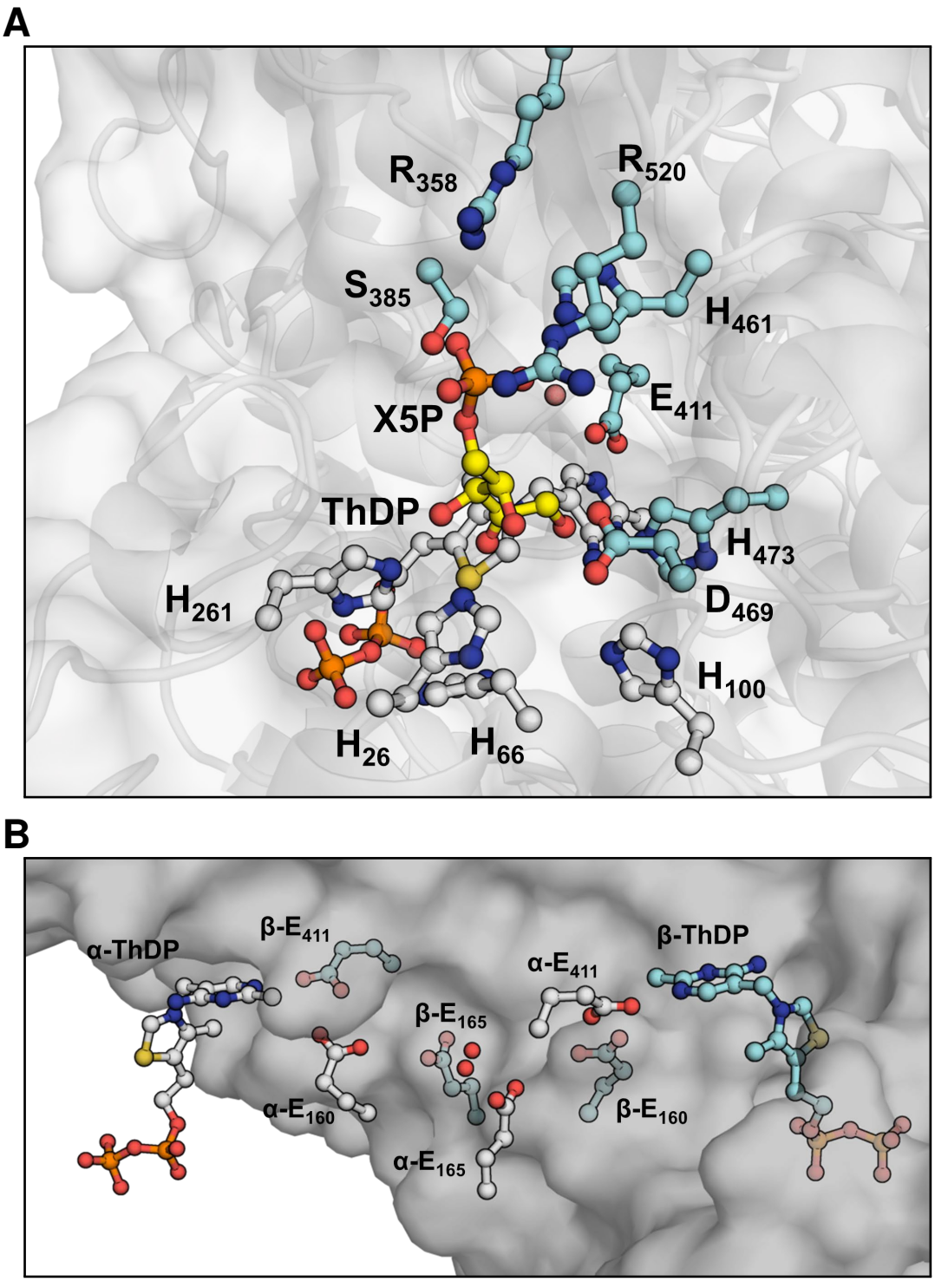

Figure 7. (A) Conserved residues in the active site of transketolases with catalytic or substrate binding function. (B) Side-view of a putative interaction channel between the active sites of transketolase dimers. The residues originating from monomer A are colored gray, the residues originating from monomer B in cyan. The substrate X5P in the docking site is colored yellow. The residues are numbered according to the *Ec*TK sequence. The water molecule conserved in virtually all ThDP-dependent enzymes is colored red.

by glutamine in animal and some protozoan transketolases), which were shown to be of high catalytic importance, with residual activity upon mutagenesis of 4.3 % (H100A) to 0.09 % (H26N) in *Saccharomyces cerevisae* transketolase. In addition, the apparent K_M is increased significantly for X5P, while remaining more or less the same for R5P. For histidine 261, the apparent K_M for both substrates is reduced (Wikner *et al.*, 1995; Wikner *et al.*, 1997). Of these, histidine 66 is the most curious case. It does not directly interact with any substrate or intermediate states during catalysis, nevertheless activity and substrate affinity are significantly impaired in the mutated enzyme. The only direct interaction of this residue is with the β-phosphate of the ThDP. Mutagenesis of histidine 26 is the most impactful out of the five. It is involved in binding of donor and acceptor substrates by formation of hydrogen bonds, and is assumed to act as acid-base catalyst during the cleavage of the covalent donor-ThDP intermediate together with histidine 261. The histidines 100 and 473 are important for the discrimination of donor and acceptor substrates by interaction with the C1-hydroxyl or -aldehyde, and are involved in orientation of dihydroxyethyl-thiamine diphosphate (DHEThDP). Mutagenesis of these residues significantly decreases the apparent affinity for X5P as well as the turnover rates. Histidine 261 is involved in cleavage of the covalent donor-ThDP intermediate together with histidine 26, acting as acid-base catalyst. In addition, it interacts with donor and acceptor before formation of the covalent adduct. However, mutagenesis of this amino acids increases the apparent affinity for both donor and acceptor.

An additional conserved feature is an acidic channel in between the two active sites of a transketolase dimer, consisting of glutamate 411, which is required for cofactor activation, glutamate 160 and 165. Furthermore, a set of water molecules contained in a pocket isolated from the solvent is involved (Fig. 7B)(Nikkola *et al.*, 1994). Residue 160 was shown to be important for reactivity and dimerization in yeast, while the importance of glutamate 165 is yet unknown (Meshalkina *et al.*, 1997). It has a similar character to an acidic channel observed between E1 subunits of the pyruvate dehydrogenase complex (Frank *et al.*, 2004). This channel was shown to be highly sensitive towards perturbations, as mutagenesis of individual residues reduced the overall complex activity

down to 3 % (Nemeria *et al.*, 2010). Half-of-the-sites reactivity seems to be prevalent in ThDP-dependent enzymes (Schröder-Tittmann *et al.*, 2013) and was also postulated for transketolase (Sevostyanova *et al.*, 2009). Furthermore, there are additional proteins showing a putative communication channel, e.g. *Lactobacillus plantarum Lp*POX (Neumann and Tittmann, 2014) or *Bifidobacterium breve* xylulose/fructose phosphoketolase (XFPK). Thus, a channel like this could be the facilitator for inter-subunit communication.

When a suitable donor-substrate enters the active site, the activated C2 of the ThDP performs a nucleophilic attack on the carbonyl carbon (typically the C2 of the sugar). This yields a covalent, tetrahedral alkoxide. The alkoxide abstracts a proton from the N4'-amine of the ThDP, forming a stable intermediate. Cleavage of the sugar is performed by acid-base catalysis. The histidines 26 and 261 work together to abstract a proton from the C3-OH. Subsequent rearrangements result in cleavage of the C2-C3 bond and formation of the first product, as well as the Breslow intermediate. In absence of substrate, the equilibrium of this reversible reaction is strongly on the side of the covalent sugar-ThDP-adduct, in a manner that allows observation of only the covalent adduct *in crystallo* and in NMR studies. This mechanism most probably serves to protect the Breslow intermediate from protonation by the solvent (Asztalos *et al.*, 2007). In presence of an acceptor substrate, the first product is displaced. The nucleophile Breslow intermediate then attacks the carbonyl carbon (typically C1, as it is an aldose), forming a new bond. The resulting alkoxide is then protonated by histidine 261, and the C2α-OH is deprotonated by the N4'-imine of the ThDP. Bond rearrangement then results in breaking of the C2α-C2 bond and release of the final product, as well as restoration of the initial state of the active site, with an ylidene-species at the thiazolium and the APH^+ species.

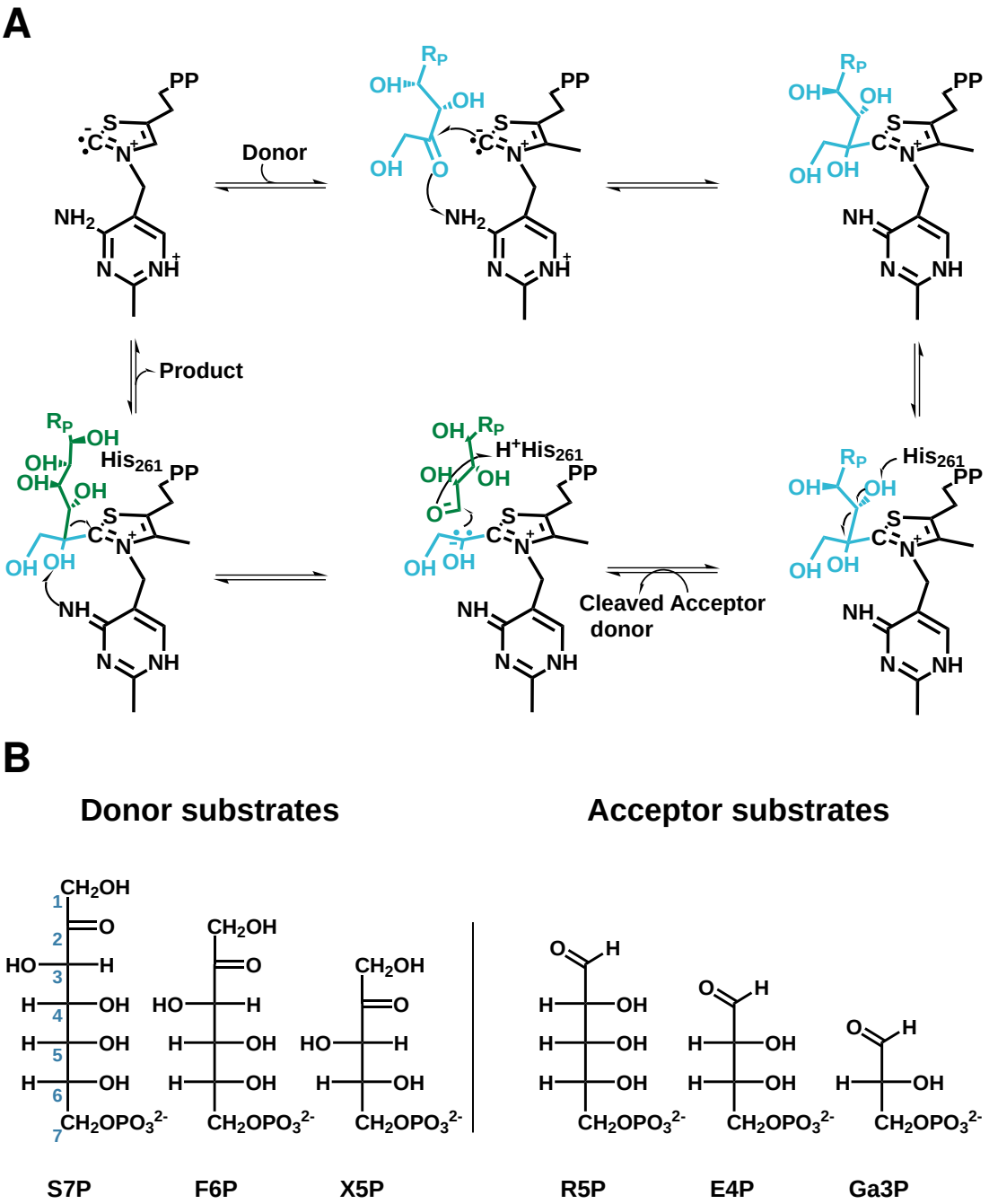

Figure 8. (A) Reaction cycle of transketolase. Transketolase catalyzes the transfer of a two-carbon unit from a donor ketose (blue) to an acceptor aldose (green). Only the carbanion form of the Breslow intermediate is displayed. R_P denotes the respective carbohydrate chain including the phosphoester group. **(B) Physiological substrates.** S7P: sedoheptulose 7-phosphate, F6P: fructose 6-phosphate, X5P: xylulose 5-phosphate, R5P: ribose 5-phosphate, E4P: erythrose 4-phosphate, Ga3P: glyceraldehyde 3-phosphate. S7P carbons are numbered according to the order referenced in the text.

1.2.4 Pyruvate Oxidase

Pyruvate oxidase belongs to the class of oxidoreductases. As such, it also employs flavin adenine dinucleotide as cofactor in addition to thiamine diphosphate. It is mainly present in bacteria and sparsely in archea and eukaryotes. The classical pyruvate:oxygen 2-oxidoreductase, as present in *Lactobacillus plantarum*, is used to transform excess pyruvate into acetyl-phosphate, which harbors a high-energy ester bond. This may be used for generation of ATP from ADP by acetate kinase. The process seems to be essential in *lactobacilli* (Götz and Sedewitz, 1991). Opposed to the pyruvate:ubiquinone 2-oxidoreductase from *E. coli*, molecular oxygen is required as electron acceptor, yielding H_2O_2. As mentioned before, a putative communication channel between the monomers of a functional dimer was observed *in crystallo*, corroborated by binding studies suggesting half-of-the-sites activity (Schröder-Tittmann *et al.*, 2013, Neumann and Tittmann, 2014).

Structurally, *Lp*POX shares many features with other ThDP-dependent enzymes. It forms a dimer of dimers, and each active site is formed by both monomers of the functional dimer, the PYR-domain of one subunit and the PP-domain of the other binding ThDP conjointly. The activation is performed by the canonical glutamate residue (Glutamate 59 in *Lp*POX).

Compared to transketolase (TK), there is a notable absence of polar residues surrounding the reactive C2 of the thiazolium. In TK there are five histidines in a proximity of 6 Å or less. Only one residue with a comparable distance is present in *Lp*POX, glutamate 483, which is located above the thiazolium ring, pointing towards it. ThDP is further surrounded by a valine, a phenylalanine, an isoleucine and a proline, forming a relatively hydrophobic active site (Muller and Schulz, 1993). The two phenylalanines 121 and 479 are most probably involved in the transfer of reducing equivalents towards FAD, with an arginine located close to Phe479, poised to stabilize the negatively charge build up during transfer. Two serines, located close to the aminopyrimidine moiety are involved in coordination of the substrate phosphate (Wille *et al.*, 2006). For catalysis, ThDP is activated as described before, yielding a reactive ylide species. This species attacks

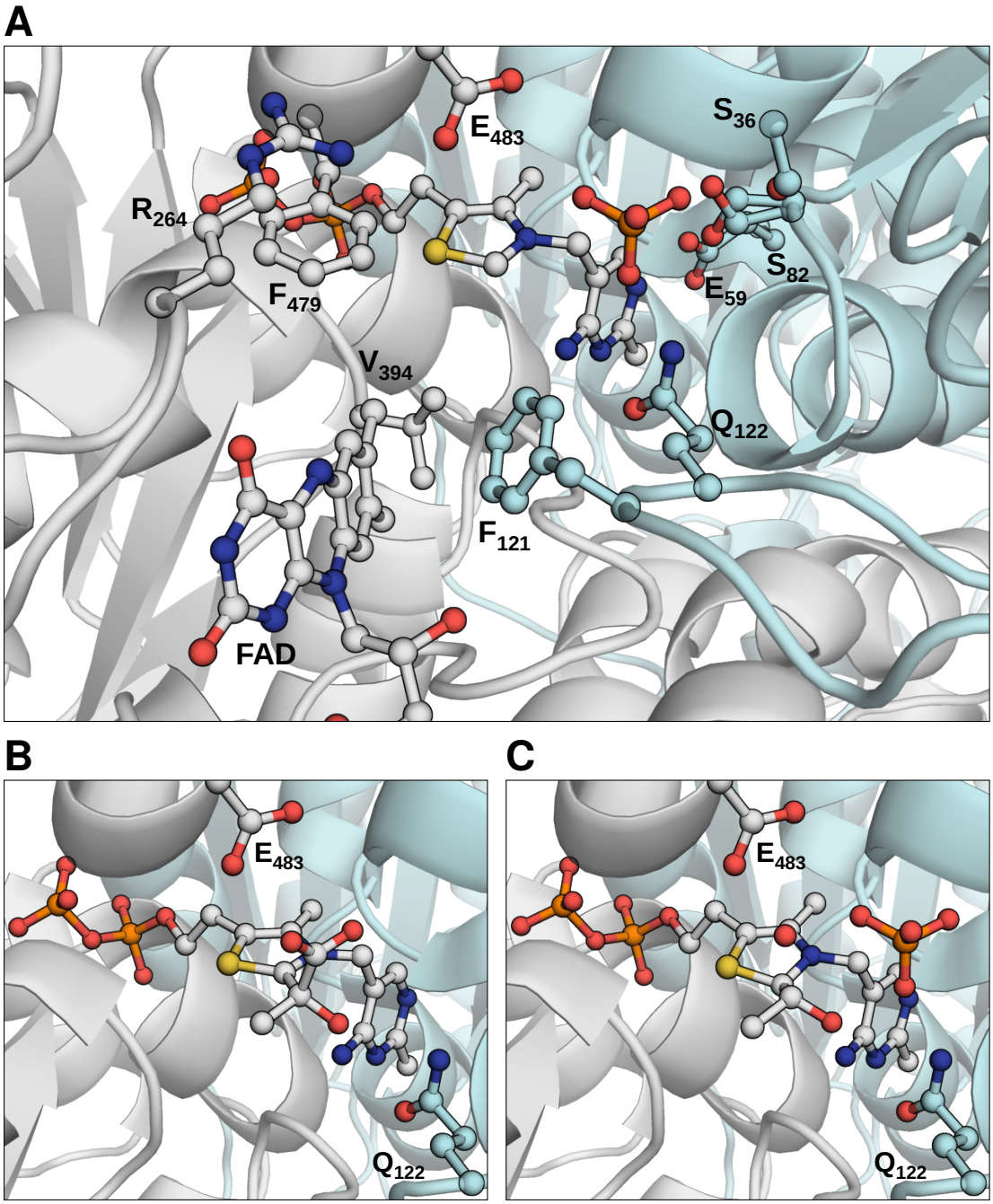

Figure 9. (A) Active site of *Lactobacillus plantarum* pyruvate oxidase in ground state. The residues stemming from monomer A of the dimer are displayed in grey, the ones from monomer B in cyan. The residues implicated in substrate coordination and catalytic function are shown and annotated (PDB 4KGD). **(B) Geometry of the tetrahedral pre-decarboxylation intermediate LThDP in pyruvate oxidase.** The residues Q_{122} and E_{483} which interact with the intermediate are shown (PDB 2EZ8). **(C) Geometry of the non-planar post-decarboxylation intermediate HEThDP.** The residue Q_{122} which interact with the intermediate is shown, as well as interacting water coordinated by E_{483} (PDB 4FEE).

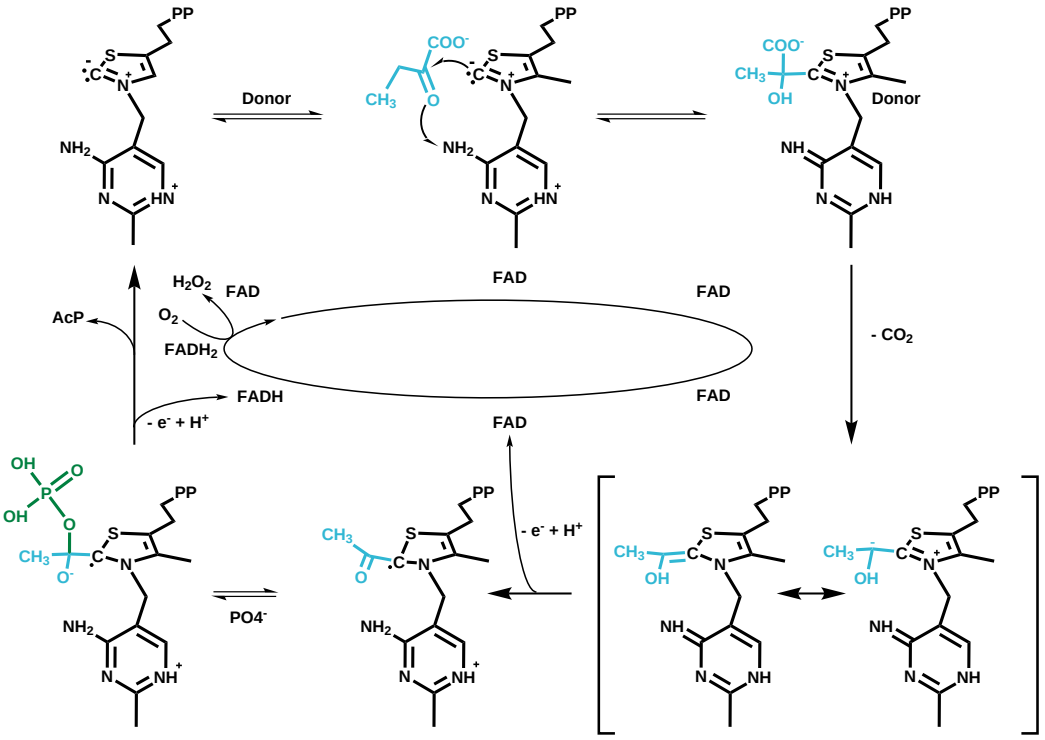

Figure 10. Reaction cycle of *Lactobacillus plantarum* pyruvate oxidase. *Lp*POX catalyzes the transfer of acetate from a pyruvate (blue) to phosphate (green), while transferring reducing agents to molecular oxygen via the cofactor FAD (Meyer *et al.*, 2012).

the carbonyl atom of the first substrate pyruvate, forming the covalent adduct LThDP. As with transketolase, the proton donor for the carbonyl-oxygen is most probably the N4' of the, at this stage of catalysis, positively charged aminopyrimidinium moiety (Tittmann *et al.*, 2003). The intermediate is then decarboxylated. Decarboxylation is most probably driven by the apolar environment of the active site. As the optimal activity of *Lp*POX is reached between pH 5.7 and 6, the carboxyl group of pyruvate, with a pK_A of 2.5, is almost completely deprotonated and thereby charged negatively. Thus, removal of the of the carboxyl group yielding uncharged CO_2 and the formally neutral carbanion/enamine Breslow-intermediate is promoted (Crosby and Lienhard, 1970; Tittmann *et al.*, 2000). As mentioned before, the following oxidation of the intermediate, required to facilitate nucleophilic attack of phosphate, proceeds via a radical mechanism. Transfer of the first reduction equivalent occurs with a rate of approximately 329 s^{-1}, followed by a very fast second step (> 800 s^{-1}) in the presence of phosphate. In the absence of phosphate,

this step only occurs with a rate of around 3 s^{-1}, followed by a slow hydrolysis to acetate (Tittmann *et al.*, 2005). Phosphate was shown not to be positioned in a manner suited for mediating transfer of reducing equivalents from the HEThDP-radical (Wille *et al.*, 2006). Furthermore, it was shown that phosphate does not react with acetyl-thiamine diphosphate (AcThDP) in solution (Gruys *et al.*, 1987). From these data it was assumed that it reacts with the neutral HEThDP-radical, forming an anionic radical, likely with a low reduction potential, prone to electron transfer. The formation of this species is most probably reason for the requirement of phosphate for the second transfer step. Release of acetyl-phosphate and oxidation of $FADH_2$ by molecular oxygen restores the enzyme for a new catalytic cycle (Fig. 10). Phosphorolysis and FAD reoxidation seem to be the rate limiting steps (Tittmann *et al.*, 2000).

Both of the two polar residues in proximity to the reactive site were already investigated in more detail. Mutagenesis studies of alanine and glutamine variants of Glu_{483} strongly suggested a role as H-bond donor in the orientation of the carboxyl-group of LThDP, as well as in the proper orientation of phosphate for the nucleophilic attack on the HEThDP-radical, retaining activities between 5-20 %, ruling out a function as acid-base catalyst in the reaction (Meyer, 2008). Glutamine 122 seems to be of importance for binding and orientation of the substrate, as was evidenced by NMR-studies. These revealed a reduction of the rate for formation of LThDP by down to 2 %, impacting all subsequent steps of catalysis (Böhme, 2007).

1.3 Motivation

The ThDP-dependent enzymes are a broad and well studied family of enzymes. However, there are still questions unanswered that surfaced when the first structures of a ThDP-dependent enzyme, the transketolase of *Saccharomyces cerevisae*, was solved, and more appeared in the years after.

Early structural investigation of *Saccharoymces cerevisae* transketolase (*Sc*TK) showed the presence of an acidic network between the two active sites of a TK dimer (Nikkola *et al.*, 1994). Initial studies on this network revealed importance in cofactor binding and dimerization (Meshalkina *et al.*, 1997). A similar network was examined in the E1 subunit of the pyruvate dehydrogenase complex, where mutagenesis of the constituents resulted in significant reductions of activity (Frank *et al.*, 2004; Nemeria *et al.*, 2010). This work aimed to further investigate the importance of this channel with regards to active site communication and modulation of ThDP reactivity.

ThDP-dependent enzymes show a flanking of the activating glutamate by a water molecule in hydrogen bond distance. *Ec*TK offers the relatively unique option to displace this water by mutagenesis of a coordinating amino acid. Therefore, elucidation of the importance of the conserved water in ThDP- dependent enzymes using the example of *Ec*TK was a further aim of this thesis.

A unique feature of *Ec*TK is the presence of two distinct conformations of ThDP (Lüdtke, 2012). It was assumed that the distribution of the two conformations is controlled by protonation of the phosphate anchor, and that it is important for separation of the reactants during catalysis. One goal of this thesis was to put this assumption to trial, and to elucidate the factors involved.

Further, this thesis aimed to elucidate the mechanism by which the nature of the first, virtually universal intermediate in ThDP-dependent catalysis is controlled, after the canonical character of the Breslow intermediate as carbanion/enamine was questioned by preceding works (Cavazza *et al.*, 2006; Meyer *et al.*, 2012). As examples *Lp*POX and *Ec*TK were chosen, as they have opposed requirements of the intermediate in regards to the character of their acceptor molecules.

It was further aspired to understand the mechanism of the antivitamin 2'-methoxythiamine diphosphate, the only naturally occurring ThDP analogue (Reddick *et al.*, 2001). Preceding studies delivered a wealth of functional and mechanistic information regarding the targets of MeOThDP, but did not elucidate the direct mode of action by which inhibition is achieved (Nemeria *et al.*, 2016).

By pushing the crystallographic resolution of *Ec*TK structures in both the resting state and with substrates, it was aspired to gain more insights regarding mechanistic details of catalysis and substrate recognition.

2 Materials & Methods

2.1 Materials

2.1.1 Chemicals

Substance	Supplier
Acetic acid	Carl Roth GmbH & Co. KG (Karlsruhe, Germany)
Acrylamide	Carl Roth GmbH & Co. KG (Karlsruhe, Germany)
Agar	AppliChem GmbH (Darmstadt, Germany)
Agarose (Low EEO)	AppliChem GmbH (Darmstadt, Germany)
Ammonium chloride	Carl Roth GmbH & Co. KG (Karlsruhe, Germany)
Bovine serum albumin (BSA)	AppliChem GmbH (Darmstadt, Germany)
Bradford reagent, 5x	SERVA Electrophoresis GmbH (Heidelberg, Germany)
Bromphenol blue, sodium salt	AppliChem GmbH (Darmstadt, Germany)
Bovine serum albumin (BSA)	AppliChem GmbH (Darmstadt, Germany)
Calcium chloride, hexahydrate	Carl Roth GmbH & Co. KG (Karlsruhe, Germany)
Carbenicillin, disodium salt	AppliChem GmbH (Darmstadt, Germany)
Coomassie Brilliant Blue G250	AppliChem GmbH (Darmstadt, Germany)
2,6-dichlorophenolindophenol (DCPIP)	Merck KgaA (Darmstadt, Germany)
Dimethylsulfoxide (DMSO)	Sigma-Aldrich (Munich, Germany)
Dithioerythritol (DTE)	AppliChem GmbH (Darmstadt, Germany)
Ethanol (denatured)	Apotheke Frau Magerkuth (Göttingen, Germany)
Ethanol (purest)	Nordhäuser Spirituosen GmbH (Nordhausen, Germany)
Ethidium bromide	Carl Roth GmbH & Co. KG (Karlsruhe, Germany)
Ethylenediaminotetraacetic acid (EDTA)	AppliChem GmbH (Darmstadt, Germany)
Ethylene glycol	AppliChem GmbH (Darmstadt, Germany)
Flavin adenine dinucleotide disodium salt di-hydrate (FAD)	AppliChem GmbH (Darmstadt, Germany)
Flavin mononucleotide monosodium salt di-hydrate (FMN)	AppliChem GmbH (Darmstadt, Germany)
D-Fructose 6-phosphate, disodium salt hydrate	Sigma-Aldrich (Munich, Germany)
D-Glucose	AppliChem GmbH (Darmstadt, Germany)
Glycerol (anhydrous)	AppliChem GmbH (Darmstadt, Germany)
Glycine	Carl Roth GmbH & Co. KG (Karlsruhe, Germany)

Glycylglycine	AppliChem GmbH (Darmstadt, Germany)
Guanidinium chloride	AppliChem GmbH (Darmstadt, Germany)
Hydrochloric acid (37 %)	Carl Roth GmbH & Co. KG (Karlsruhe, Germany)
Imidazole	AppliChem GmbH (Darmstadt, Germany)
Kanamycin sulfate	AppliChem GmbH (Darmstadt, Germany)
D-Lactose	AppliChem GmbH (Darmstadt, Germany)
Magnesium chloride, hexahydrate	Carl Roth GmbH & Co. KG (Karlsruhe, Germany)
Magnesium sulfate, hydrate	Carl Roth GmbH & Co. KG (Karlsruhe, Germany)
Manganese(II) chloride, tetrahydrate	AppliChem GmbH (Darmstadt, Germany)
β-Mercaptoethanol	Carl Roth GmbH & Co. KG (Karlsruhe, Germany)
2′-methoxythiamine diphosphate (MeOThDP)	Prof. Tadhg Begley (Texas A&M University, USA)
Methylacetylphosphonate (MAP)	Synthesis facility MPI for Biophysical Chemistry (Göttingen, Germany)
Nicotinamide adenine dinucleotide (NADH)	AppliChem GmbH (Darmstadt, Germany)
Piperazine-N,N′-bis(2-ethanesulfonic acid) (PIPES)	AppliChem GmbH (Darmstadt, Germany)
Phenylmethanesulfonylfluoride (PMSF)	AppliChem GmbH (Darmstadt, Germany)
Phosphoric acid (85 %)	Carl Roth GmbH & Co. KG (Karlsruhe, Germany)
Polyethylene glycol (PEG) 6000	Carl Roth GmbH & Co. KG (Karlsruhe, Germany)
Potassium chloride	Carl Roth GmbH & Co. KG (Karlsruhe, Germany)
Potassium di-hydrogen phosphate anhydrous	AppliChem GmbH (Darmstadt, Germany)
D-Ribose 5-phosphate, disodium salt dihydrate	Sigma-Aldrich (Munich, Germany)
Sodium chloride	AppliChem GmbH (Darmstadt, Germany)
Sodium dodecyl sulfate (SDS)	AppliChem GmbH (Darmstadt, Germany)
di-Sodium hydrogen phosphate anhydrous	AppliChem GmbH (Darmstadt, Germany)
Sodium hydroxide	AppliChem GmbH (Darmstadt, Germany)
N,N,N',N'-Tetramethylethylenediamine (TEMED)	Carl Roth GmbH & Co. KG (Karlsruhe, Germany)
Thiamine hydrochloride	AppliChem GmbH (Darmstadt, Germany)
Thiamine diphosphate	Sigma-Aldrich (Munich, Germany)
2-Amino-2-hydroxymethyl-propane-1,3-diol (Tris)	AppliChem GmbH (Darmstadt, Germany)
Tryptone	Carl Roth GmbH & Co. KG (Karlsruhe, Germany)

D-Xylulose 5-phosphate, sodium salt	Sigma-Aldrich (Munich, Germany)
Yeast extract	Carl Roth GmbH & Co. KG (Karlsruhe, Germany)

2.1.2 Enzymes

Enzyme	**Supplier**
DNaseI (bovine pancreas)	AppliChem GmbH (Darmstadt, Germany)
*Dpn*I	Thermo Fisher Scientific (Braunschweig, Germany)
Glucose oxidase (*Aspergillus niger*)	Sigma-Aldrich (Munich, Germany)
α-Glycerophosphate dehydrogenase (rabbit muscle)	Sigma-Aldrich (Munich, Germany)
Lysozyme (chicken egg white)	AppliChem GmbH (Darmstadt, Germany)
Phusion polymerase	Thermo Fisher Scientific (Braunschweig, Germany)
Triosephosphate isomerase (rabbit muscle)	Sigma-Aldrich (Munich, Germany)

2.1.3 Primers

All primers were supplied by Sigma-Aldrich (Munich, Germany). In the case of mutagenesis primers, the targeted codon is bold, the mismatches red.

Mutagenesis Primers

Primer	**Sequence (5'-3')**
*Ec*TK$_{H66A}$ Fwd	CCAACGGC**GCG**GGCTCCATGC
*Ec*TK$_{H66A}$ Rev	GCATGGAGCC**CGC**GCCGTTGG
*Ec*TK$_{E160Q}$ Fwd	GCTGCATGATG**CAA**GGCATCTCCCACG
*Ec*TK$_{E160Q}$ Rev	CGTGGGAGATGCC**TTG**CATCATGCAGC
*Ec*TK$_{E160A}$ Fwd	GCTGCATGATG**GCG**GGCATCTCCCACG
*Ec*TK$_{E160A}$ Rev	CGTGGGAGATGCC**CGC**CATCATGCAGC
*Ec*TK$_{E165A}$ Fwd	GCATCTCCCAC**GCG**GTTTGCTCTCTGG
*Ec*TK$_{E165A}$ Rev	CCAGAGAGCAAAC**CGC**GTGGGAGATGC
*Ec*TK$_{E165Q}$ Fwd	GGAAGGCATCTCCCAC**CAA**GTTTGCTCTCTGG

*Ec*TK$_{E165Q}$ Rev	CCAGAGAGCAAAC**TTG**GTGGGAGATGCCTTCC
*Ec*TK$_{E165D}$ Fwd	GCATCTCCCAC**GAT**GTTTGCTCTCTGG
*Ec*TK$_{E165D}$ Rev	CCAGAGAGCAAAC**ATC**GTGGGAGATGC
*Ec*TK$_{E165N}$ Fwd	GCATCTCCCAC**AAC**GTTTGCTCTCTGG
*Ec*TK$_{E165N}$ Rev	CCAGAGAGCAAAC**GTT**GTGGGAGATGC
*Ec*TK$_{H261N}$ Fwd	CACGACTCC**AAC**GGTGCGCCGCTG
*Ec*TK$_{H261N}$ Rev	CAGCGGCGCACC**GTT**GGAGTCGTG
*Ec*TK$_{T433Q}$ Fwd	CTGCCGTACACCTCC**CAG**TTCCTGATG
*Ec*TK$_{T433Q}$ Rev	CATCAGGAA**CTG**GGAGGTGTACGGCAG
*Ec*TK$_{T433V}$ Fwd	CTGCCGTACACCTCC**GTG**TTCCTGATG
*Ec*TK$_{T433V}$ Rev	CATCAGGAA**CAC**GGAGGTGTACGGCAG
*Lp*POX$_{Q122H}$ Fwd	GGATACGTTC**CAC**GAAATGAATGAGAATCC
*Lp*POX$_{Q122H}$ Rev	GGATTCTCATTCATTTC**GTG**GAACGTATCC
*Lp*POX$_{E483I}$ Fwd	GGATTTATCAAAGAT**ATC**CAGGAAGATACTAATCAG
*Lp*POX$_{E483I}$ Rev	CTGATTAGTATCTTCCTG**GAT**ATCTTTGATAAATCC

Sequencing primers

Primer	**Sequence (5'-3')**
*Ec*TK Fwd 651	TCATGACGCGGCATCTATCAAA
*Ec*TK Rev 851	TGAGCATAGATTTCAGACGGGATTT
*Ec*TK Fwd 1301	TTCGTGGAATACGCACGTAA
*Lp*POX Fwd 501	TCCAGTCGATTTACCATGGCAA
*Lp*POX Rev 701	TACTCATTAATGGAATTTTCAACGTTTTAC
*Lp*POX Fwd 1201	GAATCGACATTTGAAATTAACGC

2.1.4 Strains

Strain name	Supplier
E. coli BL21Star™	Thermo Fisher Scientific (Braunschweig, Germany)
E. coli C600	Agilent Technologies Deutschland GmbH, Waldbronn
E. coli DH5α™	Thermo Fisher Scientific (Braunschweig, Germany)
E. coli XL1-Blue	Agilent Technologies Deutschland GmbH, Waldbronn

2.1.5 Kits and Solutions

Item	Supplier
DNA Gel Loading Dye (6x)	Thermo Fisher Scientific (Braunschweig, Germany)
dNTP mix (10 mM each)	Thermo Fisher Scientific (Braunschweig, Germany)
GC-buffer	Thermo Fisher Scientific (Braunschweig, Germany)
Gel Filtration LMW Calibration Kit	GE Healthcare Europe (Munich, Germany)
Gel Filtration Standard	Bio-Rad Laboratories GmbH (Munich, Germany)
HF-buffer	Thermo Fisher Scientific (Braunschweig, Germany)
NucleoSpin™ Plasmid Kit	Macherey-Nagel (Düren, Germany)
NucleoSpin™ Gel&PCR Clean-Up Kit	Macherey-Nagel (Düren, Germany)
Pierce™ Unstained Protein MW Marker	Thermo Fisher Scientific (Braunschweig, Germany)

2.1.6 Commodities

Material	Supplier
ActiLoops™ (0.1 - 0.4 mm)	Molecular Dimensions (Suffolk, UK)
Cover plates, 18 mm (siliconized)	Jena Bioscience GmbH, (Jena, Germany)
Cryoloops (0.05 - 0.5 mm)	Hampton Research Corp, (CA, USA)
Crystallization plates, greased	Hampton Research Corp, (CA, USA)
Spin-X UF® 6&20 (5 kDa - 50 kDa)	Corning GmbH (Berlin, Germany)
ZelluTrans/Roth®, 3.5 kDa	Carl Roth GmbH & Co. KG (Karlsruhe, Germany)

2.1.7 Devices

Cell disruption

Item	Supplier
M-110S Microfluidizer	Microfluidics (Newton, MA, USA)
Sonoplus GM 70	Bandelin GmbH & Co. KG (Berlin, Germany)

Fast protein liquid chromatography

Item	Supplier
ÄKTAprime plus	GE Healthcare Europe (Munich, Germany)
ÄKTApurifier	GE Healthcare Europe (Munich, Germany)
HiLoad™ 26/10 Q-Sepharose™ HP	GE Healthcare Europe (Munich, Germany)
HiPrep™ 26/10 desalting	GE Healthcare Europe (Munich, Germany)
HisPrep™ FF 5 mL	GE Healthcare Europe (Munich, Germany)
Superdex™ 200 HiLoad™ 16/60	GE Healthcare Europe (Munich, Germany)
Superloop (50 mL, 150 mL)	GE Healthcare Europe (Munich, Germany)

Centrifuges and rotors

Item	Supplier
Avanti™ JXN-26	Beckmann Coulter GmbH (Krefeld, Germany)
Avanti™ J-20XPI	Beckmann Coulter GmbH (Krefeld, Germany)
Avanti™ HP-30I	Beckmann Coulter GmbH (Krefeld, Germany)
Rotor JLA-8.1000	Beckmann Coulter GmbH (Krefeld, Germany)
Rotor JA-10	Beckmann Coulter GmbH (Krefeld, Germany)
Rotor JA-25.50 Ti	Beckmann Coulter GmbH (Krefeld, Germany)
Rotor JA-30.50 Ti	Beckmann Coulter GmbH (Krefeld, Germany)
Rotor JLA-8.1000	Beckmann Coulter GmbH (Krefeld, Germany)
Centrifuge tubes	Beckmann Coulter GmbH (Krefeld, Germany)
Eppendorf 5810R	Eppendorf AG (Wesseling-Berzdorf, Germany)
Rotor A-4-81	Eppendorf AG (Wesseling-Berzdorf, Germany)
Mikro 200	Hettich GmbH & Co. KG (Tuttlingen, Germany)
Rotor 2424 B	Hettich GmbH & Co. KG (Tuttlingen, Germany)
Universal 320R	Hettich GmbH & Co. KG (Tuttlingen, Germany)
Rotor 1420 A/B	Hettich GmbH & Co. KG (Tuttlingen, Germany)
Rotor 1617 A	Hettich GmbH & Co. KG (Tuttlingen, Germany)
Rotor 1620 A	Hettich GmbH & Co. KG (Tuttlingen, Germany)

Spectroscopy

Item	Supplier
Chirascan plus CD spectrometer	Applied Photophysics Ltd., UK
Fluoromax 4 spectrofluorometer	HORIBA Europe GmbH, Oberursel
NanoDrop 2000	Thermo Scientific, USA
AV401 NMR spectrometer	Bruker, USA
Stopped-flow system SX.20	Applied Photophysics Ltd., UK
UV-vis spectrometer, V-650	Jasco GmbH, (Groß-Umstade, Germany)
UV-vis spectrometer, V-630	Jasco GmbH, (Groß-Umstade, Germany)
Suprasil precision cuvettes QS	Hellma GmbH & Co.KG (Mühlheim, Germany)

X-ray data collection

Item	Supplier
MicroMax™-007 rotating anode X-ray generator	Rigaku Corp., (MI, USA)
X-stream™ 2000 Cryogenic Crystal Cooler	Rigaku Corp., (MI, USA)
Mar 345dtb image plate	marXperts GmbH (Norderstedt, Germany)
MicroMax™-003 sealed tube X-ray generator	Rigaku Corp., (MI, USA)
800 Cryostream Cooler	Oxford Cryosystems (Oxford, UK)
PILATUS3 R 200K-A	DECTRIS Ltd. (Baden-Daetwill, CH)

Miscellaneous

Item	Supplier
Arium®pro VF	Sartorius AG (Göttingen, Germany)
Thermocycler TProfessional	Biometra (Göttingen, Germany)
miniDAWN TREOS™ Light Scattering Instrument	Wyatt Technology Corporation (Santa Barbara, USA)
Optilab T-rEX Refractive Index Detector	Wyatt Technology Corporation (Santa Barbara, USA)
pH-electrode Minitrode	Hamilton Bonaduz AG (Bonaduz, Switzerland)
pH-electrode InLab® Easy DIN	Mettler-Toledo GmbH (Giessen, Germany)

2.2 Methods

2.2.1 Molecular Biology

The gene encoding *Escherichia coli* transketolase in the pGSJ427 vector was initially provided by Prof. Dr. Georg Sprenger (Institute of Microbiology, University of Stuttgart). In this construct, a C-terminal His_6-tag is fused to the protein. The gene itself is under control of its native promoter which is constitutively active and independent of external induction for protein expression. As resistance marker, the gene encoding for β-lactamase is present (Sprenger *et al.*, 1995, Asztalos, 2008). *Lp*POX is encoded on the plasmid pBP200, containing an ampicillin resistance marker under control of a *lac*-operon regulated *tac*-promoter. The plasmid was initially provided by Prof. Dr. Rainer Rudolph, University of Halle.

2.2.1.1 Polymerase Chain Reaction (PCR)

Mutants were generated by site-directed mutagenesis PCR. Desired bases were exchanged by using partially mismatching oligonucleotides, according to a QuikChange-protocol adapted to *Phusion* DNA-polymerase. The PCR conditions were adjusted to the requirements of the respective primers. All used primers are listed in table 2, section 2.1.3. To remove all remaining template DNA with the unmodified sequence, 5 units of DpnI were added after PCR and the mix was incubated for $\sim$16 hours.

2.2.1.2 Agarose Gel Electrophoresis

Horizontal agarose gel electrophoresis was performed using 1% agarose gels, with 1x TAE buffer (40 mM Tris, 20 mM acetate, 1 mM EDTA, pH 8.5). Samples were prepared by mixing with 6x DNA loading dye. Visualization of DNA molecules was achieved by incubation in a 2 $\mu g/ml$ ethidium bromide solution for 10 minutes and subsequent detection using UV-light in an image documentation system.

2.2.1.3 Preparation and Transformation of Chemocompetent Cells

Preparation of chemocompetent cells and transfection of plasmids into cells was performed as described previously (Inoue *et al.*, 1990). Minor adaptations were introduced, such as growing the cells at 37 °C instead of 18 °C, and plating the transformed cells directly after 1 hour of incubation without transferring them to melted agar.

2.2.1.4 Isolation of Plasmid DNA

The isolation of plasmid DNA from transformed *E. coli* cells was performed using a NucleoSpin™ Plasmid kit, following the manufacturers instructions.

2.2.1.5 Determination of DNA Concentrations

All DNA concentrations were determined using a NanoDrop2000 device, using an average extinction coefficient of $1\ A_{260} = \frac{50\ ng}{\mu L \cdot cm}$.

2.2.1.6 DNA Sequencing

Sequencing of isolated plasmid DNA was performed by GATC Biotech, Konstanz. The samples were prepared according to their requirements. For sequencing, self-designed primers were employed, as listed in table 3, section 2.1.3.

2.2.2 Protein Chemistry

2.2.2.1 Expression of *Ec*TK

A single 20 ml culture of LB medium (1 % ($^{w}/_{v}$) tryptone, 0.5 % ($^{w}/_{v}$) yeast extract, 0.5 % ($^{w}/_{v}$) NaCl) was inoculated with multiple colonies of E. coli BL21 Star™(DE3) carrying the respective *Ec*TK variant. After 16 h of growth at 37 °C, this culture was used to inoculate a 250 ml culture, which was grown for 10 h at 37 °C. 500 ml main cultures were then inoculated to an OD_{600} of 0.1 using this culture, after spinning down and resuspension in fresh medium to remove possible β-lactamase secretions. Furthermore, the main cultures were supplemented with 50 µg/ml thiamine hydrochloride

and 100 µg/ml carbenicillin. After 16 h at 37 °C and 200-220 RPM, for baffled/non-baffled flasks respectively, the cells were harvested by centrifugation at 5769 x g for 20 minutes at 4 °C. The pellets were shock-frozen using liquid nitrogen and stored at -20 °C till usage.

2.2.2.2 Purification of *Ec*TK

For purification, cell pellets were resuspended in buffer A (20 mM Tris, 20 mM imidazole, 300 mM NaCl, pH 8.0) with addition of 1 mM DTE, 200 µM PMSF, 1 mM $MgSO_4$, 10 µg/ml lysozyme and 5 µg/ml DNase I using 3 ml per gram of pellet. Disruption was performed after complete resuspension of the pellet by stirring at 4 °C, using three to four cycles at a Microfluidizer (450 kilopascal). Cell debris was removed by centrifugation (75,000 x g; 45 min; 6 °C). The supernatant was loaded onto a Ni-NTA column equilibrated with buffer A (20 mM Tris pH 8.0, 20 mM imidazole, 300 mM NaCl). After loading, the column was washed with 5 CV buffer A or till baseline was reached. Elution was performed using a gradient over 100 ml to 100% of buffer B (20 mM Tris, 200 mM imidazole, 300 mM NaCl, pH 8.0). After elution, the protein was left on ice in elution buffer overnight. For buffer exchange, the volume of the protein solution was decreased to $\leq$ 5 ml by ultrafiltration (Corning Spin-X UF, 50 kDa MWCO) and then loaded onto a HiPrep 26/10 desalting column equilibrated with the desired buffer, 50 mM GlyGly pH 7.9 for crystallization, pH 7.6 for all other assays.

2.2.2.3 Expression of *Lp*POX

*Lp*POX was expressed in *E. coli* C600, using the inducing ZYP-5052 auto-inducing medium composition according to Studier, 2005. The medium was supplemented with 37 µg/ml thiamine hydrochloride, 30 µg/ml flavin mononucleotide, 50 µg/ml carbenicillin and 50 µg/ml kanamycin. Main cultures were grown to an OD_{600} of approximately 0.7 at 37 °C, before reducing the temperature to 16 °C for up to 72 hours at 200 RPM in non-baffled flasks. Cells were harvested by centrifugation at 5769 x g for 20 minutes at 4 °C. The pellets were shock-frozen using liquid nitrogen, and stored at -20 °C till usage.

2.2.2.4 Purification of *Lp*POX

*Lp*POX was purified as untagged protein. The pellets were resuspended in buffer A (20 mM KH_2PO_4, 100 μM ThDP, 1 mM $MgSO_4$, pH 6.0), further supplemented with 200 μM PMSF, 1 mM $MgSO_4$, 10 μg/ml lysozyme, 5 μg/ml DNase I and 100 μM FAD, 3 ml per gram of cells. The cells were incubated at 4 °C under constant stirring till the solution became homogeneous and smooth. Lysis was performed using a microfluidizer at 450 kPa. Cell debris was separated by centrifugation (75.000 x g, 45 min, 6 °C). Purification was performed by initial fractional ammonium sulfate precipitation, in two steps to 23 % ($^w/_v$) and 35 % ($^w/_v$) , at 6 °C. After each step, centrifugation was performed to separate the soluble and insoluble fractions (75.000 x g, 20 min, 6 °C). After the first step, the supernatant was used further. After the second step, the pellet was gently resuspended in buffer A. To prepare the protein for subsequent anion-exchange chromatography, dialysis was performed. Two steps were performed, each with a ratio of buffer A to protein of 1:40, over night at 6 °C. The protein was then subjected to a HiLoad™ 26/10 Q-Sepharose. After loading and washing, the protein was eluted using a linear gradient of buffer B (500 mM KH_2PO_4, 100 μM ThDP, 1 mM $MgSO_4$, pH 6.0) over 3 column volumes. Further purification was performed using a Superdex™ 200 HiLoad™ 16/60 gel filtration column, in buffer C (200 mM KH_2PO_4, 100 μM ThDP, 1 mM $MgSO_4$, pH 6.0).

2.2.2.5 SDS-Polyacrylamide Gel Electrophoresis (SDS-PAGE)

To check the homogeneity of purified proteins, SDS-PAGE was performed. The gels consisted of a stacking gel (5% acrylamide (37.5:1), 125 mM Tris, 0.1% ($^w/_v$) SDS, pH 6.8) and a separating gel (12% acrylamide (37.5:1), 375 mM Tris, 0.1% ($^w/_v$) SDS, pH 8.0). Samples for SDS-PAGE were mixed with sample buffer (0.1 M Tris, 25% ($^v/_v$) glycerol, 2% ($^w/_v$) SDS, 0.02% ($^w/_v$) bromophenol blue, 2.5% β-mercaptoethanol, pH 6.8) and incubated for 5 minutes at 95°C. After loading, the gel was run at 1 mA/cm^2. The gel was stained (0.25% ($^w/_v$) Coomassie Brilliant Blue G250, 30% ($^v/_v$) ethanol, 6% ($^v/_v$) acetic acid) and afterwards non-protein bound dye was removed by washing

with destaining solution (30% ($^{v}/_{v}$) ethanol, 10% ($^{v}/_{v}$) acetic acid).

2.2.2.6 Determination of Protein Concentrations

All *Ec*TK concentrations were determined using an extinction coefficient ε_{280} of 94.770 $M^{-1}cm^{-1}$ (ProtParam). The concentrations of holo-*Lp*POX were determined using the FAD signal at 407 nm of 11.600 $M^{-1}cm^{-1}$ (Tittmann *et al.*, 2000). Protein concentrations of samples with cofactors or of unknown homogeneity were determined using an assay based on the Bradford method (Bradford, 1976). Fresh calibrations were performed shortly before use, using commercially obtained Bradford reagent and bovine serum albumin.

2.2.2.7 Reconstitution of *Ec*TK with Cofactors

The concentrations of the cofactors ThDP and MeOThDP were determined according to the extinction coefficients given in table 1. Before each measurement requiring active *Ec*TK, the enzyme was reconstituted by adding the respective cofactor and $CaCl_2$ as required and incubating for at least 20 minutes on ice. Unless stated otherwise, all reconstitutions were performed with 300 µM cofactor and 2.5 mM $CaCl_2$.

Table 1. Extinction coefficients for ThDP and MeOThDP

Cofactor	ε [$M^{-1}cm^{-1}$]	Citation
ThDP	$\varepsilon_{273.5}$ = 7,757	(Schellenberger and Hübner, 1966)
MeOThDP	ε_{267} = 11,300	(Koppel *et al.*, 1962)

2.2.3 Biophysical Methods

2.2.3.1 Kinetic steady-State Assays

2.2.3.1.1 *Escherichia coli* transketolase

Characterization of the transketolase-catalyzed native reaction, the formation of glyceraldehyde 3-phosphate (Ga3P) and sedoheptulose 7-phosphate (S7P) from xylulose 5-phosphate (X5P) and ribose 5-phosphate (R5P) was performed using a coupled assay. It links the formation of Ga3P to the consumption of NADH (ε_{340} = 6220 $M^{-1}cm^{-1}$) via the two auxiliary enzymes triosephosphate isomerase (TIM) and α-glycerophosphate dehydrogenase from rabbit muscle (GDH). TIM converts Ga3P to dihydroxyacetone phosphate (DHAP), which is in turn irreversibly reduced by GDH to glycerol 3-phosphate (G3P), oxidizing one molecule of NADH to NAD+ in the process (Smeets *et al.*, 1971; Tsolas and Joris, 1975; Kochetov, 1982). For a typical measurement series, 0.005 mg/ml ($\sim$ 68 nM) EcTK, 250 μM NADH, $\sim$ 4.55 U GDH, $\sim$ 45.5 U TIM, 300 μM ThDP, 2.5 mM $CaCl_2$, 5 mM R5P and 0.02 – 6 mM X5P were mixed in 50 mM GlyGly, pH 7.6. The measurement was performed at 25 °C, 340 nm. Due to the fact that the commercially obtained X5P contained slight Ga3P impurities, the reaction mix was incubated for 1-2 minutes before adding EcTK. The auxiliary enzymes, stored in 4.8 M ammonium sulfate were dialyzed two times against 1 L of 50 mM GlyGly, pH 7.6, for at least 16 hours in total. Using the initial rate of NADH oxidation, the turnover per second was calculated for each substrate concentrations. To obtain the maximum rate and the

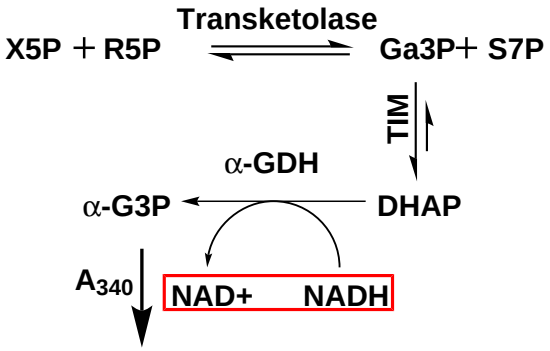

Figure 11. Schematic depiction of the coupled steady state assay. Transketolase interconverts X5P and R5P to S7P and Ga3P. Ga3P is transformed to DHAP by TIM, which is reduced to α-glycerophosphate by GDH.

Michaelis constant, these were fitted according to equation 1, where k_{cat} represents the maximal turnover number, K_M the Michaelis constant, [S] the substrate concentration and k_{app} the turnover number at the respective substrate concentration.

$$k_{app} = \frac{k_{cat} \cdot [S]}{K_M + [S]} \quad (1)$$

To determine the apparent K_D values for ThDP in different variants or for different cofactors, this assay was performed at a fixed concentration of substrates, and the enzyme incubated at varying cofactor concentrations before being added to the reaction. Classic hyperbolic plots were fitted according to equation 1, plots showing a tight-binding phase where $K_D \leq$ [Enzyme] were fitted according to a mixed quadratic-hyperbolic function.

$$v_{app} = \left(\frac{V_{max}^{tight}}{2[E_0]} \cdot [([S_0] + [E_0] + K_D^{tight}) - \sqrt{([S_0] + [E_0] + K_D^{tight})^2 - 4[S_0] \cdot [E_0]} \right) + \left(\frac{V_{max}^{loose} \cdot [S_0]}{K_D^{loose} + [S_0]} \right) \quad (2)$$

E_0 represents employed enzyme concentration and S_0 the employed cofactor concentration, V_{max} and K_D are named according to the phase (adapted from Steinmetz *et al.*, 2010).

2.2.3.1.2 *Lactobacillus plantarum* pyruvate oxidase

Steady-state kinetics of *Lp*POX were measured using an assay coupling electron transfer in the course of catalysis to reduction of the artificial electron acceptor 2,6-dichlorphenolindophenol (DCPIP), with an ε_{600} of 17.700 $M^{-1}cm^{-1}$ in the oxidized state (Tittmann *et al.*, 1998). Each turnover event results in reduction of one molecule of DCPIP, turning it non-absorbing at 600 nm. A standard assay mix consisted of 0.1 - 100 mM pyruvate, 100 µM DCPIP and 5 µg/ml-20 µg/ml of *Lp*POX in 20 mM KH_2PO_4, 100 µM ThDP, 1 mM $MgSO_4$, pH 6.0. Both substrates were preincubated before addition of *Lp*POX to allow the background reactions of DCPIP to take place. The measurements were started by addition of *Lp*POX, at 25 °C and 600 nm. The linear initial phase was used for rate determination, and the plot was fitted according to equation 1, or in the

case of apparent substrate excess inhibition by pyruvate according to the following equation, where k_{cat} describes the maximum turnover number per second, K_M the Michaelis-constant, K_I the inhibitory constant and [S] the initial substrate concentration.

$$k_{app} = \frac{k_{cat}}{1 + \frac{K_M}{[S]} + \frac{[S]}{K_I}} \tag{3}$$

2.2.3.2 Stopped-Flow Spectroscopy

As observing fast kinetics with common methods is impossible, stopped-flow spectroscopy was employed. Using a SX20 stopped-flow spectrometer paired with a photomultiplier or a photodiode array, processes occurring on a time-scale of milliseconds to seconds were resolved.

2.2.3.2.1 Single-Wavelength Kinetics

Escherichia coli transketolase

Transketolase displays two distinct intra-molecular charge transfer bands stemming from the interactions of the thiazolium and the aminopyrimidine moieties of ThDP. These were assigned to the 4′-aminopyrimidine (AP) and the 1′,4′-iminopyrimidine (IP) species, and thereby to increasing activation of the enzyme (depletion of AP) and formation of the tetrahedral sugar-ThDP adduct (increase of IP) (Fig. 12) (Kochetov and Usmanov, 1970; Lüdtke, 2012). Substrate binding, intermediate formation and cofactor binding were followed using a photomultiplier for fructose 6-phosphate, β-hydroxypyruvate (HPA) and thiamine diphosphate. All measurements except for ThDP-binding were performed in 50 mM GlyGly, 300 μM ThDP, 2.5 mM $CaCl_2$, pH 7.6. For the ThDP binding measurements, the buffer did not contain any ThDP. The respective concentration ranges, observed wavelengths and temperatures are given in table 2. Fitting of the raw data was performed according to a single- (Eq. 4) or double-exponential (Eq. 5) equation:

$$A(t) = a_1 \cdot e^{-k_1^{obs} \cdot t} + y_0 \tag{4}$$

$$A(t) = a_1 \cdot e^{-k_1^{obs} \cdot t} + a_2 \cdot e^{-k_2^{obs} \cdot t} + y_0 \tag{5}$$

A(t) is the absorbance at the time t, *a* represents the amplitude of the respective phase,

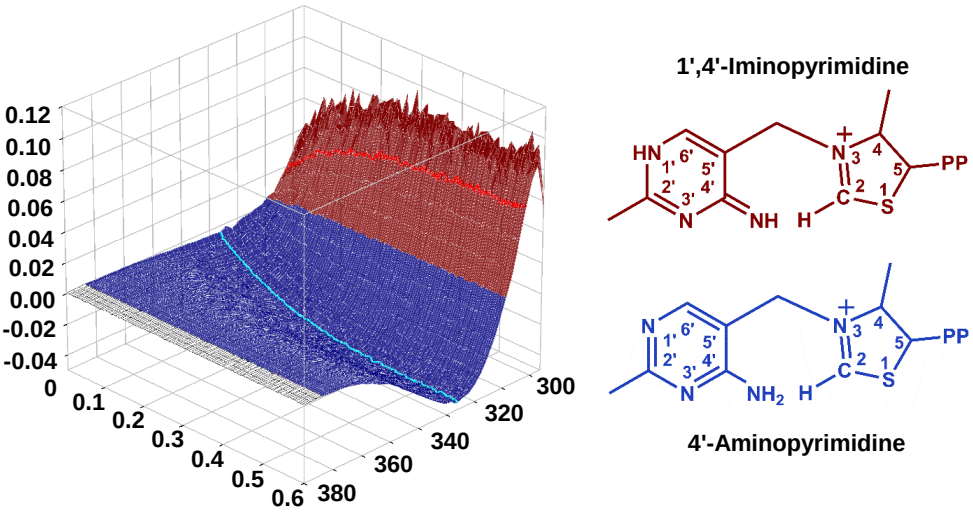

Figure 12. 3D difference plot of the *Ec*TK charge-transfer bands after substrate addition. The band displayed in blue corresponds to the AP species and the band displayed in red to the IP species. Exemplary trajectories for the AP species (cyan) and the IP species (red) are highlighted.

k^{obs} the rate constant and y_0 the y-offset.

Reactions displaying a first-order or pseudo-first order dependency were fitted according to a normal hyperbolic equation, where k_{max} describes the rate of intermediate formation, K_S the apparent dissociation constant of the respective intermediate and [S] the substrate concentration.

$$v = \frac{k_{max} \cdot [S]}{K_S + [S]} \tag{6}$$

Fitting of data following a sigmoidal dependency was performed using the Hill-equation, where n, the Hill-coefficient, denotes the theoretical number of cooperating partners, k_{max} the maximal reaction velocity, K_S the apparent dissociation constant and [S] the substrate concentration.

$$v = \frac{k_{max} \cdot [S]^n}{K_S^n + [S]^n} \tag{7}$$

Reversible reactions were fitted according to a modified hyperbolic equation, where k_{off} describes the *off*-rate of intermediate formation, k_{on} the *on*-rate of intermediate formation, K_S the apparent dissociation constant of the respective intermediate and [S] the substrate concentration.

$$v = k_{off} + \frac{k_{on} \cdot [S]}{K_S + [S]} \tag{8}$$

Lactobacillus plantarum pyruvate oxidase

In *Lp*POX, stopped-flow methods were used to follow reduction of the cofactor FAD under aerobic and anaerobic conditions, as well as binding of the substrate mimic methylacetylphosphonate (MAP). The intrinsic signal at 457 nm was used for tracking the reduction of FAD, the signal of the intermediate at 310 nm to study the binding of MAP (Tittmann *et al.*, 2000, Meyer, 2008). All measurements were performed at 25 °C. Pyruvate and MAP in concentration ranges of 0.1 - 100 mM and 1 - 40 mM were employed, with *Lp*POX concentrations of 1.5 mg/ml and 2.5 mg/ml, respectively.

To observe anaerobic reduction of FAD, molecular oxygen was removed from all components using glucose oxidase and glucose at final concentrations of 0.54 mg/ml and 4.7 mM, respectively. After 5 minutes, nearly complete removal of molecular oxygen was observed.

Table 2. Parameters used for stopped-flow single-wavelengths measurements of *Ec*TK and *Lp*POX.

Substrate	Wavelength [nm]	Concentration [mM]	Temp. [°C]
F6P	305	0.05 - 10	4
	325	0.05 - 10	4
HPA	400	0.1 - 2.5	25
ThDP	325	0.03 - 25	25
Pyruvate	457	0.1 - 100	25
MAP	310	1 - 40	25

2.2.3.2.2 Spectra of *Escherichia coli* transketolase

Spectra of holoenzyme and substrates F6P or HPA were obtained by using a photodiode array. Final concentrations of 3 mg/ml EcTK and 0 – 5 mM F6P or were employed. All measurements were performed in 50 mM GlyGly, 300 µM ThDP, and 2.5 mM $CaCl_2$, pH 7.9, at 25 °C. After shooting, the mixture was incubated for 5 – 100 seconds, and spectra were recorded for 10 seconds with 2 spectra per second. These spectra were averaged. Three measurements were performed for each concentration.

2.2.3.3 Circular Dichroism Spectroscopy

Circular dichroism spectroscopy was used to investigate the binding of ThDP to the apo-transketolase, the formation of the characteristic charge-transfer bands, as well as to gauge the binding of phosphate to *Lp*POX.

2.2.3.3.1 Cofactor Binding

The capability of binding the cofactor in *Ec*TK was verified by incubating 1.2 mg/ml of transketolase in 50 mM GlyGly, 300 µM ThDP, 2.5 mM $CaCl_2$, pH 7.6. After incubation for 20 minutes, a spectrum was recorded from 290 - 400 nm, at 20 °C. Successful recombination was indicated by formation of the characteristic charge-transfer bands around 300 nm for the iminopyrimidine form and 325 nm for the aminopyrimidine form (Kochetov and Usmanov, 1970; Heinrich *et al.*, 1971; Nemeria *et al.*, 2009).

2.2.3.3.2 ThDP Titration

For the ThDP titration, 1.2 mg/ml of transketolase in 50 mM GlyGly, 2.5 mM $CaCl_2$, pH 7.6 was titrated with increasing concentrations of ThDP. After addition of ThDP, the mix was incubated for 20 minutes. For each concentration, 5 - 10 spectra were collected from 250 to 400 nm, with a step size of 0.5 nm and an accumulation time of 0.3 seconds. These were then averaged, and corrected for the background stemming from buffer and ThDP.

2.2.3.3.3 pH Titration

The dependence of charge-transfer band formation on the pH was investigated by a pH titration (Lüdtke *et al.*, 2013). This titration was performed in a two-component buffer system consisting of 20 mM MES and 20 mM GlyGly. The measurement was performed in a 101-QS cuvette. The pH was adjusted inside the cuvette using a Minitrode pH electrode, by addition of 1 M Tris base. For each pH, 6 spectra were measured from 250 to 400 nm, with a step size of 0.5 nm and a accumulation time of 0.3 seconds.

These were corrected for the increase in volume, as well as for buffer background, and averaged. All measurements were performed at a protein concentration of 1.2 mg/ml, at 20 °C. Fitting of the obtained $\log_{10}(|\text{mdeg}_{324\text{-}326}|)$ vs pH was performed according to equation 9.

$$\Theta = \Theta_{max} - log(1 + 10^{(pK_a - x)}) \tag{9}$$

2.2.3.3.4 Phosphate Titration

To determine the binding affinity of potassium phosphate to *Lp*POX, the enzyme was transferred to 25 mM MES, 50 µM ThDP, 0.5 mM $MgSO_4$, pH 6.0. Successive spectra of 4.5 mg/ml *Lp*POX from 295 - 550 nm were recorded at 25 °C while stepwise increasing the phosphate concentration. The averages of three measurements for the AP-form at 333 nm and the the IP-form at 300 nm were plotted and fitted according to the following equation, where K_D describes the dissociation constant of phosphate, y_0 the y-offset and [S] the phosphate concentration.

$$\text{CD} = y_0 + \frac{\text{CD}_{max} \cdot [S]}{K_D + [S]} \tag{10}$$

2.2.3.4 Fluorescence Spectroscopy

2.2.3.4.1 Cofactor Titration

To obtain the nanomolar dissociation constants of ThDP and MeOThDP, fluorescence spectrometry was performed. All experiments were performed in a 3.5 ml 101-QS cuvette. The measurements were done at a concentration of EcTK of 0.1 µM, in 50 mM GlyGly, 3 mM $CaCl_2$, pH 7.6. The respective cofactor was titrated stepwise. For reconstitution, the mix was left to incubate for 20 minutes on ice and subsequently 5 minutes in the device for temperature adjustment. The samples were excited at 295 nm (3 nm slit width), and spectra were recorded from 310-450 nm (5 nm slit width), at an integration time of 0.1 s using a Horiba FluoroMax-4, under constant stirring at 25 °C.

In addition, a titration with buffer instead of cofactor was performed to account for the inner filter effect and dynamic quenching (Asztalos, 2008). For MeOThDP, the cofactor was also titrated to buffer to account for excimer formation.

The recorded spectra were corrected for the Raman peak, and the relative quenching at 340 nm calculated. The rel. quenching of the cofactor titration was corrected by the rel. quenching observed in the buffer titration, and in the case of MeOThDP for the excimer fluorescence. The obtained data was fitted according to a double hyperbolic equation accounting for two-phasic binding, where Q_{max} represents the maximum relative quenching of the respective phase.

$$Q = \frac{Q^1_{max} \cdot [\text{Cofactor}]}{K^1_D + [\text{Cofactor}]} + \frac{Q^2_{max} \cdot [\text{Cofactor}]}{K^2_D + [\text{Cofactor}]} \tag{11}$$

2.2.3.5 Nuclear Magnetic Resonance Spectroscopy (NMR)

The determination of the H/D exchange rate at the reactive C2 of MeOThDP was performed as previously described, substituting ThDP with MeOThDP (Kern *et al.*, 1997, Tittmann *et al.*, 1998). The investigation of formation of possible covalent intermediates in *Ec*$TK_{MeOThDP}$ was performed as described previously, but with an incubation temperature of 20 °C (Tittmann *et al.*, 2003, Asztalos *et al.*, 2007). All measurements were performed using the AV401 NMR spectrometer of the Institute of Organic and Biomolecular Chemistry, Göttingen.

2.2.4 X-Ray Crystallography

2.2.4.1 Crystallization

Crystallization of *Ec*TK was performed using the hanging-drop vapor diffusion method, according to conditions previously described (Asztalos *et al.*, 2007). The apoenzyme, concentrated to 12 - 20 mg/ml, was reconstituted with 5-10 mM ThDP or 1 mM MeOThDP, 5 mM $CaCl_2$ in 50 mM GlyGly (pH 7.9) and incubated on ice for at least 20 minutes. The well solution consisted of 18-24 % ($^w/_v$) PEG 6000, 2 % ($^v/_v$) glycerol, in 50 mM GlyGly (pH 7.9), at a total volume of 500 µl per well. In each well, 2 drops were set up,

using 3 µl of protein solution mixed with 3 µl of well solution. The drops were mixed by pipetting. Plates were stored at 4-6 °C. To optimize crystal growth the plates were seeded by microseeding, after 24 hours of equilibration. For this purpose, pre-existing crystals were crushed in well solution using a fine needle, and distributed amongst the fresh drops by streak-seeding, using the same needle. Subsequently, the plates were stored and crystals grew over the course of 7-14 days. Cryoprotection was performed by incubating the crystals for 5-10 seconds in 20 % ($^{w}/_{v}$) PEG 6000, 30 % ($^{v}/_{v}$) ethylene glycol, 5 mM ThDP (1 mM MeOThDP), 10 mM $CaCl_2$, 50 mM GlyGly, pH 7.9.
Soaking of crystals with X5P or R5P was performed using cryoprotectant solution with 100 mM X5P or R5P, adjusted for pH, for varying amounts of time. Soaking with HPA was performed in 20 % ($^{w}/_{v}$) PEG 6000, 15 % ($^{v}/_{v}$) ethylene glycol, 5 mM ThDP, 10 mM $CaCl_2$, 50 mM GlyGly, pH 7.9, with 40 mM HPA.

2.2.4.2 Data collection

Prior to synchrotron data collection, crystals were tested for diffraction potential, mosaicity, twinning or ice rings. For this, the rotating anode of the department of Molecular Structural Biology, Göttingen was used (as described in Materials), using CuKα radiation, which corresponds to a wavelength of 1.54 Å. Datasets of adequately diffracting crystals were collected at the synchrotron facilities of the Deutsches Elektronen-Synchrotron (DESY) and the European Synchrotron Radiation Facility (ESRF). All collected datasets are listed in table 4, appendix.

2.2.4.3 Refinement

The obtained data sets were processed using the *XDS* program package (Kabsch, 2010). All subsequent refinement steps were performed using the *PHENIX* suite (Adams *et al.*, 2010), with constant quality control using the MolProbity server (Davis *et al.*, 2007, Chen *et al.*, 2010). The phase was determined by using the rigid body method in *PHENIX.REFINE*, employing a *Ec*TK_{WT} structure as model. For variants whose unit cell parameters diverged from those of the wild type, a wild type monomer was used

for molecular replacement, using *PHENIX.PHASER* (McCoy *et al.*, 2007). CIF files were generated using the *PRODRG* server (Schüttelkopf and van Aalten, 2004). RMSD values were calculated using *LSQMAN* (Kleywegt, 1996), atom counts and statistics were generated using *MOLEMAN2* (Kleywegt, 1997).

3 Results

3.1 Biochemical and Structural Analysis of *Ec*TK Glu_{160} and Glu_{165}

The very first crystal structures of *Saccharoymces cerevisae* transketolase revealed an acidic, solvent-inaccessible channel reaching from one monomer to the other monomer of a functional dimer (Nikkola *et al.*, 1994). This channel is also present in *Ec*TK, being formed by the following interaction partners, in sequence: αThDP-βE411-αE160-H_2O-βE165-2 H_2O-αE165-H_2O-βE160-αE411-βThDP, where α and β denote the different monomers. To elucidate the function of the channel as a whole, as well as of the highly conserved individual constituents, the following variants were created: E160Q, E160A, E165Q, and E165A. The substituent amino acids were chosen to disrupt potential proton transfers in glutamine variants and the hydrogen bond network in alanine variants.

Investigation of the thiamine binding capability by circular dichroism spectrometry revealed that both variants of glutamate 165 were incapable of binding thiamine, or at least of forming the characteristic charge transfer bands associated with ThDP binding in transketolase (Kochetov and Usmanov, 1970; Heinrich *et al.*, 1971). The variants of glutamate 160 retained this capability (Fig. 54, Appendix). Comparing the elution profile of *Ec*TK_{E165Q} to a protein standard and dimeric *Ec*TK_{WT} on a gel filtration column showed later elution of *Ec*TK_{E165Q} by approximately 6 minutes, close to the peak of conalbumin with a molecular weight of 75 kDa, hinting towards monomerization. This result was further supported by multi angle light scattering (MALS), which estimated a molecular weight of around 90 kDa for the constituents of the *Ec*TK_{E165Q}-peak. Additional variants, *Ec*TK_{E165D} and *Ec*TK_{E165N}, were generated for position 165. Of these two, *Ec*TK_{E165D} retained the ability to bind ThDP (Fig. 54, Appendix), and was subjected to further biochemical characterization.

In the steady-state assay (Fig. 13A), *Ec*TK_{E160Q} exhibited a k_{cat} of 67.4 ± 0.6 s^{-1} (127 % of *Ec*TK_{WT}), and a K_M of 0.73 ± 0.02 mM (2-fold increase), while the k_{cat} of *Ec*TK_{E160A} was 36.4 ± 0.3 s^{-1} (68 %), with a K_M of 0.26 ± 0.01 mM (1.4-fold decrease), compared to 53.01 ± 0.45 s^{-1} and 0.37 ± 0.01 mM for *Ec*TK_{WT}. The ThDP-binding

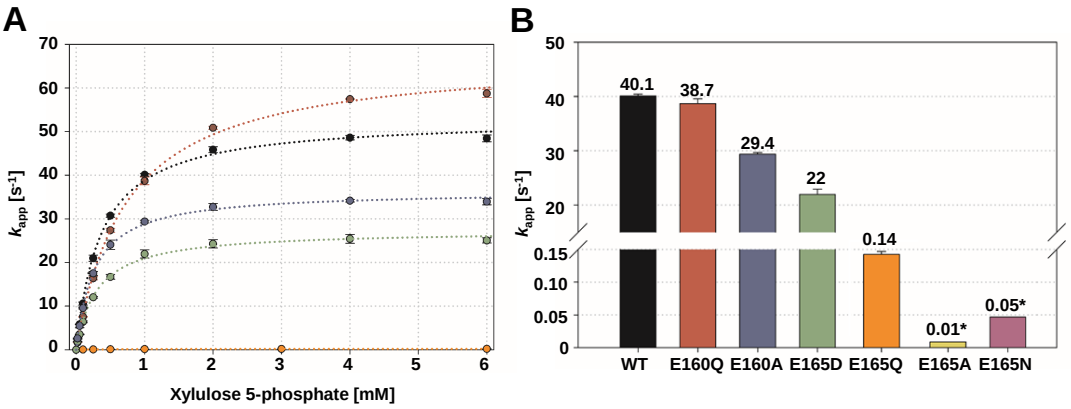

Variant	k_{cat} [s^{-1}]	K_M [mM]	$k_{app.}^{1\ mM}$ [s^{-1}]
*Ec*TK$_{WT}$	53.01 ± 0.45	0.37 ± 0.01	40.1
*Ec*TK$_{E160Q}$	67.4 ± 0.6	0.73 ± 0.02	38.7
*Ec*TK$_{E160A}$	36.4 ± 0.3	0.26 ± 0.01	29.4
*Ec*TK$_{E165D}$	27.3 ± 0.3	0.31 ± 0.01	22
*Ec*TK$_{E165Q}$	0.2 ± 0.0	0.47 ± 0.03	0.14
*Ec*TK$_{E165N}$	nd	nd	0.01
*Ec*TK$_{E165A}$	nd	nd	0.05

Figure 13. (A) Steady-state kinetics of *Ec*TK$_{WT}$ and variants of E160 and E165. *Ec*TK$_{WT}$ is shown in black, *Ec*TK$_{E160Q}$ in red, *Ec*TK$_{E160A}$ in blue, *Ec*TK$_{E165D}$ in green and *Ec*TK$_{E165Q}$ in orange. The assay was performed as described before (Section 2.2.3.1), all plots were fitted according to equation 1 (Section 2.2.3.1). **(B) Comparison of turnover rates at 1 mM X5P.** *Ec*TK$_{WT}$ is shown in black, *Ec*TK$_{E160Q}$ in red, *Ec*TK$_{E160A}$ in blue, *Ec*TK$_{E165D}$ in green, *Ec*TK$_{E165Q}$ in orange, *Ec*TK$_{E165N}$ in yellow and *Ec*TK$_{E165A}$ in purple. Values denoted with * were obtained by single measurement, values denoted with nd were not determined, the standard deviations of the respective fits are given $k_{app.}^{1\ mM}$ denotes the rate constant obtained at 1 mM X5P.

variant of glutamate 165, *Ec*TK$_{E165D}$ showed a k_{cat} of 27.3 ± 0.3 s^{-1} (51 %), with a K_M of 0.31 ± 0.01 mM (1.2-fold decrease). In addition, *Ec*TK$_{E165Q}$ was characterized, showing a minuscule k_{cat} of 0.2 ± 0.004 s^{-1} (>1 %), with a K_M of 0.47 ± 0.03 mM (1.3-fold increase). The reaction velocities of the variants *Ec*TK$_{E165A}$ and *Ec*TK$_{E165N}$ were recorded for comparison, at a concentration of 1 mM X5P. They exhibited activities of less than 0.1 percent of the wild type.

By correlating formation of the 4′-aminopyrimidine (AP)- and 1′,4′-iminopyrimidine (IP)-bands present in holo-*Ec*TK to pH using circular dichroism spectroscopy, it is possible to determine the pK_A of the aminopyrimidine N4', which is responsible for activation of C2

and in turn for formation of the intramolecular charge-transfer bands. With a decreasing pH of the solvent, the equilibrium of the three species of the aminopyrimidine moiety shifts from the signature-less, protonated 1′,4′-aminopyrimidinium species (APH^+) to the unprotonated and spectroscopically active IP and AP forms. To determine the impact of the respective mutations, pH-titrations were performed. The measurements were complicated by the fact that the pI value of *Ec*TK is around 5.6, which is, at least for the variants *Ec*TK_{E160A} and *Ec*TK_{E160Q} in the onset of AP-band formation. Furthermore the AP-band of *Ec*TK displays a blue-shift at increasing pH-values. Only small shifts of the apparent pK_A from 5.47 $\pm$ 0.01 for *Ec*TK_{WT} to 5.57 $\pm$ 0.01 in *Ec*TK_{E160Q}, 5.37 $\pm$ 0.02 in *Ec*TK_{E160A} and of 6.06 $\pm$ 0.03 in *Ec*TK_{E165D} were observed, as shown in figure 56 (Appendix).

Utilizing the absorbance of the AP-band at 325 nm correlated to holoenzyme formation, we investigated the kinetics of ThDP-binding for *Ec*TK_{WT}, *Ec*TK_{E160Q} and *Ec*TK_{E160A}, to verify whether the substitution close to the activating glutamate and the putative pK_A-shift observed have any impact. This measurement was performed using stopped-flow spectroscopy and revealed two exponential phases, the fast, first phase being the dominant one as judged by amplitude. Using the first phase to account for the majority of binding events, the apparent K_D for ThDP derived from AP-formation is more or less the same for the variants, 2.17 $\pm$ 0.1 mM for *Ec*TK_{E160Q} and 2.53 $\pm$ 0.1 mM for *Ec*TK_{E160A}, compared to a value of 2.46 $\pm$ 0.1 mM for the wild type. The velocity of band formation did not differ greatly between *Ec*TK_{WT} (3.89 $\pm$ 0.06 s^{-1}) and *Ec*TK_{E160A} (3.43 $\pm$ 0.05 s^{-1}), but in *Ec*TK_{E160Q} it is reduced to 1.8 $\pm$ 0.03 s^{-1}. Furthermore, all fits were sigmoid, with an n-value of 1.53 $\pm$ 0.06 for *Ec*TK_{WT}, 1.37 $\pm$ 0.07 for *Ec*TK_{E160Q} and 1.32 $\pm$ 0.04 for *Ec*TK_{E160A}.

The second phase saturates much faster in the variants, with an apparent K_S of 3.5 $\pm$ 0.4 mM in *Ec*TK_{WT}, 0.43 $\pm$ 0.04 mM in *Ec*TK_{E160Q} and 0.21 $\pm$ 0.02 in *Ec*TK_{E160A}. The apparent k_{max} are similar, being 0.11 s^{-1}.

Investigation of the depletion and formation of the charge-transfer bands as shown in figure 12 (Section 2.2.3.2) was performed to investigate the behavior of *Ec*TK_{WT},

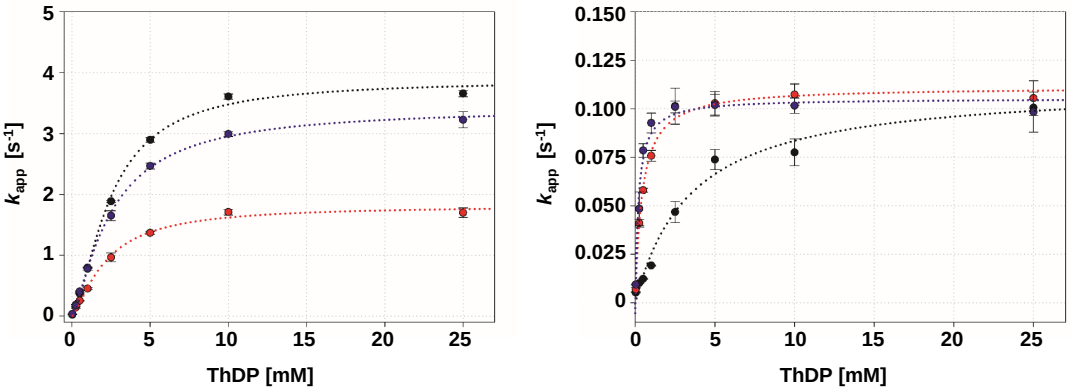

Variant	k_1^1 [s^{-1}]	$K^1_{S\,app.}$ [mM]	n	k_1^2 [s^{-1}]	$K^2_{S\,app.}$ [mM]
EcTK_{WT}	3.89 ± 0.06	2.46 ± 0.09	1.53 ± 0.06	0.11 ± 0.00	3.5 ± 0.4
EcTK_{E160A}	3.43 ± 0.05	2.53 ± 0.08	1.32 ± 0.04	0.11 ± 0.00	0.21 ± 0.02
EcTK_{E160Q}	1.82 ± 0.03	2.18 ± 0.11	1.37 ± 0.07	0.11 ± 0.00	0.43 ± 0.04

Figure 14. Microscopic kinetic constants of AP-band formation in *Ec*TK_{WT}, *Ec*TK_{E160Q} and *Ec*TK_{E160A}. The fast phase 1 is shown on the left, the slow phase 2 on the right. *Ec*TK_{WT} is shown in black, *Ec*TK_{E160Q} in red and *Ec*TK_{E160A} in blue. The data of phase 1 were fitted according to the Hill equation (Equation 7, Section 2.2.3.2.1), those of phase 2 to according to a hyperbolic equation 6 (Section 2.2.3.2.1).

EcTK_{E160Q} and *Ec*TK_{E160A} in the pre-steady state using stopped-flow spectroscopy. The formation of the tetrahedral complex was monitored by observing the IP-band at 304 nm. The AP-form depletion was monitored at 325 nm. This species is not directly required for catalysis, and thereby provides more catalytically active IP and APH^+ while depleting. As shown in figure 15, *Ec*TK_{WT} shows a faster depletion of the AP-band, with a rate of 503 ± 191.5 s^{-1} compared to 197.9 ± 59.3 s^{-1} for *Ec*TK_{E160Q} and 237.3 ± 58.9 s^{-1} for *Ec*TK_{E160A}. All plots show off-rates. These are 14.6 ± 6.4 s^{-1} for *Ec*TK_{WT}, 5.6 ± 2.4 s^{-1} for *Ec*TK_{E160Q} and 8.1 ± 2.6 s^{-1} for *Ec*TK_{E160A}. The apparent K_S values are not much different between variants, 6.1 ± 0.7 for *Ec*TK_{WT}, 7.3 ± 1.4 for *Ec*TK_{E160Q} and 4 ± 0.7 s^{-1} for *Ec*TK_{E160A}. However, as saturation could not be reached in the covered concentration range as the reaction became too fast to reliably fit after a certain point, the quality of the hyperbolic fits does not allow any definitive statements.

The formation of the tetrahedral intermediate could be followed to saturating conditions, giving an on-rate of 194.6 ± 3.5 s^{-1} for *Ec*TK_{WT}, 138.9 ± 3.3 s^{-1} for *Ec*TK_{E160Q} and 149.2 ± 3.3 s^{-1} for *Ec*TK_{E160A}. No off-rate was observed in *Ec*TK_{WT}, but in *Ec*TK_{E160Q} (3.3

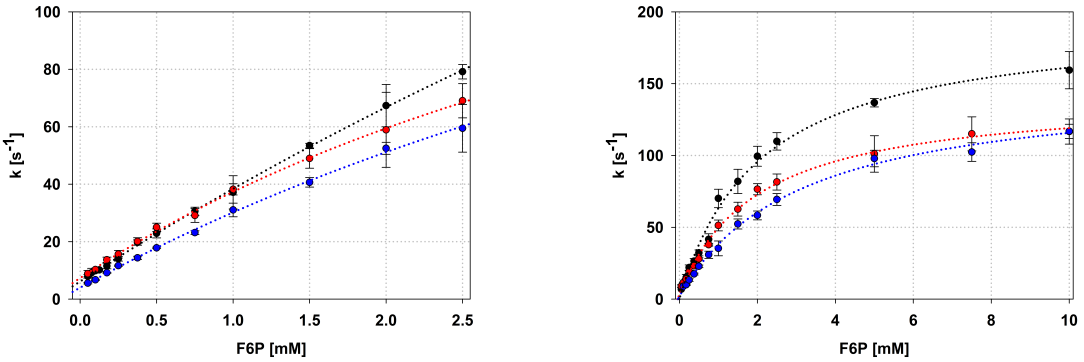

Variant	k_1^{AP} [s^{-1}]	k_{-1}^{AP} [s^{-1}]	$K_{s\,app.}^{AP}$ [mM]	k_1^{IP} [s^{-1}]	k_{-1}^{IP} [s^{-1}]	$K_{s\,app.}^{IP}$ [mM]
EcTK_{WT}	503 ± 191.5	14.6 ± 6.4	6.1 ± 0.7	194.6 ± 3.5	nd	2.1 ± 0.1
EcTK_{E160Q}	197.9 ± 59.3	5.6 ± 2.4	7.3 ± 1.4	138.9 ± 3.8	3.3 ± 2	2 ± 0.2
EcTK_{E160A}	237.3 ± 58.9	8.1 ± 2.6	4 ± 0.7	149.2 ± 3.3	1.8 ± 1.5	3.1 ± 0.2

Figure 15. Depletion of the AP-species (left) and formation of the IP-species (right). *Ec*TK_{WT} is shown in black, *Ec*TK_{E160Q} in red and *Ec*TK_{E160A} in blue. The data were fitted according to equation 8.

± 2 s^{-1}) and *Ec*TK_{E160A} (1.8 ± 1.5 s^{-1}). The apparent K_S value for formation of the intermediate was 2.1± 0.1 mM for *Ec*TK_{WT}, 2 ± 0.2 mM for *Ec*TK_{E160Q} and 3.1 ± 0.2 mM for *Ec*TK_{E160A}. Additionally, formation of the enamine-intermediate from the artificial donor substrate HPA was observed. The formation of this intermediate encompasses activation of the cofactor, attack on the donor-carbonyl of the substrate, protonation and formation of the tetrahedral β-hydroxylactyl-ThDP intermediate and decarboxylation. It is in a manner similar to the IP-band formation, but substrate cleavage is in this case virtually irreversible and allows to gauge the state of the proton relay formed by Glu_{160}, Glu_{411} and the AP-moiety. As shown in figure 58 (Appendix), neither variant saturates in the technically feasible concentration range, so the data were fitted according to the linear equation 12.

$$k_{app} = k_{off} + k_{on} \cdot [S] \tag{12}$$

Thus, it is only possible to determine $\frac{k_{on}}{K_S}$. This value was 5.5 ± 0.14 $s^{-1}mM^{-1}$ for *Ec*TK_{WT}, 5.1 ± 0.18 $s^{-1}mM^{-1}$ for *Ec*TK_{E160Q} and 1.3 ± 0.04 $s^{-1}mM^{-1}$ for *Ec*TK_{E160A}.

As prior results for *Ec*TK_{E160Q} were unusual, i.e. the increased k_{cat}, the behavior of this variant compared to the wild type was further investigated. The apparent K_M for ThDP under pseudo-physiological conditions was determined by performing steady-state as-

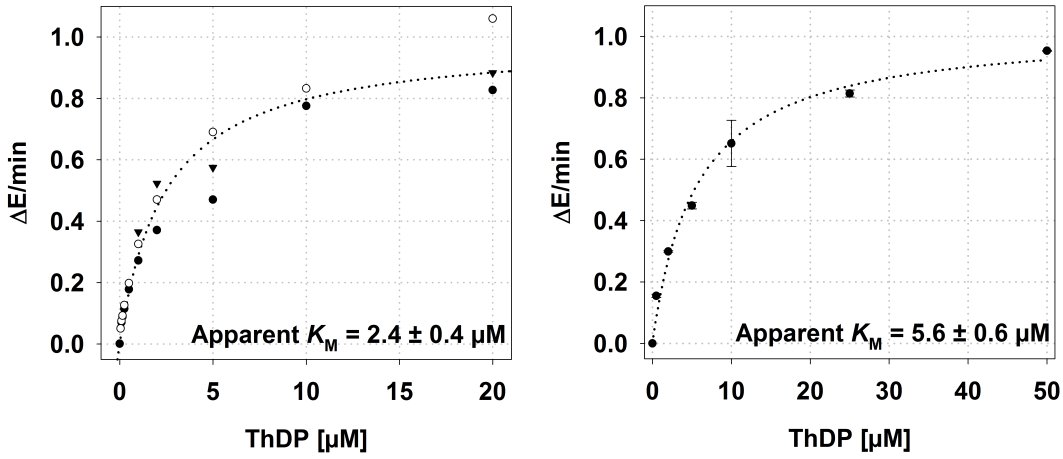

Figure 16. Plot of maximal velocities for *Ec*TK$_{WT}$ (left) and *Ec*TK$_{E160Q}$ (right) versus ThDP-concentration. As the scattering for *Ec*TK$_{WT}$ was relatively large, the data points are displayed as individual values. Fitting was performed according to equation 6.

says at a fixed concentration of X5P, with varying concentrations of ThDP. The apparent K_M values for ThDP calculated from the data were 2.4 $\pm$ 0.4 µM for *Ec*TK$_{WT}$ and 5.6 $\pm$ 0.6 µM for *Ec*TK$_{E160Q}$. As the reaction velocity increased over time at each ThDP concentration, the maximal velocities near the end of each measurement were chosen for plotting. A comparative dataset using a reduced amount of enzyme to obtain better initial velocities yielded an apparent K_M of 17.4 $\pm$ 2.1 µM for *Ec*TK$_{E160Q}$, corresponding to a threefold increase. Comparison of progress curves reveals a slower reconstitution of *Ec*TK$_{E160Q}$ under steady-state conditions. *Ec*TK$_{WT}$ reaches its maximum reaction velocity at a thiamine concentration of 0.5 µM after less than 1200 seconds, with a 3.4-fold increase from initial activity to maximal activity. For *Ec*TK$_{E160Q}$ the activity is still increasing after 1200 seconds, having already increased six-fold over initial activity, but still being slower than *Ec*TK$_{WT}$ (Fig. 59).

A crystallographic data set of *Ec*TK$_{E165Q}$ was obtained to a resolution of 2.156 Å (R_{work} = 20.9 %, R_{free} = 26.2 %). The unit cell diverged from the usually obtained unit cell parameters on the a-axis by approximately 6 Å. No density for the cofactor ThDP could be observed. Overlaying a monomer of *Ec*TK$_{E165Q}$ and *Ec*TK$_{WT}$ revealed a comparatively low divergence for the aligned monomer (RMSD 0.81 Å), but a clear

displacement of the interacting monomer in the functional dimer (overall RMSD 1.83 Å). Furthermore, two regions of each monomer were disordered in a manner that only allowed observation of partial or even no electron density, from residue 186 to 199 and residue 381 to 387. 2mFo-DFc density for Glu_{165} was only visible for the main chain at 1 σ, with some possible density for the side chain becoming visible at 0.7 σ. Based on the modeled orientation, the normal interaction partners of Glu_{165} are not in range. In *Ec*TK_{WT}, the carboxyl group interacts with the backbone nitrogen of Gly_{161} (second monomer) and Gly_{413} directly, but in *Ec*TK_{E165Q} these contacts cannot be formed (Fig. 17). The opposing loop containing Gly_{413} is very flexible (average atomic displacement parameter $(ADP)_{409\text{-}413}$ in *Ec*TK_{E165Q}: 60, 5 in *Ec*TK_{WT}), and the only possible interaction for Gln_{165} is the backbone oxygen of Val_{409}. In *Ec*TK_{E165Q}, the water interacting with Glu_{165} and Glu_{160} in *Ec*TK_{WT}, as well as Glu_{160} itself do not show any electron density and are therefore highly flexible or not present at all.

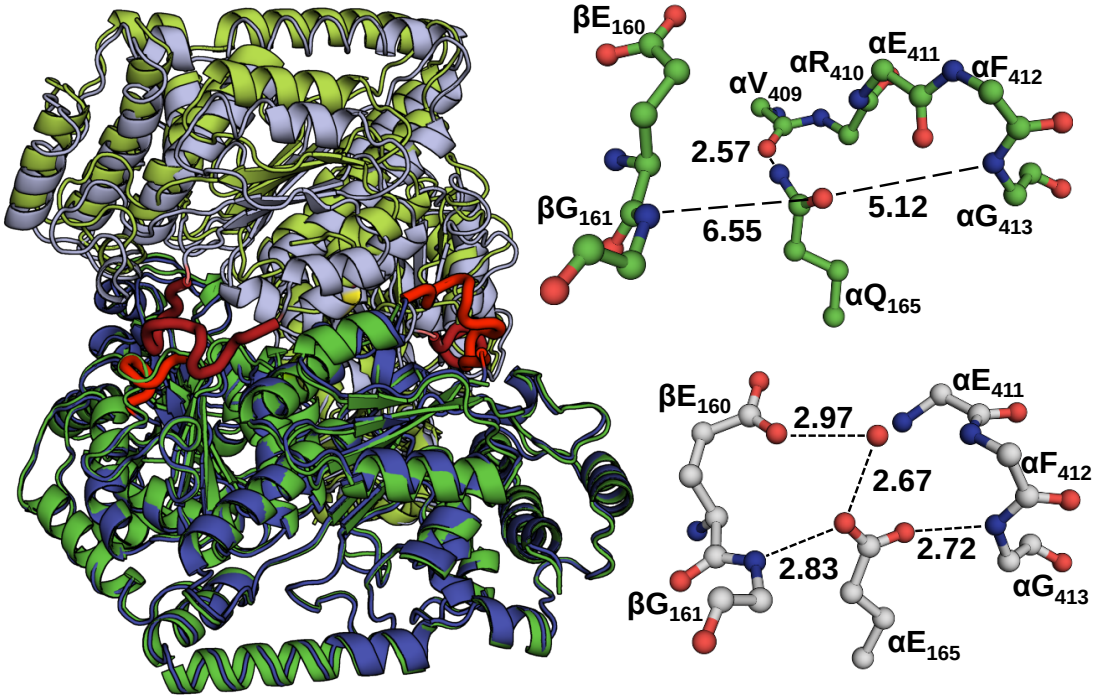

Figure 17. Overlay of the dimers of *Ec*TK_{WT} and *Ec*TK_{E165Q} as observed in the crystal (left), interactions of Gln_{165} (top right) and Glu_{165} (bottom right). The respective monomers of *Ec*TK_{WT} are shown in blue hues, these of *Ec*TK_{E165Q} in green hues. The disordered regions are shown in red hues (PDB *Ec*TK_{WT}: 1QGD). The distances between Gln_{165} and the interaction partners observed in *Ec*TK_{WT} are indicated by long dashes. Actual interactions are indicated by short dashes.

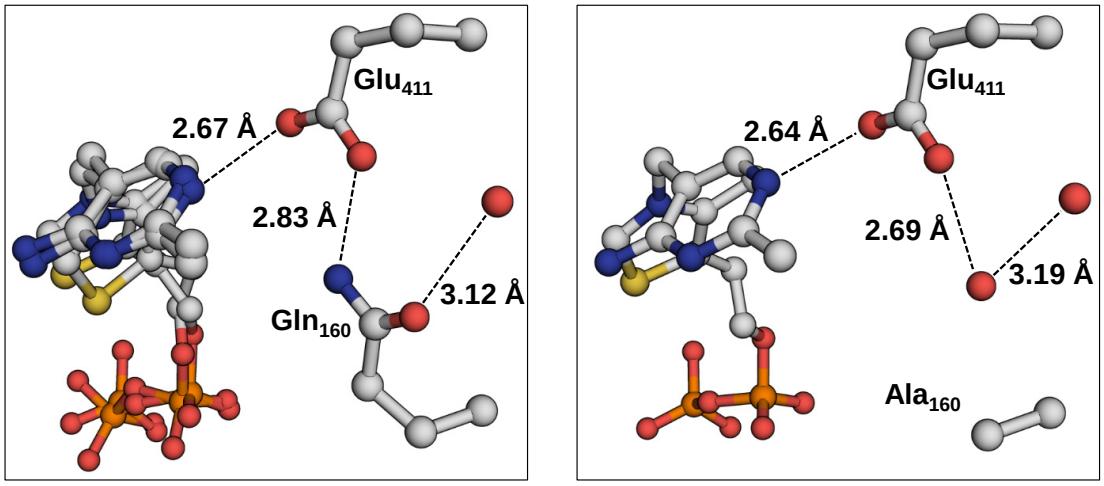

Figure 18. Comparison of interactions of Glu_{411} in *Ec*TK_{E160Q} and *Ec*TK_{E160A}. The distances between ThDP, Glu_{411}, Gln_{160} or Ala_{160}/H_2O and the next interacting water are displayed.

Both *Ec*TK_{E160Q} (1.3 Å, R_{work} = 13.6 %, R_{free} = 15.9 %) and *Ec*TK_{E160A} (1.7 Å, R_{work} = 14.8 %, R_{free} = 18.7 %) could be crystallized. In *Ec*TK_{E160A}, a water molecule was present close to the former position of the glutamate carboxyl-group. In both structures, the distance between Glu_{411} and the next interaction partner, Gln or H_2O increased significantly from 2.57 Å in *Ec*TK_{WT} to 2.83 Å in *Ec*TK_{E160Q} and 2.69 Å in *Ec*TK_{E160A}. However, the distance between Glu_{411} and the water molecule situated close to the second carboxyl-oxygen decreased in the variants, from 2.73 in *Ec*TK_{WT} to 2.69 in *Ec*TK_{E160Q} and 2.65 in *Ec*TK_{E160A}. Furthermore, the distance between position 160 and the next water also increased from 2.97 Å to 3.12 Å in *Ec*TK_{E160Q} and 3.19 Å in *Ec*TK_{E160A}, which is greater than the normally observed distance for hydrogen bonds (Fig. 18). Overall, all the distances observed between the constituents of the network increased in the variants compared to *Ec*TK_{WT}, except for the H_2O-H_2O distance at the midpoint (Table 3). In addition, the water molecule(s) at the midpoint of the network behave markedly different in *Ec*TK_{E160A} compared to *Ec*TK_{WT} and *Ec*TK_{E160Q} (Fig. 60, Appendix). In all variants there is non-spherical mFo-DFc density observable when no waters are build, but in *Ec*TK_{WT} and *Ec*TK_{E160Q}, the density is shaped like an hourglass, while in *Ec*TK_{E160A} it is more of a stretched sphere. As such, there was only one water molecule modeled in *Ec*TK_{E160A}, while in *Ec*TK_{WT} and *Ec*TK_{E160Q}, two molecules

Table 3. Comparison of interactions in the putative communication channel of *Ec*TK$_{WT}$, *Ec*TK$_{E160Q}$ and *Ec*TK$_{E160A}$. The distances in Å between all interacting partners are displayed in order for all variants.

Variant	$\alpha N'_1$-βE_{411}	βE_{411}-αX_{160}	αX_{160}-H_2O	H_2O-βE_{165}	βE_{165}-H_2O	H_2O-H_2O
*Ec*TK$_{WT}$	2.62	2.57	2.97	2.67	2.91	2.97
*Ec*TK$_{E160Q}$	2.67	2.83	3.12	2.66	2.98	2.89
*Ec*TK$_{E160A}$	2.64	2.69	3.19	2.68	3.42	2.88
Variant	H_2O-αE_{165}	αE_{165}-H_2O	H_2O-βX_{160}	βX_{160}-αE_{411}	αE_{411}-$\beta N'_1$	
*Ec*TK$_{WT}$	2.94	2.67	2.97	2.57	2.61	
*Ec*TK$_{E160Q}$	3.01	2.67	3.10	2.84	2.67	
*Ec*TK$_{E160A}$	3.19	2.63	3.18	2.82	2.69	

were build. As there is a significant mFo-DFc-density visible between the two water molecules, the possibility exists that it is one water molecule occupying two distinct positions in a very ordered manner. In *Ec*TK$_{E160A}$, this mobility seems to be present too, as mFo-DFc-density is visible mirrored through the water. The waters built at these densities were used to determine the distances in table 3.

In summary, exchange of Glu$_{160}$ for alanine or glutamine results in a variety of changes. The pK_A of the N4′ is apparently increased, the binding of ThDP occurs more slowly, formation of both the tetrahedral intermediate and the enamine are impacted, more severely in *Ec*TK$_{E160A}$. In the steady-state, *Ec*TK$_{E160Q}$ displays both an increased k_{cat} and K_M, while the k_{cat} of *Ec*TK$_{E160A}$ is reduced, with a comparative K_M. Structural investigation revealed a rearrangement of the hydrogen-bond network around Glu$_{411}$ in both, as well as of the midpoint water in *Ec*TK$_{E160A}$. Glu$_{165}$ proved to be vital for dimerization, as only *Ec*TK$_{E165D}$ remained viable. It revealed a 50 % reduction of k_{cat}, and structural investigation of *Ec*TK$_{E165Q}$ showed a significant impact on dimerization and disordering of several regions of the individual monomers.

3.2 Biochemical and Structural Investigation of *Ec*TK Thr$_{433}$

One common feature observed in all ThDP-dependent enzymes investigated structurally is the presence of a water molecule isolated from the solvent, in hydrogen bond distance to the activating glutamate which is often further flanked by an amino acid with acid-base catalyst properties. In most enzymes it is not possible to displace this water, as it is

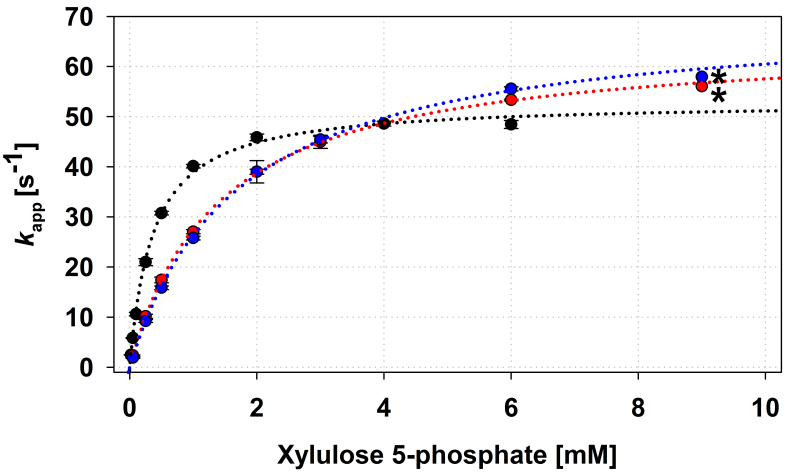

Variant	k_{cat} [s^{-1}]	K_M [mM]	Catalytic Efficiency [$mM^{-1}s^{-1}$]
EcTK_{WT}	53.01 ± 0.45	0.37 ± 0.01	143.3
EcTK_{T433Q}	65.45 ± 0.51	1.38 ± 0.03	47.4
EcTK_{T433V}	73.67 ± 0.93	1.68 ± 0.06	43.9

Figure 19. Steady-state kinetics of *Ec*TK_{T433Q} and *Ec*TK_{T433V}. The assay was performed as described before (Section 2.2.3.1). Displayed are the measured triplicates including error bars for *Ec*TK_{WT} (black), *Ec*TK_{T433Q} (red) and *Ec*TK_{T433V} (blue). The hyperbolic fits according to equation 1 are displayed as dotted curves. Data points denoted with * are single measurements. The table displays the numerical values obtained for k_{cat}, K_M and the catalytic efficiency.

interacting only with the main chain. In transketolase however, it is in hydrogen bond distance to threonine 433. It was exchanged against glutamine or valine, a nonpolar and a hydrophobic amino acid, to displace the water and investigate its role.

Beginning with the pH-titration, using AP-band formation as observed by CD-spectroscopy as a marker, the change in apparent pK_A of the Glu_{411}-ThDP proton relay was probed. Both variants showed a delayed onset of the AP-band compared to *Ec*TK_{WT}, as observed for the variants of Glu_{160} before. The pK_A-values obtained from the plotted band intensities according to equation 9 were 5.25 ± 0.04 for *Ec*TK_{T433Q} and 5.8 ± 0.03 for *Ec*TK_{T433V}. However, as the number of points is small, these values are not trustworthy. Onset of the band does not even begin before a pH of 5.4, so a pK_A at 5.25 is most probably wrong. To control the impact of these differences, steady-state assays were performed. They revealed an increase of k_{cat} for both *Ec*TK_{T433Q} and *Ec*TK_{T433V}, to 65.45 ± 0.51 s^{-1} and 73.67 ± 0.93 s^{-1} respectively, compared to 53.01 ± 0.45 s^{-1} for

*Ec*TK$_{WT}$. However, the K_M increased quite significantly, from 0.37 $\pm$ 0.01 in *Ec*TK$_{WT}$, to 1.38 $\pm$ 0.03 in *Ec*TK$_{T433Q}$ and 1.68 $\pm$ 0.06 in *Ec*TK$_{T433V}$. This corresponds to an increase of k_{cat} of 23 % in *Ec*TK$_{T433Q}$ and 39 % in *Ec*TK$_{T433V}$, with a 3.7-fold decrease in affinity for X5P for *Ec*TK$_{T433Q}$ and a 4.5-fold decrease for *Ec*TK$_{T433V}$ (Fig. 19). These changes result in an approximate 3-fold reduction of the catalytic efficiency.

Crystallization of both variants was performed in the ground state (*Ec*TK$_{T433Q}$: 1.25 Å, R_{work} = 11.3 %, R_{free} = 13.4 %; *Ec*TK$_{T433V}$: 1.13 Å, R_{work} = 11 %, R_{free} = 12.9 %) and with substrate X5P (*Ec*TK$_{T433Q}$: 1.47 Å, R_{work} = 14.9 %, R_{free} = 16.3 %; *Ec*TK$_{T433V}$: 1.15 Å, R_{work} = 11 %, R_{free} = 13.2 %). The ground state structures of both variants showed a structure very similar to that of *Ec*TK$_{WT}$ (RMSD *Ec*TK$_{T433Q}$: 0.32 Å, *Ec*TK$_{T433V}$: 0.33 Å), but in both the water coordinated by Thr$_{433}$ is displaced. In *Ec*TK$_{T433Q}$, a water molecule is closely situated to the position formerly occupied by the side chain hydroxy-group of Thr$_{433}$, while the new side chain points away, towards the main chain of Phe$_{437}$ and Val$_{438}$, displacing these slightly. The newly incorporated water interacts with the main chain amine of Gln$_{433}$ and the side chain carbonyl, as well as with the original water molecule. For this water, the interaction distance to Glu$_{411}$ stays identical at 2.72 Å, but both the interaction with the new water and the main chain carbonyl of Ala$_{380}$ increase to 2.80 Å, from 2.76 Å to Ala$_{380}$ and 2.69 Å to the former carbonyl of Thr$_{433}$ in *Ec*TK$_{WT}$. The interactions of Glu$_{411}$ did not change much, the distance to the aminopyrimidine N1′ increased from 2.62 to 2.64 Å, while the distance to Glu$_{160}$ decreased from 2.57 to 2.54 Å. In *Ec*TK$_{T433V}$, the displacement of the water is more pronounced. The interaction distance with Ala$_{380}$ decreases from 2.76 to 2.66 Å, while that with Glu$_{411}$ increases from 2.72 to 2.82 Å, and the water itself is displaced from its position in *Ec*TK$_{WT}$ by 1.36 Å. The oxygen of Glu$_{411}$ interacting with N1′ shifts by 0.36 Å, resulting in an increase of the distance to N1′ from 2.62 to 2.7 Å and making a change of the angle of the interacting glutamate oxygen relative to the aminopyrimidine plane from -7.4 ° to 2.2 ° necessary. In both variants, the water molecules display increased ADPs compared to *Ec*TK$_{WT}$. In *Ec*TK$_{T433Q}$, both the original and the newly incorporated water display an ADP of around 10, in *Ec*TK$_{T433V}$ it is 13, opposed to 6 in *Ec*TK$_{WT}$.

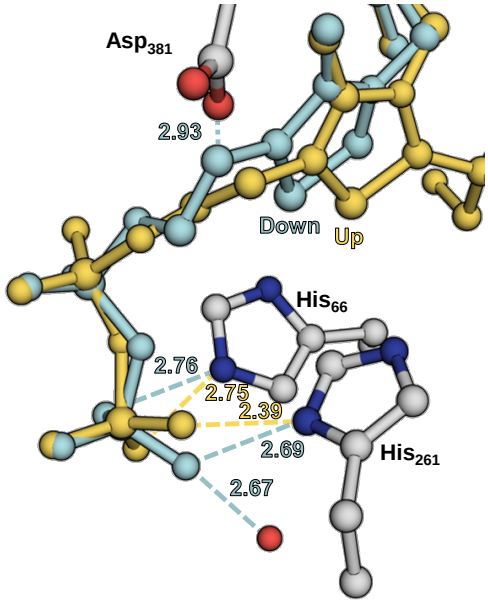

Figure 20. Interactions of ThDP in up- and down-conformation in *Ec*TK$_{T433V}$. The up-conformer is shown in yellow, the down-conformer in cyan. Possible interaction partners involved in control of the flexibility are shown with their respective interaction distances in Å.

A further prominent feature is the notable absence of the up-conformation of ThDP in the ground state of both variants. There is a small amount of positive mFo-DFc density observable at the up-position of S1 of the thiazolium, however in a negligible intensity. Furthermore, the otherwise pronounced alternate conformations of the diphosphate-anchor are absent, with only weak positive mFo-DFc density observable (Fig. 61, Appendix). Inversely, there is nearly full occupation of the tetrahedral X5P-ThDP intermediate observed in crystals soaked with X5P, with around 17 % down observed in *Ec*TK$_{T433V}$ and no observation in *Ec*TK$_{T433Q}$. Overall, the structures are highly similar to the ground state, with only minor changes (RMSD *Ec*TK$_{T433Q}$: 0.099 Å, *Ec*TK$_{T433V}$: 0.094 Å). Except for the interaction partners of X5P, ThDP itself, and possibly Asp$_{381}$ and Leu$_{116}$, no movement is observed. However, there are some changes of the interactions between the two conformations of ThDP and the protein environment. In the down-conformer, the beta-phosphate interacts with His$_{66}$ at 2.76 Å, His$_{261}$ at 2.69 Å and a water molecule at 2.67 Å. Furthermore, the strictly conserved Asp$_{381}$ is in range of the methylene bridge at 2.93 Å. In the up-conformer, the distance to His$_{66}$ stays practically the same, at 2.75 Å, but the distance to His$_{261}$ decreases drastically to

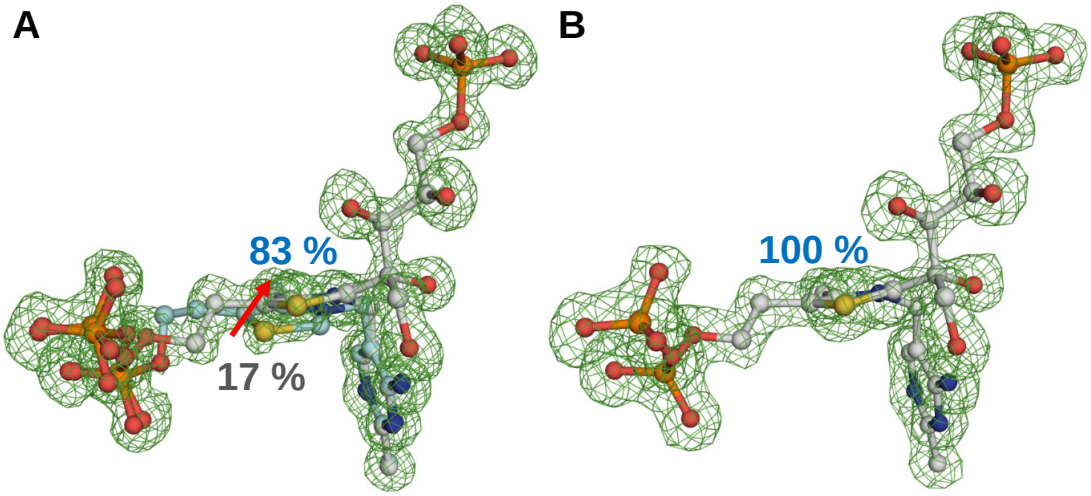

Figure 21. mFo-DFc omit maps of ThDP and X5P-ThDP in *Ec*TK$_{T433V}$ (A) and *Ec*TK$_{T433Q}$ (B). The mFo-DFc densities are contoured at 3 σ. The maps were generated by running 0 cycles of *PHENIX.REFINE* after removal of the respective components from the pdb file. The movement of the cofactor from down- to up conformation is indicated by the red arrow. The distributions of the respective conformations are shown in grey (down) and blue (up).

2.39 Å. Both the interactions with the water molecule and Asp$_{381}$ are lost. Additionally, the ADP observed for His$_{261}$ is significantly higher than that of the other active site residues, with an average of 11.8 for the side chain, compared to His$_{66}$ with 7.1 and His$_{473}$ with 7. In total, the C2 and S1 of the thiazolium move 1.35 Å between the two conformations. The movement of the diphosphate-methylene-thiazolium joint is clearly visible, as the positions of diphosphate and methylene bridge are distinct between ground- and X5P-bound state.

To summarize the results, the exchange of Thr$_{433}$ by both valine and glutamine causes an apparent pK_A-shift, increases the k_{cat} by 20-40 %, but also increases the apparent K_M values 3.7- to 4.5-fold. Structural investigation revealed no removal, but only displacement of the water molecule coordinated by Thr$_{433}$, accompanied by changes in the orientation of Glu$_{411}$. Furthermore, in both ground state structures close to 100 % of ThDP were present in the down-conformation while in the structures with covalently bound X5P, 80-100 % were present in the up-conformation.

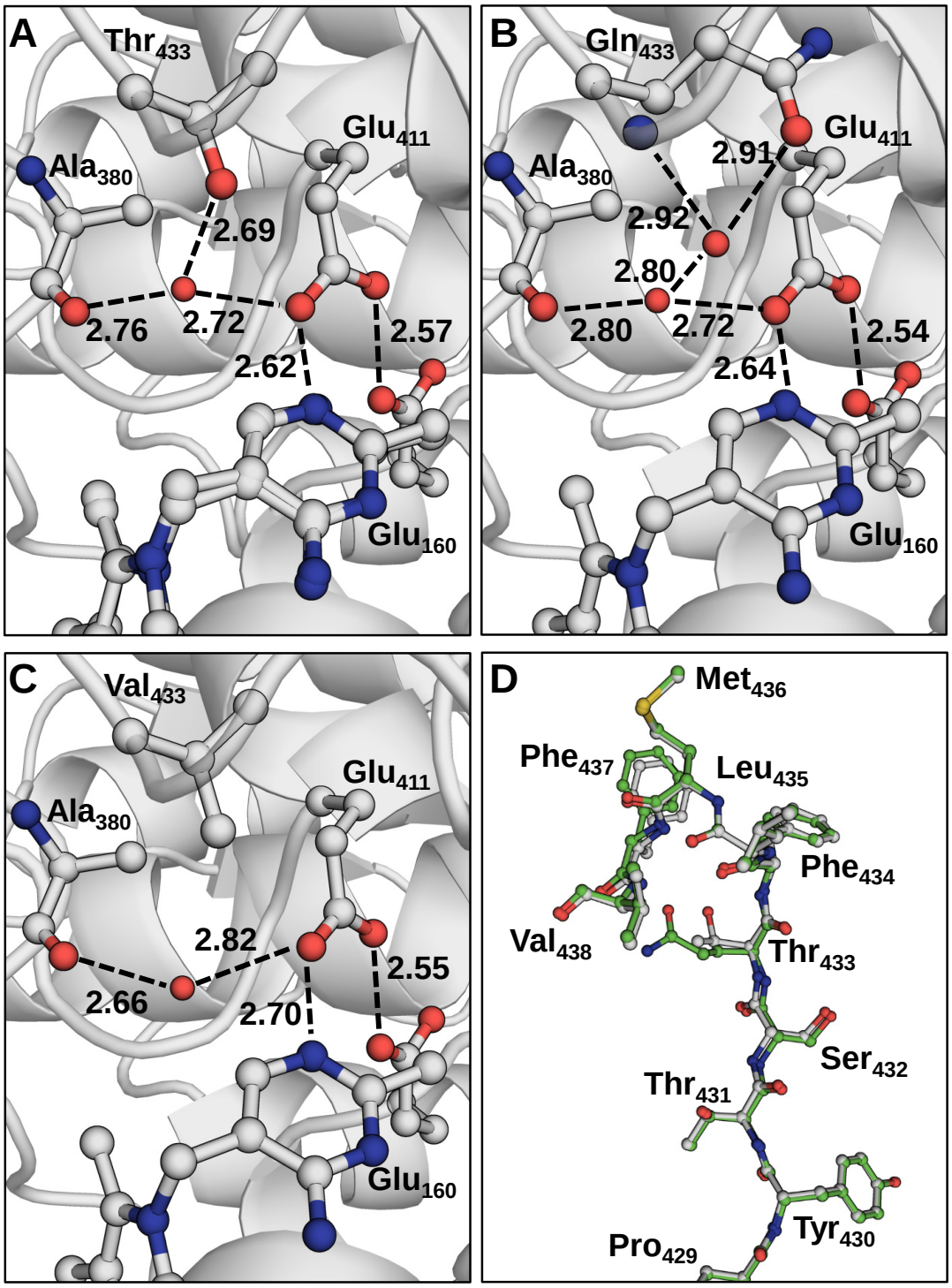

Figure 22. Comparison of the water interaction network in *Ec*TK$_{WT}$ (A), *Ec*TK$_{T433Q}$ (B) and *Ec*TK$_{T433V}$ (C). The interactions formed by Glu$_{411}$ and the adjacent water are shown in marked dashes and the distance displayed in Å. In *Ec*TK$_{T433Q}$, an additional water molecule is present. **Loop disorder caused by mutagenesis of Thr$_{433}$ to glutamine in *Ec*TK$_{T433Q}$ (D).** A slight displacement is observed in the region from Tyr$_{430}$ to Val$_{438}$ in both monomers of *Ec*TK$_{T433Q}$ (green), *Ec*TK$_{WT}$ (grey) is shown for comparison.

3.3 Investigation of the Mode of Action of 2′-Methoxythiamine Diphosphate

The bacimethrin derived ThDP-analogue 2′-methoxythiamine diphosphate (Fig. 5, Section 1.2.1) is the only naturally occurring ThDP analogue. It inhibits a set of highly important metabolic enzymes in bacteria, amongst them transketolase. To understand why the activity is reduced for MeOThDP reconstituted enzymes, we employed *Ec*TK to elucidate the mechanism.

*Ec*TK is purified as apoenzyme in absence of ThDP and a bivalent metal cation. As such, it readily allows insertion of cofactor analogues and is thereby designated for studies like this. Reconstitution with ThDP is commonly controlled by CD spectroscopy, as it results in the formation of the characteristic charge-transfer bands around 325 nm and 295 nm, as described before for UV-Vis spectroscopy (Section 2.2.3.2). Incubation of *Ec*TK with increasing concentrations MeOThDP resulted in no visible formation of the characteristic charge-transfer complexes, only a slight decrease of the signal from 300 to 320 nm, accompanied by formation of an absorbance band in normal UV-Vis, where free MeOThDP is not absorbing (Fig. 62, Appendix). According to these data a preliminary K_D of approximately 50 μM was estimated. A steady-state assay was

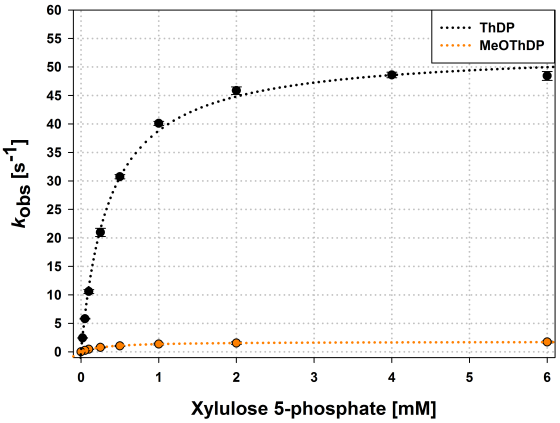

Cofactor	k_{cat} [s^{-1}]	K_M app. [mM]
ThDP	53.01 ± 0.45	0.37 ± 0.01
MeOThDP	1.8 ± 0.06	0.33 ± 0.04

Figure 23. Steady-state kinetics of MeOThDP reconstituted *Ec*TK. The assay was performed as described before (Section 2.2.3.1). Displayed are the measured triplicates including error bars for the ThDP (black) and MeOThDP (orange) reconstituted enzyme. The hyperbolic fits according to equation 1 are displayed as dotted curves. The table displays the numerical values obtained for k_{cat} and K_M.

performed using saturating concentrations of MeOThDP according to the estimation. The k_{cat} was determined to 1.8 $\pm$ 0.06 s^{-1}, a decrease to 3.4 % compared to the wild type. The apparent K_M decreased to 0.33 $\pm$ 0.04 mM, an increase in apparent affinity of approximately 11 % (Fig. 23). It was also observed that the reaction velocity increased over the total course of the measurement, with an increase of 10-20 % from the first to the last measurement of each triplicate.

To further compare the respective affinities of *Ec*TK for the two cofactors, a cofactor titration was performed. Although it is not understood how, it was shown that binding of ThDP quenches the intrinsic fluorescence of *Ec*TK (Asztalos, 2008). Both cofactors were titrated stepwise to $EcTK_{WT}$. A double hyperbolic dependency of the quenching on cofactor concentration was observed for both. The apparent K_D for the main phase with ThDP was calculated to 258 $\pm$ 5.2 nM, the apparent K_D for the main phase of MeOThDP to 15.09 $\pm$ 2.45 μM (Fig. 24 C), which corresponds to an 60-fold increase. We further investigated the apparent binding under substrate turnover, to simulate *in vivo* conditions. Here, an apparent K_M of 2 $\pm$ 0.2 μM was observed for ThDP and an apparent K_M of 21.9 $\pm$ 2.2 μM for MeOThDP in the dominant phase displaying low affinity, corresponding to an 11-fold decrease of apparent affinity, and 0.01 $\pm$ 0.005 μM in the high-affinity phase, an apparent 20-fold increase (Fig. 24 A and B).

NMR studies were employed to obtain the distribution of intermediates in the presence of only the donor substrates X5P and fructose 6-phosphate (F6P), and to obtain the rate of H/D-exchange at the C2 of the thiazolium ring (Kern *et al.*, 1997, Tittmann *et al.*, 2003, Asztalos, 2008). As shown in figure 25, only minimal amounts of covalent adduct are formed between cofactor and substrate in $EcTK_{MeOThDP}$, with a population of approximately 15 %. When incubated with F6P, small amounts of dihydroxyethyl-thiamine diphosphate were observed. Furthermore, a significantly decreased rate of H/D-exchange at the C2 was observed. In $EcTK_{ThDP}$ this exchange occurs with a rate of 313 $\pm$ 41 s^{-1} while it is reduced to 2.9 $\pm$ 1.1 s^{-1} in $EcTK_{MeOThDP}$. This is even below the rate observed in the *Ec*TK variant E411A (11 $\pm$ 3.6 s^{-1}), where the activating glutamate is removed (Asztalos, 2008).

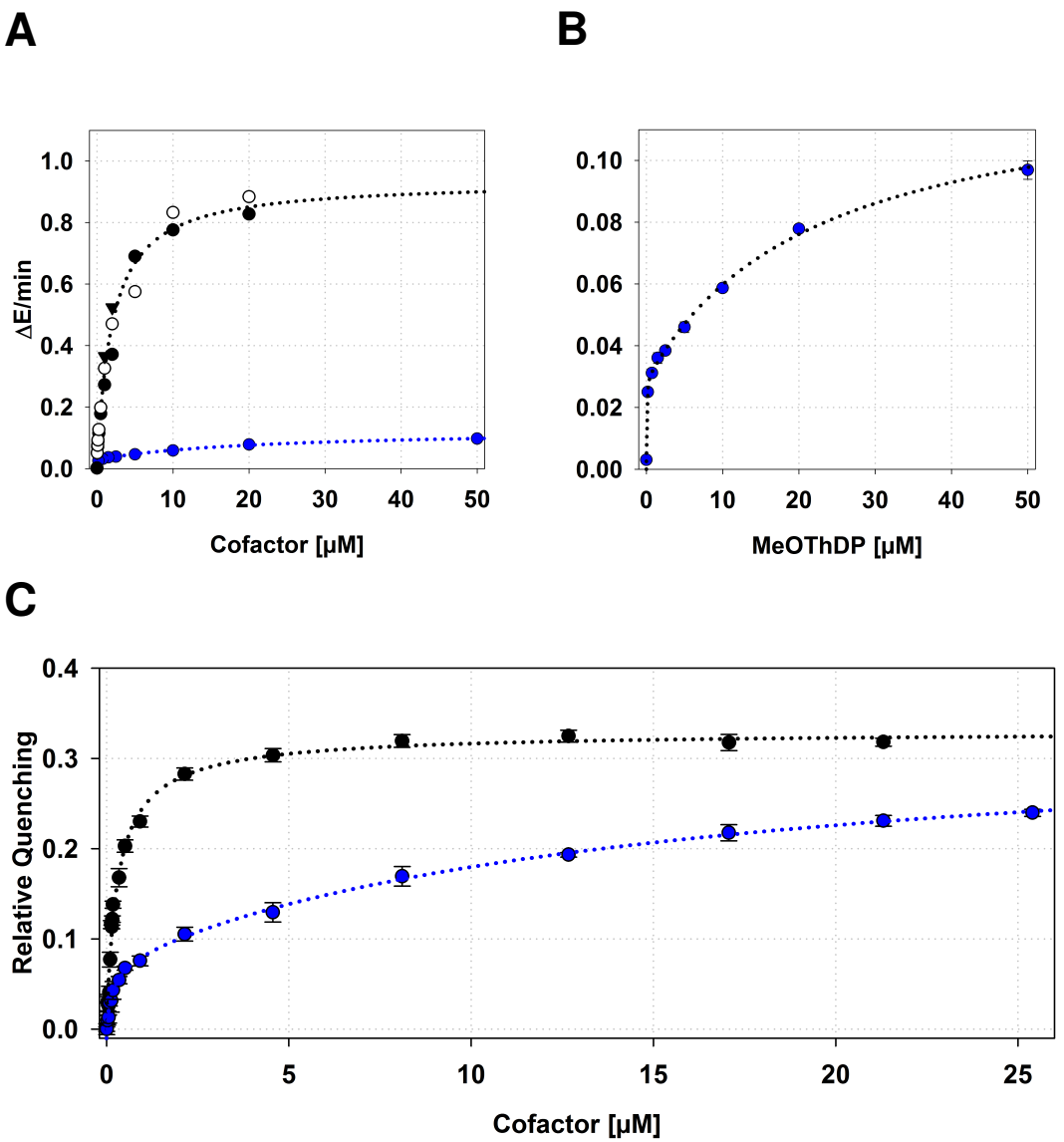

Figure 24. (A) Comparison of ThDP and MeOThDP binding as observed under steady-state conditions. Rates at differing ThDP concentrations are shown as individual points (white and black circles, triangles), those for MeOThDP in blue. The data for ThDP were fitted according to equation 1, those for MeOThDP according to equation 2. **(B) Display of the binding of MeOThDP to ThDP, as observed in the steady-state assay.** As a small, tight-binding phase was present the data were fitted according to equation 2. **(C) Comparison of ThDP and MeOThDP binding as observed by fluorescence titration.** The relative quenching, corrected for excimers, is plotted against the ThDP (black) or MeOThDP (blue) concentration. Both plots were fitted according to equation 11.

Generation of crystals of *Ec*TK$_{MeOThDP}$ and collection of datasets to atomic resolution were successful. Data sets were collected of a ground state crystal and one soaked with 100 mM X5P. The structure of *Ec*TK$_{MeOThDP}$ in the ground state was refined to 0.92 Å

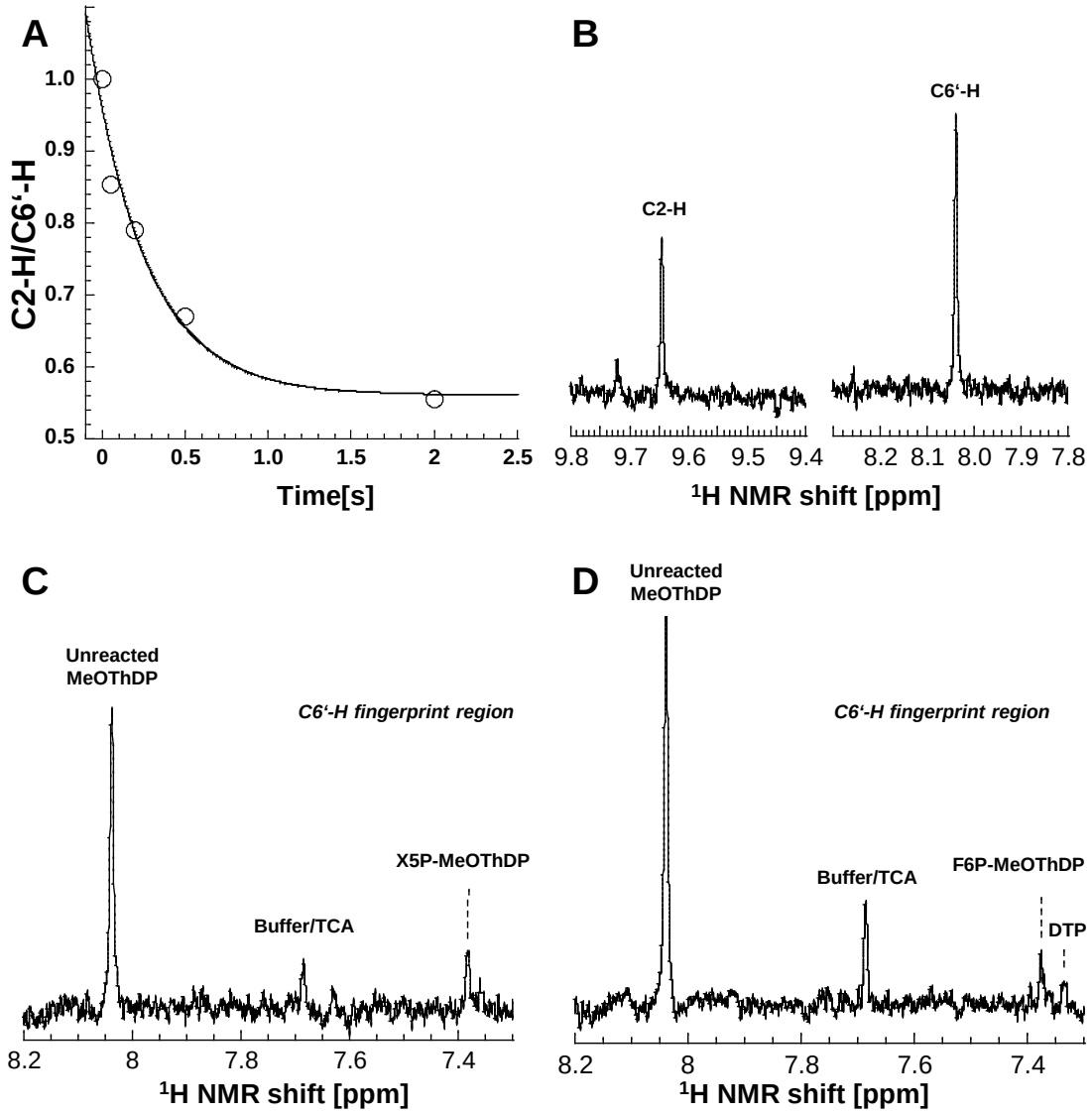

Figure 25. Intermediate distribution and cofactor activation measured by NMR. Shown are the kinetics of H/D exchange at the C2-atom (A), the NMR spectra at full exchange (B), and the spectra obtained after incubation with X5P (C) and F6P (D). DTP denotes the dihydroxyethyl-thiamine diphosphate intermediate. All measurements were performed by Prof. Dr. Kai Tittmann at the NMR device of the Institute for Organic and Biomolecular Chemistry.

(R_{work} = 10.9 %, R_{free} = 11.9 %), the structure with X5P to 0.95 Å (R_{work} = 10.3 %, R_{free} = 11.4 %). The ground state structure clearly revealed small but significant differences for the binding of MeOThDP compared to ThDP, while overall the structures are very similar with an RMSD of 0.39 Å. The aminopyrimidine moiety, as well as the methylene bridge and the thiazolium ring are shifted by 0.3 to 0.8 Å (e.g. N1': 0.76 Å, N4': 0.56 Å,

C2: 0.68 Å). Furthermore, the carboxyl-oxygen of Glu_{411} interacting with N4' is displaced by 0.66 Å. In sum, these changes result in an increase of the N4'- Glu_{411}-O distance length from 2.62 Å to 3.64 Å and a compression of the Glu_{411}-Glu_{160} distance to 2.49 Å. Here, positive mFo-DFc density is clearly visible at the midpoint between Glu_{411} and Glu_{160} (Fig. 63, Appendix).

A further interesting observation is the displacement of Phe_{437} in a magnitude similar to that of the aminopyrimidine ring (Fig. 28 A). A closer look at the methoxy group of MeOThDP reveals a strained geometry. The standard tetrahedral angle for a methyl-methoxy group is 111.7 °, which is increased to 114.8 ° in enzyme bound MeOThDP (Fig. 28B). When displaying the VDW-radii of the protein environment in direct proximity to the methoxy-methyl group, it is revealed that the methyl group is tightly nestled into the position were the number of clashes is the lowest (Fig. 28C). A further feature is the absence of a clearly defined second conformation of the thiazolium. While it is visible for the pyrophosphate, only little positive mFo-DFc density is observed at the expected positions (Fig. 64, Appendix). Overall, the flexibility of MeOThDP seems reduced compared to ThDP, with an ADP of 9 for MeOThDP and 9.8 for ThDP. However, for the aminopyrimidine moiety the ADP are 5.1 for ThDP and 8.6 for MeOThDP (Fig. 26), indicating a destabilization of the interaction with the binding pocket.

In the structure with X5P the substrate is present in the docking site, but not covalently bound. The distance between the carbonyl atom of X5P and the reactive C2 of the thiazolium is 4.05 Å. In total, counting alternate conformations, 13 interactions are formed between X5P and the protein environment. The sugar OH-groups interact with

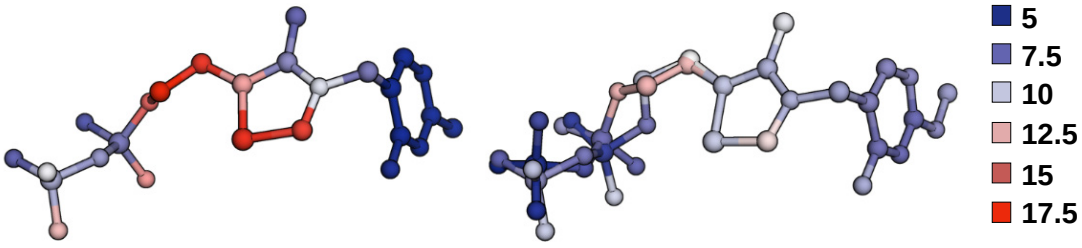

Figure 26. B-factors of enzyme bound ThDP (left) and MeOThDP (right). The ADP are displayed as colors, increasing from blue to red.

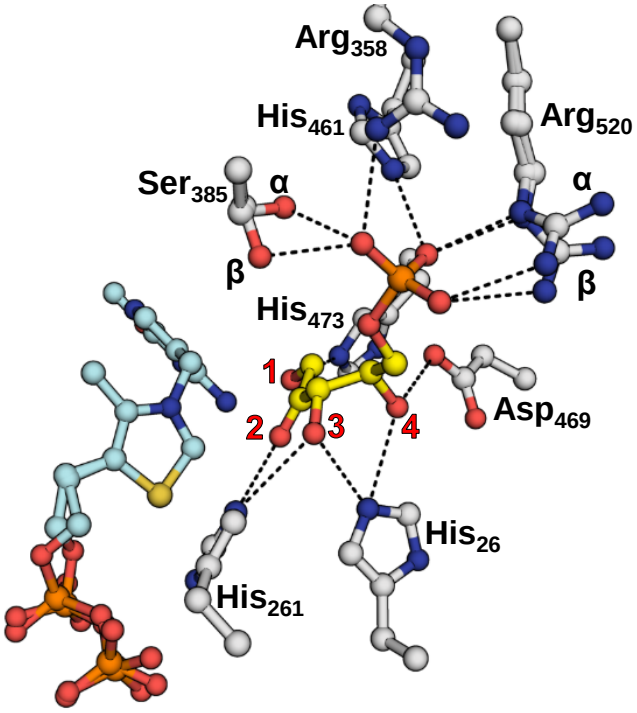

Figure 27. Interactions of X5P with the protein environment in *Ec*TK$_{\mathbf{MeOThDP}}$. All interactions of of X5P with the protein environment are indicated by dashes. For residues with multiple conformations the dominant one is labeled α, the lesser one β. X5P is colored yellow, ThDP cyan, the OH-groups of X5P are numbered in red.

the histidines 26, 261 and 473, as well as Asp$_{469}$. The phosphate moiety interacts with the arginines 358 and 520, as well as Ser$_{385}$ and His$_{461}$ (Fig. 27). Both Ser$_{385}$ and Arg$_{520}$ display alternate conformations in a distribution close to 1:1, both of which interact with the identical phosphate-oxygen. Interestingly, the presence of X5P seems to improve the binding of MeOThDP. The aminopyrimidine ring is fit into its pocket more tightly, decreasing the distance from Glu$_{411}$ to N1′ from 3.64 to 3.42 Å.

In summary, investigation of the cofactor analogue MeOThDP showed that interaction with *Ec*TK is weaker than that of the native cofactor ThDP, as it binds slower and shows a higher K_D, evidenced by two different assays. The classical charge-transfer bands are absent for enzyme reconstituted with MeOThDP. NMR studies showed a retarded formation of covalent sugar-MeOThDP complexes, as well as a significantly reduced activation rate of the cofactor. Crystallography showed a slightly different binding of MeOThDP compared to ThDP, as well as the presence of unbound X5P in the binding site, allowing analysis of substrate binding.

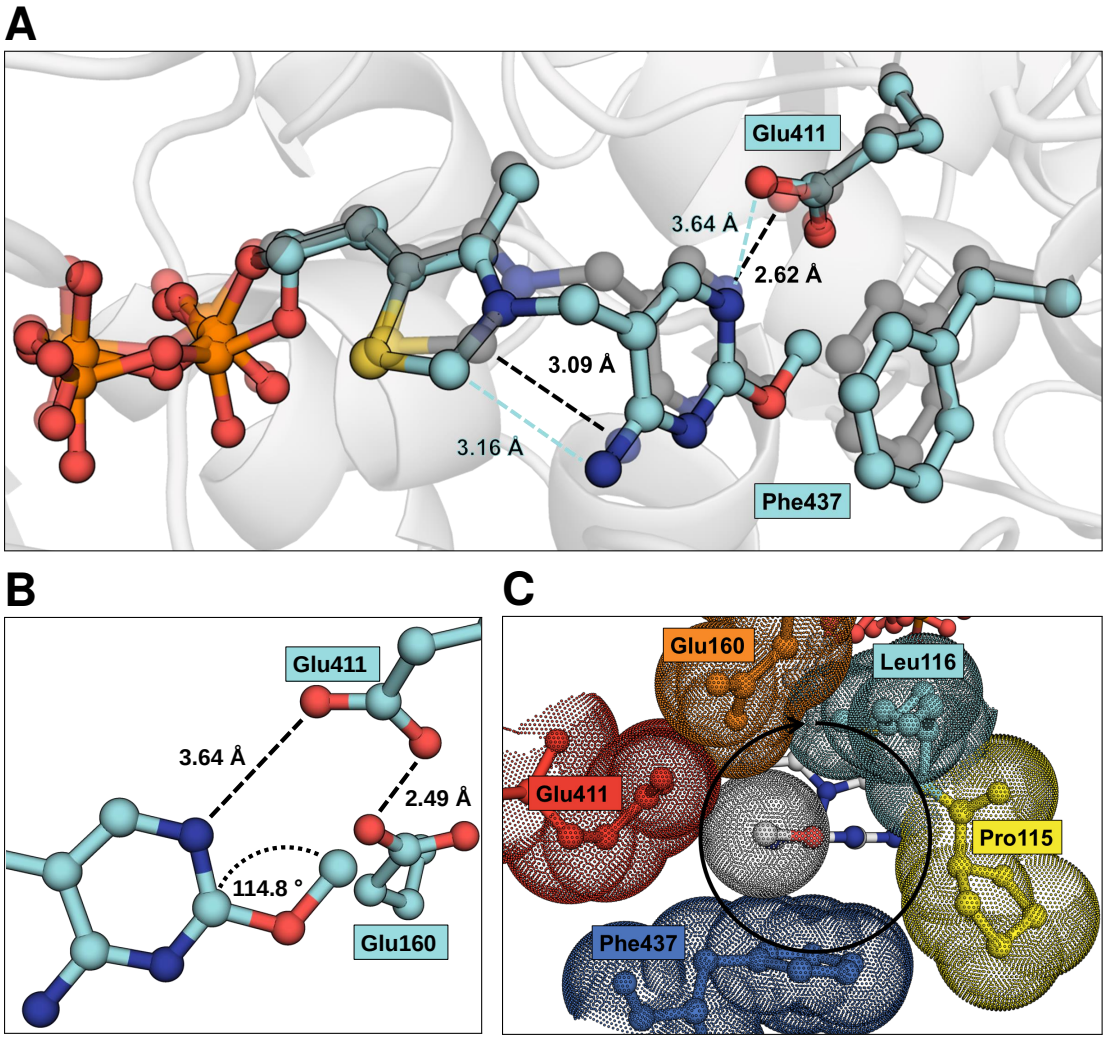

Figure 28. (A) Comparison of ThDP and MeOThDP bound in *E. coli* TK. ThDP is shown in gray, MeOThDP in cyan. The respective distances for the intramolecular proton transfer between C2 and N4′ as well as for the inter-molecular proton transfer between Glu_{411} and N1′ are shown, as well as the main interaction partners for the AP-ring, Glu_{411} and Phe_{437}. **(B) Geometry of the MeO-function and interaction with Glu_{411}.** Displayed are the tetrahedral angle of the methoxy group, the distance of N1' to Glu_{411} and the compressed hydrogen bond between Glu_{411} and Glu_{160}. **(C) Visualization of the VDW radii of the methoxy methyl group and the surrounding amino acids.** The VDW radius of the methyl function is shown in white, the radii of the surrounding residues in their respective colors. The arrow displays the outer limit of the van-der-Waals radius of the methyl group when rotating around the C2′-O2′ axis.

3.4 Biochemical and Structural Investigation of *Ec*TK His_{261}

Of all structurally characterized ThDP-dependent enzymes, *Ec*TK displays an unique feature. The cofactor is present in two distinct conformations, termed up and down, in which both the pyrophosphate moiety and the thiazolium ring show clear alternate conformations (Lüdtke, 2012).

This movement could be important to separate the reactants during the course of reaction, to stop religation of the first product after cleavage of the tetrahedral substrate-ThDP complex. As these are present in both ground state and substrate bound state, it is not fully understood how this conformational change is promoted, but an induction of the conformational change by substrate binding can be ruled out essentially. It was assumed that the β-phosphate of the pyrophosphate moiety is protonated in the course of reaction, and the whole diphosphate moiety acts as joint, forcing the thiazolium into the second conformation. There are two acid-base catalysts interacting with the diphosphate, the histidines 66 and 261, which could control the distribution of the two conformations. Histidine 261 is directly interacting with the C3-OH of ThDP-bound X5P and is assumed to be the acid-base catalyst for substrate cleavage. Histidine 66 does not interact directly with the substrate or any intermediate, only via a water molecule interacting with the C2-OH of the tetrahedral X5P-ThDP adduct and DHEThDP. This part will focus on the investigations on His_{261}.

Kinetic investigation of *Ec*TK_{H261N} revealed varying reduction of all catalytic rates. In the steady-state assay, k_{cat} was reduced to 0.24 $\pm$ 0.002 s^{-1}, corresponding to 0.5 % of wild type activity, while the K_M was apparently decreased to 0.07 $\pm$ 0.003 mM, a five-fold increase in apparent affinity (Fig. 29). The pre-steady state kinetics observing the depletion of the AP-form, concomitant with formation of catalytically active IP and APH^+, and accumulation of the IP-form, concomitant with formation of the tetrahedral intermediate mirrored these results. In *Ec*TK_{H261N} it was possible to reach saturation for AP-depletion, with a k_{max} of 128.51 $\pm$ 2.72 s^{-1}, and an apparent K_S of 5.86 $\pm$ 0.29 mM. The IP form displayed a k_{max} of 110.3 $\pm$ 4.01 s^{-1}, and an apparent K_S of 5.17 $\pm$ 0.35 mM.

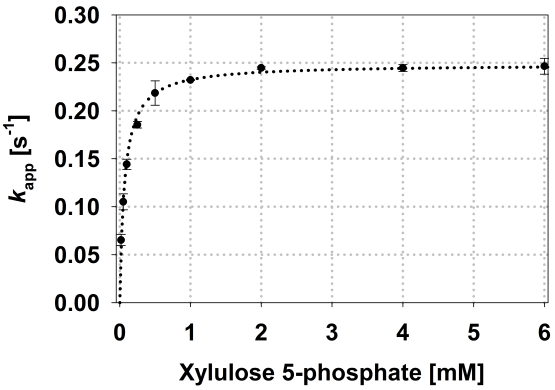

Variant	k_{cat} [s^{-1}]	K_M [mM]
EcTK_{WT}	53.01 ± 0.45	0.37 ± 0.01
EcTK_{H261N}	0.24 ± 0.00	0.07 ± 0.00

Figure 29. Steady-state kinetics of *Ec*TK_{H261N}. The assay was performed as described before (Section 2.2.3.1). The measured triplicates are displayed, the fit according to equation 1 is shown as dotted line. The table displays the numerical values obtained for k_{cat} and K_M.

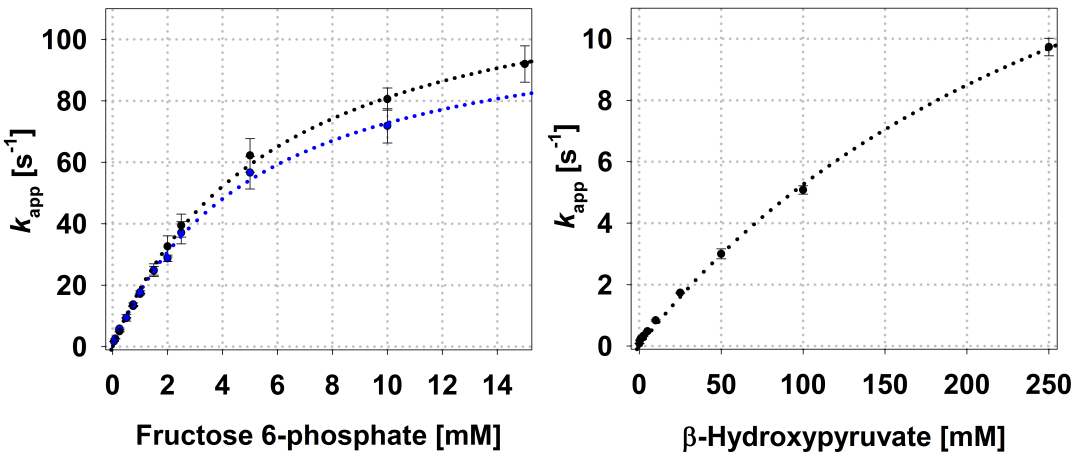

Variant	k_{max} [s^{-1}]	K_S [mM]
IP	110.3 ± 4.01	5.17 ± 0.35
AP	128.51 ± 2.72	5.86 ± 0.29
Enamine	22.16 ± 1.07	321.7 ± 24.16

Figure 30. Pre-steady-state kinetics of *Ec*TK_{H261N}, using F6P to monitor formation of the tetrahedral intermediate (left, blue) and depletion of the AP-form of the aminopyrimidine moiety (left, black), as well as HPA to monitor the formation of DHEThDP (right). The assay was performed as described before (Section 2.2.3.2). Displayed are the measured multiplicates including error bars. The hyperbolic fits according to equation 1 are displayed as dotted curves. The table displays the numerical values obtained for k_{max} and K_S.

Furthermore, it was possible to reach sufficient coverage in the reaction with HPA to perform a hyperbolic fit, giving a k_{max} of 22.16 $\pm$ 1.07 s^{-1}, and an apparent K_D of 321.7 $\pm$ 24.16 mM.

Crystallization and data collection of both *Ec*TK_{H261N} in the ground state, as well as soaked with substrate X5P was successful. However, both structures revealed the presence of the cofactor in up- and down-conformation, as observed in *Ec*TK_{WT}, with a 50:50 distribution in the ground state. In presence of X5P, around 70 % of the cofactor formed the covalent X5P-ThDP adduct, while 30 % remained in down-conformation (Fig. 31). In both states, the region from His_{258} to Gly_{262} is disordered, the introduced Asn_{261} being present in two badly defined conformations, as shown in figure 65 (Appendix). The positioning of ThDP relative to *Ec*TK_{WT} does change by a small margin, with a total movement of the C2 by 0.36 Å (Fig. 66, Appendix).

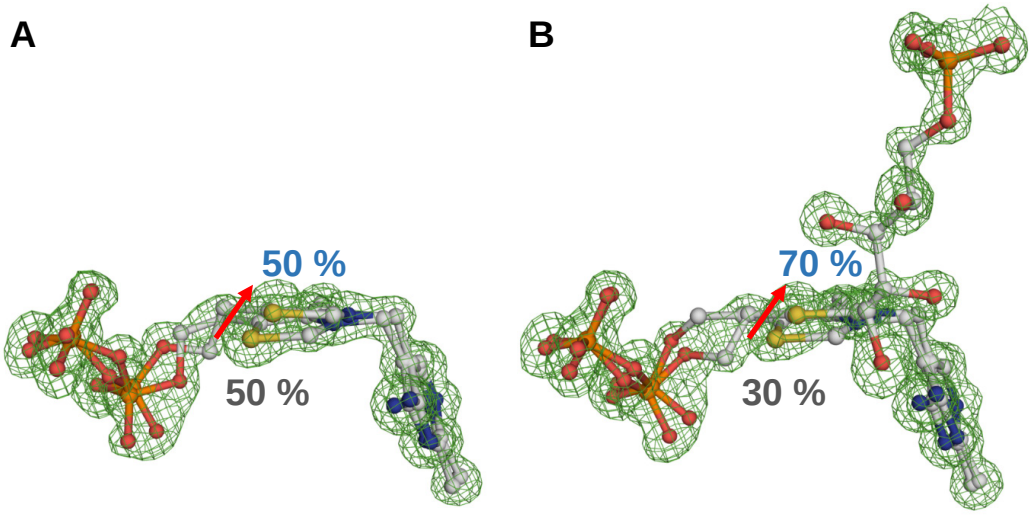

Figure 31. mFo-DFc omit maps of ThDP (A) and X5P-ThDP (B) in *Ec*TK_{H261N}. The mFo-DFc densities are contoured at 3 σ. The maps were generated by running 0 cycles of *PHENIX.REFINE* after removal of the respective components from the pdb file. The movement of the cofactor from down- to up conformation is indicated by the red arrow. The distributions of the respective conformations are shown in grey (down) and blue (up).

3.5 Examination of Tautomeric Control in Transketolase and Pyruvate Oxidase

Recent research revealed the presence of non-aromatic ThDP-adducts with keto-character, in both non-enzymatic (Berkessel *et al.*, 2010) and enzymatic environments (Amara *et al.*, 2007, Meyer *et al.*, 2012) (see figure 4, Section 1.2.1). This is opposed to the decade old assumption that resonance stabilization, as observed in the classical carbanion/enamine (di)hydroxyethyl intermediate, outweighs the increased stability of ketones over alcohols. It does however explain why reactions with nucleophilic acceptor substrates, e.g. phosphate take place, as it offers a electrophilic center to attack.

To investigate how the putative keto-intermediate is formed in *Lp*POX and avoided in *Ec*TK, variants were generated of the polar residues surrounding and interacting with the intermediate.They were mutated to the respective counterpart in the other enzyme. Five variants were created in total, *Ec*TK$_{H66A}$, *Ec*TK$_{H100A}$, *Ec*TK$_{H473Q}$, *Lp*POX$_{Q122H}$ and *Lp*POX$_{E483I}$.

As shown in figure 32, the dihydroxyethyl-ThDP intermediate in *Ec*TK interacts directly via the 1-OH with His$_{473}$, via the 2-OH with His$_{100}$ or water mediated with His$_{66}$. In *Lp*POX, the hydroxyethyl-ThDP directly interacts with Gln$_{122}$, and via the acceptor

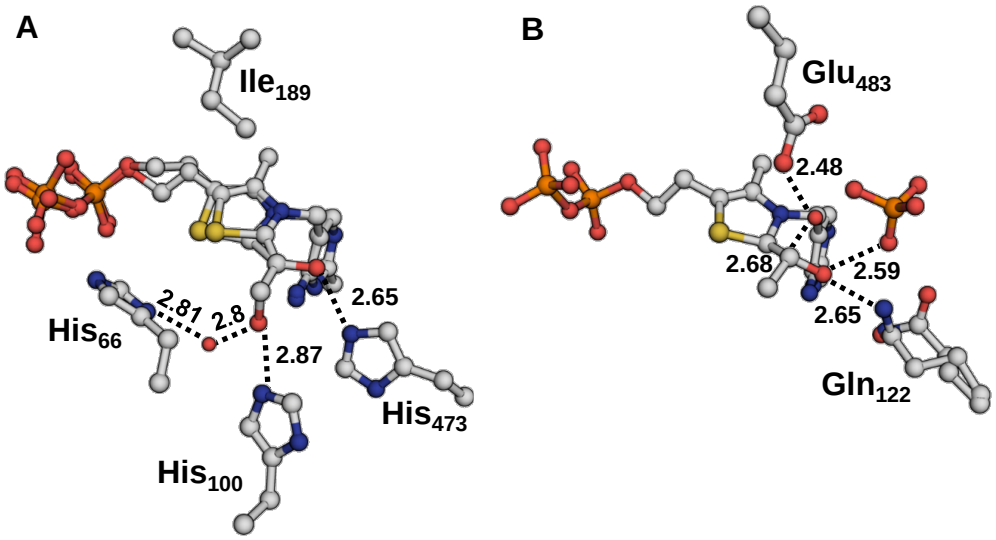

Figure 32. Comparison of the active sites of *Ec*TK (A) and *Lp*POX (B). The respective interaction partners and their equivalents in *Ec*TK and *Lp*POX are indicated, as well as their interaction distance in Å (*Lp*POX: 4FEE, *Ec*TK taken from Lüdtke, 2012).

substrate phosphate and a water molecule with Glu_{483}.

3.5.1 Transketolase

All three variants were investigated for their capability to bind ThDP, as required for catalysis. All of them retained their ability to bind ThDP, as evidenced by circular dichroism spectroscopy (Fig. 67, Appendix). However, the intensity of the characteristic charge transfer band resulting from the aminopyrimidine species was much less pronounced in *Ec*TK_{H100A}, and the minimum of the band shifted from around 325 nm to 316 nm in *Ec*TK_{H66A}. *Ec*TK_{H473Q} behaves similarly to *Ec*TK_{WT} in regards to pattern and intensity. Comparing the three variants of *Ec*TK in the steady-state assay yielded a significant reduction of k_{cat}, as well as an increase of K_M for all of them. For *Ec*TK_{H66A}, the k_{cat} was reduced to 8.92 $\pm$ 0.2 s^{-1}, which corresponds to an decrease by over 80 % compared to *Ec*TK_{WT}. The K_M increased to 1.34 $\pm$ 0.08 mM, an 3.6-fold increase, resulting in a total decrease of the catalytic efficiency from 143.3 $\pm$ 1.3 $mM^{-1}s^{-1}$ to 6.7 $\pm$ 0.2 $mM^{-1}s^{-1}$, a reduction by over 95 %. In *Ec*TK_{H100A}, the k_{cat} was reduced by over 90 % to 3.82 $\pm$ 0.12 s^{-1} and the K_M increased 4.2-fold to 1.54 $\pm$ 0.13 mM. This correlates to a reduction of the catalytic efficiency by over 98 %, to 2.48 $\pm$ 0.13 $mM^{-1}s^{-1}$. The effects were even more pronounced in *Ec*TK_{H473Q}, where k_{cat} was reduced to 3.81 $\pm$ 0.11 s^{-1}, a loss in activity of more than 90 %. The K_M is markedly increased to 4.42 $\pm$ 0.27 mM,

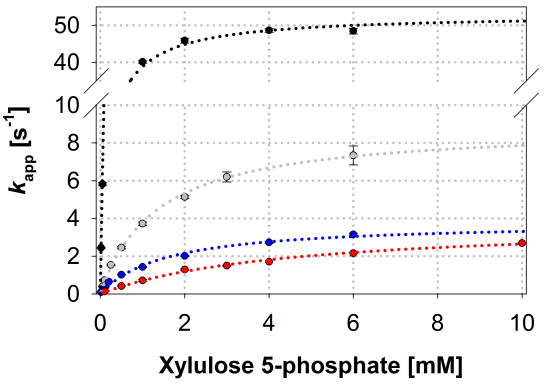

Variant	k_{cat} [s^{-1}]	K_M [mM]
EcTK_{WT}	53.01 $\pm$ 0.45	0.37 $\pm$ 0.01
EcTK_{H66A}	8.92 $\pm$ 0.20	1.34 $\pm$ 0.08
EcTK_{H100A}	3.82 $\pm$ 0.12	1.54 $\pm$ 0.13
EcTK_{H473Q}	3.81 $\pm$ 0.11	4.42 $\pm$ 0.27

Figure 33. Steady-state kinetics of *Ec*TK_{WT} (black), *Ec*TK_{H66A} (gray), *Ec*TK_{H100A} (blue) and *Ec*TK_{H473Q} (red). The assay was performed as described before (Section 2.2.3.1). The measured triplicates are displayed, the fit according to equation 1 is shown as dotted line. The table displays the numerical values obtained for k_{cat} and K_M.

an 11.9-fold decrease in apparent affinity. This results in a decrease of the catalytic efficiency to 0.86 $\pm$ 0.04 $mM^{-1}s^{-1}$, a relative reduction by more than 99 %.

To further investigate whether the mutations have an impact on the character of the intermediate, circular dichroism spectra were recorded of the enzyme after addition of HPA, which irreversibly forms DHEThDP by virtue of its decarboxylation. Therefore, it is more feasible for this investigation than the natural sugar substrates, which mainly form the tetrahedral substrate-ThDP complexes. The difference spectra obtained after addition of HPA to *Ec*TK_{WT} and the variants revealed marked differences. The band intensity is distinctly weaker in all variants. In *Ec*TK_{H66A}, the peak is flatter, and its maximum is blue-shifted by around 10 nm. In *Ec*TK_{H100A} and *Ec*TK_{H473Q}, there is a red-shift of about 5 nm observable (Fig. 34 A). A similar trend was observed in the UV-vis spectra. *Ec*TK_{WT} shows formation of enamine and IP-form of the pyrimidine at 300 nm, depletion of the AP-form at around 325 nm and formation of the assumed enolate-form of DHEThDP in a broad band around 400 nm (Lüdtke, 2012; Paulikat, 2014). In all variants, the latter form is absent. In *Ec*TK_{H100A} and *Ec*TK_{H473Q}, a small peak around 360 nm becomes visible instead, possibly overlapping the AP-band which seemingly does not deplete. In all variants, formation of a peak around 300 nm is observed, with a reduced amplitude compared to *Ec*TK_{WT}, and a blue-shift by 4-5 nm in *Ec*TK_{H100A} (Fig. 34 B). The kinetics of enamine formation were observed using the stopped-flow technique. They revealed a significant reduction of $\frac{k_{max}}{K_S}$, compared to *Ec*TK_{WT} (5.5 $\pm$ 0.14 $s^{-1}mM^{-1}$). For *Ec*TK_{H66A}, it was reduced to 0.29 $\pm$ 0.005 $mM^{-1}s^{-1}$, a reduction to 5 %. In both, *Ec*TK_{H100A} and *Ec*TK_{H473Q}, it was reduced to 0.03 $\pm$ 0.001 $mM^{-1}s^{-1}$, corresponding to a reduction by over 99 % (Fig. 34 C).

NMR data recorded previously revealed the cleavage of the usual tetrahedral sugar-ThDP intermediate in *Ec*TK_{H100A} (Diederichs, 2009). Therefore, to detect if this intermediate has an UV-Vis signature, spectra of *Ec*TK_{WT} and variants with F6P were recorded. These revealed nearly no depletion of the AP-band around 325 nm after 40 seconds in *Ec*TK_{H100A} and *Ec*TK_{H473Q}, compared to *Ec*TK_{WT}, and the formation of a weaker, but broader band with a minimum at 320 nm in *Ec*TK_{H66A}. In all variants, formation

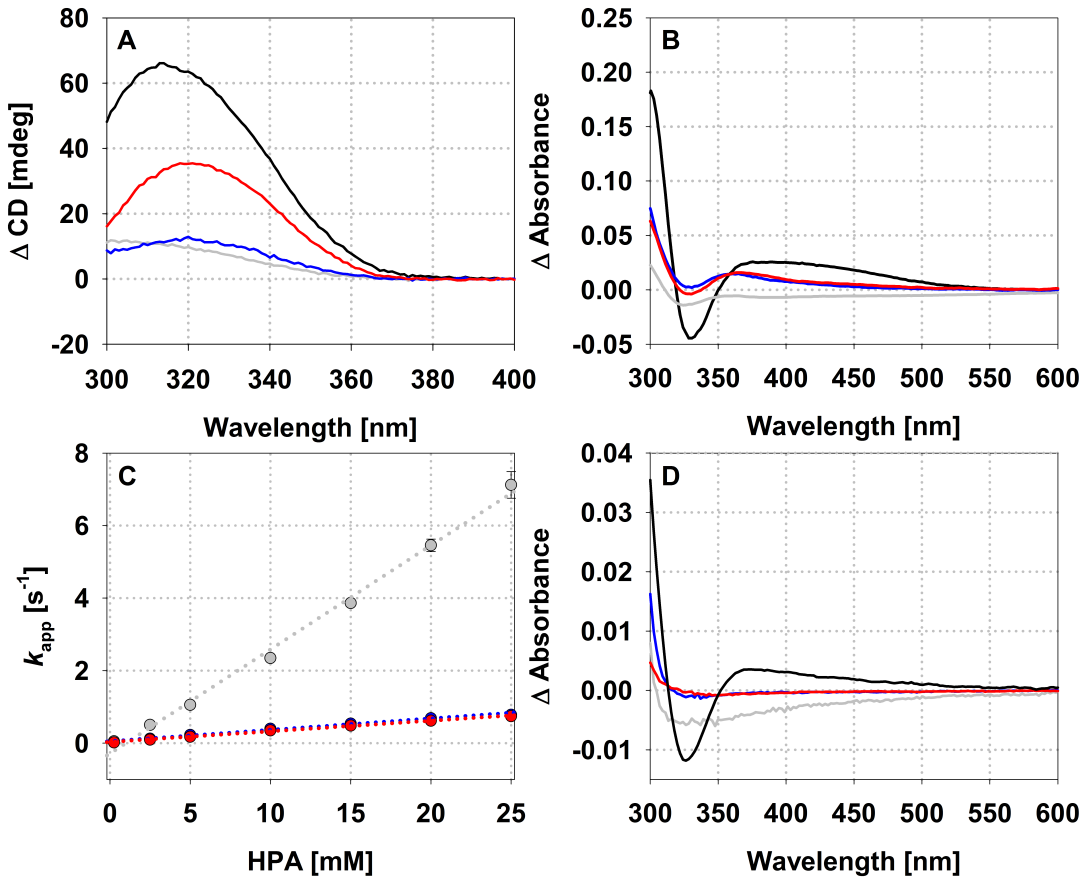

Figure 34. (A) CD difference spectra of transketolase variants after addition of HPA. Difference spectra were obtained by subtracting the CD spectra of incubated protein from the holoenzyme, corrected for buffer and HPA. *Ec*TK_{WT} is shown in black, *Ec*TK_{H66A} in gray, *Ec*TK_{H100A} in blue and *Ec*TK_{H473Q} in red. **(B) UV-vis difference spectra of transketolase variants after addition of HPA.** UV-vis difference spectra were obtained using the stopped-flow technique and corrected similar to the CD-spectra. **(C) Formation of the enamine as observed by stopped-flow spectroscopy.** Formation of the enamine was observed at 300 nm, the transients were fitted according to equation 4, the plot according to equation 12. **(D) UV-vis difference spectra of transketolase variants after addition of F6P.** The difference spectra were obtained by subtracting the spectra recorded 40 seconds after addition of 500 μM F6P from the ground state spectra.

of a band below 300 nm could be observed. These were shifted compared to that of the IP-band of *Ec*TK_{WT}, towards 280 nm where enzyme and ThDP absorb, making further observation impossible. The enolate band around 400 nm was again absent in all variants.

Longer incubation with increased F6P concentrations for *Ec*TK_{H100A} and *Ec*TK_{H473Q}

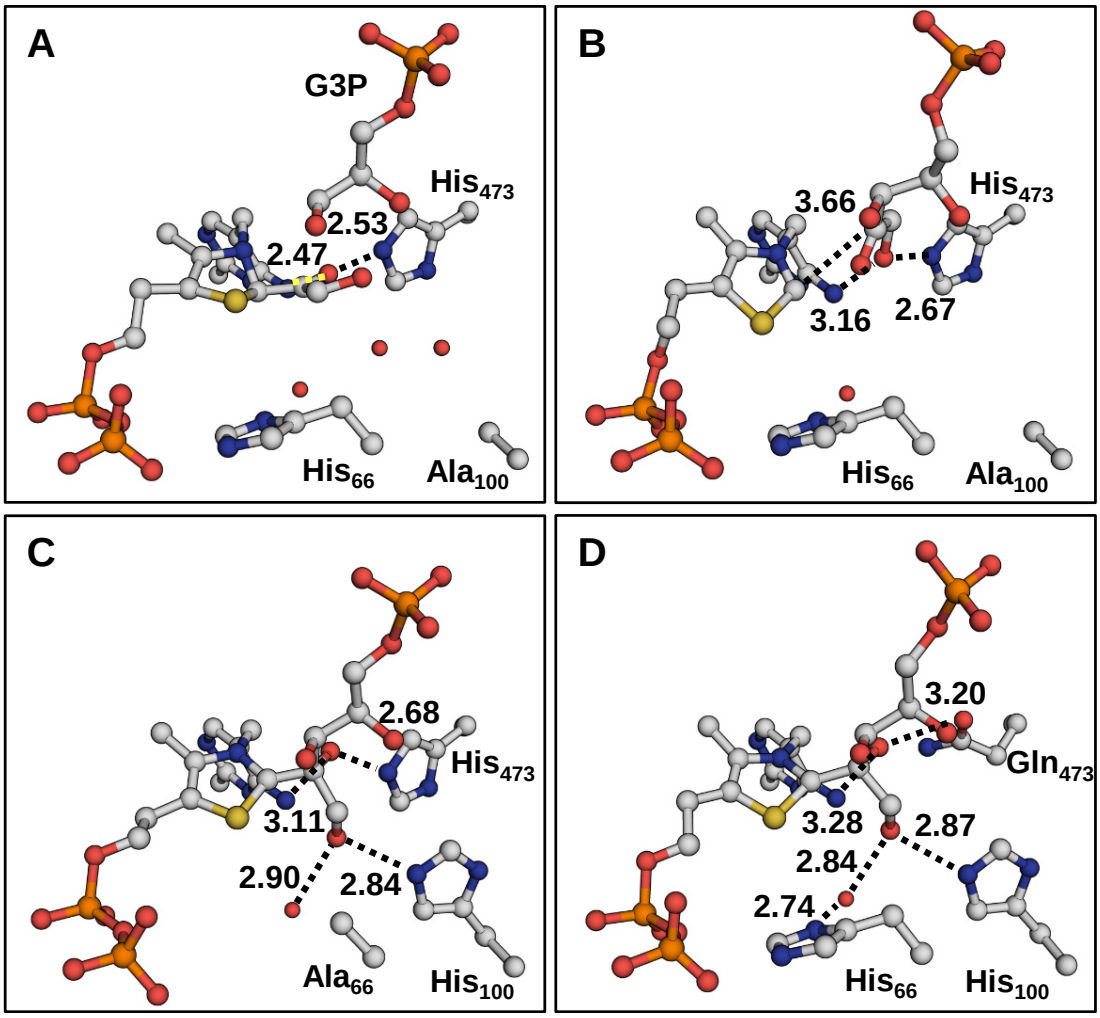

Figure 35. Crystal structures of *Ec*TK$^{AKD}_{H100A}$ (A), *Ec*TK$_{H100A}$ (B), *Ec*TK$_{H66A}$ (C) and *Ec*TK$_{H473Q}$ (D) soaked with X5P. The intermediates, non-covalently bound sugars and amino acids interacting with O1 and O2 of the intermediates are shown. The interaction distances are given in Å.

showed depletion of a broad band with a local minimum around 320 nm, most probably the AP-band, but no formation of the IP-band, as was seemingly observed at the lower F6P concentrations (Fig. 68, Appendix).

To obtain structural information, crystallization was successfully attempted for all variants. Of *Ec*TK$_{H100A}$, a dataset of a crystal soaked with X5P was collected during the diploma thesis of Ann-Kristin Diederich, but not thoroughly refined (Diederichs, 2009). The final refinements were performed during this thesis (1.73 Å, R_{work} = 14.7 %, R_{free} = 17.3 %). This structure will from here on be referenced as *Ec*TK$^{AKD}_{H100A}$. The space group of the crystal diverged from the commonly observed $P2_12_12_1$, it crystallized in $P2_1$. The

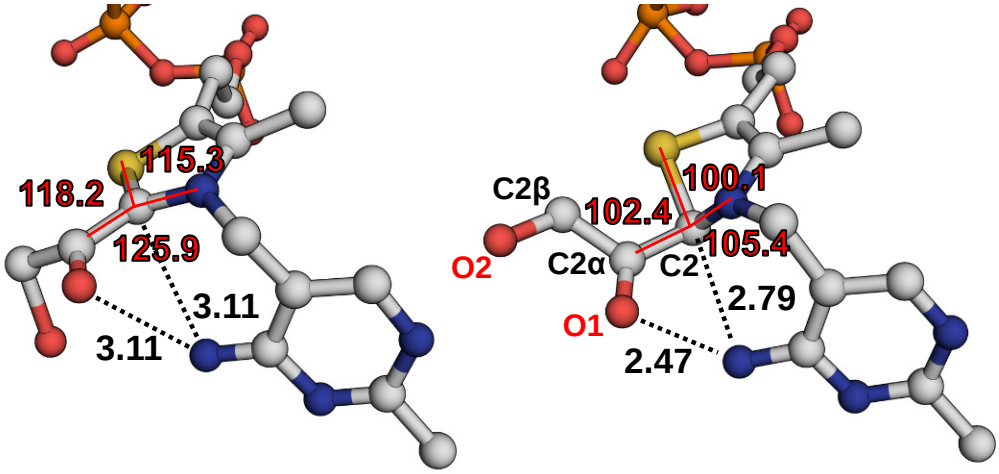

Figure 36. Comparison of *Ec*TK$_{WT}$ (left) and *Ec*TK$^{AKD}_{H100A}$ (right). The angles between the respective substituents are shown in red. The distances in Å to the N4′ are shown in black. Important atoms are labeled according to the nomenclature employed in the text (Data for *Ec*TK$_{WT}$ taken from Lüdtke, 2012).

cleavage observed by NMR was also present *in crystallo*, ThDP being present as the C2-adduct dihydroxyethyl-thiamine diphosphate, with density for the cleaved G3P being present at the phosphate binding site (Fig. 72 C, Appendix). The adduct itself shows a clear displacement of the C2 relative to structures of *Ec*TK$_{WT}$ with the DHEThDP intermediate (Lüdtke, 2012). While in *Ec*TK$_{WT}$ the intermediate is nearly planar with slight distortions, in *Ec*TK$^{AKD}_{H100A}$ the C2 is clearly displaced out of the thiazolium plane, by about 0.35 Å. In addition, the geometry of the C2 in *Ec*TK$_{WT}$ is trigonal, with substituent angles around 120 °. The geometry of the C2 in *Ec*TK$^{AKD}_{H100A}$ is more tetrahedral in character, with angles between 100 ° and 105 °. The distances between N4′ of the aminopyrimidine and C2 of the thiazolium, as well as the O1 of the dihydroxyethyl-moiety are significantly decreased in *Ec*TK$^{AKD}_{H100A}$. In *Ec*TK$_{WT}$, both of them are 3.11 Å, while in the variant they are decreased to 2.47 Å for N4′-O1 and 2.79 Å for N4′-C2 (Fig. 36). The intermediate itself only exhibits clear electron density around the C2α and O1 of the dihydroxyethyl, C2β and O2 do not exhibit clear densities (Fig. 72C, Appendix).

Datasets of the variants *Ec*TK$_{H66A}$ (1.09 Å, R_{work} = 11.3 %, R_{free} = 13.1 %), *Ec*TK$_{H473Q}$ (1.5 Å, R_{work} = 16.7 %, R_{free} = 19.6 %) as well as an additional dataset of *Ec*TK$_{H100A}$ (1.15 Å, R_{work} = 11.9 %, R_{free} = 13.7 %) soaked with X5P were collected. The datasets obtained for *Ec*TK$_{H66A}$ and *Ec*TK$_{H473Q}$ revealed normal formation of the tetrahedral

X5P-intermediate, with minimal changes in geometry compared to *Ec*TK$_{WT}$. In the structure of *Ec*TK$_{H100A}$, this time crystallized in space group $P2_12_12_1$, X5P did not bind to ThDP, despite soaking for 5 minutes, but remained in the docking site (Fig. 35). The interaction distances of X5P and the protein environment in *Ec*TK$_{H100A}$ are shown in table 13. Crystals of *Ec*TK$_{H66A}$ and *Ec*TK$_{H473Q}$ soaked with the artificial substrate HPA to generate the DHEThDP intermediate showed formation of normal, planar DHEThDP, as observed in *Ec*TK$_{WT}$ (Fig. 71, Appendix).

An interesting feature observed in a structure of *Ec*TK$_{H66A}$ in the resting state was the presence of only one conformation not corresponding to either up- or down-conformation, as observed in *Ec*TK$_{WT}$ (Fig. 69, Appendix). Furthermore, similar to *Ec*TK$_{H261N}$, the removal of His$_{66}$ induces disorder in the region around His$_{261}$. Interestingly, His$_{26}$ adopts a conformation which is in hydrogen-bonding distance to the β-phosphate of the diphosphate moiety, with a distribution of 76 % in the new conformation and 24 % in the standard conformation (Fig. 70, Appendix).

3.5.2 Pyruvate oxidase

Variants of *Lp*POX displayed significantly reduced reactivities for both macro- and microscopic rates compared to *Lp*POX$_{WT}$ (data for *Lp*POX$_{WT}$ taken from Meyer, 2008 and provided Lisa-Marie Funk). In the steady-state assay, the k_{cat} of *Lp*POX$_{Q122H}$ decreased by over 99 % to 0.27 $\pm$ 0.01 s^{-1}, compared to 41 s^{-1} for *Lp*POX$_{WT}$. The K_M increased to 13.9 $\pm$ 1.5 mM, corresponding to a decrease of apparent affinity by over 90 %, compared to 1.3 $\pm$ 0.2 in *Lp*POX$_{WT}$. In *Lp*POX$_{E483I}$, a reduction of the reaction velocity could be observed at pyruvate concentrations higher than 25 mM. Thus, it was fitted according to equation 3, which describes substrate excess inhibition. The k_{cat} of this variant was reduced to 4.12 $\pm$0.07 s^{-1}, a decrease by 90 %. The K_M was not as strongly affected, it increased by 46 % to 1.9 $\pm$ 0.1 mM. The apparent K_I obtained from the fit according to substrate excess inhibition was 309 $\pm$ 39 mM (Fig. 37).

Using the cofactor FAD as probe for electron transfer velocities in presence and absence of the native electron acceptor oxygen revealed further differences. In the presence of

oxygen, a short steady state can be observed where the rate of reduction is equal to the rate of oxidation. In the exemplary traces shown here, at 50 mM pyruvate, this state began at around 0.02 seconds in *Lp*POX$_{WT}$, and continued for about 0.04 seconds. The average ratio of oxidized to reduced FAD during this time was 55 %, and full reduction was achieved after approximately 2.14 seconds (data provided by Lisa-Marie Funk). For *Lp*POX$_{Q122H}$, the steady state began only after about 3.5 seconds, lasting for approx. 7.5 seconds, at an oxidation/reduction ratio of 0.98, and full reduction was achieved after approximately 500 seconds. Thus, it is significantly slower than *Lp*POX$_{WT}$. In *Lp*POX$_{E483I}$, the effects were less pronounced. The steady state began after 0.04 seconds and lasted for 0.55 seconds, at a ratio of 0.56 of oxidized to reduced FAD. Full reduction was achieved after 2.7 seconds (Fig. 38).

In the absence of oxygen, only one cycle of electron transfers per catalytic subunit takes place. As such, measurement of FAD reduction provides a compound rate for substrate binding, decarboxylation, as well as the two electron transfers, one of them induced by attack of phosphate. This rate was reduced by over 99 % in *Lp*POX$_{Q122H}$ compared to *Lp*POX$_{WT}$, dropping from 137.2 s^{-1} to 1 s^{-1}. The apparent K_D obtained from this measurement increased 2.3-fold, from 2.6 $\pm$ 0.07 mM to 6 $\pm$ 0.3 mM. A sigmoid

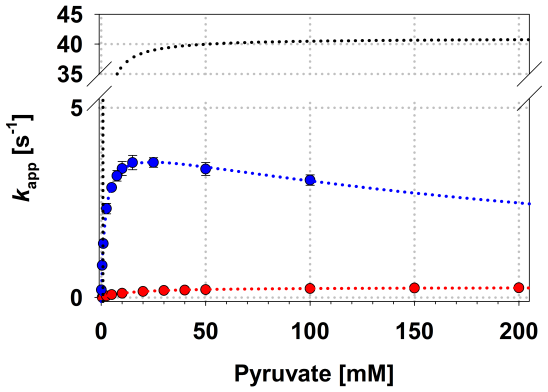

Variant	k_{cat} [s^{-1}]	K_M [mM]	K_I [mM]
*Lp*POX$_{WT}$	41 $\pm$ nd	1.3 $\pm$ 0.2	nd
*Lp*POX$_{Q122H}$	0.27 $\pm$ 0.01	13.9 $\pm$ 1.5	nd
*Lp*POX$_{E483I}$	4.12 $\pm$ 0.07	1.9 $\pm$ 0.1	309 $\pm$ 39

Figure 37. Steady state kinetics of *Lp*POX$_{Q122H}$ (red), *Lp*POX$_{E483I}$ (blue) and *Lp*POX$_{WT}$ (black). The assay was performed as described before (Section 2.2.3.1). The measured triplicates are displayed including error bars. The data for *Lp*POX$_{Q122H}$ were fitted according to equation 1, those for *Lp*POX$_{E483I}$ according to equation 3. The table displays the numerical values obtained for k_{cat}, K_M and K_I. The data for *Lp*POX$_{WT}$ were taken from Meyer, 2008.

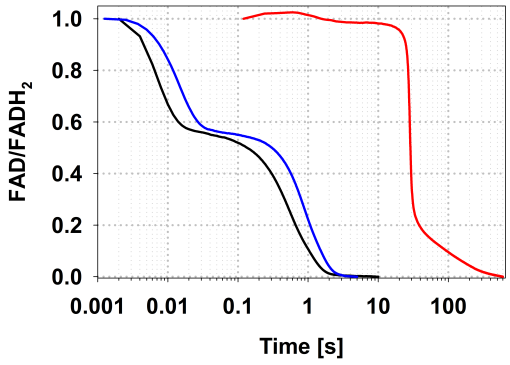

Variant	t_0^{ss} [s]	$\frac{FAD}{FADH_2}$ [%]	t_t^{ss} [s]	t_{red} [s]
*Lp*POX$_{WT}$	0.02	0.55	0.04	2.14
*Lp*POX$_{Q122H}$	3.50	0.98	7.50	approx. 500
*Lp*POX$_{E483I}$	0.04	0.56	0.055	2.7

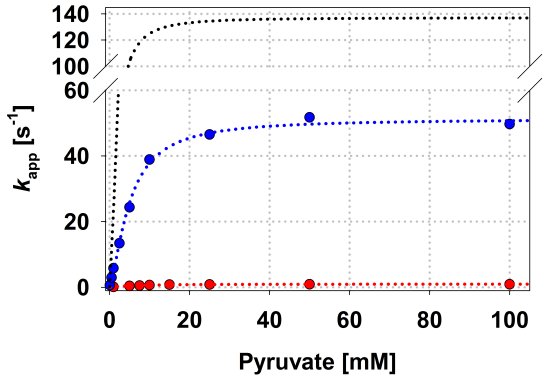

Variant	k_{max} [s^{-1}]	K_D [mM]	n
*Lp*POX$_{WT}$	137.2 ± 1.3	2.60 ± 0.07	1.72 ± 0.07
*Lp*POX$_{Q122H}$	1 ± 0.0	6 ± 0.3	1.35 ± 0.1
*Lp*POX$_{E483I}$	51.3 ± 0.5	5.0 ± 0.1	1.47 ± 0.05

Figure 38. (Top) Stopped flow traces of *Lp*POX$_{Q122H}$ (red), *Lp*POX$_{E483I}$ (blue) and *Lp*POX$_{WT}$ (black) in the presence of oxygen at 50 mM pyruvate. The traces are averages of at least three individual measurements. The rate of oxidized to reduced FAD is shown as a function of time. The table displays the numerical values obtained for the approximate start of the steady state t_0^{ss}, the average reduction level of FAD during the steady state $\frac{FAD}{FADH_2}$, the approximate duration of the steady state t_t^{ss} and the total time till full reduction of FAD t_{red}. The data for *Lp*POX$_{WT}$ were kindly provided by Lisa-Marie Funk. **(Bottom) Plot of the reduction rate of *Lp*POX$_{Q122H}$ (red), *Lp*POX$_{E483I}$ (blue) and *Lp*POX$_{WT}$ (black) in the absence of oxygen versus the pyruvate concentration.** The averages of at least three measurements are shown for each concentration. The data were fitted according to the sigmoid Hill-equation 7. The table displays the values of the obtained maximal reduction velocity k_{max}, the apparent K_D for pyruvate and the Hill-coefficient n. The data for *Lp*POX$_{WT}$ were kindly provided by Lisa-Marie Funk.

tendency was observed with an Hill-factor of 1.35 ± 0.1, compared to 1.72 ± 0.07 for *Lp*POX$_{WT}$. As before, *Lp*POX$_{E483I}$ showed less impairment. The maximal reduction rate dropped by 63 % to 51.3 ± 0.5 s^{-1}, and the K_D increased 1.9-fold to 5 ± 0.1 mM. The Hill-factor for this variant was 1.47 ± 0.05 (Fig. 38).

Like *Ec*TK, *Lp*POX displays charge-transfer bands correlated to the presence of the

imino- and aminopyrimidine species of the aminopyrimidine ring. Titrating phosphate to the enzyme causes disappearance of these bands as the protonated, signatureless aminopyrimidinium species is populated. This relation can be used to gauge the affinity of *Lp*POX for the second substrate phosphate. As this measurement requires phosphate-free buffer, some variants are unstable and become prone to aggregation. Thus, only data for *Lp*POX$_{E483I}$ could be obtained.

The apparent K_D, as observed by fitting the buffer and dilution corrected CD-signals at 333 nm at different phosphate concentrations according to equation 10 was 5.1 $\pm$ 0.6 mM (Fig. 73, Appendix). This is a significant increase in the apparent affinity for phosphate in the variant, by 5.2-fold, compared to 26.7 $\pm$ 0.3 mM in *Lp*POX$_{WT}$ (Meyer, 2008). The change in intensity for the FAD-signals is prevalent in all measurements, even with *Lp*POX$_{WT}$ (data not shown), and is probably a result of the changing buffer conditions.

Using the artificial substrate methylacetylphosphonate, the stable lactyl-thiamine diphosphate analogue phosphonolactyl-thiamine diphosphate can be generated, giving information on the velocities of substrate binding and formation of the pre-decarboxylation intermediate. Over the range of technically feasible concentrations, no saturation could be observed, the dependency of the rate of phosphonolactyl-thiamine diphosphate (PLThDP) formation on MAP concentration behaved linear. As such, the data were fitted according to the linear equation 12. This yielded an apparent rate of intermediate formation of 0.0017 $\pm$ 0.0006 s^{-1} *f*or *Lp*POX$_{Q122H}$, a reduction of over 99.9 % compared to 1.73 $\pm$ 0.33 s^{-1} in *Lp*POX$_{WT}$ (Provided by Lisa-Marie Funk). In *Lp*POX$_{E483I}$, the rate was reduced to 0.077 $\pm$ 0.001 s^{-1}, which corresponds to a decrease of over 95 %. The rate k_{off} for depletion of PLThDP could only be estimated with great error. It was reduced in the variants as well, but disproportionately to k_{on}. While in *Lp*POX$_{WT}$ it was 0.14 $\pm$ 0.46 s^{-1}, corresponding to approximately 10 % of k_{on}, in *Lp*POX$_{Q122H}$ it was 0.0014 $\pm$0.0012 s^{-1}, which is around 80 % of k_{on}. In *Lp*POX$_{E483I}$, it was 0.022 $\pm$ 0.02 s^{-1}, corresponding to approximately 30 % (Fig. 39).

Unfortunately, crystallization of the variants was not successful. Therefore, no structural

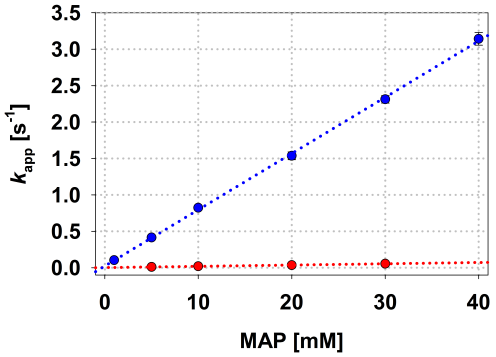

Variant	k_{on} [$mM^{-1}s^{-1}$]	k_{off} [s^{-1}]
*Lp*POX$_{WT}$	1.73 ± 0.33	0.14 ± 0.46
*Lp*POX$_{Q122H}$	0.0017 ± 0.0006	0.0014 ± 0.0012
*Lp*POX$_{E483I}$	0.077 ± 0.001	0.022 ± 0.02

Figure 39. Kinetics of PLThDP formation in *Lp*POX$_{Q122H}$ and *Lp*POX$_{E483I}$. *Lp*POX$_{Q122H}$ is shown in red, *Lp*POX$_{E483I}$ in blue. The values obtained for k_{on} and the off-rate k_{off} are given, as obtained from fitting according to the linear equation 12. *Lp*POX$_{WT}$ data were provided by Lisa-Marie Funk.

data is available to help interpret the kinetic data obtained.

In summary, these studies supported the significance of the histidines 66, 100 and 473 of *Ec*TK for substrate binding. Furthermore, a crystallographic dataset collected by Ann-Kristin Diederich and further refined during this work revealed the formation of a non-canonical intermediate in *Ec*TK$_{H100A}$. This intermediate, obtained after soaking with X5P, exhibited a broken aromaticity of the thiazolium ring, with a strong tetrahedral character of the C2, and cleaved Ga3P in the active site. The structures of *Ec*TK$_{H66A}$ and *Ec*TK$_{H473Q}$ soaked with X5P and HPA revealed classical geometries for both the tetrahedral sugar-ThDP intermediate, as well as for DHEThDP. The resting state structure of *Ec*TK$_{H66A}$ showed no presence of the distinct up- and down-conformation, only one conformation was present.

In *Lp*POX, mutagenesis of Gln$_{122}$ and Glu$_{483}$ further underpinned their importance for catalysis, especially of Gln$_{122}$, but the lack of structural data will complicate any interpretation regarding the character of the HEThDP intermediate.

3.6 Transketolase Structures in Ground- and Substrate Bound State at Atomic Resolution

To further the understanding of the individual contributions of amino acids in the active site, as well as of the general catalytic mechanism of *Ec*TK, crystallization of *Ec*TK_{WT} was performed. Structural data of different crystals of resting state *Ec*TK_{WT} at true atomic resolution could be obtained (Dataset 1: 1.00 Å, R_{work} = 10.7 %, R_{free}= 12.4 %); Dataset 2: 0.97 Å, R_{work} = 10.3 %, R_{free}= 11.1 %). The most notable feature in both structures was the negative mFo-DFc density at the C2 position of both conformations of ThDP, while for S1 both up and down conformation were clearly visible. Occupancy refinement assigned 44 % to the up and 52 % to the down conformer, indicating only 96 % occupancy for the cofactor (Fig. 74, Appendix). The lacking density at C2 was confirmed not to be radiation damage by collection of a dataset at the sealed tube MicroMax™ system of the Department of Molecular Structural Biology, Göttingen.
Another notable observation is the presence of two deviations at the Cβ of Phe_{437} of each monomer of 0.28 Å, an indicator for strain. The side chain of Phe_{437} is located atop the aminopyrimidine moiety of ThDP in face-to-face geometry, in a distance of

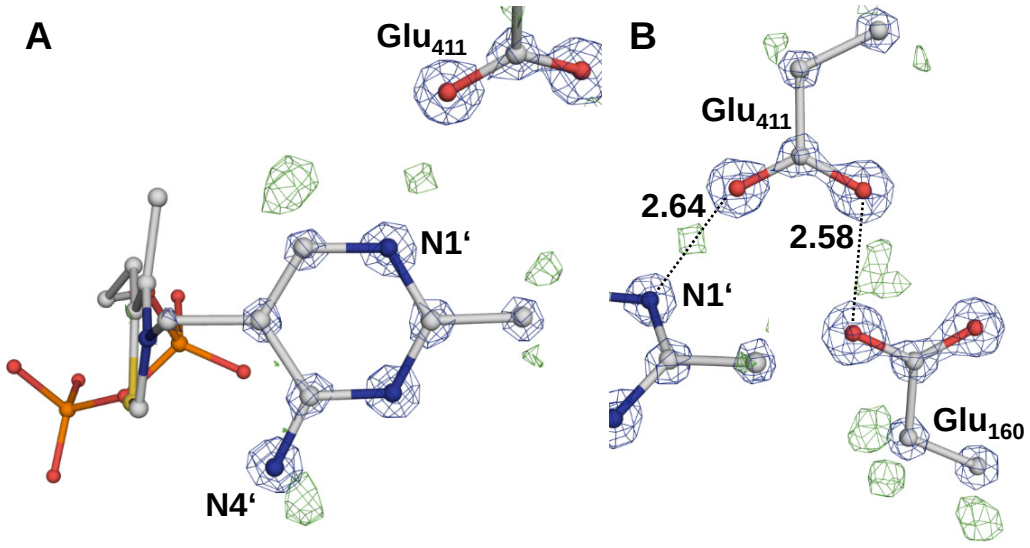

Figure 40. Protonation of ThDP (A) and Glu_{411} (B) in resting state *Ec*TK_{WT}. The 2mFo-DFc density is contoured at 4 σ, the mFo-DFc density at 2.5 σ. The hydrogen-omit map was generated by running 0 cycles of *PHENIX.REFINE* after removal of riding hydrogens from the pdb file. For ThDP, only the density of the aminopyrimidine ring is shown.

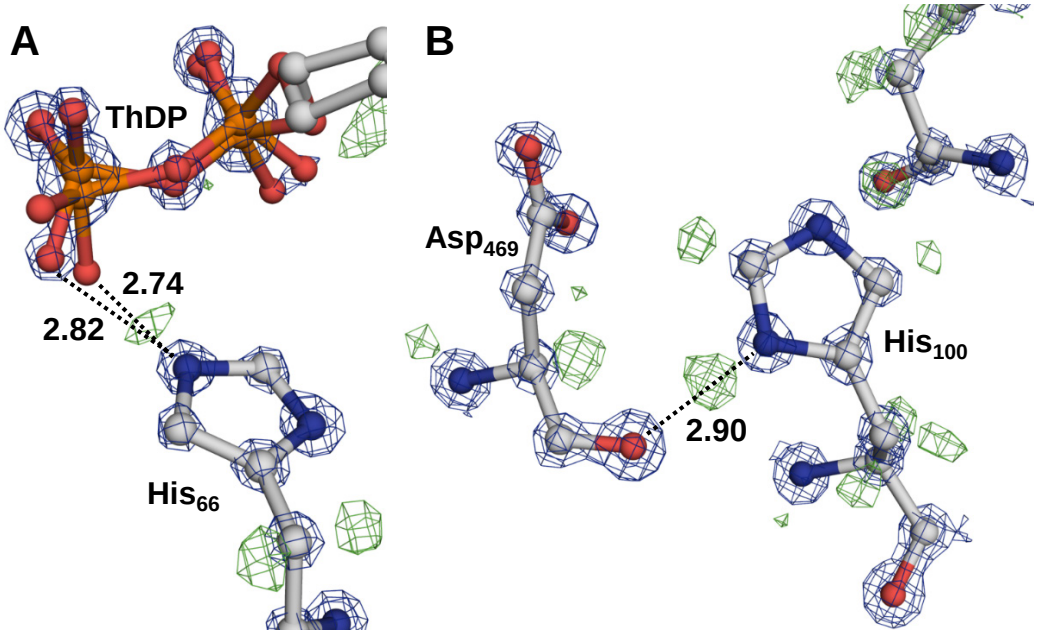

Figure 41. Protonation of His_{66} and His_{100} in resting state *Ec*TK_{WT}. The 2mFo-DFc density is contoured at 3.5 σ, the mFo-DFc density at 2.5 σ. The hydrogen-omit map was generated by running 0 cycles of *PHENIX.REFINE* after removal of riding hydrogens from the pdb file. For ThDP. Image A was generated using dataset 1, image B using dataset 2.

approximately 3.5 Å (Fig. 75, Appendix). Investigation of anisotropies of residues in the active site supported a prior finding of high anisotropies in His_{473}, along the bond-axis, interpreted as histidine flipping (Fig. 76, Appendix) (Neumann and Tittmann, 2014). Further residues displaying comparatively high anisotropy were His_{461}, as well as the arginines 358 and 520, which are involved in substrate binding.

The quality of these datasets allowed the observation of hydrogen atoms. It was possible to assign the species of the cofactor to the iminopyrimidine form by observing the protonation state of N1′ and N4′ of ThDP in dataset 1. Both of them seem to harbor one hydrogen, as shown in figure 40A.

Despite the visibility of hydrogens in the solvent-isolated parts of the enzyme, only few could be assigned in the solvent-accessible active site, namely at His_{66} in dataset 1 and at His_{100} in dataset 2. Both of them donate their hydrogen atom to a hydrogen bond, His_{66} to the β-phosphate of ThDP and His_{100} to the backbone oxygen of Asp_{469}.

Three datasets of individual *Ec*TK_{WT} crystals soaked with substrate X5P were collected. Dataset 1 was recorded at the DESY, to a resolution of 0.97 Å (R_{work} = 11.1 %, R_{free}=

12.5 %), dataset 2 was recorded at the Department of Molecular Structural Biology, Göttingen, to a resolution of 1.3 Å (R_{work} = 13.4 %, R_{free}= 16.1 %) and dataset 3 at the DESY, to a resolution of 1.04 Å (R_{work} = 12.4 %, R_{free}= 14.1 %). Interestingly, only low amounts of covalent adduct were present among all structures. Instead, they revealed a number of states between docking site-bound X5P and covalent, tetrahedral X5P-ThDP. The positive mFo-DFc density observed in the active site of dataset 1 was interpreted as X5P in the docking site (Con_1) with an occupancy of 38 % and the pre-covalent intermediate (Con_2) at an occupancy of 56 %. The interaction distances both conformations are given in table 13 (Appendix). For $Conf_1$, notable interactions are these of X5P-1-OH with His_{473}, with a very short 2.41 Å, and of the phosphate group with Ser_{385} at 2.55 Å. The X5P-C2 ThDP-C2 distance is $\geq$ 3.5 Å. In comparison, in Con_2 it moves closer towards the ThDP-C2, reducing this distance to 2.52 Å, in clash-distance. Furthermore, the C1-C2 axis of X5P rotates by approximately 150 °, inverting the orientation of 1- and 2-OH.

This turn allows interaction of the 1-OH with His_{100} at 2.85 Å, and interaction of 2-OH with His_{473}, at 2.86 Å. Furthermore, it brings the 3-OH in closer proximity of His_{26} and His_{261}, reducing the distances from 3.04 and 3.10 to 2.87 and 2.88 Å respectively, compared to Con_1. The movement brings the 4-OH closer to Asp_{469}, reducing the distance from 2.68 to 2.55 Å, while increasing the distance to His_{26} from 2.97 to 3.10 Å. Additionally, interactions with the two conformations of Ser_{385} are inverted. Con_1 interacts more closely with the first conformation, 2.55 compared to 2.74 Å, while the interaction of Con_2 is tighter to the second conformation, 2.73 compared to 2.49 Å. In addition, the interaction distance of phosphate and Arg_{520} decreases from 2.89 to 2.66 Å.

Dataset 2 was initially recorded at the sealed tube-system of the Department of Molecular Structural Biology to verify whether the presence of negative mFo-DFc density at the position of the thiazolium-C2 was caused by radiation damage. As similar effects were observed in this dataset, this was ruled out as cause. The positive mFo-DFc density observed in the active site in this dataset was interpreted as a single conformation of X5P, similar to $Conf_2$ of dataset 1, a post-turn, pre-covalent intermediate (Fig. 43). The

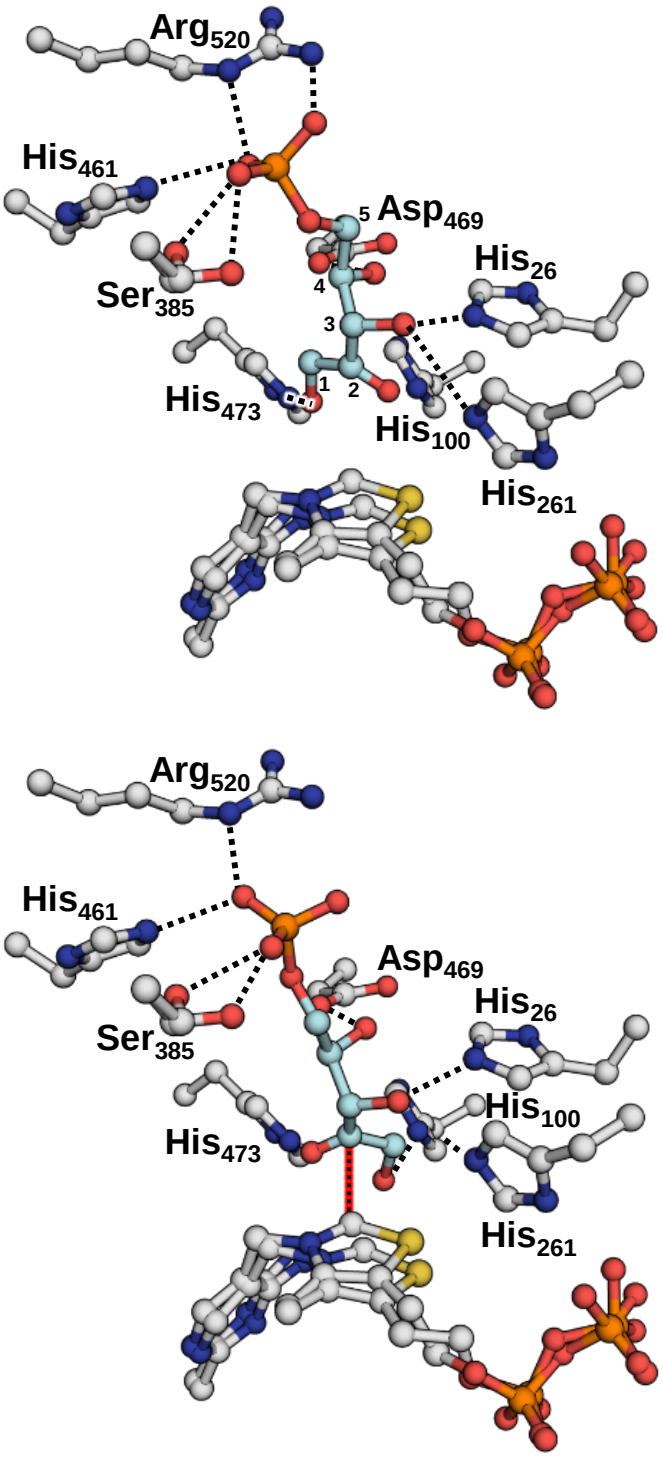

Figure 42. Coordination of X5P conformation 1 (top) and conformation 2 (bottom) in dataset 1. X5P is colored cyan, the interactions of the OH-groups to the respective partners are indicated. The clashing X5P-C2-ThDP-C2 distance is indicated in red. The X5P-carbon atoms are numbered according to the nomenclature used in this work.

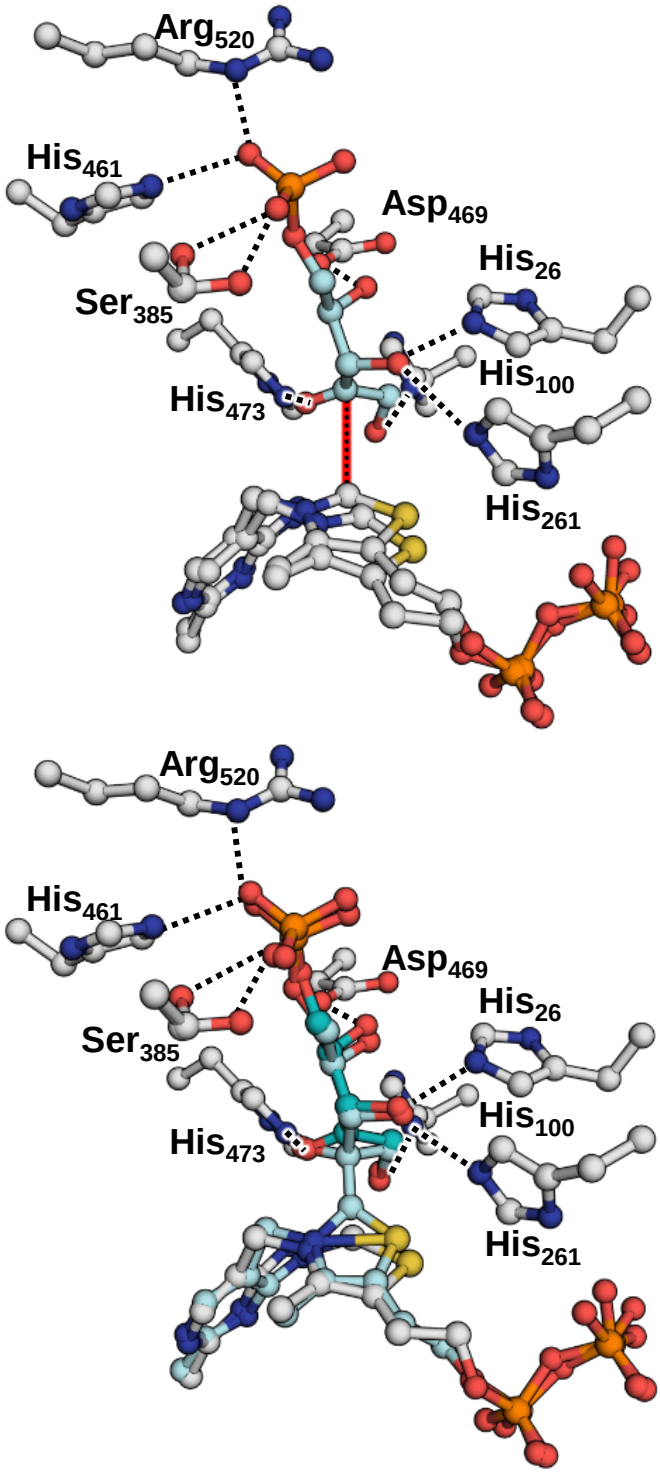

Figure 43. Coordination of X5P in dataset 2 (top) and dataset 3 (bottom). X5P and X5P-ThDP are colored cyan, the interactions of the OH-groups to the respective partners are indicated. The clashing X5P-C2-ThDP-C2 distance in dataset 2 is indicated in red.

interaction distances of the OH-groups were similar to these observed in dataset 2 (Table 13, Appendix).

In dataset 3, the mFo-DFc density was interpreted as X5P in the Michaelis-complex in short distance to ThDP (Con_1, 38 %), and the covalent, tetrahedral X5P-ThDP adduct (Con_2, 47 %) (Fig. 43). The main difference between the two conformations is the obvious reduction of the sugar-C2 to thiazolium-C2 distance from 2.90, a VDW-clashing distance, to 1.50 Å, corresponding to a covalent bond. The formation of the covalent bond is accompanied by a movement of the whole X5P, resulting in a change of interactions with the protein environment (Table 13, Appendix). The most important changes during this step are the reduction of the distance of the 3-OH to His_{26} and His_{261} from 2.94 and 2.90 to 2.90 and 2.80 Å, respectively. Furthermore, the 2-O group is brought in a distance of 3.09 Å from the N4′ of the aminopyrimidine moiety. Also, the bond length of the X5P C2-C3 bond increases from 1.53 to 1.66 Å in Con_2, as the C2-O bond length increases from 1.22 to 1.42 Å. The anisotropy of both conformations overlaps with the atom positions of the other conformation, respectively (Fig. 77, Appendix). The omit maps for the non-covalent and covalent intermediates of all three datasets are shown in figure 78 A-C, in the appendix.

Further, crystallization with acceptor substrate R5P in the active site was successful (1.03 Å, R_{work} = 11.5 %, R_{free}= 12.6 %). The mFo-DFc density observed was interpreted as being dominantly the acyclic form of R5P ($R5P_{ac}$). Possible residual density for the cyclic form was observed ($R5P_c$)(Fig. 78 D, Appendix). Refinement resulted in a distribution of 63 % acyclic to 30 % cyclic form. This is opposed to the previous observation of dominantly circular R5P *in crystallo* (Asztalos, 2008). The R5P-C1-ThDP-C2 distance for $R5P_{ac}$ is 1.56 Å, indicating a covalent bond between the two. A water molecule occupies the position otherwise taken by the C2-OH of ketose donor-substrates. The interactions with the protein of both forms are different. The 1-OH of $R5P_{ac}$ is interacting with His_{473}, at 2.72 Å. In $R5P_c$, the 1-OH is not coordinated by the enzyme. The 2-OH of both forms interacts with His_{26} and His_{261}, at distances of 3.00 and 2.74 Å in $R5P_{ac}$ and 2.97 and 3.01 Å in $R5P_c$, respectively. The 3-OH is interacting

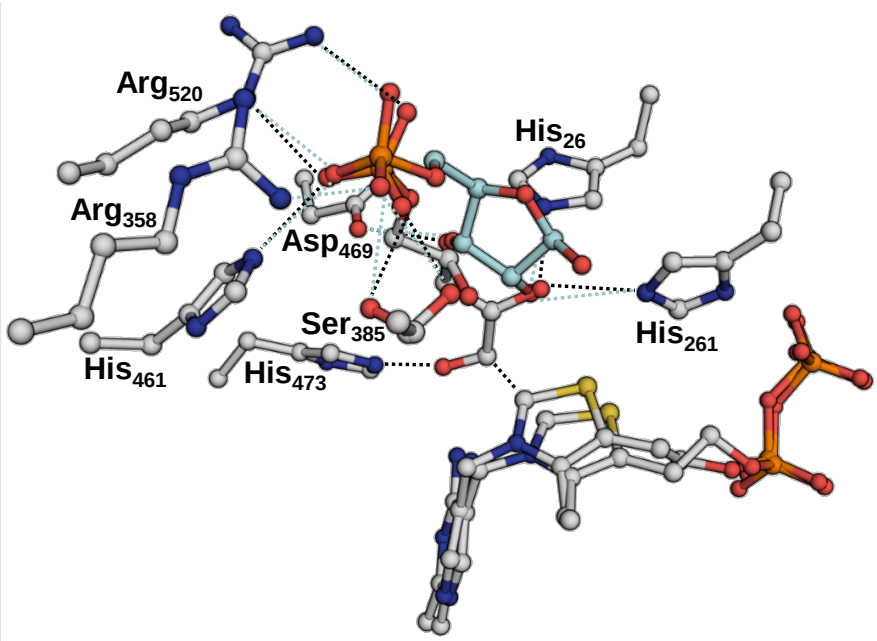

Figure 44. Coordination of linear and cyclic ribose 5-phosphate in *Ec*TK$_{WT}$. The cyclic and acyclic form of R5P are shown with their respective interaction partners in hydrogen bonding distance The interactions for the cyclic form are shown in cyan, those for the acyclic form in black.

with His_{26} and Asp_{469} in $R5P_{ac}$ (2.99 and 2.57 Å) and $R5P_c$ (2.99 and 2.83 Å). The 4-OH of $R5P_{ac}$ is uncoordinated by the protein environment, while in $R5P_c$ it forms the ether of the furanose-hemiacetal. The phosphate groups of both forms interact with Ser_{385}, His_{461} and Arg_{520}, and $R5P_c$ further interacts with Arg_{358}.

To summarize, it was possible to obtain datasets of *Ec*TK$_{WT}$ with the donor substrate X5P at different positions along the trajectory from docking site to covalent adduct. This possibly allows to trace the interactions responsible for the proper guidance of X5P to ThDP. In addition, *Ec*TK$_{WT}$ was crystallized with the acceptor substrate R5P in the active site, dominantly in the acyclic conformation. The changing interactions between the cyclic and acyclic form may give insight into the speculated ring-opening catalyzed by *Ec*TK.

4 Discussion

4.1 The Impact of the Non-Active-Site, Conserved Residues Glu_{160}, Glu_{165} and Thr_{433} in *Escherichia coli* Transketolase

The residues Glu_{160}, Glu_{165} and Thr_{433} are strictly conserved in all transketolases, as revealed by alignment of all published transketolase structures (Fig. 53, Appendix).

Early studies in *Saccharoymces cerevisae* transketolase implicated Glu_{160} in binding of ThDP and/or dimerization, and proposed a possible channel between the two active sites, comprised of αThDP-βE411-αE160-H_2O-βE165-2 H_2O-αE165-H_2O-βE160-αE411-βThDP (Meshalkina *et al.*, 1997). More recent work gave the idea that communication channels could be common in ThDP-dependent enzymes (Frank *et al.*, 2004; Nemeria *et al.*, 2010; Schröder-Tittmann *et al.*, 2013; Neumann and Tittmann, 2014).

However, the data obtained in this study, while not ruling out this assumption do not explicitly support it. The only result hinting towards any kind of cooperativity are the rate constants of 4′-aminopyrimidine-band (AP) formation depending on the concentration of ThDP, where Hill-factors over 1 were observed for the first phase. However, as these are still 1.3 in the variants, compared to 1.5 in *Ec*TK_{WT}, it seems like interaction of the assumed cooperation partners still takes place (Fig. 14, Section 3.1). While it is a noteworthy fact that the midpoint water of the speculated channel is differently placed in *Ec*TK_{E160A}, it is most probably not the cause of the observed differences between the variants. As the exchange of Glu_{160} causes rearrangements along its interaction partners, a slight reorientation of Glu_{165}, which directly interacts with the water, takes place. This changes the ground state distribution of the midpoint water (Fig. 60, Appendix).

Still, these positions must be important for transketolases *in vivo*, or else there would be variances between species, returning to the idea of ThDP binding and dimerization. The slow ThDP binding or dimerization observed in *Sc*TK under turnover conditions can also be found in *Ec*TK_{E160Q} (Fig. 59, Appendix), as shown by comparison of ThDP-binding in *Ec*TK_{WT} and *Ec*TK_{E160Q} by steady-state assay. This assay revealed a lower affinity (2.2

μM vs 5.4 μM) and slower binding of the cofactor in *Ec*TK$_{E160Q}$ (Fig. 16). In *E. coli* the intracellular concentration of free ThDP is exceedingly high, around 250 μM, mirroring the conditions in the steady-state assay (Gigliobianco *et al.*, 2013). Even at these high concentrations of ThDP, at high X5P concentrations there is a lag phase observable in *Ec*TK$_{WT}$ and *Ec*TK$_{E160Q}$. This phase is more pronounced in *Ec*TK$_{E160Q}$, as it takes longer to reach full activity than in *Ec*TK$_{WT}$ and the relative increase from initial to full activity is twice as high as in *Ec*TK$_{WT}$.

This is further supported by the 50 % reduction of the AP-formation rate indicative for ThDP-binding, as observed by stopped-flow spectroscopy, in *Ec*TK$_{E160Q}$ compared to *Ec*TK$_{WT}$. The effect is not as pronounced in *Ec*TK$_{E160A}$, with only 10 % reduction (Fig. 16, Section 3.1). As most species exhibit concentrations of free ThDP that are ten- to hundredfold lower than in *E. coli*, changes in the affinity towards ThDP could have severe impacts (Makarchikov *et al.*, 2003).

Furthermore, in the pre-steady state, for the depletion of the AP-band, both k_{on} and k_{off} are reduced in the variants by up to 60 %, indicating a reduction of the rate by which the tautomerization reactions at the aminopyrimidine moiety take place. Formation of the tetrahedral intermediate, which requires a proton from the aminopyrimidine moiety, at this stage the 4′-aminopyrimidinium species (APH$^+$), is also slowed down by 25-30 % (Fig. 15, Section 3.1). Additionally, reduced rates of enamine formation from β-hydroxypyruvate(HPA) by 10 % in *Ec*TK$_{E160Q}$ and 80 % in *Ec*TK$_{E160A}$ also hint towards a disturbance of the proton transfers involved in ThDP-activation and formation of the tetrahedral β-hydroxy-LThDP.

The steady-state assay supports this assumption. *Ec*TK$_{E160A}$ shows a 30 % reduction in k_{cat}, and an increase in apparent affinity to a K_M of 0.26 mM from 0.37 mM, which fits to the data obtained for *Sc*TK (Meshalkina *et al.*, 1997). *Ec*TK$_{E160Q}$ actually exhibits a 25 % higher k_{cat} than *Ec*TK$_{WT}$, but the K_M is also doubled to 0.73 mM (Fig. 13, Section 3.1).

The pH-titration results are not that clear, as it seems like ThDP-binding is also affected by pH-value (data not shown), thus formation of the AP-band and binding can not be

clearly separated at low pH-values. As *Ec*TK_{WT} shows onset of the AP-band at least 0.4 pH units earlier than the variants, there is definitely an effect of the substitutions close to Glu_{411} on the ground-state equilibrium. Experiments on *Ec*TK_{E411Q} showed that substitution of Glu_{411} by an isosteric amino acid without acid-base properties renders the proton relay inert against changes in solvent pH.

The pK_A-shifts, the reduced rates of formation of the tetrahedral intermediates with both X5P and HPA and the changed behavior in the steady-state assay suggest that Glu_{160} is a crucial component in controlling the pK_A of the Glu_{411}-ThDP proton relay. By this virtue it influences substrate- and cofactor affinities in the variants, as well as the velocities of the overall reaction and elementary steps.

This requirement of precise modulation of the pK_A value is prevalent in enzymes, as they do require a broad range of reactivities, stemming from only 6 amino acids with significant gaps between their respective pK_A values in solution (Harris and Turner, 2002). As such, it is necessary to adjust the pK_A of these reactive groups. There are several interaction types by which this can be achieved. Charge-charge interactions, in which two charged residues are in proximity to each other, is one of these principles. One example of this is RNase H1, where two negatively charged aspartates, trying to avoid same-charge repulsion, increase and decrease their pK_As from 4.0 to 6.1 and 2.6 (Oda *et al.*, 1994). A prominent example for the same feature with positive-charge repulsion is the 2-deoxyribose-5-phosphate aldolase DERA, where the pK_A of the Schiff base forming lysine is reduced by proximity of an additional lysine (Heine, 2001; Heine *et al.*, 2004). Of course, opposite charge interaction is possible too. In the cysteine proteases, the interaction of a cysteine-histidine pair decreases the pK_A of cysteine by up to 6 units (Pinitglang *et al.*, 1997).

The second kind of pK_A-modulating interactions are hydrogen bond interactions. One example are the serine proteases, in which an aspartate and a histidine temporarily form a bond with a distance of >2.65 Å, with an apparently shared hydrogen atom, a so called low barrier hydrogen bond (Cleland and Kreevoy, 1994; Cassidy *et al.*, 1997; Cleland *et al.*, 1998). However, these remain highly controversial, with contradicting

results claiming ionic bond character or simple short strong hydrogen bonds (Fuhrmann *et al.*, 2006). Regardless of this controversy, short bonds are common, as around 14 % of solved protein structures contain an inter-molecular hydrogen bond around 2.5 Å, some of them possibly low barrier hydrogen bonds (Lin *et al.*, 2017). Formation of a hydrogen bond is an energy gain of 1-3 $\frac{\text{kcal}}{\text{mol}}$ for normal hydrogen bonds or 7-20 $\frac{\text{kcal}}{\text{mol}}$ for the speculated low barrier hydrogen bond or short strong hydrogen bonds.

The last kind of pK_A modulation is desolvation. Situating a charged residue in an environment with a low dielectric constant, for example the hydrophobic cores of enzymes, increases the pK_A values of acidic amino acids while decreasing that of basic amino acids towards the uncharged state, as evidenced by model studies on staphylococcal nuclease (Stites *et al.*, 1991; Dwyer *et al.*, 2000). This effect that was also observed in the activation of ThDP-dependent enzymes (Jordan *et al.*, 1999).

The structures obtained for the variants may further clarify why these changes take place. In *Ec*TK$_{E160Q}$ the amide nitrogen of Gln$_{160}$ is oriented towards Glu$_{411}$ and the distance between the two is increased from a very short 2.57 Å to 2.83 Å, with the amide group having a pK_A of around 15. Calculations of the pK_A of Glu$_{160}$ in *Ec*TK$_{WT}$ using *PROPKA* resulted in a value of 15.2, which is similar to that of the glutamine amide in *Ec*TK$_{E160Q}$ (Dolinsky *et al.*, 2004). In *Ec*TK$_{E160A}$, the distance between the water occupying the position of the mutated glutamate and Glu$_{411}$ is only increased to 2.69 Å, with a changed angle. However, the p$K_A$of water in free solution is 15.7. As such, the geometry of the interaction of both variants with Glu$_{411}$ is markedly different than in *Ec*TK$_{WT}$, even though the pK_A values and the character as hydrogen-donor did not change much (Fig. 18, Section 3.1).

The importance of the well-tuned interactions of Glu$_{411}$ is further supported by the studies performed on variants of the conserved Thr$_{433}$. This threonine, at least in transketolases, is the closest interaction partner of the water flanking the activating glutamate in virtually all ThDP-dependent enzymes. As such, it was aspired to remove this water by exchanging its interaction partner for non-polar valine or sterically ill-fitting glutamine. Both variants revealed a delayed onset of the AP-band of the aminopyrimi-

dine ring in the pH-titration in a magnitude similar to that observed in the variants of Glu_{160}. This indicates a shift towards the APH^+ species, and an increased pK_A. Additionally, in a manner similar to that of *Ec*TK_{E160Q}, both of them displayed an increased k_{cat} (approximately 23 % in *Ec*TK_{T433Q}, 39 % in *Ec*TK_{T433V}) and an increase of K_M (approximately 3.7-fold in *Ec*TK_{T433Q}, 4.5-fold in *Ec*TK_{T433V}) (Fig. 19, Section 3.2). The analysis of crystallographic data showed that the water is not removed in the variants, but only displaced, while the overall structure of the protein remained unchanged. The displacement resulted in minor rearrangements of and around Glu_{411}, with the maximum increase of interaction being observed in *Ec*TK_{T433V}, where the Glu_{411}-ThDP-N1′ distance increased to 2.70 Å from 2.62 Å (Fig. 22, Section 3.2). Overall, the changes brought by mutation of Thr_{433} are similar in biochemical and structural impact to these observed in the variants of Glu_{160}. Some of the effects may stem from the reduced dynamic of ThDP. This will be discussed later.

It is quite clear that Glu_{411}, which is more or less situated in a solvent-isolated pocket (dielectric constant of yeast pyruvate decarboxylase ThDP-binding pocket = 13-15, Jordan *et al.*, 1999) requires some polar interactions to retain a pK_A at which deprotonation is favored. As shown in staphylococcal nuclease, the pK_A-shift caused by situating a glutamate in a similarly hydrophobic environment can be $\geq$ 4.3, pushing it well above 8 (Stites *et al.*, 1991; Dwyer *et al.*, 2000). Regarding the pH-optimum for *Ec*TK of 7.6, as well as the observation of full AP-formation well before that, this is highly unlikely, as such a pK_A would mean a very low incidence of cofactor protonations by Glu_{411}. So, interactions as with Glu_{160} or the conserved, proximal water are required to reduce the pK_A. Glu_{160} could do so by sharing a hydrogen, possible at the short distance of 2.57 Å to Glu_{411}, and further distribute the charge towards its proximal water. Additionally, the conserved water molecule could reduce the pK_A by offsetting the negative charge created upon proton transfer by contributing a hydrogen to a hydrogen bond. The pK_A of Glu_{411} was estimated as 6.8 by *PROPKA*, compared to 9.8 in pyruvate:ferredoxin oxidoreductase (PFOR), where the activating glutamate is flanked by a valine and an isoleucine. Estimation of the pK_A of Glu_{411} in *Ec*TK when flanked by a leucine

using *PROPKA* yielded a value of 9.45, in accordance with PFOR and staphylococcal nuclease. Thus, it seems that the interaction of Glu_{160} and Glu_{411} is important for pK_A suppression.

Assuming the offset of AP-band formation observed in the pH-titration experiments for both Glu_{160} and Thr_{433} variants is a true indicator of a pK_A-shift of about 0.4 and not an artifact of disturbed ThDP-binding, this would only indicate a change in bonding energy of around -0.5 $\frac{kcal}{mol}$ according to equation 13, where R is the ideal gas constant and T is the absolute temperature.

$$\Delta pK_A = \frac{\Delta\Delta G}{2.3 \cdot R \cdot T} \tag{13}$$

This means the protonated, traceless APH^+ state of the aminopyrimidine moiety is stabilized by approximately -0.5 $\frac{kcal}{mol}$, in both the variants of Glu_{160} and Thr_{433}. This change corresponds to the energetic contribution of approximately one weak hydrogen bond, and could be explained by the increased donor-acceptor bond distance by 0.16 Å as observed in *Ec*TK_{E160Q} (Fig. 18, Section 3.2). This means crossing the boundary from short, strong hydrogen bond to normal hydrogen bond. In *Ec*TK_{T433V}, the oxygen of Glu_{411} interacting with ThDP is shifted by 0.36 Å, most probably as result of the movement of the water molecule by 1.28 Å, this changes the angle towards ThDP by 10 ° compared to *Ec*TK_{WT} (Fig. 22, Section 3.2). For the remaining variants the cause is not as obvious, and most probably the sum of all changes in bond geometries and distances caused by the slight structural perturbation of Glu_{411}.

The increased k_{cat} and K_M values observed in *Ec*TK_{E160Q}, *Ec*TK_{T433Q} and *Ec*TK_{T433V} can be explained by this as the N4′ of the aminopyrimidine is involved in three proton transfer steps during a catalytic cycle of transketolase. First, in its 1′,4′-iminopyrimidine (IP) form it deprotonates the thiazolium C2, activating it. Then, it protonates the alkoxide at the keto-position of the substrate in the covalent, tetrahedral substrate-ThDP complex. Finally, it facilitates the disruption of the substrate-ThDP bond by deprotonation of the keto-oxygen, initiating product release. As, by virtue of the increased pK_A the likelihood of alkoxide protonation decreases, the K_M increases. By the apparent increase of the N4′-pK_A the ΔpK_A between N4′, the proton acceptor and the 2-OH, the proton donor, of

the substrate increases. An increase in the ΔpK_A of an acceptor-donor pair is correlated to an increased velocity of the proton transfer (Eigen, 1963). This increases the rate of deprotonation of the 2-OH, which is required for cleavage of the C2α-C2 bond, and therefore for product release. As product release is assumed to be the rate limiting step in transketolase catalysis, k_{cat} increases (Lüdtke, 2012).

In the end, these small disturbances result in reduced affinities for both ThDP and X5P in *Ec*TK$_{E160Q}$, reduced activities in *Ec*TK$_{E160A}$ and severely impacted K_M values for X5P in *Ec*TK$_{T433Q}$ and *Ec*TK$_{T433V}$.

Overall, the effects appear to mild for strictly invariant positions. However, taking into account that the steady-state assay for transketolase employs substrate concentrations much higher than found *in vivo*, this can be explained. Investigations on the metabolome of *E. coli* showed that, even when grown using glucose as carbon source, the concentration of the pentose phosphate pool, to which Ru5P and the two substrates X5P and R5P belong, averages around 1.3 mM (Bennett *et al.*, 2009). As these are held in equilibrium by ribose-5-phosphate isomerase and ribulose-5-phosphate epimerase, an intracellular concentration of approx. 0.4 mM can be assumed for each of the three metabolites. At these concentrations, *Ec*TK$_{E160Q}$ would be slower than *Ec*TK$_{WT}$ by about 20 %, and both variants of Thr$_{433}$ would be slower by 50 %, only taking into account the X5P concentration. The difference would further increase when moving towards less abundant growth conditions, by virtue of the increased K_M (0.33 mM X5P on glycerol, 0.017 mM on acetate).

The flanking of the activating glutamate by a conserved water molecule on one side and an acid-base catalyst on the other side is frequent in ThDP-dependent enzymes. In pyruvate dehydrogenase it is a glutamate, similar to transketolase, in cyclohexane-1,2-dione hydrolase it is tyrosine and in pyruvate oxidase histidine (Arjunan *et al.*, 2002; Loschonsky *et al.*, 2014; Muller and Schulz, 1993). In pyruvate decarboxylase, a water takes the position, which is coordinated by a histidine and a serine (Dobritzsch *et al.*, 1998). However, there are exceptions. In benzoylformat decarboxylase and acetohydroxy acid synthase a glutamine occupies the position and in the pyruvate:ferredoxin oxidoreduc-

tase a valine takes it place (Hasson *et al.*, 1998; Pang *et al.*, 2002; Cavazza *et al.*, 2006). It seems that each ThDP-dependent enzyme modulates pK_A and concomitantly reactivity of the proton relay, consisting of activating glutamate and aminopyrimidine moiety of ThDP.

This is necessary as each active site displays different polarities, which in turn influence the proton relay. The differing polarities are owed to the respective requirements by substrate and mechanism. The modulation is most probably mainly achieved by interplay of the conserved water molecule, the activating glutamate itself and the second non-ThDP interaction partner, counteracting the effects of the protein environment according to the respective requirements. It is similar to the exchange of glutamate to valine, required for catalytic fine-tuning in glyoxylate carboligase, albeit less extreme. Unfortunately, it was not possible to correlate the character of the interaction partner, and concomitantly the pK_A of the proton relay to any characteristic of the respective enzyme, be it pH-optimum, active site makeup or substrate type.

The conserved glutamate 165 plays a much more crucial part in *Ec*TK. Substitution by an uncharged amino acid virtually abolishes the ability to bind ThDP, while simply shortening the charged glutamate to an aspartate retains it (Fig. 54, Appendix). As the investigation by size exclusion gel filtration compared to standardized compounds shows, the dimerization equilibrium is strongly shifted towards the monomer in *Ec*TK_{E165Q}, as it elutes 6 minutes later than dimeric *Ec*TK_{WT}, close to conalbumin with a molecular weight of 75 kDa resembling the monomer. Dimerization being crucial in all ThDP-dependent enzymes for cofactor binding, this explains the lack of ThDP in the examined variant. Interestingly, in the crystal *Ec*TK_{E165Q} is still present as a dimer, albeit more loosely bound. This structure revealed the complete absence of ThDP, and a significantly bigger binding pocket caused by displaced loops at the monomer-monomer interaction interface (Fig. 17, Section 3.1). Overall, the B factors for both monomers average to 34.5, which is exceedingly high and reflects the much less tight packaging compared to *Ec*TK_{WT}. Among the absent or displaced residues are Ile_{187}, whose backbone oxygen is involved in coordination of the calcium ion crucial for ThDP binding, Ile_{189}, which is

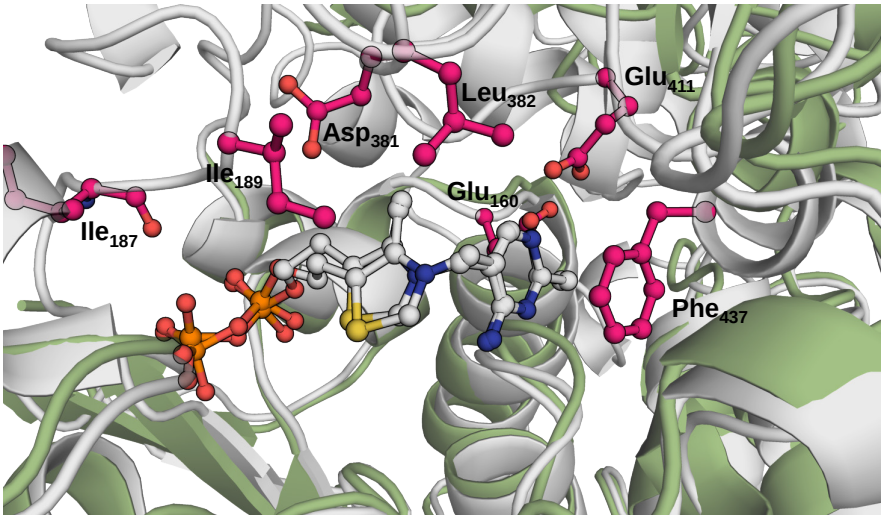

Figure 45. Overlay of active sites of *Ec*TK$_{WT}$ and *Ec*TK$_{E165Q}$ as observed *in crystallo*. *Ec*TK$_{WT}$ is shown in white, *Ec*TK$_{E165Q}$ in green. The residues interacting with ThDP absent or displaced in *Ec*TK$_{E165Q}$ are displayed in pink.

involved for proper positioning, Asp$_{381}$, implicated in monomer-monomer interaction and electrostatic interaction with ThDP, Leu$_{382}$, required for positioning of ThDP as well as Glu$_{411}$ and Phe$_{437}$ which do interact with the aminopyrimidine moiety (Fig. 45).

This disorder seems to be cascading from the missing interactions of Glu$_{165}$ with the backbone nitrogens of Gly$_{413}$ of the same and Gly$_{161}$ of the second monomer. As such, it could be holding both the loop containing Glu$_{411}$ and Glu$_{160}$ in proper position for interaction with each other and ThDP. Glu$_{160}$ seems to be further coordinated via a water molecule. The possibility of the disorder in the active site stemming from the absence of ThDP can be ruled out, as a high-resolution structure of *Ec*TK crystallized without ThDP is dominantly ordered. Unfortunately, crystallization of *Ec*TK$_{E165D}$ was not successful, but it seems like the negative charge is enough to partially rescue the functionality of the enzyme. This variant retains 50 % of k_{cat} compared to *Ec*TK$_{WT}$, with a slight decrease of the apparent K_M to 0.31 mM from 0.37 mM. The pH titration showed an increase of the AP-signal up to a pH of 9, suggesting a drastically changed pK_A or ThDP-binding in comparison to *Ec*TK$_{WT}$, most probably caused by a moderate disordering of the loops containing the interaction partners Glu$_{411}$ and Glu$_{160}$ (Fig. 56, Appendix).

This magnitude of importance of a single residue distal of the active site is seldom

observed, as one discovers them mostly by accident, or using structural data as starting point. One further example for such a structurally important position in *Ec*TK is Asp_{381}, forming three hydrogen bonds to the neighboring monomer. It was shown to be highly important for proper function of *Sc*TK, despite being not involved in catalysis (Meshalkina *et al.*, 1997). Mutations reducing enzyme activities below a certain threshold compared to the wild type are commonly unrecognized, as the organism dependent on this defective enzyme is not viable, and as such rarely sequenced. Examples of mutations at the dimer interface causing disease are for example observed in the human dihydrolipoamide dehydrogenase (Ambrus *et al.*, 2016), or in the human protein deglycase DJ-1, where exchange of a single aspartate in a short, strong hydrogen bond-pair to isoleucine significantly reduces dimerization and ordering of the protein (Lin *et al.*, 2017). It is a reasonable evolutionary approach to employ few highly impactful residues for dimer-interactions and structural integrity, as this suppresses the gradual weakening of these interactions by stepwise mutation of weakly interacting residues.

In summary, despite the apparent presence of a communication channel in transketolases, the strictly conserved residues observed could not be linked to subunit communication in this study. However, they are highly important individually, as Glu_{160} seems to regulate the pK_A of the Glu_{411}-N1′-N4′ proton relay, in conjunction with the water oriented by Thr_{433}. Glu_{165} seems to be most important for dimerization, thus explaining the high conservation.

4.2 Why is 2'-Methoxythiamine Diphosphate an Inhibitor for Thiamine Diphosphate Dependent Enzymes?

2'-methoxythiamine diphosphate is the only known naturally occurring analogue of ThDP. The precursor molecule bacimethrin, named after *Bacillus megaterium* in which it was first described was shown to posses antibiotic properties (Tanaka *et al.*, 1962). Early on it was ruled out that the antibiotic effect stems from a suppression of ThDP synthesis, on a genetic level as well as stemming from direct inhibition of biosynthetic enzymes by bacimethrin (Reddick *et al.*, 2001). *In vivo* and *in vitro* studies on targets of

MeOThDP identified the enzymes transketolase, pyruvate dehydrogenase and deoxy-D-xylulose-5-phosphate synthase of *Escherichia coli* as targets. The latest study on the subject supplied a plethora of kinetic data regarding the effect of MeOThDP, but could not pinpoint the cause of the inhibition observed in some of the enzymes. Regarding the fact that the human pyruvate dehydrogenase complex retains 50 - 75 % activity when reconstituted with MeOThDP, the chemical properties of the methoxy-aminopyrimidine ring seem not disturbed significantly. Instead, they suggested a displacement of the aminopyrimidine ring compared to ThDP, disrupting or impairing the glutamate-ThDP proton relay (Nemeria *et al.*, 2016).

Our first-time structural elucidation of MeOThDP bound to an enzyme may serve to answer this question. In the resting state, the aminopyrimidine moiety and consequentially the thiazolium moiety are displaced significantly, agreeing with the previous assumption. The crucial distance between the activating glutamate which is required for cofactor activation and the N1′ of ThDP increases from 2.62 Å to 3.62 Å (Fig. 28, Section 3.3). The former bond is a relatively short hydrogen bond while the latter is at the limit of hydrogen bonding distances. Studies in pyruvate decarboxylase (PDC) revealed that mutagenesis of the activating glutamate to aspartate reduces the activity to below 3 % (Candy *et al.*, 1996). The increase in distance between the N1′ of ThDP and aspartate was estimated to increase by around 1 Å, which would correspond to the increase observed with MeOThDP. Furthermore, the residual k_{cat} observed in *Ec*$TK_{MeOThDP}$ under steady-state conditions is around 3 %, matching the activity observed in PDC (Fig. 23, Section 3.3).

As already explained in section 3.3, the substitution of the methyl group of ThDP by a methoxy group in MeOThDP results in a strained architecture at the binding site for the aminopyrimidine moiety. The environment of the methoxy group forces it to orient towards the activating glutamate, as the number of van-der-Waals clashes is minimized in this orientation (Fig. 28, Section 3.3). This clash of binding and repulsive interactions results in the displacement of Glu_{411} towards Glu_{160}, compressing their hydrogen bond below 2.5 Å, in a manner resulting in a smeared positive mFo-DFc density between the

two interaction partners (Fig. 63, Section 3.3).

As a result of the increased interaction distance the H/D-exchange rate at the thiazolium C2, correlated with cofactor activation by the proton relay, is reduced. Thus it becomes the rate limiting step, with a rate of 2.9 $\pm$ 1.1 s^{-1} compared to 313 $\pm$ 41 s^{-1} when reconstituted with ThDP. In *Ec*TK_{WT}, release of the second product was identified as rate-limiting (Lüdtke, 2012). This defect in cofactor activation is further supported by the NMR-based analysis of intermediate distribution, where around 85 % of the cofactor molecules remained unreacted, while in *Ec*TK_{WT} only 10 % (X5P) or 20 % (F6P) of ThDP molecules do not form the tetrahedral intermediate (Fig. 25, Section 3.3).

The clash of the methoxy group and the protein environment explain the increased K_D values observed for MeOThDP in all employed assays, as binding of the cofactor is facilitated by the two independent binding sites for the diphosphate moiety and the aminopyrimidine moiety. While diphosphate binding should work properly, impacted binding of the modified aminopyrimidine ring, as evidenced by the comparatively increased ADPs (Fig. 26, Section 3.3), significantly increases the K_D. This is most probably an additive effect of two factors. The first one is the increased distance to Glu_{411}, which is by virtue of the hydrogen bond interaction a productive interaction of enzyme and cofactor (Wikner *et al.*, 1994; Candy *et al.*, 1996). The second is the misfit of the hydrophobic aminopyrimidine moiety in the desolvated and hydrophobic binding pocket. Both of these are direct consequences of the methoxy group-environment clashes.

The observation of the clash-induced misfit can be used to explain the activities observed by Nemeria *et al.*, who observed 50 - 75 % retained activity of the human pyruvate dehydrogenase complex (*h*PDHC) after reconstitution with MeOThDP, while the activities of *Escherichia coli* PDHC (*ec*PDHC) were reduced to approximately 10 %. MeOThDP was fitted into structures of the pyruvate dehydrogenase component of both human and bacterial PDHC (Arjunan *et al.*, 2002; Kato *et al.*, 2008). This fitting revealed that *h*PDHC has a more expansive and possibly more flexible binding pocket for the aminopyrimidine. The least amount of clashes with the environment is estimated to

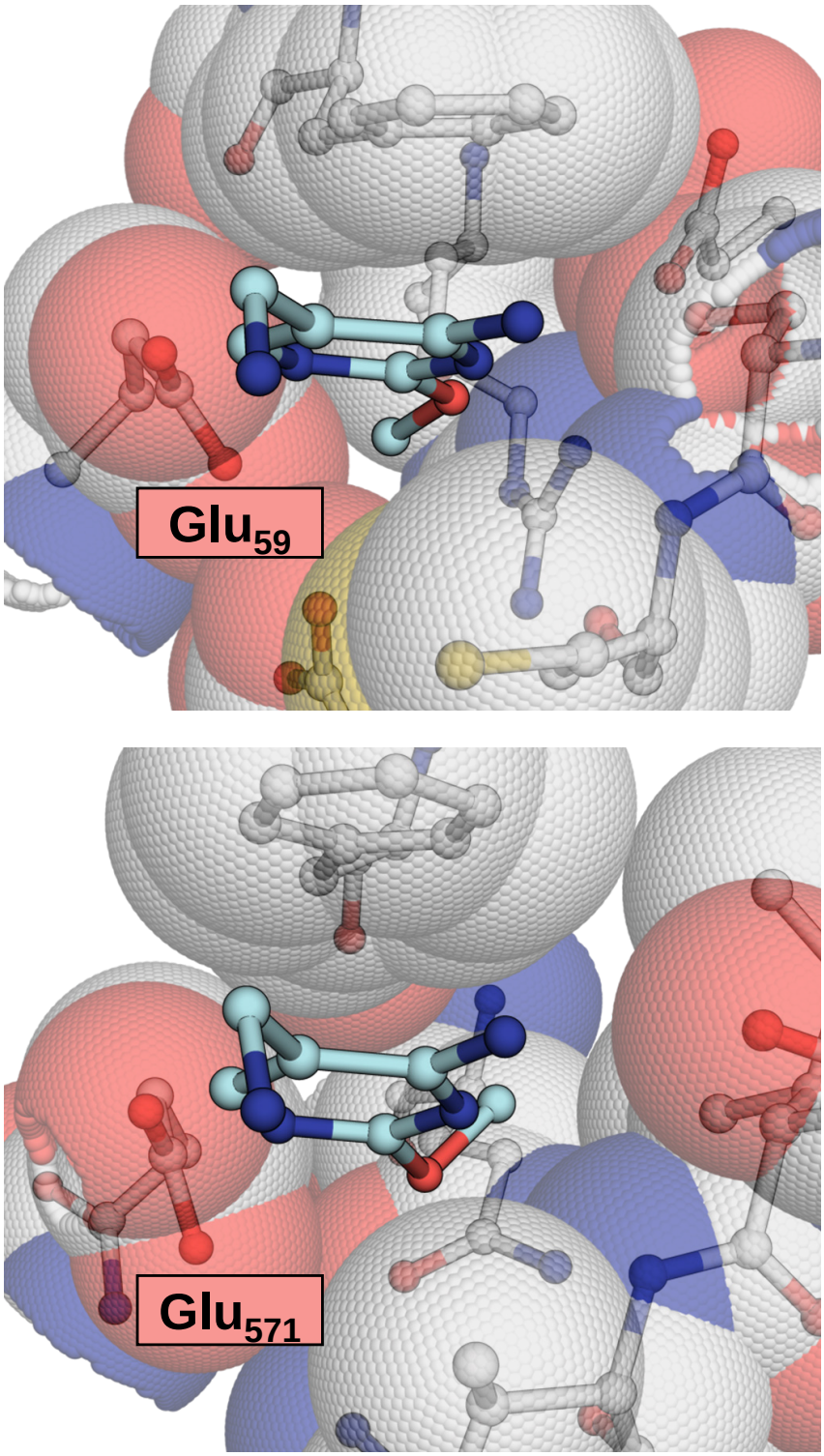

Figure 46. Fit of 2'-methoxythiamine diphosphate in *Escherichia coli* (top) and *Homo sapiens* (bottom) pyruvate dehydrogenase. MeOThDP was fitted according to the deposited electron densities of ThDP. The orientation of the methoxy group was approximated according to the lowest number of clashes.

occur when the methoxy group is oriented in an angle of approximately 60 ° to the aminopyrimidine plane, pointing away from the activating glutamate. In *ec*PDHC, the orientation causing the smallest amount of clashes is towards the activating glutamate, nearly parallel to the aminopyrimidine plane. This orientation would place the methoxy-carbon in a distance of approximately 2.4 Å to the glutamate, most probably resulting in a repulsion similar to that observed in *Ec*TK$_{MeOThDP}$ (Fig. 46). A similar binding architecture is present in *E. coli* 1-deoxy-D-xylulose 5-phosphate synthase (DXPS), in which reconstitution with MeOThDP resulted in a decrease of activity to around 10 %. The most flexible pocket to situate the methoxy group is next to the activating glutamate, resulting in clashing, repulsive interaction.

Interestingly, binding of X5P in the docking site seems to partially alleviate this effect. In the X5P-soaked structure of *Ec*TK$_{MeOThDP}$, the aminopyrimidine moiety is nestled more tightly into its binding pocket, reducing the N1′-Glu$_{411}$ distance to 3.42 Å. This is most probably a result of the clashes of the 1-OH and 2-O of X5P with the methylene bridge carbon and the C2 of MeOThDP. It seems that X5P is bound strong enough to

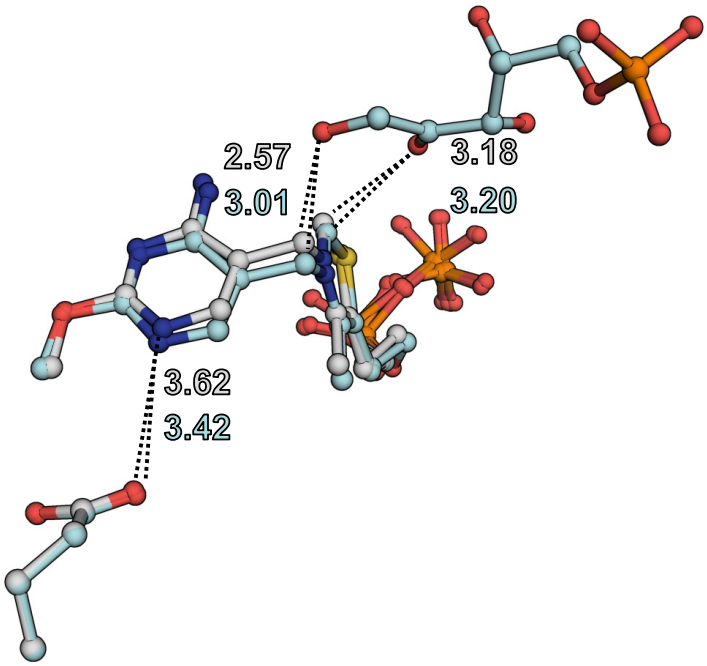

Figure 47. Movement of MeOThDP upon X5P addition. MeOThDP as observed in *Ec*TK$_{MeOThDP}$ is shown in gray, as observed in *Ec*TK$_{MeOThDP}$-X5P in cyan. The important interaction distances in Å are indicated in the respective color.

force MeOThDP in an alternate conformation. This observation would explain the lag phase observed in many steady-state progress curves at high concentrations of X5P, in *Ec*TK_{WT} and different variants (data not shown). It seems that a small population of ThDP is improperly bound, which is corrected when supplying saturating concentrations of X5P.

These differences between the accommodation capabilities of the different homologues and ThDP-dependent enzymes may be significant for possible exploration as antibiotic. The precursor molecule for 2'-methoxythiamine diphosphate, hydroxymethoxypyrimidin (bacimethrin) was already shown to inhibit bacterial growth (Nishimura and Tanaka, 1963). While the preferential insertion of this compound by the thiamine biosynthesis machinery poses a problem for bacteria, humans do not synthesize ThDP themselves. Furthermore, it seems that at least three of the five human ThDP-dependent enzymes should be resistant against adverse effects by MeOThDP. Either, because they can accommodate the methoxy group, as seen in pyruvate dehydrogenase, or because they exhibit quasi-irreversible tight binding of ThDP requiring complicated protocols for cofactor removal, as in human transketolase or human and *E. coli* oxoglutarate dehydrogenase (Mitschke *et al.*, 2010; Nemeria *et al.*, 2016). The two remaining targets in humans would be the oxoisovalerate dehydrogenase of the branched chain amino acid dehydrogenase complex, and the 2-hydroxyacyl-CoA lyase. It is likely that oxoisovalerate dehydrogenase would be able to incorporate MeOThDP, as the native methyl group is flanked by two waters, which the methoxy group could displace. Unfortunately, no structural data is available for the last ThDP-dependent enzyme, 2-hydroxyacyl-CoA lyase. However, this enzyme was never implicated in any deficiency phenotype, and as such may be dispensable for some time, especially if dietary accommodations are made (Casteels *et al.*, 2007).

The bacterial transketolases are highly similar in geometry of their aminopyrimidine binding pocket, and as such could be susceptible for MeOThDP, independent of organism. There are four major principles by which resistance may be achieved, reduction of uptake, an active ejection of the agent from the cell, modification of the target in

a manner which promotes incompatibility with the agent and active degradation or modification of the agent. These can be either achieved by random mutation or by horizontal gene transfer (Blair *et al.*, 2014). The strict conservation of the binding pocket basically rules out resistance by target modification. Regarding the high similarity of hydroxymethoxypyrimidin and hydroxymethylpyrimidin, as well as of MeOThDP and ThDP, the other three methods may be questionable as well, as discrimination of the precursors and the cofactors could prove difficult, as observed in the initial biosynthesis of MeOThDP from hydroxymethoxypyrimidin by the native synthesis machinery. As such, any kind of resistance acquired should decrease the fitness under non-selecting conditions by reduced ThDP synthesis, increased ThDP hydrolysis or overproduction of ThDP, which is very expensive (Zilles *et al.*, 2000; Lawhorn *et al.*, 2004; Jurgenson *et al.*, 2009).

This study elucidated the direct mode of action of 2'-methoxythiamine diphosphate. The inhibition of activity in certain enzymes is achieved by a one-atom modification resulting in a clash of cofactor analogue and binding pocket, which in turn increases the interaction distance of the crucial activating glutamate and the aminopyrimidine N1′. This results in significantly reduced rates of cofactor activation. In enzymes capable of accommodating the introduced methoxy group, MeOThDP is catalytically competent. Human ThDP-dependent enzymes can either bind MeOThDP in a non-inhibiting manner or display extremely tight binding of ThDP. Consequently, they should prove resistant against MeOThDP, while many crucial bacterial enzymes could be susceptible. Antibiotic properties against certain unicellular organisms were already shown under defined conditions (Drautz *et al.*, 1987). As acquiring resistances against this compound could prove difficult, an exploration of this compound as novel antibiotic may be fruitful.

4.3 New Insights in Thiamine Diphosphate Dynamics in Transketolases

Recent crystallographic studies on *Ec*TK at true atomic resolution revealed the presence of two distinct conformations of ThDP. These conformations are different in the position

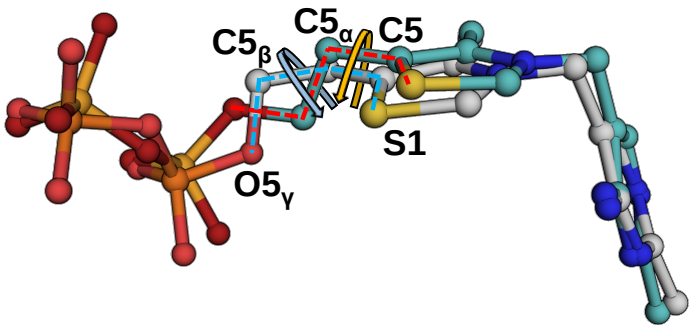

Figure 48. Movement of ThDP in resting state *Ec*TK$_{WT}$. ThDP$_{down}$ is indicated in gray, ThDP$_{up}$ in cyan. The components of the S1-C5-C5α-C5β and C5-C5α-C5β-O5γ dihedrals are named and the dihedral axes are indicated by arrows. Structural data taken from Lüdtke, 2012.

of the thiazolium ring, as well as of the diphosphate anchor, and were termed "up" and "down". As the names suggest the thiazolium ring of ThDP$_{down}$ is positioned lower than that of ThDP$_{up}$, relative to the entrance of the active site. Reevaluation of existing structural data of adequate resolution according to these findings revealed a prevalence of this dynamic in all evaluated structures. This dynamic was assumed to be important for formation of the covalent sugar-ThDP adduct, as data obtained with the non-reactive cofactor analogue N3′-pyridyl-ThDP suggested that only ThDP$_{up}$ is in bond-forming distance to the C2 of X5P. Further, the slight movement of the aminopyrimidine ring reduces the distance of N4′ and C2-O of the sugar, where protonation takes place during formation of the covalent intermediate. Movement of the cleaved dihydroxyethyl-thiamine diphosphate towards the down-conformation would serve to spatially separate it and the cleaved sugar, reducing religation frequency. Failure to do so could result in a pseudo dead-end intermediate, where transfer of the ThDP-bound C2 unit to an acceptor aldose is inhibited by a cycle of cleavage and religation. Despite the possible importance for catalysis, the cause of this movement and the absence of it in human transketolase are not yet understood (Lüdtke, 2012).

It is striking that concomitantly to the movement of the thiazolium ring a rearrangement of the diphosphate anchor takes place, while the aminopyrimidine moiety remains relatively rigid (Fig. 48). The movement of the thiazolium C2 is 0.86 Å from ThDP$_{down}$ to ThDP$_{up}$. The dihedral angles around the C5-C5α axis are ∼7.2 ° for ThDP$_{down}$, which is almost parallel, and ∼-88.2 ° in ThDP$_{up}$, almost perpendicular. The dihedral angles around the C5α-C5β axis are ∼-72.5 ° for ThDP$_{down}$, and ∼168.6 °for ThDP$_{up}$. In addition, the

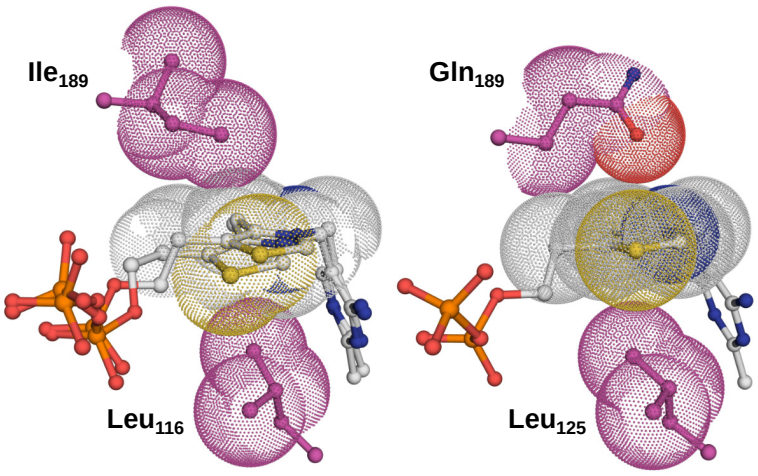

Figure 49. Interactions of the thiazolium moiety in *Ec*TK (left) and *h*TK (right). The van-der-Waals radii of the constituents of the thiazolium ring, as well as of the residues below and atop of it are indicated. Structural data taken from Lüdtke, 2012 and Mitschke *et al.*, 2010.

oxygen atoms of the phosphate anchor not interacting with the calcium ion rotate by ∼50 °. It is not possible to discern which moiety is the one responsible for initiating the movement. Further, it is unclear if the movement is of a purely stochastic nature by virtue of e.g. Brownian molecular motion, or if the enzyme is able to control the movement, for example by interactions of active site residues with the diphosphate anchor. Nevertheless, it seems like this was possibly the first observation of conformational selection enacted by a cofactor (Lüdtke, 2012).

In human transketolase, this movement is absent. According to the dihedral angles, ThDP is present in the up-conformation. However, it is sandwiched between the residues Leu_{125} and Gln_{189} (corresponding to Leu_{116} and Ile_{189} in *Ec*TK) in a tight manner not allowing movement in a magnitude as observed in *Ec*TK (Fig. 49). In *Ec*TK, the two residues form a larger gap, allowing the movement between the two distinct conformations. Should the movement towards the up-conformation indeed be crucial for substrate binding, an arrest in this position could partially explain the significantly better K_M for X5P in *Homo sapiens* transketolase (*h*TK) compared to *Ec*TK. It is ∼70 μM in *h*TK (Shaobo Dai, data not published) and ∼370 μM in *Ec*TK. Conversely, the absence of movement after substrate cleavage may contribute to the significantly reduced k_{cat} observed in *h*TK (∼3 s^{-1} vs. ∼53 s^{-1}).

This work aimed to investigate if and how the enzyme is able to steer the conformation distribution. Building on the assumption that cofactor movement is not only required

for substrate binding, but also for reactant separation, histidine 261 was targeted. This histidine is responsible for abstraction of a proton from the sugar 3-OH prior to cleavage of the substrate-ThDP complex and is in interaction distance to the diphosphate anchor. Thus, it is the ideal initiator to trigger a movement pulling apart the cleaved sugar and DHEThDP.

The mutant *Ec*TK$_{H261N}$ displayed a significantly reduced k_{cat} in the steady state, to below 0.5 % of the activity of *Ec*TK$_{WT}$, while apparently decreasing the K_M to 0.07 mM, an 5-fold increase of apparent affinity for X5P. However, most of this is probably owed to its character as the prime acid-base catalyst. The apparent reduction of K_M is thus a product of the reduced reaction velocity, which always reduces K_M, and the stabilization of the tetrahedral intermediate by drastically reducing cleavage frequency (Fig. 29, Section 3.4). In the pre-steady state kinetics, the effect is much less pronounced. While still distinctly slower than *Ec*TK$_{WT}$ in formation of the tetrahedral intermediate and depletion of the AP-form of the aminopyrimidine ring, it is clear that the rate-limiting step happens after formation of the covalent sugar-ThDP complex (Fig. 30, Section 3.4).

Structural investigation revealed that *Ec*TK$_{H261N}$ retained the movement of the cofactor, with a shift of the more populated form to ThDP$_{up}$, with slightly more than 50 % occupancy. Possibly, this could be a factor for the apparent decrease of K_M, as it would provide an increased population of cofactor in attacking distance to the X5P-C2. Soaked with X5P, a significant portion of cofactor formed the covalent X5P-ThDP adduct. The distribution was 70 % of covalent adduct, to approximately 30 % unreacted ThDP$_{down}$ (Fig. 31, Section 3.4). Reevaluation of the published *Ec*TK structure with covalently bound X5P revealed the presence of ThDP$_{down}$ (Asztalos, 2008, PDB 2R8O). It seems like non-full occupation of the covalent adduct is the normal state. As such, no significant changes in the dynamics could be observed in *Ec*TK$_{H261N}$, only a shift in the resting state to a one-to-one distribution of ThDP$_{down}$ and ThDP$_{up}$. However, the structures of the variants of Thr$_{433}$ revealed a significant decrease of the phosphate-His$_{261}$ distance to 2.39 Å. This could serve to increase the tendency of His$_{261}$ to abstract a proton from the 3-OH, as required for substrate cleavage, by stabilization of the positive charge.

The second histidine interacting with the diphosphate, histidine 66, was mutated to alanine in the course of the intermediate stabilization study. Crystallographic studies on the ground state enzyme revealed the presence of only one conformation of ThDP. The dihedral angles of this conformation correspond more to $ThDP_{down}$ than to $ThDP_{up}$. Seemingly, the only movement of the thiazolium ring observed in this variant is in the ring plane, and below it. If any movement towards the up-conformation takes place, it is in a magnitude not resolvable at 1.11 Å (Fig. 69, Appendix).

In the X5P-bound state, the thiazolium ring is elevated in a manner fitting to the covalent X5P-ThDP adduct. The diphosphate anchor is more motile compared to the resting state. This is most probably caused by the flipping of His_{26} in the ground state, where it forms a new hydrogen bond with the β-phosphate (Fig. 70, Appendix). As this residue is also important for substrate binding, this new orientation is absent in the substrate bound state, destabilizing the diphosphate. The densities observed only indicate perpendicular movement of the thiazolium, not towards the down-state.

Despite not directly interacting with the substrate, only via a water which is also present in the variant, mutagenesis of His_{66} was quite impactful. In the steady-state, k_{cat} is reduced by more than 80 % and K_M is increased 3.5-fold (Fig. 33, Section 3.5.1). Presumably, this is the result of both the destabilization of the loop around His_{261}, which is required both for substrate binding and as acid-base catalyst, and the alternate conformation of His_{26}, which is also required for substrate binding. Further, the arrest between up- and down-conformation may affect the K_M by reducing the amount of suitably oriented ThDP.

The movement is presumably a sum of opposing forces. Both His_{66} and His_{261} form interactions with the β-phosphate of both conformations. By these, they most probably offer two energetic minima to the diphosphate, resulting in the two endpoints observed as $ThDP_{down}$ and $ThDP_{up}$. However, in the up-conformation strain should be placed on the aminopyrimidine moiety, which is tightly nestled into its binding pocket, and could promote the movement back towards the down-conformation, in addition to the normal stochastic up- and down movement of the cofactor. In the substrate-bound

state, the proximity of the substrate 2-OH to N4′ serves as a backstop, suppressing full return to the down-conformation. This probably serves to keep dihydroxyethyl-thiamine diphosphate positioned for transfer of the dihydroxyethyl to the respective acceptor aldose.

Overall, it seems that His_{66} is necessary for fine-tuning the movement of the diphosphate anchor in a manner that turns undirected movement of the thiazolium ring along the ring plane to the movement required to switch between $ThDP_{down}$ and $ThDP_{up}$. There are multiple factors by which it could contribute. The first would be direct interaction with the β-phosphate. Further, in the absence of His_{66}, a significantly populated alternate conformation of His_{26} interacts with the β-phosphate, which would otherwise be repulsed by His_{66}. This new interaction could modulate the cofactor movement in a non-productive manner. In addition, the loop around His_{261} is destabilized in the absence of His_{66}. As His_{261} also interacts with the β-phosphate, the (partial) loss of two interaction partners is likely involved in changing the movement pattern.

In the covalent X5P-ThDP adduct, the sugar C2-C3 bond is no longer elongated, as it is in *Ec*TK_{WT}. It seems like the directed movement of the cofactor while the active site residues keep the sugar in place by multiple interactions is one of the driving forces of this elongation, and the absence of His_{66} changes the direction of the movement to one without contribution to catalysis.

More curious is the observation that the variants of Thr_{433}, *Ec*TK_{T433Q} and *Ec*TK_{T433V} displayed a significant shift of the equilibrium distribution of the two conformations towards $ThDP_{down}$, which nearly shows 100 % occupancy in the resting state. In the presence of substrate however, nearly all ThDP molecules form the tetrahedral intermediate. As this residue is separated from the active site by the cofactor, and forms no interaction with the diphosphate, an explanation for this behavior is hard to find. The water molecule coordinated by Thr_{433} interacts with the backbone of the neighbor of Asp_{381}, an invariant residue of high importance. Mutagenesis significantly impacted k_{cat} and K_M in *Sc*TK, reducing the activity to 3 %, and increased the apparent affinity up to 6-fold (Meshalkina *et al.*, 1997). It is at the outer limit of a van-der-Waals

clash towards the C5α of $ThDP_{down}$. Slight reorientation may remove this interaction and shift the equilibrium towards the down-conformation. Otherwise, the variants only influence Glu_{411}, which interacts with the aminopyrimidine moiety. It seems unlikely that the movement of ThDP is initiated from this rigid part of the cofactor, especially as the variant *Ec*TK_{E160Q}, which behaves similar to those of Thr_{433} kinetically, displays the normally observed 70:30 distribution of $ThDP_{down}$ to $ThDP_{up}$ in the ground state. As no obvious rearrangements of the active site take place which could explain this strong divergence, it must be assumed that the change is the result of a series of subtle changes in the protein environment making the up-conformation energetically unfavorable. This can be overcome in the presence of substrate, as formation of a covalent bond to X5P supplies additional productive interactions with the active site, making it energetically favorable. This could explain, in addition to the potential pK_A shift, the apparently increased K_M in both variants. The shifted equilibrium reduces the frequency by which a productive $ThDP_{up}$-X5P Michaelis-complex is formed, increasing K_M. As the enzyme may be more prone to the down-conformation, cleavage is more efficient resulting in a higher k_{cat}.

It seems like the concerted movement of the cofactor, as observed in *Ec*TK, introduces a further element into the enzyme. $ThDP_{down}$ and $ThDP_{up}$ are in an enzyme-induced equilibrium in the resting state and X5P forms a productive complex only with $ThDP_{up}$. This describes the simplest case of conformational selection, according to scheme 1. Conformational selection, the sampling of conformations of differing catalytic or interaction competence is normally not associated with cofactors, but with the enzyme environment itself (Monod *et al.*, 1965; Changeux and Edelstein, 2011; Vogt and Di Cera, 2012; Vogt and Di Cera, 2013).

$$E_{Down} \quad \underset{k_{UD}}{\overset{k_{DU}}{\rightleftharpoons}} \quad E_{Up} + [S] \quad \underset{k_{off}}{\overset{k_{on}}{\rightleftharpoons}} \quad E_S \qquad (1)$$

*Ec*TK-$ThDP_{up}$ is probably the productive state, as the activation barrier for the subsequent formation of the covalent adduct is significantly lowered by reduction of the soon-to-be linked carbon-carbon distance. However, as conformational selection is

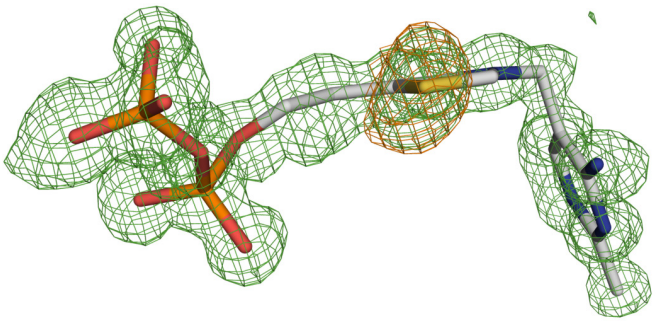

Figure 50. mFo-DFc map of *Scheffersomyces stipitis* transketolase. The mFo-DFc density is contoured at 3 σ, the density stemming from S1 is further highlighted in orange. The map was generated by running 0 cycles of *PHENIX.REFINE* refine after removal of ThDP from pdb file 5HYV.

complicated to detect when $k_{DU} > k_{on}$, definitive kinetic proof for this assumption is still missing.

Recently, the transketolase from *Scheffersomyces stipitis* (*ss*TK) was structurally elucidated at true atomic resolution, the first besides those of *E. coli* and human (Hsu *et al.*, 2016). Reevaluation of the deposited data revealed the presence of movement similar to that observed in *Ec*TK (Fig. 50). The bean shaped density observed for the sulfur atom, as well as diffuse densities observed around C5α and C5β of the thiazolium ring and the β-phosphate of the diphosphate anchor are clear indications for the directed movement between up- and down-conformation, opposed to the in-plane movement as observed in *Ec*TK$_{H66A}$.

As such, it seems like employing cofactor dynamics as a factor of catalysis is not limited to *E. coli*, but also appears (at least) in other unicellular organisms like the yeast *Scheffersomyces stipitis*. Unfortunately, no further structures of holo-transketolases with a better resolution than approximately 1.5 Å are available, the limit at which the two conformations are clearly distinguishable. Therefore, it is not possible to narrow down when and where this dynamic was abolished, and if there are any factors beside the tighter restrains placed upon the thiazolium ring by the protein environment involved.

4.4 Stabilization of the Breslow Intermediate by the Protein Environment in ThDP-dependent enzymes

The initial postulation of the Breslow intermediate assumed that delocalization of the carbanion charge into the aromatic thiazolium ring via the enamine form was necessary

for stabilization. Further, it was assumed that formation of a keto-tautomer would result in transfer of the proton from 1-OH to the thiazolium C2, resulting in formation of a tetrahedral carbon and subsequent loss of aromaticity of the thiazolium ring. While keto-intermediates were postulated for some ThDP-dependent enzymes, an external electron acceptor is always required for the reaction, as in *Lactobacillus plantarum* pyruvate oxidase (O_2), pyruvate dehydrogenase (Lipoamide) and phosphoketolase (Dehydration). This may serve to avoid tautomerization via C2.

This paradigm was challenged for the first time by the observation of an hydroxyethyl-thiamine diphosphate species which exhibited a tetrahedral character at the C2 atom in pyruvate:ferredoxin oxidoreductase (Cavazza *et al.*, 2006). It was attributed to the formation of a localized, cationic σ/n-type radical. The possibility of rearrangement to a similar species was further supported by studies in solution using 1,3,4-triphenyl-4,5-dihydro-1*H*-1,2,4-triazol-5-ylidene, an N-heterocyclic carbene, with propionic acid as substrate. The thermodynamic minimum of the resulting adduct was identified as the keto-species with a tetrahedral C2 (Berkessel *et al.*, 2010). Further support for a naturally occurring intermediate of this kind was the observation of a tetrahedral intermediate in *Lp*POX. The occurrence of a keto-HEThDP in *Lp*POX would be consequent, as the acceptor substrate phosphate is a nucleophile itself, and would be more prone to react with an electrophilic center, instead of the previously postulated C2α-localized radical species (Meyer *et al.*, 2012). For many ThDP-dependent enzymes however, a species like this would be unproductive, as a nucleophilic C2α is required, for example, in transketolases. In principle, by virtue of the V-conformation, the aminopyrimidine N4′ is positioned to mediate the transfer of a proton from the DHEThDP 2-OH to the C2 of the thiazolium in ThDP-dependent enzymes. Therefore, the identification of the factors stemming from the enzyme environment involved in the promotion or suppression of the respective intermediates was investigated.

In transketolase, three polar residues are in proximity of the dihydroxyethyl-thiamine diphosphate intermediate. His_{66}, His_{100} and, in non-animals, His_{473}. In animals, the histidine is replaced by a glutamine. His_{66} interacts with the dihydroxyethyl 1-OH

via a water molecule, while His_{100} interacts directly. His_{473} is interacting with the dihydroxyethyl 2-OH. Thus, His_{66} and His_{100} could stabilize the intermediate by distorting the geometry required for proton transfer mediated by N4′, while His_{473} was shown to flip (Neumann and Tittmann, 2014). By this flipping, it could abstract a proton from the 1-OH and remove the possibility for proton transfer. These residues were targeted to probe their importance on intermediate stabilization in *Ec*TK. In *Lp*POX, only two hydrogen-bond forming residues are in proximity of the HEThDP intermediate, Gln_{122} and Glu_{483}. Both of them were implicated in formation of the covalent intermediate, as well as positioning of lactyl-thiamine diphosphate and the second substrate phosphate. They were mutated to their equivalents in transketolase, histidine and isoleucine respectively.

The kinetic and spectroscopic investigations on the variants of transketolase revealed significant reductions of k_{cat}, while K_M increased concomitantly, decreasing the catalytic efficiency. For *Ec*TK_{H66A}, k_{cat} decreased by 80 %, K_M increased 3.6-fold. In *Ec*TK_{H100A}, k_{cat} decreased by 90 %, while K_M increased 4.2-fold. The strongest effect was observed in *Ec*TK_{H473Q}, where k_{cat}decreased by 90 % and K_M increased 11.9-fold (Fig. 33, Section 3.5.1). The spectral signatures of the intermediates obtained with fructose 6-phosphate and β-hydroxypyruvate changed markedly compared to *Ec*TK_{WT}, most prominently seen in the absence of the broad enolate band from 350 - 500 nm (Fig. 34, Section 3.5.1). The rate constants for formation of this intermediate follow a dependency on the substrate concentration identical to that for the enamine at 300 nm (not shown). It was assumed to be formed by abstraction of a proton from the 2-OH by His_{473} (Lüdtke, 2012; Paulikat, 2014). These results suggest that the formation of the enolate is susceptible to subtle perturbations of the active site.

In single-turnover experiments using HPA as substrate, the rates of enamine-formation were markedly decreased, to 5 % in *Ec*TK_{H66A} and below 1 % in *Ec*TK_{H66A} and *Ec*TK_{H473Q} (Fig. 34, Section 3.5.1).

The analysis of structural data obtained in this study, as well as of data obtained by Ann-Kristin Diederich revealed no significant deviations of the intermediates from those observed in *Ec*TK_{WT}. The only exception were the data obtained for the crystal of

*Ec*TK$_{H100A}$ soaked with X5P, crystallized in space group P2$_1$, by Ann-Kristin Diederich. Here, a non-canonical dihydroxyethyl-thiamine diphosphate intermediate was observed, where a clearly tetrahedral C2 was present, implying loss of aromaticity at the thiazolium ring (Fig. 35, Section 3.5.1). As His$_{100}$ is the primary interaction partner of the 1-OH, its absence could allow relaxation of the intermediate, allowing the distance of 2-OH and N4′ to decrease. This would allow the N4′, present as iminopyrimidine in this state and therefore receptive for a proton, to mediate a proton transfer from 2-OH to C2, generating a non-aromatic keto-DHEThDP in the process.

Interestingly, trying to recreate a crystal showing an identical intermediate resulted only in the observation of unbound X5P in the docking site (Fig. 35, Section 3.5.1). This demonstrates that His$_{100}$ is not only important to maintain the preferred state of the intermediate, but also is of high importance for positioning the substrate for nucleophilic attack by the activated ThDP-ylidene. For this, the sugar C2-C3 axis has to rotate by more than 180 °, and the C2 needs to move towards the thiazolium ring. One of the key facilitators for this movement seems to be His$_{100}$. This is further supported by its general importance to discriminate for the C1-OH group of substrates, as adequate mutagenesis to hydrophobic amino acids allows to modulate the enzyme to accept pyruvate as donor substrate, which is normally not the case (Diederichs, 2009).

In the structures of *Ec*TK$_{H66A}$, a disturbance of the cofactor dynamics could be observed, as mentioned before (Fig. 69, Appendix). As much of the conformation of intermediates is however, by virtue of the interactions of their HO-groups and the repulsion by the N4′, independent from the cofactor movement, the intermediates are similar to these observed in *Ec*TK$_{WT}$. It seems like His$_{66}$ has no impact on the nature of the intermediates and is important by interacting with the diphosphate moiety and regulating its movement. *Ec*TK$_{H473Q}$, while being the most impacted one in the steady-state assay, did not display conspicuous structural features. The geometry of the intermediate and its interactions with the active site is changed slightly, as far as it can be said at this resolution. The most striking change is a decrease of the His$_{261}$-3-OH distance by approximately 0.2 Å, which could have an impact on the rate of substrate cleavage (Fig. 35, Section 3.5.1).

In *Lp*POX, the results obtained in this study mirror those established before. In the steady-state, *Lp*POX$_{Q122H}$ displays a reduction of k_{cat} below 1 %, and an approximately 11-fold increase of K_M. This k_{cat} is even lower than that observed in mutants of the activating glutamate, but K_M is way less impacted (Fig. 37, Section 3.5.2). The investigation of the reduction rates of FAD revealed a significantly reduced rate of reduction, in both presence and absence of phosphate (Fig. 38, Section 3.5.2). Together with the markedly reduced rate of phosphonolactyl-thiamine diphosphate formation from the substrate analogue methylacetylphosphonate (Fig. 39, Section 3.5.2), this strongly supports the results of Susan Böhme that this residue is crucial for formation of the first covalent intermediate lactyl-thiamine diphosphate (Böhme, 2007). In *Lp*POX$_{E483I}$, the impacts were not as pronounced. The k_{cat} decrease to 10 %, while K_M worsened 1.5-fold. More interestingly, an apparent substrate-inhibition was observed, with an estimated K_I of 309 $\pm$ 39 mM for pyruvate (Fig. 37, Section 3.5.2). This may be caused by increasing the size of the active site. As Glu$_{483}$ occupies the position above the ThDP, and together with the substrate phosphate coordinates a water molecule further narrowing the active site, reducing its size by mutagenesis to isoleucine may give space for an additional pyruvate molecule. Pyruvate was already shown to bind in a distal site, even when hydroxyethyl-thiamine diphosphate is formed (Meyer *et al.*, 2012). At sufficiently high concentrations it could out-compete phosphate by occupying its binding site. This would in turn decrease the rate of phosphorolysis and thereby the turnover. The impact of the mutation on the pre-steady state is less pronounced. The rate of FAD-reduction in absence of oxygen is only reduced by 60 % (Fig. 38, Section 3.5.2). So, while it seems to be partially involved in positioning of substrate and intermediate formation, its main functions are located after these steps. The titration with phosphate yielded an apparently lowered K_D (Fig. 73, Appendix). This could mean that Glu$_{483}$ actually is required to destabilize phosphate-binding, and is involved in promoting phosphorolysis and substrate release, by the repulsive effect of its negative charge. The same effect could explain the impact on formation of HEThDP, as the negative charge could promote decarboxylation of LThDP. As no structural investigation

was performed, it is not reasonable to draw conclusions in regards to a possible impact of both variants on the tautomeric state of the intermediate.

In summary, this work, together with the diploma thesis of Ann-Kristin Diederichs provided evidence for the possibility to induce formation of a non-aromatic keto-dihydroxyethyl-thiamine diphosphate by removing the crucial interaction partner His_{100}. This removal seemingly allows the intermediate to adopt a conformation similar to that in *Lp*POX, and thus allows proton transfer by the N4′ yielding the new species, given enough time. While this species seemingly does not occur under steady-state conditions, as the rate-impairment is not congruent with the introduction of a dead-end intermediate, it still serves well as proof-of-principle. Not only the interaction with His_{100} may be important for the stabilization of canonical Breslow-intermediate, but also the orientation of N4′ to the 2-OH by virtue of the total geometry of the cofactors.

In *Lp*POX, the unoccupied orbital of N4′ should be pointing directly towards the hydroxyethyl OH (∠ C4′-N4′-OH: 124.2 °), while the orbitals of OH should be doing the same (∠ C2α-OH-N4′: 107.2 °), allowing for efficient proton transfer to yield an intermediate as observed *in crystallo* by Meyer *et al.*, 2012. In *Ec*TK, by virtue of strain exerted by Phe_{437} on the aminopyrimidine ring, the geometry is much less suitable, and the distance between the two is significantly bigger (2.77 vs. 3.11 Å). The absence of His_{100} reduces this distance to 2.47 Å, possibly compensating the worse geometry. Interaction with His_{473} could further serve to avoid unfavorable interactions. However, as evidenced by structural data, it is not as impactful as His_{100}. His_{66} is important for catalysis not by stabilization of the intermediate, but by directing the movement of ThDP in a productive manner between the up- and down-conformation, not in a seemingly random motion. The non-strained C2-C3 bond of X5P-ThDP underlines the importance of this controlled motion, as selectively enacted strain was postulated as a catalytic principle in transketolase (Lüdtke *et al.*, 2013).

4.5 New Insights into Substrate Binding of *Escherichia coli* Transketolase

The caption of different states of X5P on the trajectory from the docking site to the covalent adduct may help to discern the key players in facilitating this movement. The general motion towards the cofactor seems to be driven to a great extent by the interactions of the 4-OH with Asp_{469}, which in course of the movement forms a very short hydrogen bond of 2.52 Å. Such a bond should contribute considerable energy, as it falls in the regime of short, strong hydrogen bonds, with a potential energy of 7-20 $\frac{kcal}{mol}$. Further, the distances between 3-OH and the histidines 26 and 261 decrease, crossing the boundary from weak to medium hydrogen bonds. More curious is the reason for the rotation of the C2-C3 bond, which is necessary for proper positioning of the sugar C2 towards the thiazolium C2. In the unturned state, the C2-C2 distance is approximately 4 Å, but for a nucleophilic attack the distance is required to be below 3 Å (Fig. 42, Section 3.6 and table 13, Appendix)(Burgi *et al.*, 1973).

The absence of this motion in *Ec*TK_{H100A}-X5P identified this residue as important player, which is not exactly unexpected, as it was already implicated in discrimination of the 1-OH group of substrates (Diederichs, 2009). However, from the unturned position the distance between 1-OH and His_{100} is $\geq$ 4.5 Å, making random movement towards it unlikely. However, already in this state there is some clash with the up-conformation of ThDP. As such, it could be that the sugar is displaced by the cofactor dynamics, and nudged towards Asp_{469}, which helps to direct the 1-OH in interaction distance to His_{100}. As His_{100} donates a proton to the hydrogen bond with the backbone oxygen of Asp_{469} it is likely to form a stable hydrogen bond with the reoriented 1-OH (Fig. 41, Section 3.6).
A further important feature is the presence of a strained sugar C2-C3 bond in the tetrahedral X5P-ThDP adduct, as was observed in human transketolase (Lüdtke *et al.*, 2013). The bond length increases from 1.54 to 1.66 Å, which significantly weakens this bond, making it more scissile (Fig. 52). Important is the absence of strain in the non-bound intermediate, clearly showing that the strain is not induced by the interactions of the sugar with the active site, but only by formation of the tetrahedral adduct, which forces

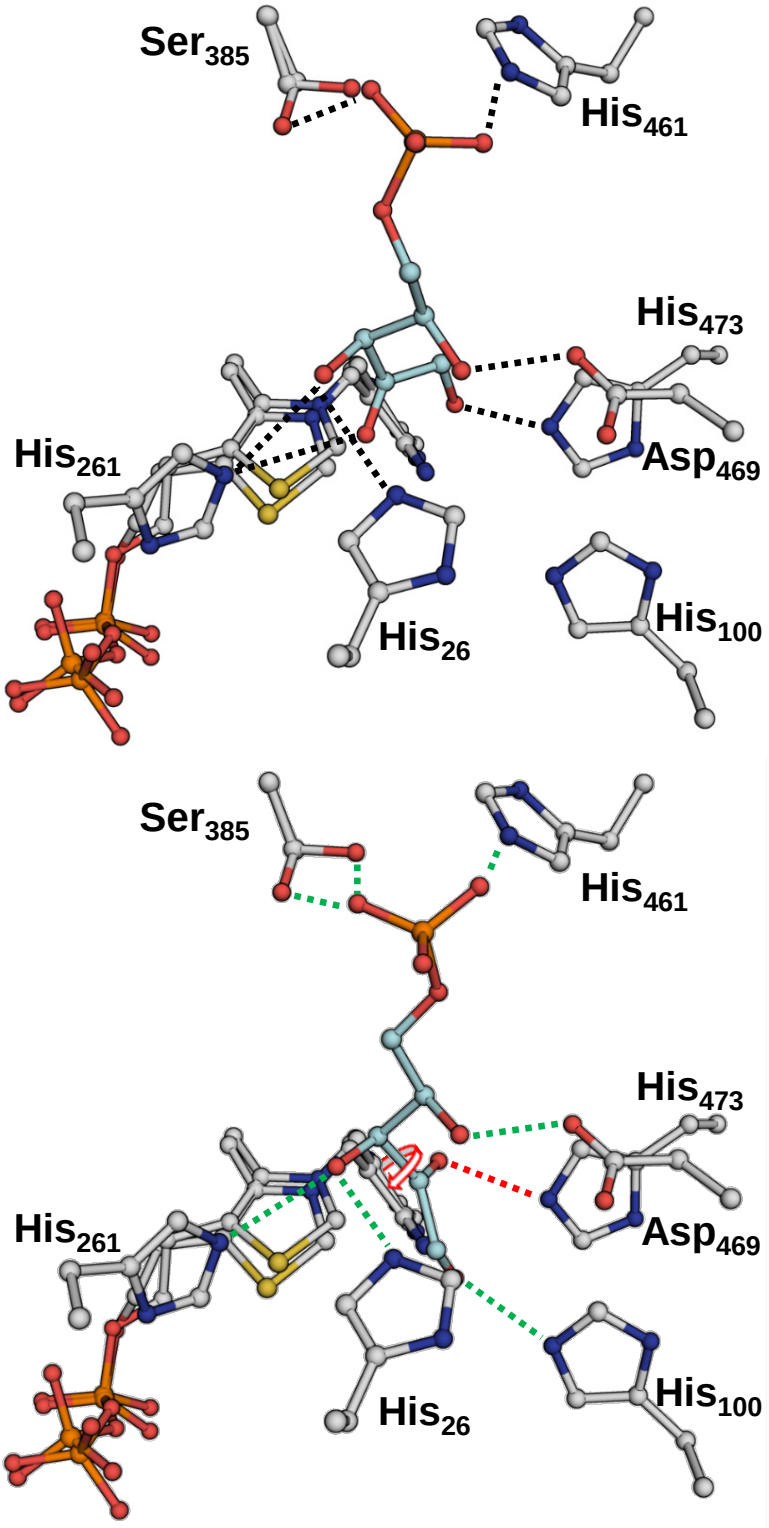

Figure 51. Movement of X5P from the docking site (top) towards the pre-covalent (bottom) position. The interaction distances of X5P are indicated by black dashes. For X5P in the pre-covalent position, red dashes indicate a relative increase of the distance compared to the docking site interaction, while green dashes indicate a reduction of the distance.

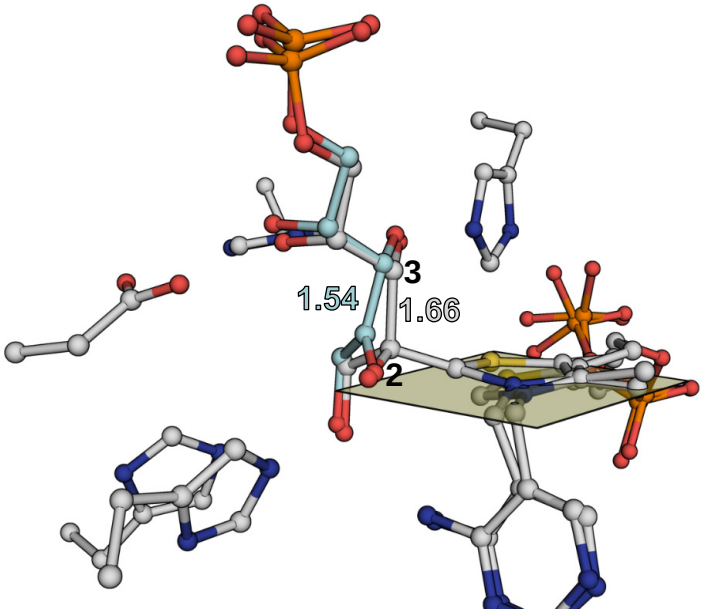

Figure 52. The strained X5P-ThDP adduct in *Escherichia coli* transketolase. X5P is shown in the covalently bound state (gray) and in the unbound state (cyan). The respective length of the sugar C2-C3 bond is indicated in Å, and the atoms are named. The plane of the thiazolium ring is indicated.

the thiazolium C2 out of plane. The strain on the plane paired with the up- and down-motion of the cofactor then introduces sufficient stress to induce the bond-elongation. As mentioned before, the intermediate formed in *Ec*TK_{H66A} does not exhibit the strained bond, showing the importance of the cofactor dynamic, at least in *Escherichia coli* transketolase.

Crystallographic investigation revealed the presence of dominantly linear R5P, while in literature mainly the circular form was observed (Asztalos *et al.*, 2007). The distribution observed here was approximately ⅔ of linear to ⅓ circular form. Additionally, the linear form protruded significantly deeper into the active site than observed before. Partially, the R5P-C1 was positioned in covalent bond distance to the thiazolium C2, and the anisotropy of C1 strongly suggested the presence of a dynamic covalent-non-covalent equilibrium (Fig. 44, Section 3.6). The formation of this unexpected intermediate is probably owed to the increased soaking time, which aimed to increase the occupancy of R5P.

There is ongoing discussion regarding the question if enzymes do catalyze the ring-opening of cyclic substrates (Tittmann, 2014). There is strong evidence supporting this assumption for some enzymes. In rabbit fructose-1,6-bisphosphate aldolase (FBP) presteady-state kinetics revealed faster Schiff-base formation than ring-opening is

observed in solution (Choi and Tolan, 2004). Further work on variants of *Thermoproteus tenax* FBP allowed capture of the cyclic intermediate, and resulted in the proposal of a concerted ring opening conjointly catalyzed by the enzyme and the phosphate group of the sugar (Lorentzen *et al.*, 2005). In transketolase, kinetic and structural data suggest the requirement of ring-opening by the enzyme. The k_{cat} of 53 s^{-1} for *Ec*TK_{WT}, or the even higher values observed in some of the variants, exceed the rate of ring-opening of R5P, estimated to be $\leq$ 50 s^{-1} at 25 °C (Pierce *et al.*, 1985). The same holds true for the reaction with F6P. Assuming that this reaction proceeds at approximately half of the speed of the reaction with X5P, k_{cat} is approximately 25 s^{-1} (Sprenger *et al.*, 1995). This exceeds the rate of ring-opening of F6P in solution at least twice (Pierce *et al.*, 1985).

The structures of *Ec*TK with cyclic R5P do not show an acid-base catalyst in proximity to the furanose oxygen. However, the phosphate group of sugar phosphates was shown to significantly contribute to the rate of ring-opening in solution by intramolecular catalysis (Pierce *et al.*, 1985). While it is not near the furanose oxygen, it could interact via the solvent. Additionally, the enzyme could exert strain on the ether-bond. The 2- and 3-OH form tighter interactions with the active site in the acyclic form, as does the phosphate moiety. This could serve to pull the ring further into the active site. However, as the anomeric 1-OH is in van-der-Waals clash distance to Ile_{189} and His_{261}, further enhanced by movement, this may weaken the ether-bond and make it more prone for protonation by the solvent, facilitating ring opening.

The structural capture of multiple states of the enzyme-X5P complex on the trajectory towards the covalent adduct allowed to identify the key-interactions required for rotation of the C2-C3 axis of X5P, as required for proper intermediate formation, as well for promotion of the movement towards the cofactor. Further, identification of the cofactor and potentially the enzyme-promoted dynamics as source of the strain on the C2-C3 bond was possible. This strain is thought to promote cleavage of the intermediate to the first product and dihydroxyethyl-thiamine diphosphate. The structure of *Ec*TK_{WT} with R5P allowed the surprising observation of a covalent R5P-ThDP complex, albeit at low occupancy, in dynamic equilibrium with non-covalently bound R5P. Further, it

allowed some speculation regarding the contribution of the enzyme environment to ring opening of cyclic sugar substrates.

5 Summary & Outlook

In this work, the importance of certain invariant residues of transketolase with no direct catalytic function was demonstrated. It elucidated the importance of the two moieties flanking the activating glutamate, namely the conserved water molecule and glutamate 160. As the glutamate is not conserved among all ThDP-dependent enzymes, it can be reasoned that this position is modified according to the needs of the individual enzyme depending on e.g. the hydrophobic character of the active site or the pH-optimum. To further the understanding regarding the importance of providing these interactions to the activating glutamate, introduction of a leucine residue at position 160 would be recommendable, as to increase the hydrophobicity of the surroundings. Further, by mutagenesis of Thr_{433} to leucine or isoleucine, a complete displacement of the conserved water molecule should be attempted. To see how the glutamate behaves with only the aminopyrimidine N1 as interaction partner, a variant with both a leucine at position 160 and a removed water should be investigated. Variants of Thr_{433} should be investigated in human transketolase, where the only contribution to the kinetic behavior of the enzyme should stem from the changed interaction with the activating glutamate, as the ThDP dynamic is absent.

Glutamate 165 was identified as a crucial structural component. Mutagenesis to an uncharged amino acid partially unraveled the enzyme, rendering it catalytically inactive, as it lost its capability to bind ThDP. To further probe the importance of single interactions for the proper fold of the enzyme, some conserved residues spring to mind. For example the salt bridge formed by Glu_{612} and Arg_{483}, the interacting triad of Arg_{492}, Ser_{559} and Glu_{560}, the interaction of Arg_{57} and Glu_{110}. However, all of these form pretty obvious intra-monomer salt bridges. More important would be interactions at the dimer-interface, such as those by Ser_{638}, Tyr_{440} or Arg_{410}.

Further, the ThDP analogue 2'-methoxythiamine diphosphate was investigated. This compound was shown to inhibit certain bacterial ThDP-dependent enzymes (Reddick *et al.*, 2001). It was not yet clear if this is owed to general catalytic incompetence, or to a binding mode different to that of ThDP. The initial results obtained by Nemeria *et al.*

pointed towards the latter, as the human pyruvate dehydrogenase retained up to 75 % activity after recombination with MeOThDP. This was verified by structural investigation of *Ec*TK recombined with MeOThDP, where a clash of the methoxy-function with the protein environment displaced the cofactor significantly. The displacement increased the crucial distance of the cofactor N1 to the activating glutamate to $\geq$ 3.5 Å, reducing the activation rate of the thiazolium C2 to approximately 3 s^{-1}, compared to around 300 s^{-1} in the ThDP-reconstituted enzyme. This was further supported by the observation of primary unreacted cofactor after incubation with substrate in NMR experiments as well as in crystallographic studies. The apparent resistance of human ThDP-dependent enzymes against this compound, either by very tight binding of ThDP or by being able to accommodate MeOThDP in a manner allowing for only marginally reduced activity may make MeOThDP a promising candidate for probing as antibiotic. Yet, obtaining the K_I of MeOThDP in human and *E. coli* transketolase and pyruvate dehydrogenase to gauge the competitiveness of the analogue should be performed.

Investigation of the dynamics of the cofactor, observed not only in *Escherichia coli* but also in *Scheffersomyces stipitis* (Hsu *et al.*, 2016), revealed that the main actor in directing the movement is histidine 66. Mutagenesis of this residue to alanine changed the motion to one along the thiazolium ring plane, instead of up- and downwards. The absence of this movement in human transketolase can be explained by restriction of this movement by the residues below and atop of the thiazolium ring, which form a tighter pocket than observed *Ec*TK and *ss*TK. To rule out that the planar movement in the resting state is not induced by the interaction with the new conformation of His_{26}, a double mutant should be generated to probe this issue. In general, crystal structures of transketolases from additional organisms will be necessary to determine when, why and how the dynamics were lost in evolution from bacteria and yeast to human transketolase.

Building on the data provided by Ann-Kristin Diederichs, the (de)-stabilization of the classical carbanion/enamine Breslow intermediate in *Ec*TK was further investigated. The three histidines flanking the intermediate were mutated and the variants characterized. While all variants significantly impact the catalytic efficiency by reduction of both, reaction

velocity and apparent substrate affinity, only His_{100} revealed an importance for the character of the intermediate. In the dataset collected and initially refined by Ann-Kristin Diederichs, a intermediate clearly deviating from planarity was observed. Further refinement confirmed the angles of the thiazolium C2 to be more tetrahedral in character. The bond of the C2α to its oxygen was more similar in character to a double-bond, as far as it is reasonable to state at a resolution of 1.7 Å. This further supports the idea that a keto-intermediate is indeed the thermodynamic minimum of the Breslow intermediate, and that the enzyme needs to stabilize the carbanion/enamine form when required for catalysis (Berkessel *et al.*, 2010; Meyer *et al.*, 2012). It should be aimed to obtain a crystal of the new intermediate at true atomic resolution, which failed during this work. Further, the variants of *Lp*POX need to be characterized structurally, to allow a statement regarding the character of their respective intermediates. Unfortunately, there are no methods to detect ketones in solution suitable to preserve the enzyme environment, as they require denaturing conditions. Using NMR to investigate the character of the intermediate against the enzyme background would be a very demanding method, even when using ^{13}C or ^{17}O labeled substrates.

Pushing the resolution limits of the intermediate-enzyme complexes of *Ec*TK with substrates X5P and R5P to true atomic resolution allowed to shed some light on the mechanism by which movement of X5P towards the cofactor, as well as the reorientation of the C1 and C2 group take place. His_{100} was identified as a key player in the rotary motion, as well as Asp_{469} for the movement towards the active site by virtue of formation of a very short hydrogen bond. The structure of *Ec*TK with R5P allowed observation of a lowly populated covalent R5P-ThDP species, and mainly linear R5P. A possible contribution of the enzyme environment to ring opening by exerting strain on the furanose ether was discussed. To investigate this notion, datasets of variants of the residues Asp_{469}, His_{26}, His_{261} and possibly His_{473} soaked with R5P under standardized conditions should be collected. Further kinetic investigation regarding R5P binding should be performed by stopped-flow spectrometry and isothermal calorimetry.

6 Appendix

Table 4. Collected Datasets. Given are the variant, the place of data collection, the soaking conditions and the final resolution to which the structures were refined.

Crystal	Collection	Soaking	Resolution [Å]
*Ec*TK$_{E165Q}$	ESRF Grenoble	No soaking	2.156
*Ec*TK$_{E160Q}$	DESY Hamburg	No soaking	1.3
*Ec*TK$_{E160Q}$	DESY Hamburg	No soaking	1.7
*Ec*TK$_{H261N}$	DESY Hamburg	No soaking	1.03
*Ec*TK$_{H261N}$	DESY Hamburg	100 mM X5P	1.09
*Ec*TK$_{MeOThDP}$	DESY Hamburg	No soaking	0.92
*Ec*TK$_{MeOThDP}$	DESY Hamburg	100 mM X5P	0.95
*Ec*TK$_{T433Q}$	DESY Hamburg	No soaking	1.25
*Ec*TK$_{T433Q}$	DESY Hamburg	100 mM X5P	1.47
*Ec*TK$_{T433V}$	DESY Hamburg	No soaking	1.13
*Ec*TK$_{T433V}$	DESY Hamburg	100 mM X5P	1.15
*Ec*TK$_{H66A}$	DESY Hamburg	No soaking	1.11
*Ec*TK$_{H66A}$	DESY Hamburg	100 mM X5P	1.09
*Ec*TK$_{H66A}$	DESY Hamburg	40 mM HPA	1.25
*Ec*TK$_{H100A}$	DESY Hamburg	100 mM X5P	1.15
*Ec*TK$_{H473Q}$	DESY Hamburg	100 mM X5P	1.5
*Ec*TK$_{H473Q}$	DESY Hamburg	40 mM HPA	1.6
*Ec*TK$_{WT}$	DESY Hamburg	No soaking	0.97
*Ec*TK$_{WT}$	DESY Hamburg	No soaking	1.00
*Ec*TK$_{WT}$	DESY Hamburg	100 mM X5P	0.93
*Ec*TK$_{WT}$	DESY Hamburg	100 mM X5P	1.04
*Ec*TK$_{WT}$	MSB Göttingen	100 mM X5P	1.3
*Ec*TK$_{WT}$	DESY Hamburg	100 mM R5P	1.05

Table 5. Refinement statistics of *Ec*TK$_{E160A}$, *Ec*TK$_{E160Q}$ and *Ec*TK$_{E165Q}$

	***Ec*TK$_{E160A}$**	***Ec*TK$_{E160Q}$**	***Ec*TK$_{E165Q}$**
Data collection			
Parameters			
Space group	$P2_12_12_1$	$P2_12_12_1$	$P2_12_12_1$
Cell dimensions			
a,b,c [Å]	90.00, 101.93, 133.18	89.76, 101.68, 132.84	96.38, 102.35, 132.04
α,β,γ [deg]	90, 90, 90	90, 90, 90	90, 90, 90
Resolution [Å]	50 – 1.7	47.48 – 1.3	48.08 - 2.156
R_{meas}	17.4 (76.2)	11.2 (91.4)	15 (71.6)
I/σ(I)	11.24 (2.36)	15.15 (2.96)	7.36 (1.95)
CC-half (%)	99.7 (92.4)	99.9 (78.7)	99.3 (75)
Completeness [%]	99.9 (99.3)	100 (100)	96.8 (98.8)
Redundancy	13.1 (12.7)	12.9 (12.9)	3.89 (3.93)
Refinement			
Resolution [Å]	47.6 – 1.7	47.48 – 1.3	48.08 - 2.156
Unique Reflections	134582	577753	68815
R_{work}, R_{free} [%]	14.8, 18.7	13.6, 15.9	21.14, 26.15
No. of Atoms			
Protein (Chain A,B)	5231, 5251	5408, 5410	5023, 4977
Water	1589	1641	705
Ligands	104	182	16
B factors [Å^2]			
Protein (Chain A,B)	12.5, 12.9	12.8, 12.9	34.7, 34.2
Water	24.13	26.1	33.4
Ligands	16.34	17.3	34.9
Wilson B factor [Å^2]	13.1	10.7	27.1
RMSD			
Bond Length [Å]	0.017	0.008	0.003
Bond Angles [deg]	1.62	1.31	0.67
Ramachandran			
Outliers [%]	0.00	0.00	0.46
Allowed [%]	1.76	1.79	3.17
Favored [%]	98.24	98.21	96.37

Table 6. Refinement statistics of *Ec*TK$_{T433V}$, *Ec*TK$_{T433V}$-X5P and *Ec*TK$_{T433Q}$

	***Ec*TK$_{T433V}$**	***Ec*TK$_{T433V}$-X5P**	***Ec*TK$_{T433Q}$**
Data collection			
Parameters			
Space group	$P2_12_12_1$	$P2_12_12_1$	$P2_12_12_1$
Cell dimensions			
a,b,c [Å]	89.71, 101.80, 132.52	89.54, 101.81, 132.53	89.64, 101.86, 132.45
α,β,γ [deg]	90, 90, 90	90, 90, 90	90, 90, 90
Resolution [Å]	50 – 1.13	50 – 1.15	50 - 1.25
R_{meas}	8.5 (98.3)	9.2 (96.2)	8.2 (83)
I/σ(I)	23.01 (3.45)	18.01(2.81)	23.65 (3.83)
CC-half (%)	100 (85.2)	100 (78.1)	100 (89.1)
Completeness [%]	100 (100)	99.9 (99.9)	100 (100)
Redundancy	13.3 (13)	8.9 (8.4)	13.4 (12.9)
Refinement			
Resolution [Å]	44.27 – 1.13	42.42 – 1.15	47.54 - 1.25
Unique Reflections	449572	425737	332727
R_{work}, R_{free} [%]	11, 12.9	11, 13.6	11.3, 13.4
No. of Atoms			
Protein (Chain A,B)	5154, 5217	5187, 5213	5127, 5197
Water	1352	1465	1460
Ligands	120	206	147
B factors [Å^2]			
Protein (Chain A,B)	10, 9.9	9.9, 9.9	11.2, 11.1
Water	22.9	24.4	25
Ligands	12.3	11.8	17.4
Wilson B factor [Å^2]	8.6	8.7	9.6
RMSD			
Bond Length [Å]	0.008	0.009	0.007
Bond Angles [deg]	1.21	1.59	1.05
Ramachandran			
Outliers [%]	0.00	0.00	0.46
Allowed [%]	2.19	1.89	1.89
Favored [%]	97.81	98.11	98.11

Table 7. Refinement statistics of *Ec*TK$_{T433Q}$-X5P, *Ec*TK$_{H261N}$ and *Ec*TK$_{H261N}$-X5P

	***Ec*TK$_{T433Q}$-X5P**	***Ec*TK$_{H261N}$**	***Ec*TK$_{H261N}$-X5P**
Data collection			
Parameters			
Space group	$P2_12_12_1$	$P2_12_12_1$	$P2_12_12_1$
Cell dimensions			
a,b,c [Å]	89.65, 102.02, 132.76	89.88, 101.82, 132.73	89.70, 102.10, 132.85
α,β,γ [deg]	90, 90, 90	90, 90, 90	90, 90, 90
Resolution [Å]	50 – 1.47	50 – 1.03	50 - 1.09
R_{meas}	10.8 (99.8)	7.3 (88.2)	6.7 (88.4)
I/σ(I)	17.24 (2.65)	13.85(2.52)	20.23 (3.2)
CC-half (%)	99.9 (77.7)	99.9 (62.0)	100 (81.5)
Completeness [%]	100 (100)	99.3 (97.3)	100 (99.9)
Redundancy	8.99 (8.95)	5.7 (4.1)	10.3 (9)
Refinement			
Resolution [Å]	44.34 – 1.47	47.28 – 1.03	47.65 - 1.09
Unique Reflections	206225	591955	503080
R_{work}, R_{free} [%]	14.9, 16.3	10.1, 11.4	10.5, 12.3
No. of Atoms			
Protein (Chain A,B)	5178, 5239	5352, 5320	5353, 55358
Water	987	1438	1372
Ligands	162	211	234
B factors [Å^2]			
Protein (Chain A,B)	12.2, 12.1	10.7, 10.7	11.5, 11.4
Water	20.1	25	26.1
Ligands	15.2	14.7	13.8
Wilson B factor [Å^2]	11.3	8.7	9.9
RMSD			
Bond Length [Å]	0.008	0.01	0.01
Bond Angles [deg]	1.4	1.54	1.52
Ramachandran			
Outliers [%]	0.00	0.00	0.00
Allowed [%]	1.81	1.81	1.73
Favored [%]	98.191	98.19	98.27

Table 8. Refinement statistics of *Ec*TK$_{MeOThDP}$, *Ec*TK$_{MeOThDP}$-X5P and *Ec*TK$_{H66A}$

	***Ec*TK$_{MeOThDP}$**	***Ec*TK$_{MeOThDP}$-X5P**	***Ec*TK$_{H66A}$**
Data collection			
Parameters			
Space group	$P2_12_12_1$	$P2_12_12_1$	$P2_12_12_1$
Cell dimensions			
a,b,c [Å]	89.55, 101.91, 132.96	89.76, 102.08, 133.13	89.89, 102.19, 133.30
α,β,γ [deg]	90, 90, 90	90, 90, 90	90, 90, 90
Resolution [Å]	50 – 0.92	50 – 0.95	50 - 1.11
R_{meas}	9.5 (61.4)	8.1 (88.6)	10.3 (91.8)
I/σ(I)	9.73 (2.22)	12.46 (2.42)	12.49 (2.48)
CC-half (%)	99.4 (66.8)	99.8 (63.3)	99.9 (68.4)
Completeness [%]	93.8 (61.6)	98.9 (96.6)	99.1 (98.2)
Redundancy	4.2 (2.9)	6.1 (5)	6.5 (6)
Refinement			
Resolution [Å]	47.685 – 0.92	47.658 – 0.95	47.65 - 1.11
Unique Reflections	780617	751411	475687
R_{work}, R_{free} [%]	10.9, 11.9	10.3, 11.4	12.7, 14.4
No. of Atoms			
Protein (Chain A,B)	5592, 5557	5491, 5527	5337, 5316
Water	1453	1418	1498
Ligands	222	230	123
B factors [Å^2]			
Protein (Chain A,B)	8.3, 8.6	9, 9.1	10.5, 10.5
Water	22.8	23	22.9
Ligands	12.5	12.5	13.7
Wilson B factor [Å^2]	7.6	7.6	8.3
RMSD			
Bond Length [Å]	0.007	0.009	0.007
Bond Angles [deg]	1.2	1.5	1.11
Ramachandran			
Outliers [%]	0.00	0.00	0.08
Allowed [%]	1.81	1.83	2.04
Favored [%]	98.191	98.17	97.89

Table 9. Refinement statistics of *Ec*TK$_{H66A}$-X5P, *Ec*TK$_{H66A}$-HPA and *Ec*TK$^{AKD}_{H100A}$

	***Ec*TK$_{H66A}$-X5P**	***Ec*TK$_{H66A}$-HPA**	***Ec*TK$^{AKD}_{H100A}$**
Data collection			
Parameters			
Space group	$P2_12_12_1$	$P2_12_12_1$	$P12_11$
Cell dimensions			
a,b,c [Å]	89.73, 102.08, 133.91	89.61, 102.04, 132.64	86.73, 73.12, 106.78
α,β,γ [deg]	90, 90, 90	90, 90, 90	90, 94.35, 90
Resolution [Å]	50 – 1.09	50 – 1.25	50 - 1.73
R_{meas}	9.2 (92.1)	10.7 (110.4)	6.1 (30.5)
I/σ(I)	13.91 (2.54)	21.07 (3.09)	15.3 (4.4)
CC-half (%)	99.4 (72)	100 (81.8)	
Completeness [%]	99.4 (98.6)	97.0 (95.2)	98 (92.2)
Redundancy	6.5 (5.9)	13.6 (13.3)	2.8 (2.6)
Refinement			
Resolution [Å]	47.7 – 1.09	80.8 – 1.25	28.8 - 1.73
Unique Reflections	500483	288673	136250
R_{work}, R_{free} [%]	11.3, 13.1	14.4, 16.3	14.7, 17.3
No. of Atoms			
Protein (Chain A,B)	5316, 5297	5260, 5304	5108, 5129
Water	1502	1553	1749
Ligands	179	138	176
B factors [Å^2]			
Protein (Chain A,B)	9.7, 9.8	11.1, 10.9	16.7, 15.5
Water	23.5	24.1	29.7
Ligands	13.8	14.4	26.2
Wilson B factor [Å^2]	8.4	9.5	15.4
RMSD			
Bond Length [Å]	0.007	0.006	0.005
Bond Angles [deg]	1.11	1.01	1.10
Ramachandran			
Outliers [%]	0.00	0.00	0.08
Allowed [%]	1.58	1.81	2.2
Favored [%]	98.42	98.19	97.8

Table 10. Refinement statistics of *Ec*TK$_{H100A}$-X5P, *Ec*TK$_{H473Q}$-X5P and *Ec*TK$_{H100A}$-HPA

	***Ec*TK$_{H100A}$-X5P**	***Ec*TK$_{H473Q}$-X5P**	***Ec*TK$_{H473Q}$-HPA**
Data collection			
Parameters			
Space group	$P2_12_12_1$	$P2_12_12_1$	$P2_12_12_1$
Cell dimensions			
a,b,c [Å]	90.00, 101.81, 133.00	90.05, 101.93, 133.17	89.60, 101.82, 132.65
α,β,γ [deg]	90, 90, 90	90, 90, 90	90, 90, 90
Resolution [Å]	50 – 1.15	50 – 1.5	50 - 1.6
R_{meas}	9.4 (77.7)	12.1 (54.2)	17.6 (83.7)
I/σ(I)	13.8 (2.5)	12.81 (3.54)	17.6 (83.7)
CC-half (%)	99.9 (70)	99.8 (86.1)	99.9 (90.3)
Completeness [%]	99.2 (95.1)	98.5 (97.2)	99.9 (99.9)
Redundancy	6.3 (4.9)	6.8 (6.8)	20.1 (19.4)
Refinement			
Resolution [Å]	80.84 – 1.15	47.6 – 1.5	47.6 - 1.6
Unique Reflections	426431	192581	159742
R_{work}, R_{free} [%]	11.9, 13.7	16.7, 19.6	17.7, 19.7
No. of Atoms			
Protein (Chain A,B)	5290, 5260	5237, 5264	5079, 5149
Water	1777	1590	1466
Ligands	134	114	110
B factors [Å^2]			
Protein (Chain A,B)	9.3, 9.6	9, 9.3	11.5, 11.2
Water	22.1	22.2	20.8
Ligands	13.2	14.4	12.1
Wilson B factor [Å^2]	8	8.5	10.6
RMSD			
Bond Length [Å]	0.007	0.01	0.006
Bond Angles [deg]	1.15	1.5	1
Ramachandran			
Outliers [%]	0.00	0.00	0.00
Allowed [%]	1.96	1.89	2.11
Favored [%]	98.04	98.11	97.89

Table 11. Refinement statistics of *Ec*TK_{WT}-1, *Ec*TK_{WT}-X5P-1 and *Ec*TK_{WT}-X5P-2

	***Ec*TK$_{WT}$-1**	***Ec*TK$_{WT}$-X5P-1**	***Ec*TK$_{WT}$-X5P-2**
Data collection			
Parameters			
Space group	$P2_12_12_1$	$P2_12_12_1$	$P2_12_12_1$
Cell dimensions			
a,b,c [Å]	89.91, 101.83, 132.62	89.69, 101.80, 132.81	89.83, 101.71, 132.88
α,β,γ [deg]	90, 90, 90	90, 90, 90	90, 90, 90
Resolution [Å]	50 – 1.00	50 – 0.97	50 - 1.3
R_{meas}	7.3 (84.2)	8.5 (102.5)	10.3 (95.9)
$I/\sigma(I)$	11.8 (1.8)	11 (1.6)	9.7 (1.4)
CC-half (%)	99.9 (56)	99.9 (46.4)	99.7 (50.3)
Completeness [%]	95.3 (93.2)	98.0 (98.2)	99.7 (99.5)
Redundancy	4.5 (3.2)	4.3 (3.4)	4.2 (2.9)
Refinement			
Resolution [Å]	47.3 – 1.00	42 – 0.97	42 - 1.30
Unique Reflections	636280	695908	296333
R_{work}, R_{free} [%]	10.7, 12.4	11.1, 12.5	13.4, 16.1
No. of Atoms			
Protein (Chain A,B)	5397, 5329	5226, 5283	5235, 5265
Water	1424	1510	1703
Ligands	216	222	178
B factors [Å^2]			
Protein (Chain A,B)	9.5, 9.5	8.2, 8.2	10.2, 10.4
Water	23.7	22.1	25.3
Ligands	11.7	9.2	12.9
Wilson B factor [Å^2]	7.8	6.8	9.1
RMSD			
Bond Length [Å]	0.008	0.008	0.009
Bond Angles [deg]	1.22	1.24	1.15
Ramachandran			
Outliers [%]	0.00	0.00	0.00
Allowed [%]	1.89	1.66	1.59
Favored [%]	98.11	98.34	98.41

Table 12. Refinement statistics of *Ec*TK_{WT}-X5P-3, *Ec*TK_{WT}-R5P and *Ec*TK_{WT}-2

	***Ec*TK$_{WT}$-X5P-3**	***Ec*TK$_{WT}$-R5P**	***Ec*TK$_{WT}$-2**
Data collection			
Parameters			
Space group	$P2_12_12_1$	$P2_12_12_1$	$P2_12_12_1$
Cell dimensions			
a,b,c [Å]	89.81, 101.86, 132.92	89.61, 101.76, 132.69	89.83, 101.79, 132.96
α,β,γ [deg]	90, 90, 90	90, 90, 90	90, 90, 90
Resolution [Å]	50 – 1.04	50 – 1.03	50 – 0.97
R_{meas}	19.4 (143.5)	7.5 (88.9)	7.4 (105.4)
$I/\sigma(I)$	17.3 (3.1)	18.4 (2.5)	18.2 (2.2)
CC-half (%)	99.9 (65.4)	100.0 (73.4)	100.0 (64.7)
Completeness [%]	98.5 (96.5)	99.9 (99.9)	100.0 (99.9)
Redundancy	43 (33.4)	8.7 (7.5)	8.5 (6.7)
Refinement			
Resolution [Å]	47.6 – 1.04	47.5 – 1.03	47.5 - 0.97
Unique Reflections	569829	592063	711584
R_{work}, R_{free} [%]	12.4, 14.1	11.1, 12.5	10.3, 11.1
No. of Atoms			
Protein (Chain A,B)	5294, 5303	5296, 5303	5372, 5369
Water	1597	1469	1542
Ligands	228	219	192
B factors [Å^2]			
Protein (Chain A,B)	8.9, 9	9.3, 9.5	8.5, 8.6
Water	22.3	19.1	22.2
Ligands	10.9	11.8	10.7
Wilson B factor [Å^2]	7.8		7
RMSD			
Bond Length [Å]	0.008	0.008	0.008
Bond Angles [deg]	1.54	1.28	1.28
Ramachandran			
Outliers [%]	0.00	0.00	0.00
Allowed [%]	1.81	1.58	1.88
Favored [%]	98.19	98.42	98.12

Table 13. Interactions of xylulose 5-phosphate in transketolase. The interaction distances of the respective sugar hydroxy/oxygen groups and their interaction partners are displayed in Å. Alternate conformations are indicated by α and β, the primary conformation is named α. The presence of multiple conformations of X5P is indicated by *C1* and *C2*. The absence of interactions between partners is indicated by ni, the absence of the interaction partner in the protein by nb.

X5P	**Protein**	**Distance** [Å]							
		*Ec*TK$_{MeOThDP}$	Dataset 1		Dataset 2	Dataset 3		*Ec*TK$_{H100A}$	Asztalos *et al.*, 2007
			C1	*C2*		*C1*	*C2*		
C2	Thiazolium-C2	ni	ni	2.52	2.93	2.90	1.50	ni	1.51
1-OH	His$_{100}$	ni	ni	2.85	2.78	2.81	2.90	nb	2.83
	His$_{473}$	2.69	2.41	3.16	3.01	2.88	2.71	2.67	ni
	AP-N4′	ni	ni	ni	ni	ni	ni	3.16	ni
2-OH	His$_{261}$	3.07	ni	ni	ni	ni	ni	3.15	ni
	His$_{473}$	ni	ni	2.86	2.85	2.88	2.71	ni	2.66
	AP-N4′	ni	ni	3.08	ni	ni	3.09	ni	3.10
3-OH	His$_{26}$	3.08	3.04	2.87	2.86	2.94	2.90	3.15	3.03
	His$_{261}$	3.08	3.10	2.88	2.96	2.95	2.80	2.96	2.80
4-OH	His$_{26}$	2.99	2.97	3.1	3.09	3.14	2.96	2.97	2.98
	Asp$_{469}$	2.68	2.68	2.55	2.52	2.55	2.63	2.63	2.63
Phos-OH	Arg$_{358}$	3.04	ni	ni	ni	ni	ni	ni	ni
	Ser$_{385}$-α	2.65	2.55	2.73	2.65	2.77	2.62	2.58	2.66
	Ser$_{385}$-β	2.72	2.74	2.49	2.43	2.39	2.47	2.59	2.60
	His$_{461}$	2.77	2.78	2.74	2.75	2.77	2.75	2.76	2.8
	Arg$_{520}$-Nε-α	2.79	2.89	2.66	2.69	2.72	2.73	2.74	2.82
	Arg$_{520}$-Nε-β	2.81	nb	nb	nb	nb	nb	nb	nb
	Arg$_{520}$-Nη-α	2.94	3.03	ni	ni	ni	ni	3.08	ni
	Arg$_{520}$-Nη-β	2.98	nb	nb	nb	nb	nb	nb	nb

Appendix

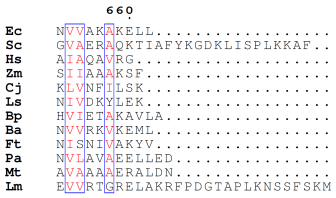

Figure 53. Protein-sequence alignment of all structurally elucidated transketolases. The sequences were taken from the Uniprot database, structural data from the protein data bank, alignment was performed using T-Coffee, the figure was generated using ESPript 3.0. Ec: *Escherichia coli*, Sc: *Saccharomyces cerevisae*, Hs: *Homo sapiens*, Zm: *Zea mays*, Cj: *Campylobacter jejuni*, Ls: *Lactobacillus salivarius*, Bp: *Burkholderia pseudomallei*, Ba: *Bacillus anthracis*, Ft: *Francisella tularensis*, Pa: *Pseudomonas aeruginosa*, Mt: *Mycobacterium tuberculosis*, Lm: *Leishmania mexicana*.

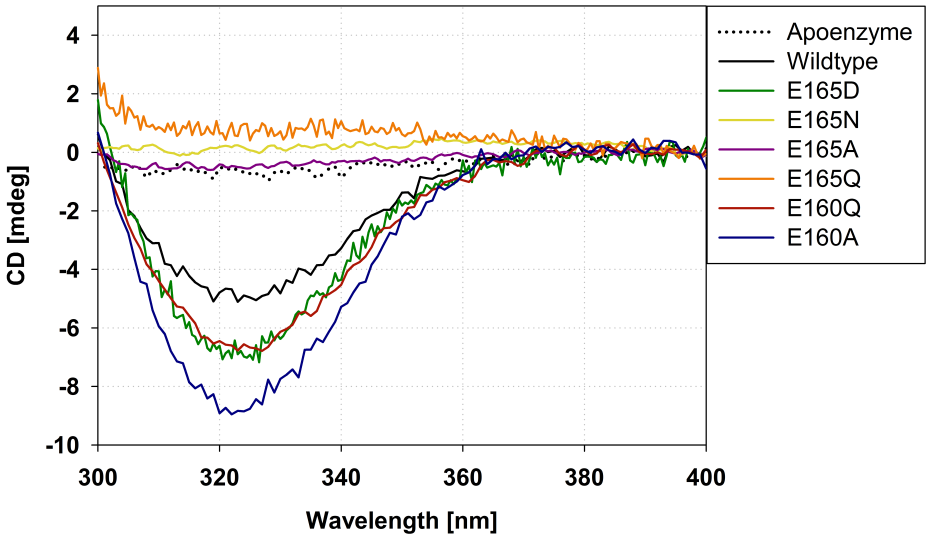

Figure 54. CD-spectra of reconstituted *Ec*TK$_{WT}$ and variants of glutamate 160 and 165. Except for apo-*Ec*TK$_{WT}$, all spectra shown were recorded at full ThDP saturation, or in case of non-binding variants at 300 μM ThDP.

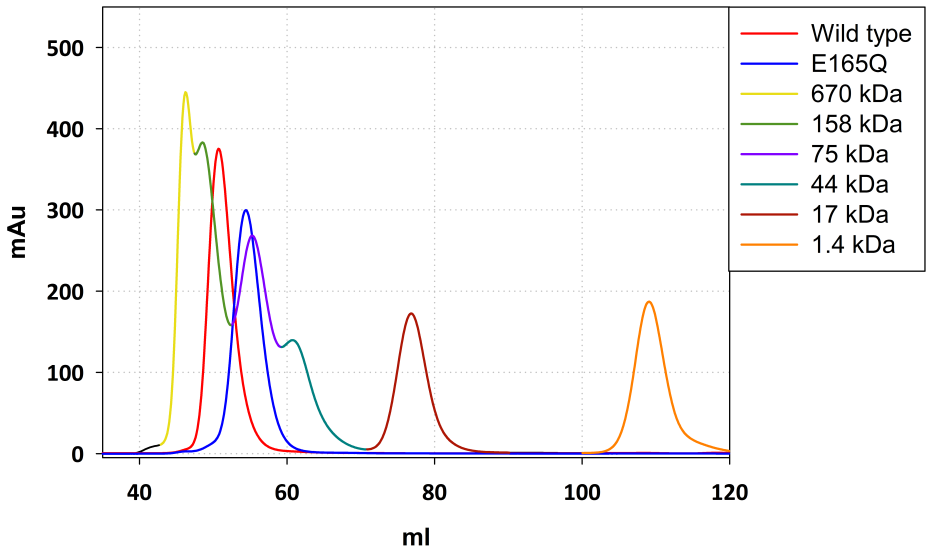

Figure 55. The chromatogram of *Ec*TK$_{E165Q}$ on an S75 column compared to *Ec*TK$_{WT}$ and a standard. The standard was mixed from the BioRad gel filtration standard (in descending weight: thyroglobulin, γ-globulin, ovalbumin, myoglobin, cyanocobalamin) and the GE gel filtration standard (conalbumin, 75 kDa).

A

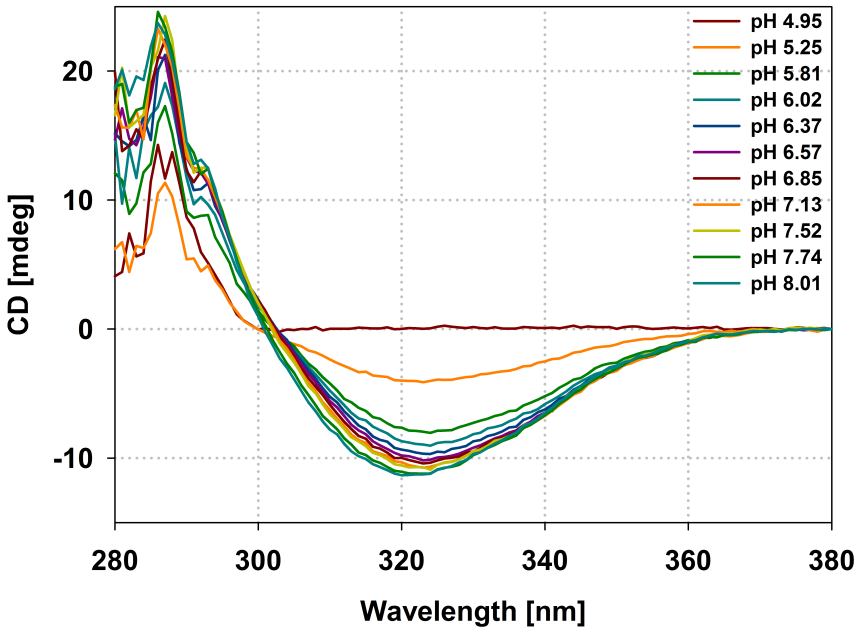

B

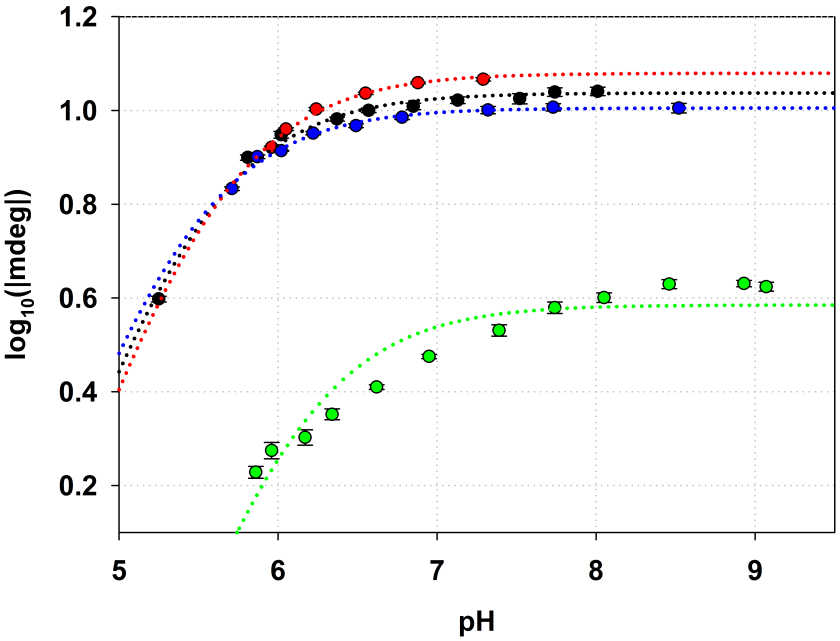

Figure 56. (A) Exemplary pH-titration of *Ec*TK$_{WT}$. The spectra are corrected for baseline and dilution. **(B) Plot of average log$_{10}$(|mdeg$_{324-326}$|) versus pH.** *Ec*TK$_{WT}$ is shown in black, *Ec*TK$_{E160A}$ in blue, *Ec*TK$_{E160Q}$ in red and *Ec*TK$_{E165D}$ in green. The data were fitted according to equation 5.

A

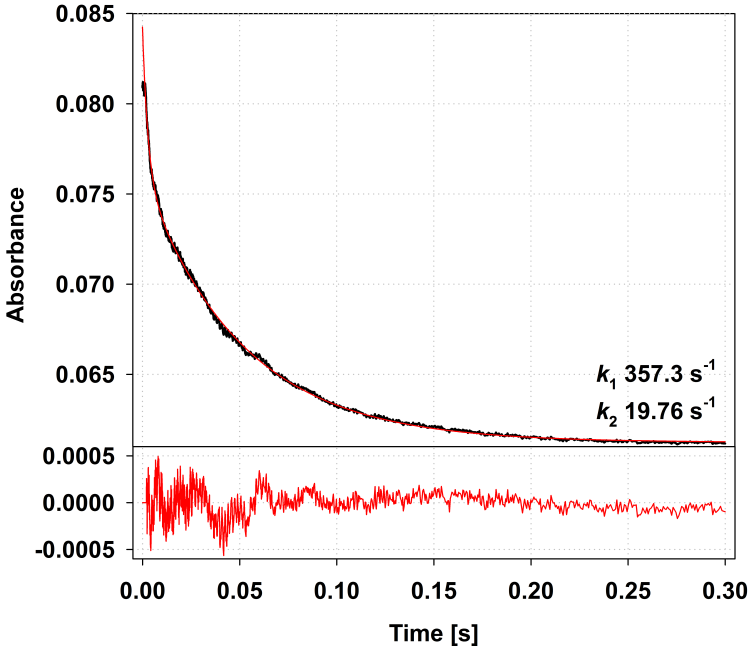

B

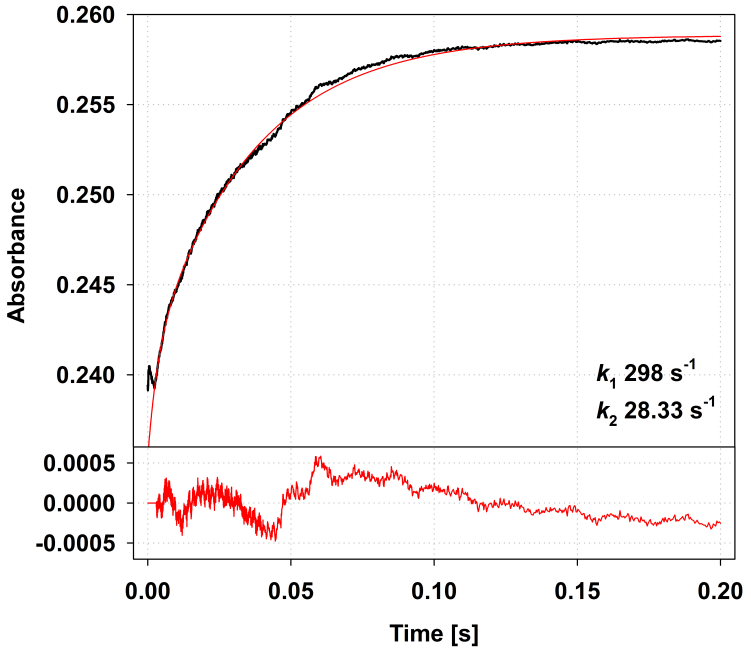

Figure 57. Exemplary transient for the depletion of the AP-band (A) and formation of the IP-band (B). Transients were recorded at 0.5 mM F6P. Both transients are averaged from multiple measurements and thus do not reflect the actual values used for plotting. The data were fitted according to equation 5.

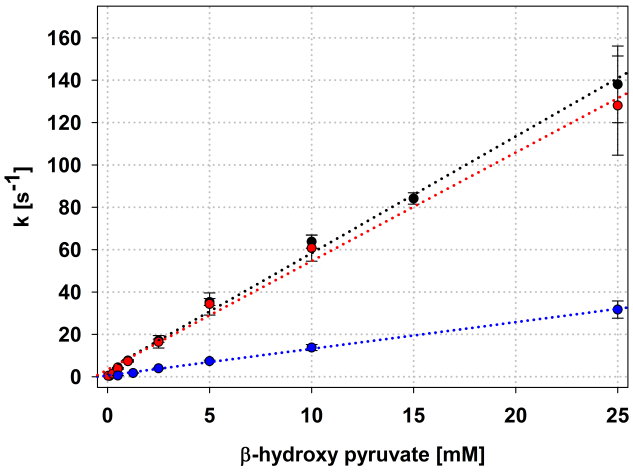

Variant	$\frac{k_{on}}{K_S}$ $s^{-1}mM^{-1}$
*Ec*TK$_{WT}$	5.5 ± 0.14
*Ec*TK$_{E160Q}$	5.1 ± 0.18
*Ec*TK$_{E160A}$	1.2 ± 0.04

Figure 58. Dependency of enamine formation on the β-hydroxypyruvate concentration in *Ec*TK$_{WT}$, *Ec*TK$_{E160Q}$ and *Ec*TK$_{E160A}$. *Ec*TK$_{WT}$ is shown in black, *Ec*TK$_{E160A}$ in blue and *Ec*TK$_{E160Q}$ in red. The plotted data were fitted according to equation 12.

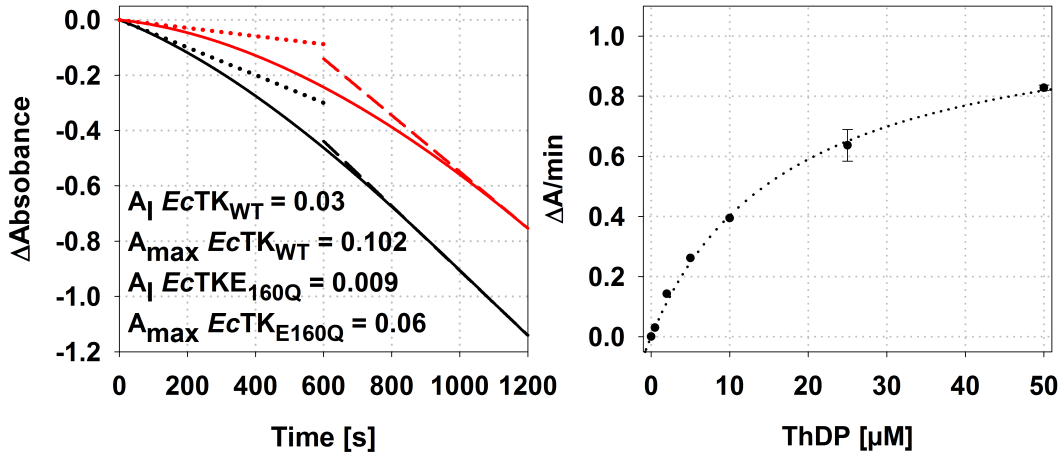

Figure 59. (Left) Exemplary progress curves for the determination of the K_M of ThDP. Progress curves were recorded at 0.5 μM ThDP of *Ec*TK$_{WT}$ (black) and *Ec*TK$_{E160Q}$ (red). The initial (A$_I$) and maximal (A$_{max}$) rates are expressed in $\frac{\Delta Absorbance}{min}$. **(Right) Plot of initial velocities at low enzyme concentrations for *Ec*TK$_{E160Q}$.** Measurements were performed at 0.5 μg/ml. The data were fitted according to equation 1.

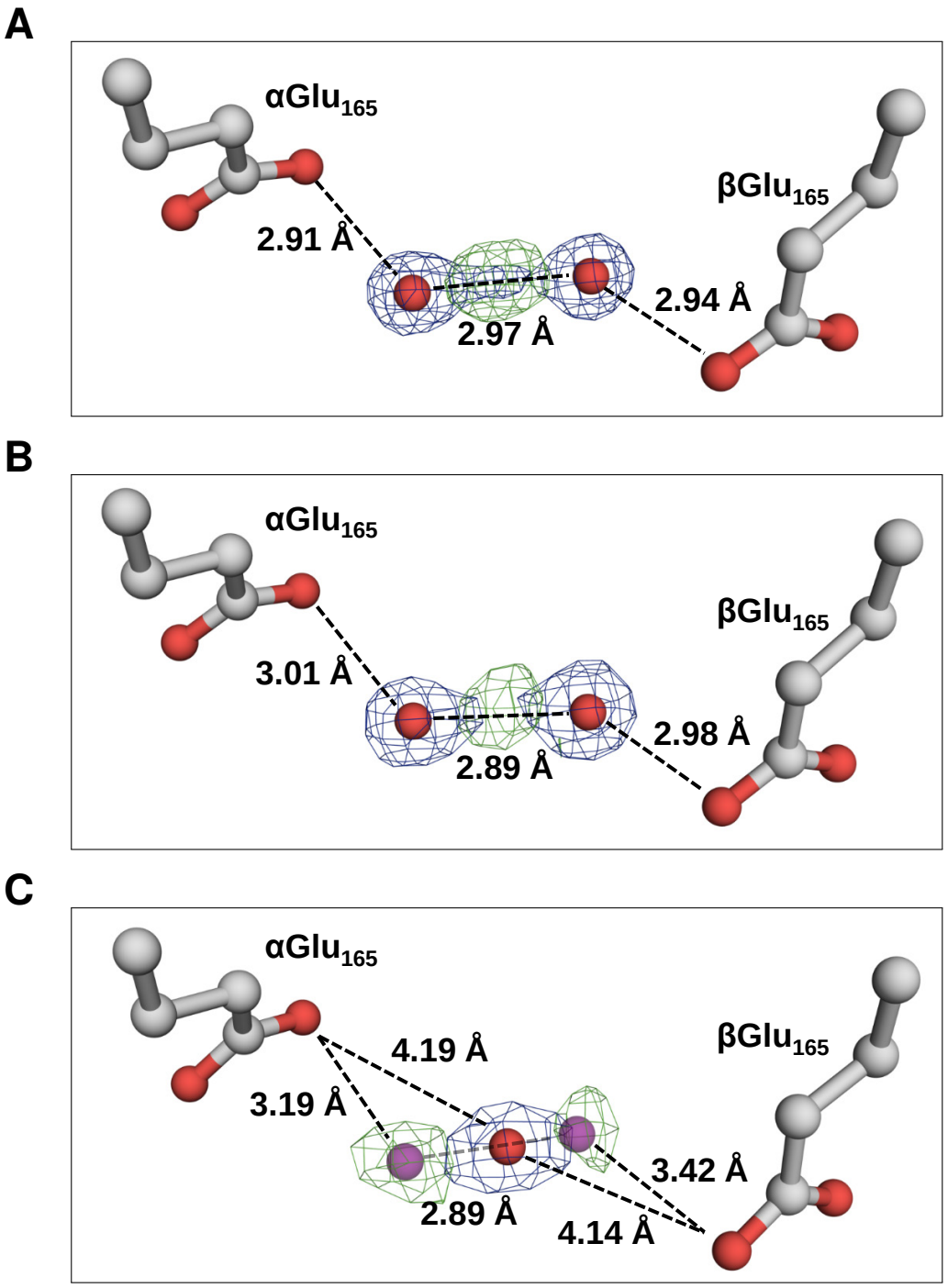

Figure 60. Comparison of the midpoint water(s) in the putative communication channel of *Ec*TK$_{WT}$ (A), *Ec*TK$_{E160Q}$ (B) and *Ec*TK$_{E160A}$ (C). The distances in Å between the water molecules and Glu$_{165}$ are given. The 2mFo-DFc density is contoured at 1 σ, the mFo-DFc density at 2.5 σ. The maps were generated at resolutions of 0.94 Å (*Ec*TK$_{WT}$), 1.3 Å (*Ec*TK$_{E160Q}$) and 1.7 Å (*Ec*TK$_{E160A}$).

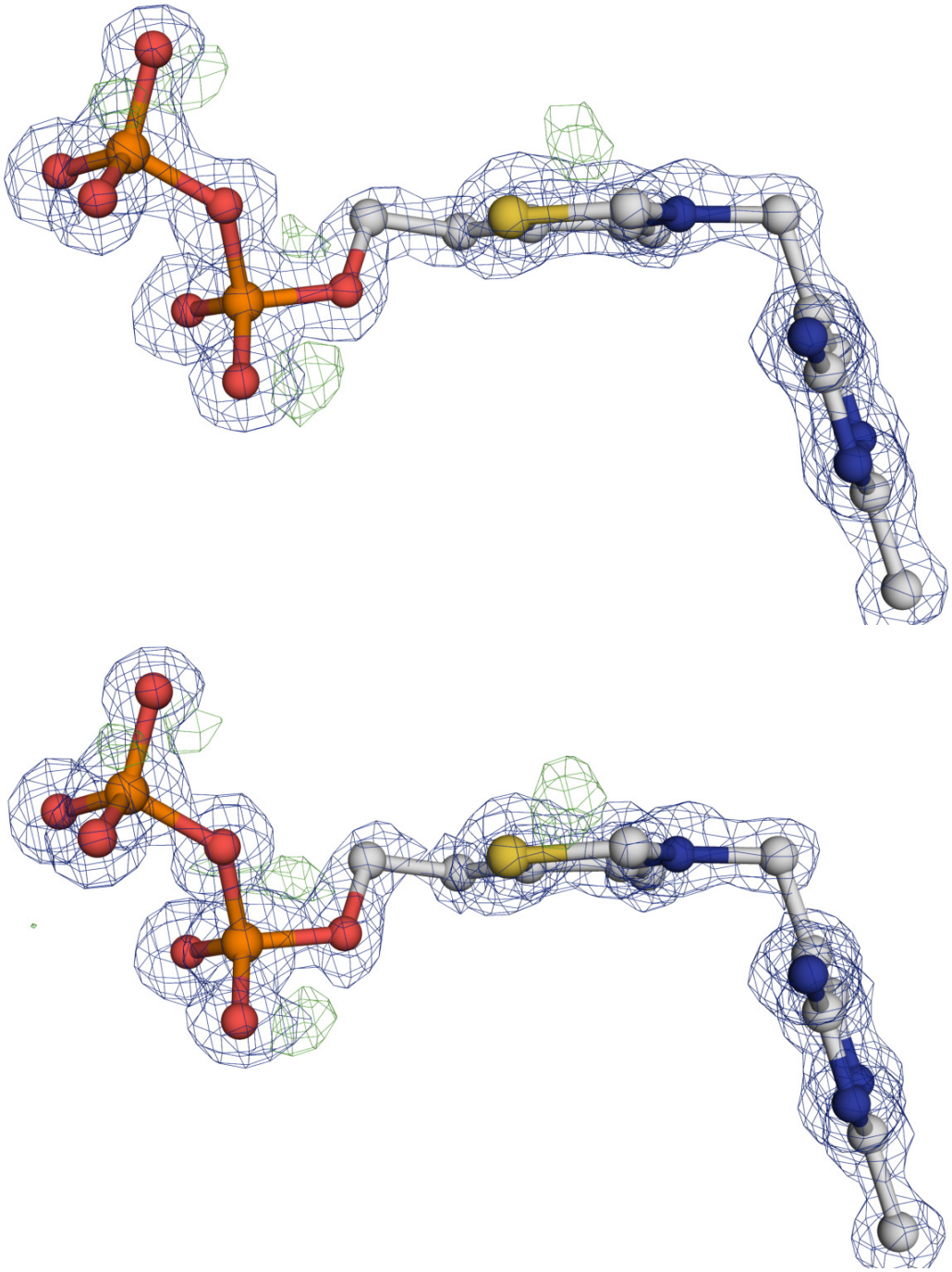

Figure 61. Electron densities around ThDP in *Ec*TK$_{T433Q}$ (top) and *Ec*TK$_{T433V}$ (bottom). The 2mFo-DFc densities are contoured at 1.5 σ, the mFo-DFc densities at 3.5 σ. As no negative mFo-DFc densities were observed in this part of the maps, none are shown.

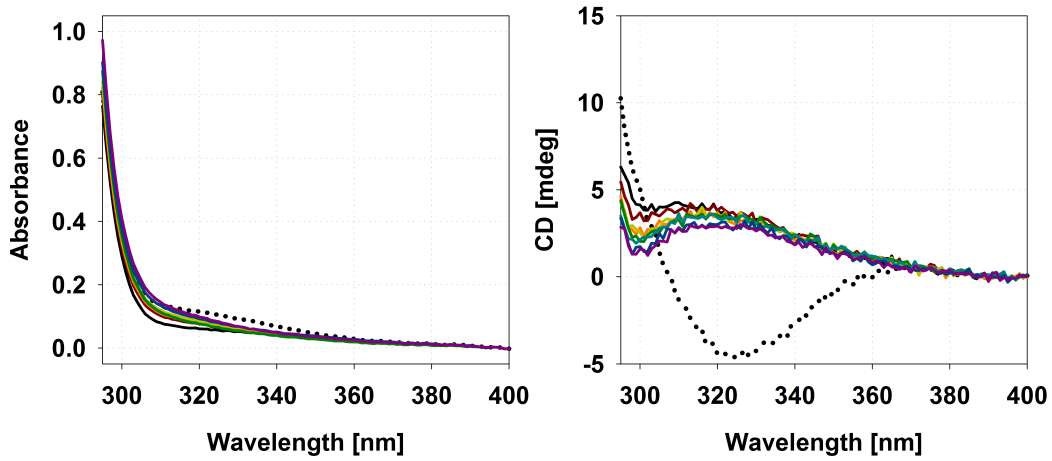

Figure 62. Titration of MeOThDP as observed by UV-Vis (left) and CD (right). The apoenzyme is shown as solid black line, enzyme reconstituted with saturating ThDP as dotted black line. The MeOThDP concentration increases from red (12.5 μM) to purple (150 μM).

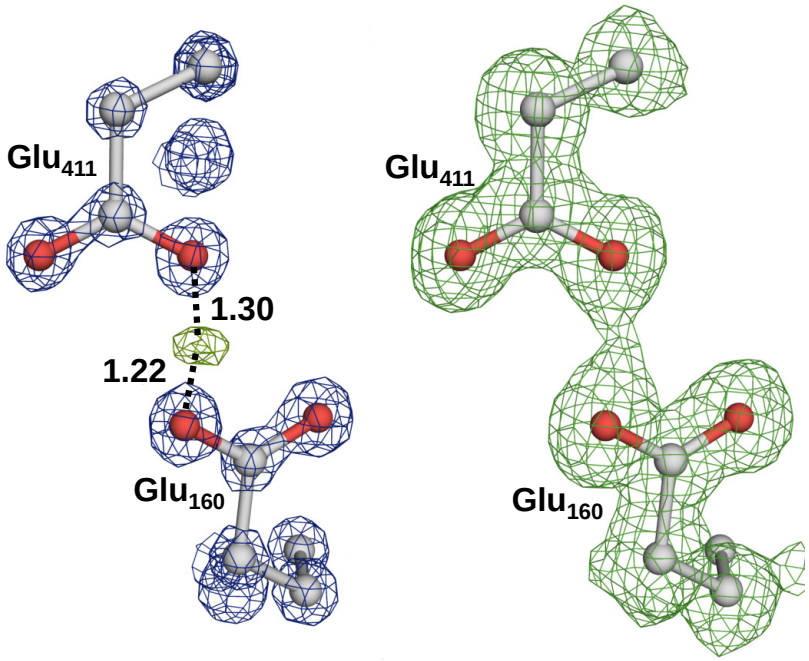

Figure 63. Electron densities of Glu_{411} and Glu_{160} in *Ec*$TK_{MeOThDP}$ (A). The 2mFo-DFc density is contoured at 2.5 σ, the mFo-DFc density at 4 σ, the theoretical distances to the mFo-DFc center are indicated. **Omit map of Glu_{411} and Glu_{160} (B).** The maps were generated by running 0 cycles of PHENIX after removal of the respective components from the pdb file. The density is contoured at 3.5 σ.

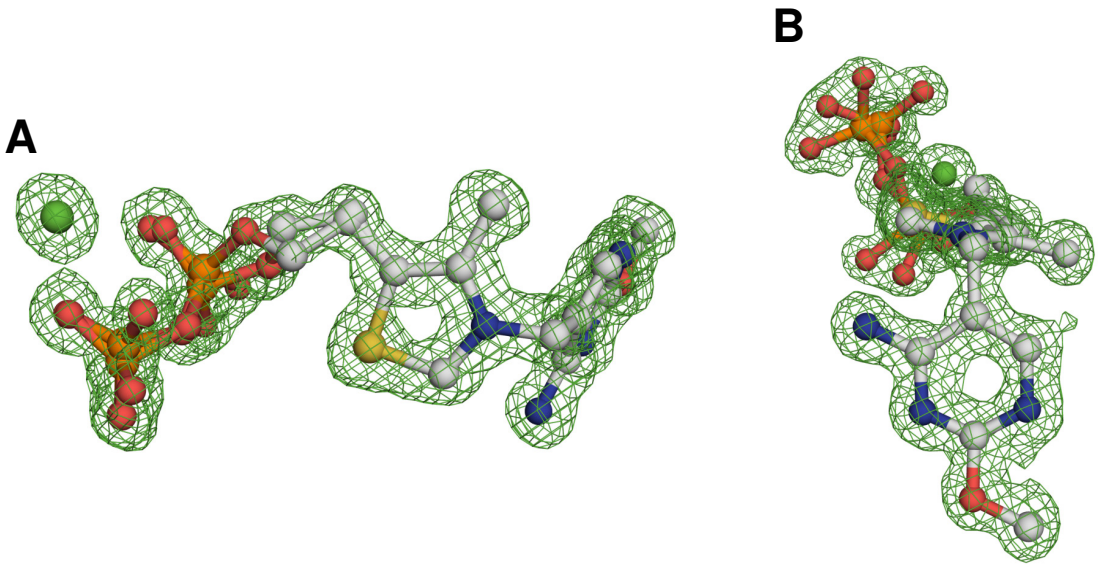

Figure 64. Omit maps of enzyme-bound MeOThDP in the active site of *Ec*TK. The mFo-DFc density is contoured at 3 σ. Shown are the orientation facing the thiazole and the pyrophosphate moieties **(A)** and the orientation facing the methoxypyrimidine ring **(B)**. The calcium ion is colored green.

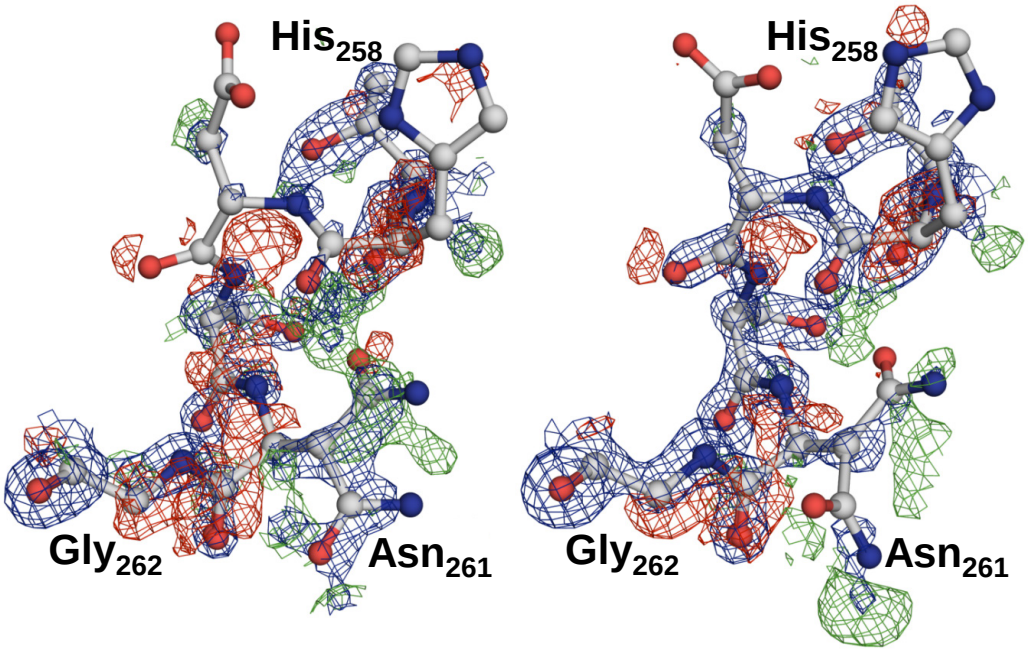

Figure 65. 2mFo-DFc and mFo-DFc maps of the region Gly_{262} to His_{258} in *Ec*TK_{H261N} ground state (left) and with covalently bound X5P (right). The 2mFo-DFc densities are contoured at 1 σ, the mFo-DFc densities at 3 σ. Asn_{261} and the limits of the disordered region are labeled.

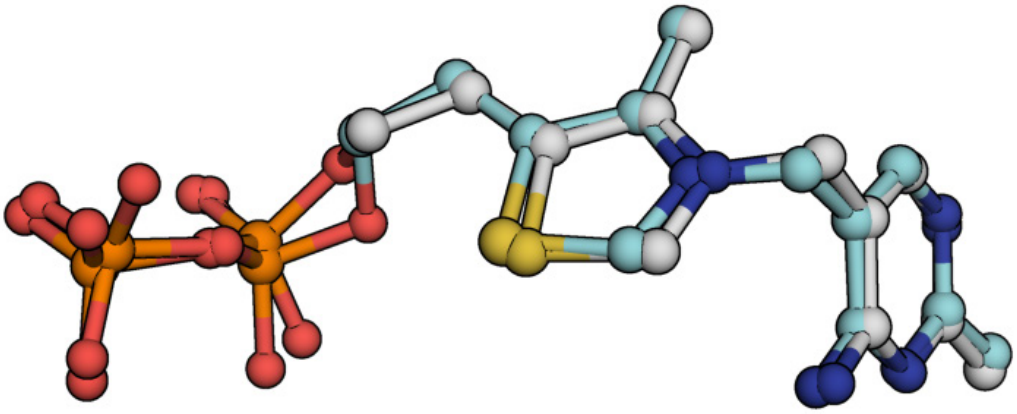

Figure 66. Overlay of the down-conformer of ThDP in *Ec*TK$_{WT}$ (gray) and *Ec*TK$_{H261N}$ (cyan). The alignment of *Ec*TK$_{WT}$ and *Ec*TK$_{H261N}$ was performed using secondary-structure matching in *COOT*, using both monomers.

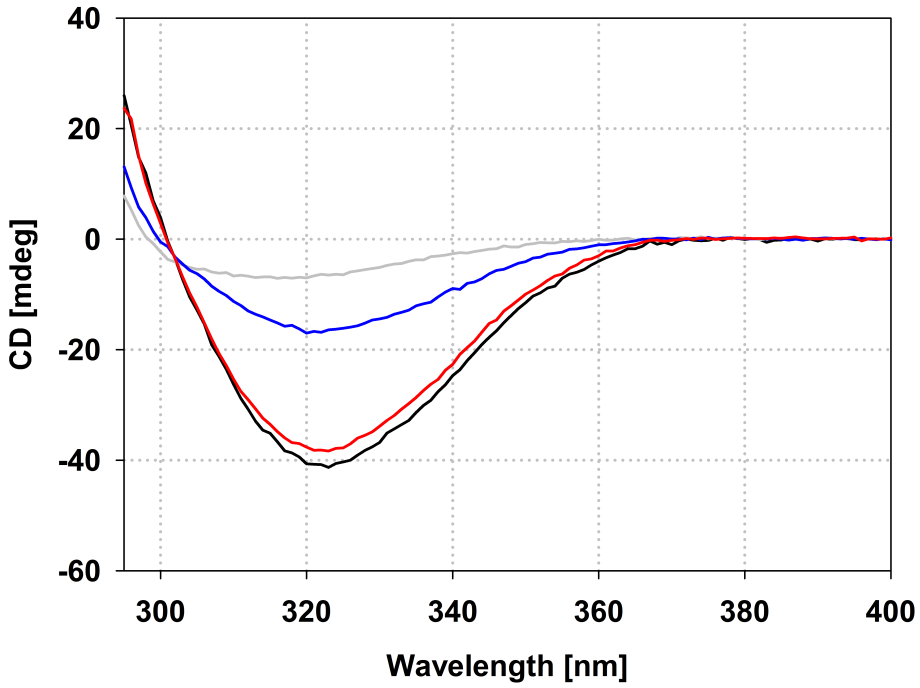

Figure 67. CD-spectra of reconstituted *Ec*TK$_{WT}$ and histidine variants. *Ec*TK$_{WT}$ is shown in black, *Ec*TK$_{H66A}$ in gray, *Ec*TK$_{H100A}$ in blue and *Ec*TK$_{H473Q}$ in red. All spectra shown were recorded at a concentration of 300 μM ThDP.

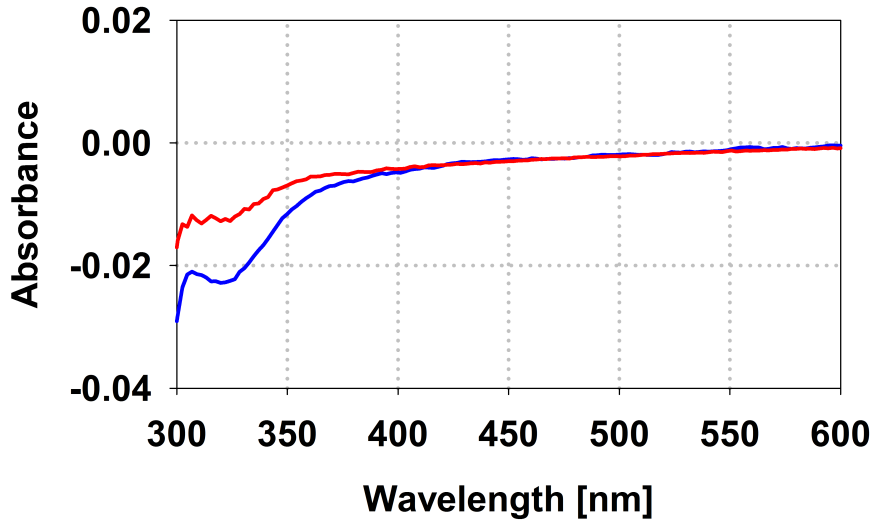

Figure 68. UV-vis difference spectra of *Ec*TK$_{H100A}$ (blue) and *Ec*TK$_{H473Q}$ (red) 120 s after addition of 5 mM fructose 6-phosphate. The spectra were recorded using the stopped flow technique, and corrected for buffer and enzyme absorbance.

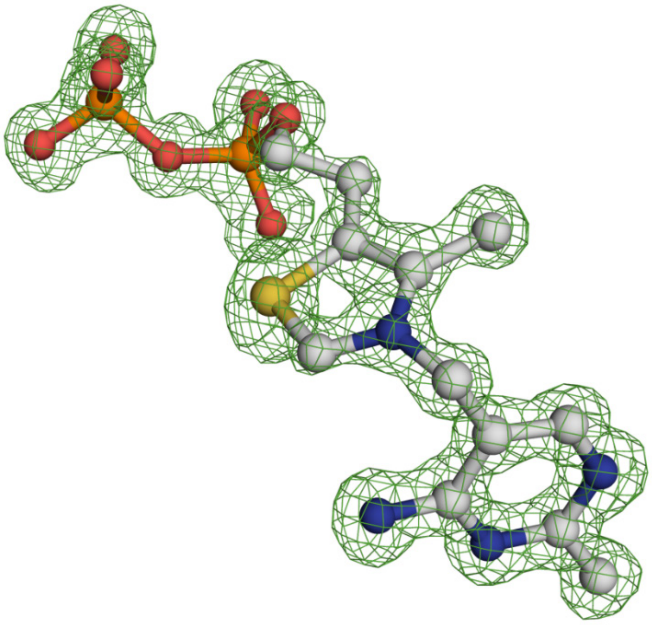

Figure 69. Omit map of ThDP in *Ec*TK$_{H66A}$. The mFo-DFc density is contoured at 3.5 σ. The map was generated by running 0 cycles of *PHENIX.REFINE* after removal of ThDP from the pdb file.

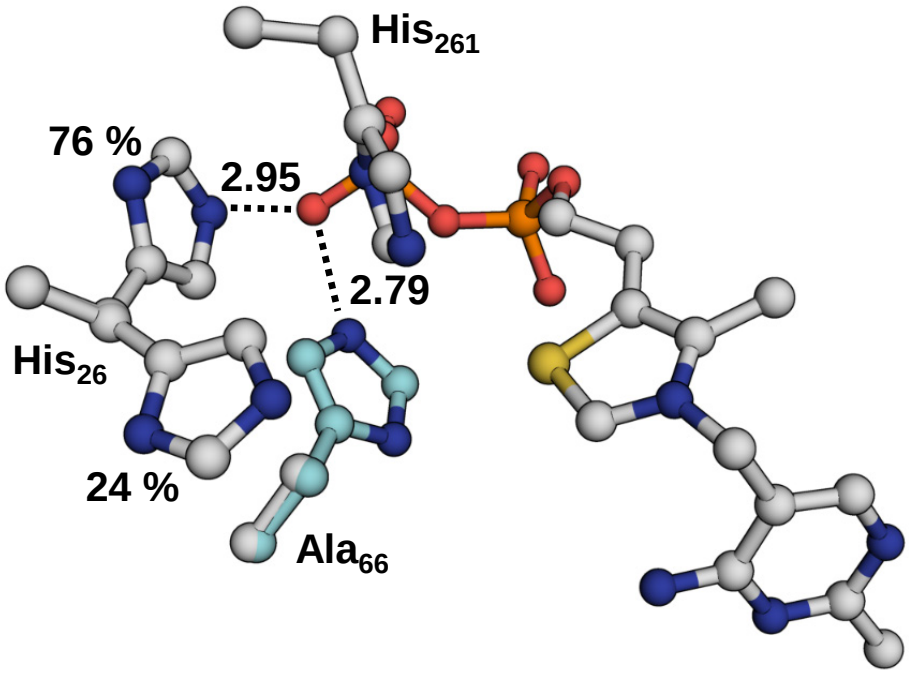

Figure 70. Interactions of ThDP with His$_{26}$ in *Ec*TK$_{H66A}$. The cyan histidine represents the orientation of His$_{66}$ in *Ec*TK$_{WT}$. The interaction distances of His$_{66}$ and His$_{26}$ as well as the occupancies of the two conformations of His$_{26}$ are indicated.

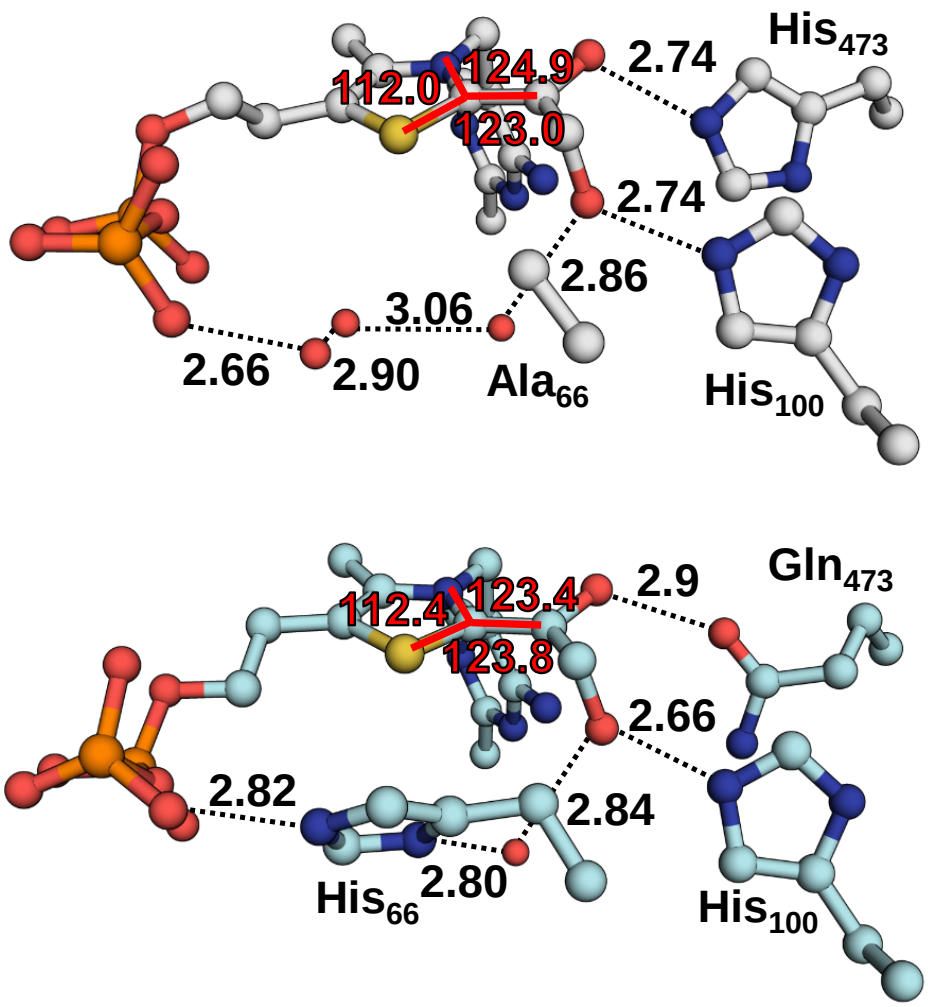

Figure 71. Geometry and interactions of the dihydroxyethyl-thiamine diphosphate-intermediate in *Ec*TK$_{H66A}$ (top) and *Ec*TK$_{H473Q}$ (bottom). The angles of C2-substituents are indicated in red. The interaction distances between DHEThDP and the environment are indicated.

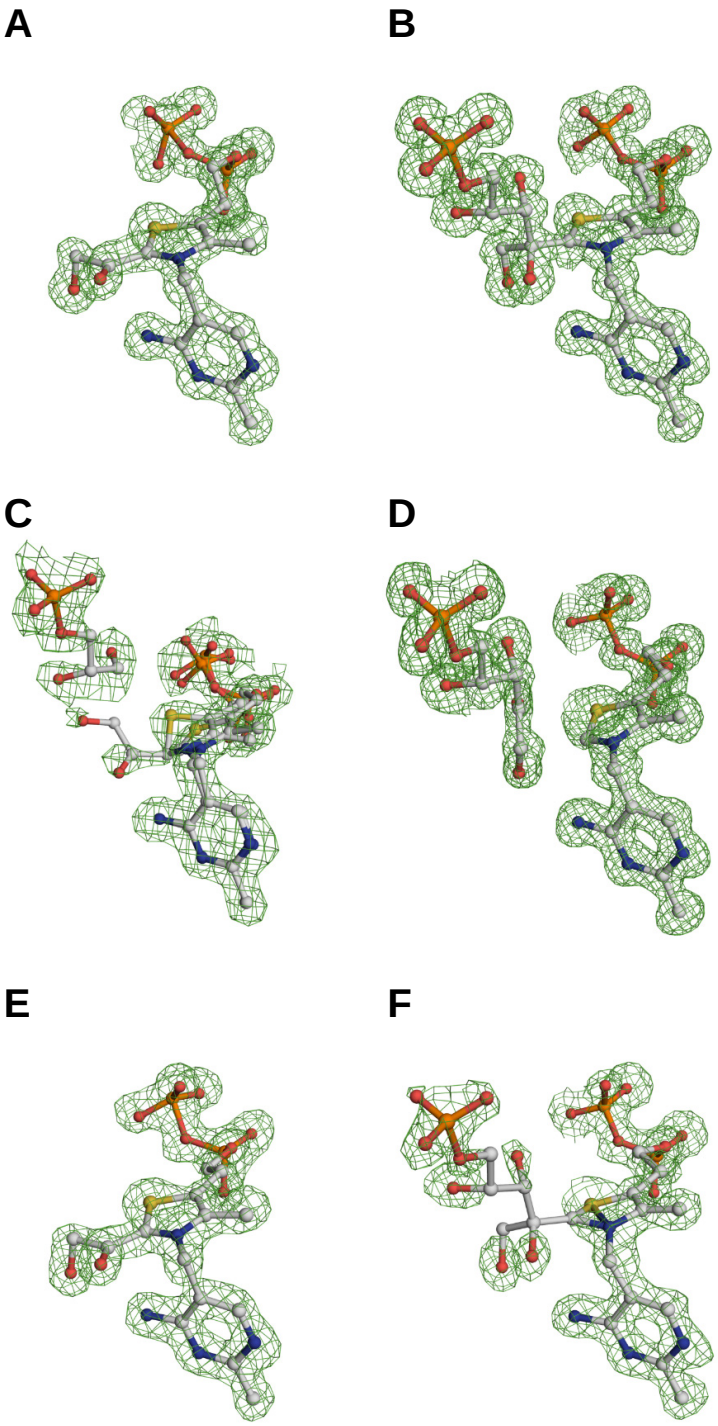

Figure 72. OMIT maps of *Ec*TK$_{H66A}$ with HPA (A)and X5P (B), *Ec*TK$_{H100A}$ in P2$_1$ (C) and P2$_1$2$_1$2$_1$ (D) with X5P and *Ec*TK$_{H473Q}$ with HPA (E) and X5P (F). The mFo-DFc densities are contoured at 3 σ. The maps were generated by running 0 cycles of *PHENIX.REFINE* after removal of the respective ligands from the pdb file.

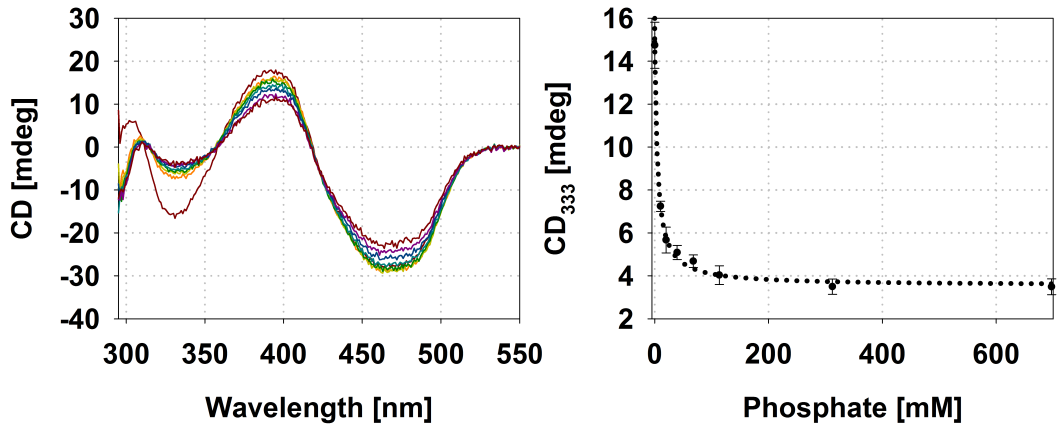

Figure 73. Exemplary phosphate titration curves of *Lp*POX$_{E483I}$ (left), plot of the CD signal at 333 nm versus the phosphate concentration (right). One of three titrations is shown as example, corrected for buffer and dilution. The aminopyrimidine band is visible at 333 nm, the iminopyrimidine band at 300 nm. The corrected signals at 333 nm were used to generate the plot, which was fitted according to equation 10.

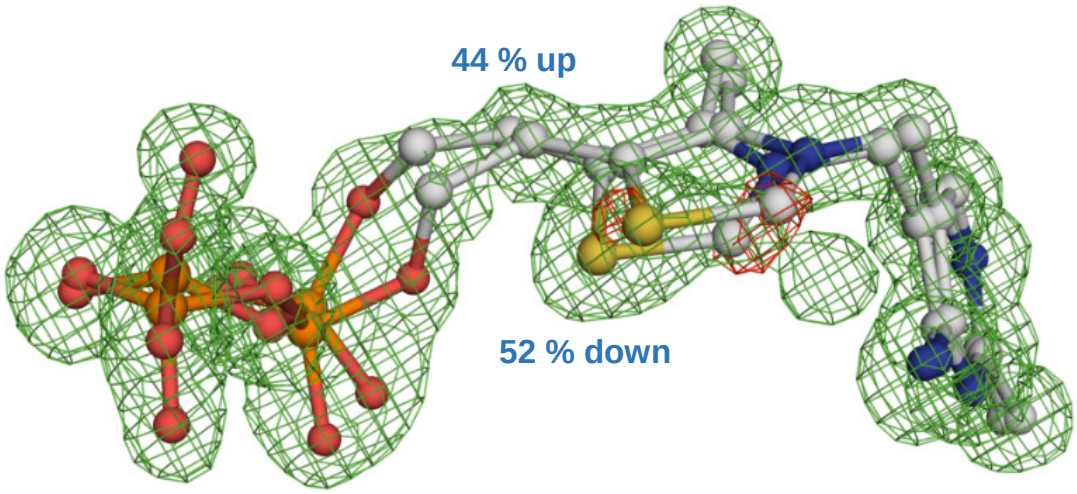

Figure 74. mFo-DFc omit map (green) and negative mFo-DFc (red) of ThDP in *Ec*TK$_{WT}$. The mFo-DFc omit density is contoured at 3 σ. The negative mFo-DFc is contoured at 2.5 σ. The map was generated by running 0 cycles of *PHENIX.REFINE* after removal of ThDP from the pdb file, using dataset 1.

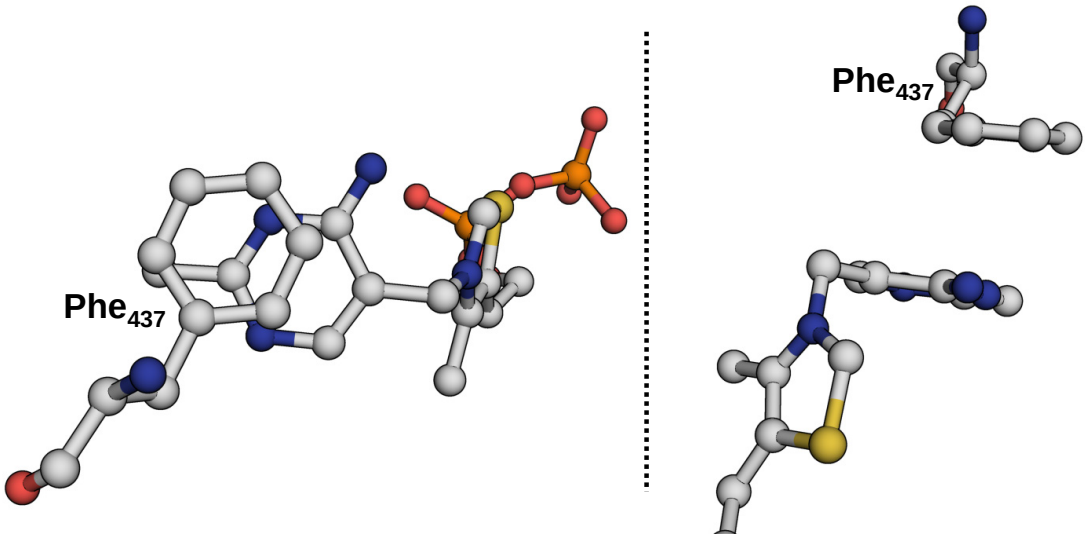

Figure 75. Positioning of Phe_{437} in *Ec*TK_{WT}. Shown are top (left) and side (right) view. Phe_{437} exhibits a total Cβ-deviation of 0.28 Å.

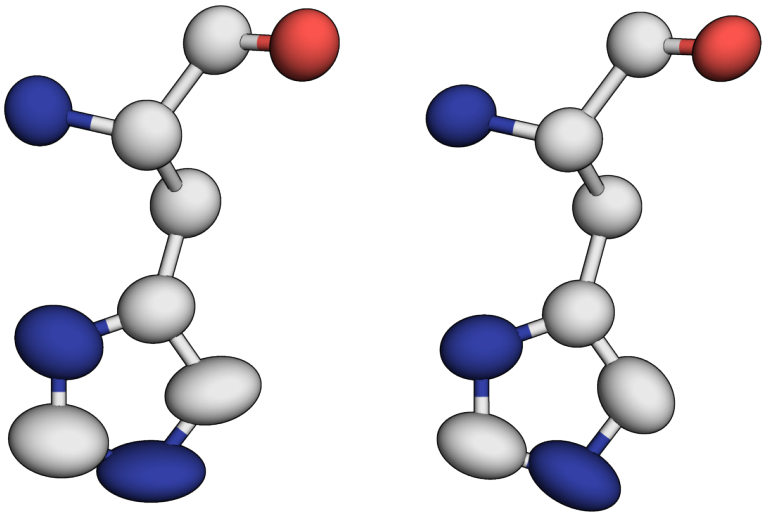

Figure 76. Anisotropy of His_{473} in resting state *Ec*TK_{WT}. Shown are the histidines of both monomers.

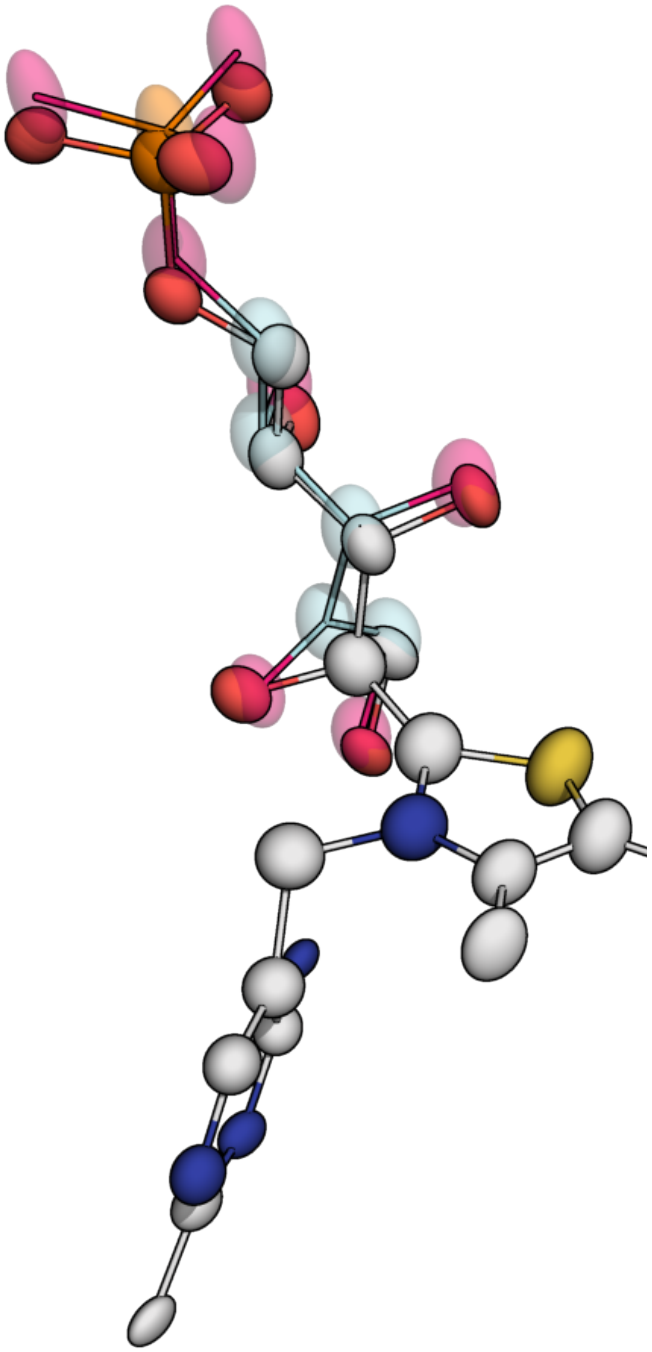

Figure 77. Anisotropy of non-bound and covalently bound X5P in *Ec*TK$_{WT}$dataset 3. The non-bound X5P is shown in cyan, with pink oxygens, the covalently bound X5P in grey, with red oxygens.

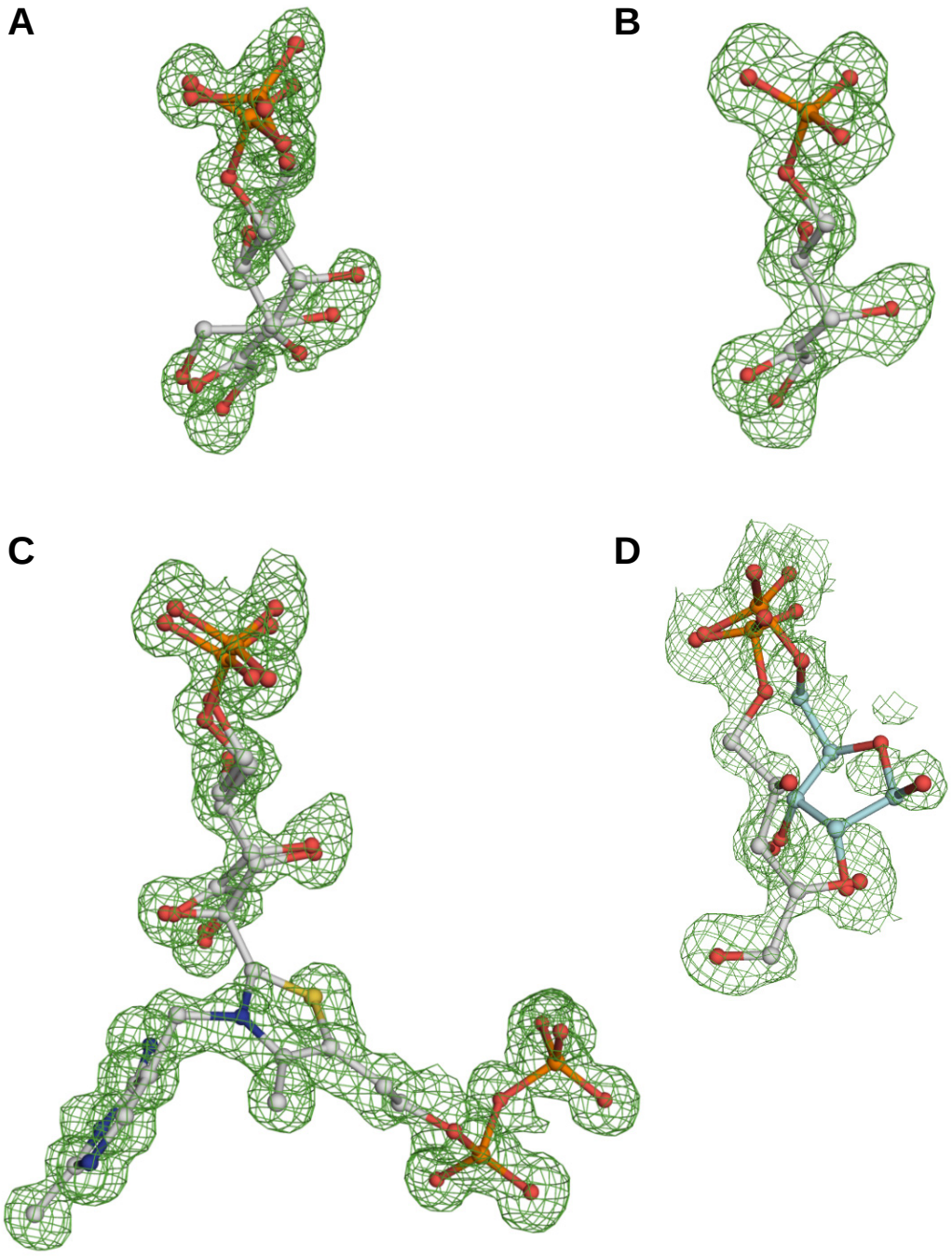

Figure 78. mFo-DFc omit map of X5P in *Ec*TK$_{WT}$ for dataset 1 (A), dataset 2 (B) and dataset 3 (C), and R5P in *Ec*TK$_{WT}$ (D). The mFo-DFc omit density is contoured at 3 σ. The map was generated by running 0 cycles of *PHENIX.REFINE* after omitting of the respective intermediates from the pdb file.

References

Adams, P. D.; Afonine, P. V.; Bunkóczi, G.; Chen, V. B.; Davis, I. W.; Echols, N.; Headd, J. J.; Hung, L.-W.; Kapral, G. J.; Grosse-Kunstleve, R. W.; McCoy, A. J.; Moriarty, N. W.; Oeffner, R.; Read, R. J.; Richardson, D. C.; Richardson, J. S.; Terwilliger, T. C.; Zwart, P. H. (2010): "PHENIX: a comprehensive Python-based system for macromolecular structure solution." *Acta Crystallogr D Biol Crystallogr* 66 (Pt 2), pp. 213–221.

Affaticati, P. E.; Dai, S.-B.; Payongsri, P.; Hailes, H. C.; Tittmann, K.; Dalby, P. A. (2016): "Structural Analysis of an Evolved Transketolase Reveals Divergent Binding Modes." *Scientific Reports* 6 (1).

Amara, P.; Fdez. Galván, I.; Fontecilla-Camps, J.; Field, M. (2007): "The Enamine Intermediate May Not Be Universal to Thiamine Catalysis." *Angewandte Chemie International Edition* 46 (47), pp. 9019–9022.

Ambrus, A.; Wang, J.; Mizsei, R.; Zambo, Z.; Torocsik, B.; Jordan, F.; Adam-Vizi, V. (2016): "Structural alterations induced by ten disease-causing mutations of human dihydrolipoamide dehydrogenase analyzed by hydrogen/deuterium-exchange mass spectrometry: Implications for the structural basis of E3 deficiency." *Biochimica et Biophysica Acta* 1862 (11) (11), pp. 2098–2109.

Arjunan, P.; Nemeria, N.; Brunskill, A.; Chandrasekhar, K.; Sax, M.; Yan, Y.; Jordan, F.; Guest, J. R.; Furey, W. (2002): "Structure of the pyruvate dehydrogenase multienzyme complex E1 component from Escherichia coli at 1.85 A resolution." *Biochemistry* 41 (16) (16), pp. 5213–5221.

Asztalos, P. (2008): "Untersuchungen zu molekularen, strukturellen und biokatalytischen Aspekten des Vitamin B1-abhängigen Enzyms Transketolase A aus *Escherichia coli*." PhD thesis. Martin-Luther-Universität Halle.

Asztalos, P.; Parthier, C.; Golbik, R.; Kleinschmidt, M.; Hübner, G.; Weiss, M. S.; Friedemann, R.; Wille, G.; Tittmann, K. (2007): "Strain and near attack conformers in enzymic thiamin catalysis: X-ray crystallographic snapshots of bacterial transketolase in covalent complex with donor ketoses xylulose 5-phosphate and fructose 6-phosphate,

and in noncovalent complex with acceptor aldose ribose 5-phosphate." *Biochemistry* 46 (43), pp. 12037–12052.

Auhagen, E (1932): "Co-carboxylase, ein neues Co-enzym der alkoholischen Gärung." *Z. Physiol. Chem.* 204 (3-4), pp. 149–167.

Backstrom, A. D.; McMordie, R. A. S.; Begley, T. P. (1995): "Biosynthesis of Thiamin I: The Function of the thiE Gene Product." *J. Am. Chem. Soc.* 117 (8), pp. 2351–2352.

Bay, A. R. (2012): *Beriberi in Modern Japan: The Making of a National Disease*. UNIV OF ROCHESTER PR. 230 Seiten.

Bennett, B. D.; Kimball, E. H.; Gao, M.; Osterhout, R.; Dien, S. J. V.; Rabinowitz, J. D. (2009): "Absolute metabolite concentrations and implied enzyme active site occupancy in Escherichia coli." *Nature Chemical Biology* 5 (8), pp. 593–599.

Berkessel, A.; Elfert, S.; Etzenbach-Effers, K.; Teles, J. H. (2010): "Aldehyde Umpolung by N-Heterocyclic Carbenes: NMR Characterization of the Breslow Intermediate in its Keto Form, and a Spiro-Dioxolane as the Resting State of the Catalytic System." *Angewandte Chemie International Edition* 49 (39), pp. 7120–7124.

Bettendorff, L.; Hennuy, B.; De Clerck, A.; Wins, P. (1994): "Chloride permeability of rat brain membrane vesicles correlates with thiamine triphosphate content." *Brain Res* 652 (1), pp. 157–160.

Bettendorff, L.; Kolb, H. A.; Schoffeniels, E. (1993): "Thiamine triphosphate activates an anion channel of large unit conductance in neuroblastoma cells." *J Membr Biol* 136 (3), pp. 281–288.

Bettendorff, L.; Wirtzfeld, B.; Makarchikov, A. F.; Mazzucchelli, G.; Frédérich, M.; Gigliobianco, T.; Gangolf, M.; De Pauw, E.; Angenot, L.; Wins, P. (2007): "Discovery of a natural thiamine adenine nucleotide." *Nat Chem Biol* 3 (4), pp. 211–212.

Bettendorff, L.; Lakaye, B.; Kohn, G.; Wins, P. (2014): "Thiamine triphosphate: a ubiquitous molecule in search of a physiological role." *Metab Brain Dis* 29 (4), pp. 1069–1082.

Böhme, S. (2007): *Analyse der katalytischen Funktion der hydrophilen Aminosäuren Glutamat 483 und Glutamin 122 im aktiven Zentrum der Pyruvatoxidase aus Lactobacillus plantarum.*

Blair, J. M. A.; Webber, M. A.; Baylay, A. J.; Ogbolu, D. O.; Piddock, L. J. V. (2014): "Molecular mechanisms of antibiotic resistance." *Nature Reviews Microbiology* 13 (1), pp. 42–51.

Bradford, M. M. (1976): "A rapid and sensitive method for the quantitation of microgram quantities of protein utilizing the principle of protein-dye binding." *Anal Biochem* 72 (1-2), pp. 248–254.

Breslow, R. (1958): "On the mechanism of thiamine action. IV. 1 Evidence from studies on model systems." *J. Am. Chem. Soc.* 80 (14), pp. 3719–3726.

– (1957): "Rapid deuterium exchange in thiazolium salts 1." *J. Am. Chem. Soc.* 79 (7), pp. 1762–1763.

Breslow, R.; Appayee, C. (2013): "Transketolase reaction under credible prebiotic conditions." *Proc Natl Acad Sci U S A* 110 (11), pp. 4184–4187.

Burgi, H. B.; Dunitz, J. D.; Shefter, E. (1973): "Geometrical reaction coordinates. II. Nucleophilic addition to a carbonyl group." *Journal of the American Chemical Society* 95 (15), pp. 5065–5067.

Candy, J. M.; Koga, J.; Nixon, P. F.; Duggleby, R. G. (1996): "The role of residues glutamate-50 and phenylalanine-496 in Zymomonas mobilis pyruvate decarboxylase." *Biochemical Journal* 315 (3), pp. 745–751.

Cassidy, C. S.; Lin, J.; Frey, P. A. (1997): "A new concept for the mechanism of action of chymotrypsin: The role of the low-barrier hydrogen bond †." *Biochemistry* 36 (15), pp. 4576–4584.

Casteels, M.; Sniekers, M.; Fraccascia, P.; Mannaerts, G.; Veldhoven, P. V. (2007): "The role of 2-hydroxyacyl-CoA lyase, a thiamin pyrophosphate-dependent enzyme, in the peroxisomal metabolism of 3-methyl-branched fatty acids and 2-hydroxy straight-chain fatty acids". *Biochemical Society Transactions* 35 (5), pp. 876–880.

Cavazza, C.; Contreras-Martel, C.; Pieulle, L.; Chabrière, E.; Hatchikian, E. C.; Fontecilla-Camps, J. C. (2006): "Flexibility of thiamine diphosphate revealed by kinetic crystallographic studies of the reaction of pyruvate-ferredoxin pxidoreductase with pyruvate." *Structure* 14 (2), pp. 217–224.

Chabriere, E. (2001): "Crystal structure of the free radical intermediate of pyruvate:ferredoxin oxidoreductase." *Science* 294 (5551), pp. 2559–2563.

Changeux, J.-P.; Edelstein, S. (2011): "Conformational selection or induced fit? 50 years of debate resolved." *F1000 Biology Reports* 3, p. 19.

Chen, V. B.; Arendall 3rd, W. B.; Headd, J. J.; Keedy, D. A.; Immormino, R. M.; Kapral, G. J.; Murray, L. W.; Richardson, J. S.; Richardson, D. C. (2010): "MolProbity: all-atom structure validation for macromolecular crystallography." *Acta Crystallogr D Biol Crystallogr* 66 (1), pp. 12–21.

Choi, K. H.; Tolan, D. R. (2004): "Presteady-State Kinetic Evidence for a Ring-Opening Activity in Fructose-1,6-(bis)phosphate Aldolase." *Journal of the American Chemical Society* 126 (11), pp. 3402–3403.

Cleland, W. W.; Frey, P. A.; Gerlt, J. A. (1998): "The low barrier hydrogen bond in enzymatic catalysis." *Journal of Biological Chemistry* 273 (40), pp. 25529–25532.

Cleland, W.; Kreevoy, M. (1994): "Low-barrier hydrogen bonds and enzymic catalysis." *Science* 264 (5167), pp. 1887–1890.

Cooper, L. E.; O'Leary, S. E.; Begley, T. P. (2014): "Biosynthesis of a Thiamin Antivitamin in Clostridium botulinum." *Biochemistry* 53 (14), pp. 2215–2217.

Crosby, J.; Lienhard, G. E. (1970): "Mechanisms of thiamine-catalyzed reactions. Kinetic analysis of the decarboxylation of pyruvate by 3,4-dimethylthiazolium ion in water and ethanol." *J. Am. Chem. Soc.* 92 (19), pp. 5707–5716.

Davis, I. W.; Leaver-Fay, A.; Chen, V. B.; Block, J. N.; Kapral, G. J.; Wang, X.; Murray, L. W.; Arendall 3rd, W. B.; Snoeyink, J.; Richardson, J. S.; Richardson, D. C. (2007): "MolProbity: all-atom contacts and structure validation for proteins and nucleic acids." *Nucleic Acids Res* 35 (Web Server issue), pp. 375–383.

Diederichs, A.-K. (2009): *Catalytic role of a conserved histidine for substrate binding and conversion in transketolase from E. coli.*

Dobritzsch, D; König, S; Schneider, G; Lu, G (1998): "High resolution crystal structure of pyruvate decarboxylase from Zymomonas mobilis. Implications for substrate activation in pyruvate decarboxylases." *The Journal of Biological Chemistry* 273 (32) (32), pp. 20196–20204.

Dolinsky, T. J.; Nielsen, J. E.; McCammon, J. A.; Baker, N. A. (2004): "PDB2PQR: an automated pipeline for the setup of Poisson-Boltzmann electrostatics calculations." *Nucleic Acids Research* 32 (Web Server issue), pp. 665–667.

Drautz, H.; Messerer, W.; Zähner, H.; Breiding-Mack, S.; Zeeck, A. (1987): "Metabolic products of microorganisms. 239. Bacimethrin isolated from Streptomyces albus. Identification, derivatives, synthesis and biological properties." *The Journal of Antibiotics* 40 (10), pp. 1431–1439.

Dudeja, P. K.; Tyagi, S.; Gill, R.; Said, H. M. (2003): "Evidence for a carrier-mediated mechanism for thiamine transport to human jejunal basolateral membrane vesicles." *Dig Dis Sci* 48 (1), pp. 109–115.

Dwyer, J. J.; Gittis, A. G.; Karp, D. A.; Lattman, E. E.; Spencer, D. S.; Stites, W. E.; E., B. G.-M. (2000): "High apparent dielectric constants in the interior of a protein reflect water penetration." *Biophysical Journal* 79 (3), pp. 1610–1620.

Eigen, M. (1963): "Protonenübertragung, Säure-Base-Katalyse und enzymatische Hydrolyse. Teil I: Elementarvorgänge." *Angewandte Chemie* 75 (12), pp. 489–508.

Eijkman, C. (1897): "Eine Beri Beri-ähnliche Krankheit der Hühner." *Archiv für pathologische Anatomie und Physiologie und für klinische Medicin* 148 (3), pp. 523–532.

Enders, D.; Grossmann, A.; Fronert, J.; Raabe, G. (2010): "N-heterocyclic carbene catalysed asymmetric cross-benzoin reactions of heteroaromatic aldehydes with trifluoromethyl ketones." *Chem Commun (Camb)* 46 (34), pp. 6282–6284.

Fitzpatrick, T. B.; Thore, S. (2014): "Complex behavior: from cannibalism to suicide in the vitamin B1 biosynthesis world." *Curr Opin Struct Biol* 29, pp. 34–43.

Flanigan, D. M.; Romanov-Michailidis, F.; White, N. A.; Rovis, T. (2015): “Organocatalytic reactions enabled by N-Heterocyclic carbenes.” *Chemical Reviews* 115 (17), pp. 9307–9387.

Frank, R. A. W.; Titman, C. M.; Pratap, J. V.; Luisi, B. F.; Perham, R. N. (2004): “A molecular switch and proton wire synchronize the active sites in thiamine enzymes.” *Science* 306 (5697) (5697), pp. 872–876.

Frédérich, M.; Delvaux, D.; Gigliobianco, T.; Gangolf, M.; Dive, G.; Mazzucchelli, G.; Elias, B.; De Pauw, E.; Angenot, L.; Wins, P.; Bettendorff, L. (2009): “Thiaminylated adenine nucleotides. Chemical synthesis, structural characterization and natural occurrence.” *FEBS J* 276 (12), pp. 3256–3268.

Fuhrmann, C. N.; Daugherty, M. D.; Agard, D. A. (2006): “Subangstrom crystallography reveals that short ionic hydrogenbonds, and not a His-Asp low-barrier hydrogen bond, stabilize the transition state in serine protease catalysis”. *Journal of the American Chemical Society* 128 (28), pp. 9086–9102.

Gigliobianco, T.; Lakaye, B.; Wins, P.; El Moualij, B.; Zorzi, W.; Bettendorff, L. (2010): “Adenosine thiamine triphosphate accumulates in Escherichia coli cells in response to specific conditions of metabolic stress.” *BMC Microbiol* 10, p. 148.

Gigliobianco, T.; Gangolf, M.; Lakaye, B.; Pirson, B.; Ballmoos, C. von; Wins, P.; Bettendorff, L. (2013): “An alternative role of FoF1-ATP synthase in Escherichia coli: synthesis of thiamine triphosphate.” *Scientific Reports*.

Grijns, G (1901): “Over polyneuritis gallinarum.” *Geneeskundig Tijdschrift voor Nederlandsch-Indie* 43, pp. 3–110.

Gruys, K. J.; Halkides, C. J.; Frey, P. A. (1987): “Synthesis and properties of 2-acetylthiamin pyrophosphate: an enzymatic reaction intermediate.” *Biochemistry* 26 (24), pp. 7575–7585.

Götz, F.; Sedewitz, L. (1991): “Biochemistry and physiology of thiamin diphosphate enzymes.” Ed. by Bisswanger, H.; Ullrich, J. Verlag Chemie Weinheim. Chap. Physiological role of pyruvate oxidase in ther aerobic metabolism of Lactobacillus plantarum. Pp. 286–293.

Guerrini, I.; Thomson, A. D.; Cook, C. C. H.; McQuillin, A.; Sharma, V.; Kopelman, M.; Reynolds, G.; Jauhar, P.; Harper, C.; Gurling, H. M. D. (2005): "Direct genomic PCR sequencing of the high affinity thiamine transporter (SLC19A2) gene identifies three genetic variants in Wernicke Korsakoff syndrome (WKS)." *Am J Med Genet B Neuropsychiatr Genet* 137B (1), pp. 17–19.

Hachisu, Y.; Bode, J. W.; Suzuki, K. (2003): "Catalytic intramolecular crossed aldehyde-ketone benzoin reactions: A novel synthesis of functionalized preanthraquinones." *J. Am. Chem. Soc.* 125 (28), pp. 8432–8433.

Hailes, H. C.; Rother, D.; Müller, M.; Westphal, R.; Ward, J. M.; Pleiss, J.; Vogel, C.; Pohl, M. (2013): "Engineering stereoselectivity of ThDP-dependent enzymes." *FEBS J* 280 (24), pp. 6374–6394.

Harris, T. K.; Turner, G. J. (2002): "Structural basis of perturbed pKa values of catalytic groups in enzyme active sites." *IUBMB Life (International Union of Biochemistry and Molecular Biology: Life)* 53 (2), pp. 85–98.

Hasson, M. S.; Muscate, A; McLeish, M. J.; Polovnikova, L. S.; Gerlt, J. A.; Kenyon, G. L.; Petsko, G. A.; Ringe, D (1998): "The crystal structure of benzoylformate decarboxylase at 1.6 A resolution: diversity of catalytic residues in thiamin diphosphate-dependent enzymes." *Biochemistry* 37 (28) (28), pp. 9918–9930.

Hawkins, C. F.; Borges, A.; Perham, R. N. (1989): "A common structural motif in thiamin pyrophosphate-binding enzymes." *FEBS Lett* 255 (1), pp. 77–82.

Heine, A. (2001): "Observation of covalent intermediates in an enzyme mechanism at atomic resolution." *Science* 294 (5541), pp. 369–374.

Heine, A.; Luz, J. G.; Wong, C.-H.; Wilson, I. A. (2004): "Analysis of the class I aldolase binding site architecture based on the crystal structure of 2-deoxyribose-5-phosphate aldolase at 0.99A resolution." *Journal of Molecular Biology* 343 (4) (4), pp. 1019–1034.

Heinrich, C. P.; Noack, K; Wiss, O (1971): "A circular dichroism study of transketolase from baker's yeast." *Biochemical and biophysical research communications* 44 (2) (2), pp. 275–279.

Hsu, L.-J.; Hsu, N.-S.; Wang, Y.-L.; Wu, C.-J.; Li, T.-L. (2016): "Structural and biochemical interrogation on transketolase from Pichia stipitis for new functionality." *Protein Eng Des Sel* 29 (11), pp. 513–522.

Hulshoff-Pol, M. (1902): "Katjang idjo, un nouveau medicament contre le béri-béri [Katjang idjo (mung beans), a new treatment for beri-beri]." *Janus* 7, pp. 524–581.

Inoue, H.; Nojima, H.; Okayama, H. (1990): "High efficiency transformation of Escherichia coli with plasmids." *Gene* 96 (1), pp. 23–28.

Jansen, B.; Donath, W. (1926): "On the isolation of the anti-beriberi vitamin." *OProc K Acad Wet Amsterdam* 29, pp. 1389–1400.

"Thiamine - Catalytic Mechanisms in Normal and Disease States" (2003). Ed. by Jordan, F.; Patel, M. S. . CRC Press. Chap. Biosynthesis of Thiamine and Its Phosphorylated Terms.

Jordan, F.; Li, H.; Brown, A. (1999): "Remarkable stabilization of zwitterionic intermediates may account for a billion-fold rate acceleration by thiamin diphosphate-dependent decarboxylases †." *Biochemistry* 38 (20), pp. 6369–6373.

Jurgenson, C. T.; Begley, T. P.; Ealick, S. E. (2009): "The structural and biochemical foundations of thiamin biosynthesis." *Annu Rev Biochem* 78, pp. 569–603.

Kabsch, W. (2010): "XDS." *Acta Crystallogr D Biol Crystallogr* 66 (2), pp. 125–132.

Kaplun, A.; Binshtein, E.; Vyazmensky, M.; Steinmetz, A.; Barak, Z.; Chipman, D. M.; Tittmann, K.; Shaanan, B. (2008): "Glyoxylate carboligase lacks the canonical active site glutamate of thiamine-dependent enzymes." *Nat Chem Biol* 4 (2), pp. 113–118.

Kato, M.; Wynn, R. M.; Chuang, J. L.; Tso, S.-C.; Machius, M.; Li, J.; Chuang, D. T. (2008): "Structural basis for inactivation of the human pyruvate dehydrogenase complex by phosphorylation: role of disordered phosphorylation loops." *Structure (London, England : 1993)* 16 (12) (12), pp. 1849–1859.

Kern, D.; Kern, G.; Neef, H.; Tittmann, K.; Killenberg-Jabs, M.; Wikner, C.; Schneider, G.; Hübner, G. (1997): "How thiamine diphosphate is activated in enzymes." *Science* 275 (5296), pp. 67–70.

Kleywegt, G. J. (1996): “Use of non-crystallographic symmetry in protein structure refinement.” *Acta Crystallographica Section D Biological Crystallography* 52 (4), pp. 842–857.

Kleywegt, G. J. (1997): “Validation of protein models from Calpha coordinates alone.” *Journal of Molecular Biology* 273 (2) (2), pp. 371–376.

Kluger, R.; Tittmann, K. (2008): “Thiamin diphosphate catalysis: enzymic and nonenzymic covalent intermediates.” *Chem Rev* 108 (6), pp. 1797–1833.

Kochetov, G. A. (1982): “Transketolase from yeast, rat liver, and pig liver.” *Methods Enzymol* 90 (E), pp. 209–223.

Kochetov, G. A.; Usmanov, R. A. (1970): “Charge transfer interactions in transketolase-thiamine pyrophosphate complex.” *Biochemical and Biophysical Research Communications* 41 (5) (5), pp. 1134–1140.

Koppel, H. C.; Springer, R. H.; Robins, R. K.; Cheng, C. C. (1962): “Pyrimidines. X. (Antibiotics. II) Synthesis of Bacimethrin, 2-Methoxy Analog of Thiamine, and Related Alkoxypyrimidines 1.” *The Journal of Organic Chemistry* 27 (10), pp. 3614–3617.

Laforenza, U.; Patrini, C.; Alvisi, C.; Faelli, A.; Licandro, A.; Rindi, G. (1997): “Thiamine uptake in human intestinal biopsy specimens, including observations from a patient with acute thiamine deficiency.” *Am J Clin Nutr* 66 (2), pp. 320–326.

Lawhorn, B. G.; Gerdes, S. Y.; Begley, T. P. (2004): “A genetic screen for the identification of thiamin metabolic genes.” *Journal of Biological Chemistry* 279 (42), pp. 43555–43559.

Li, G.-Q.; Dai, L.-X.; You, S.-L. (2007): “Thiazolium-derived N-heterocyclic carbene-catalyzed cross-coupling of aldehydes with unactivated imines.” *Chem. Commun.* (8), pp. 852–854.

Lin, J.; Pozharski, E.; Wilson, M. A. (2017): “Short carboxylic acid–carboxylate hydrogen bonds can have fully localized protons.” *Biochemistry* 56 (2), pp. 391–402.

Lohmann, K; Schuster, P (1937): “Untersuchungen über die Cocarboxylase.” *Biochem Z.* 294, pp. 188–214.

Lonsdale, D. (2006): “A review of the biochemistry, metabolism and clinical benefits of thiamin(e) and its derivatives.” *Evid Based Complement Alternat Med* 3 (1), pp. 49–59.

Lorentzen, E.; Siebers, B.; Hensel, R.; Pohl, E. (2005): “Mechanism of the Schiff Base Forming Fructose-1,6-bisphosphate Aldolase: Structural Analysis of Reaction Intermediates‡.” *Biochemistry* 44 (11), pp. 4222–4229.

Loschonsky, S.; Wacker, T.; Waltzer, S.; Giovannini, P. P.; McLeish, M. J.; Andrade, S. L. A.; Müller, M. (2014): “Extended reaction scope of thiamine diphosphate dependent cyclohexane-1,2-dione hydrolase: from C-C bond cleavage to C-C bond ligation.” *Angewandte Chemie (International ed. in English)* 53 (52) (52), pp. 14402–14406.

Lüdtke, S. (2012): “Structural and sunctional studies on vitamin B1- dependent, human and bacterial transketolases.” PhD thesis. Georg-August-University Göttingen.

Lüdtke, S.; Neumann, P.; Erixon, K. M.; Leeper, F.; Kluger, R.; Ficner, R.; Tittmann, K. (2013): “Sub-ångström-resolution crystallography reveals physical distortions that enhance reactivity of a covalent enzymatic intermediate.” *Nat Chem* 5 (9), pp. 762–767.

Maji, B.; Breugst, M.; Mayr, H. (2011): “N-heterocyclic carbenes: organocatalysts with moderate nucleophilicity but extraordinarily high Lewis basicity.” *Angew Chem Int Ed Engl* 50 (30), pp. 6915–6919.

Makarchikov, A. F.; Lakaye, B.; Gulyai, I. E.; Czerniecki, J.; Coumans, B.; Wins, P.; Grisar, T.; Bettendorff, L. (2003): “Thiamine triphosphate and thiamine triphosphatase activities: from bacteria to mammals.” *Cellular and Molecular Life Sciences (CMLS)* 60 (7), pp. 1477–1488.

McCoy, A. J.; Grosse-Kunstleve, R. W.; Adams, P. D.; Winn, M. D.; Storoni, L. C.; Read, R. J. (2007): “Phaser crystallographic software.” *J Appl Crystallogr* 40 (4), pp. 658–674.

Meshalkina, L.; Nilsson, U.; Wikner, C.; Kostikowa, T.; Schneider, G. (1997): “Examination of the thiamin diphosphate binding site in yeast transketolase by site-directed mutagenesis.” *Eur J Biochem* 244 (2), pp. 646–652.

Meyer, D. (2008): “Kinetische und strukturelle Untersuchung der Katalysemechanismen ausgewählter Kofaktor-abhängiger Enzyme - Implikationen für die Decarboxylierung von α-Ketosäuren durch Thiamindiphosphat-abhängige Enzyme.” PhD thesis. Martin-Luther-University Halle-Wittenberg.

Meyer, D.; Neumann, P.; Ficner, R.; Tittmann, K. (2013): “Observation of a stable carbene at the active site of a thiamin enzyme.” *Nat Chem Biol* 9 (8), pp. 488–490.

Meyer, D.; Neumann, P.; Koers, E.; Sjuts, H.; Lüdtke, S.; Sheldrick, G. M.; Ficner, R.; Tittmann, K. (2012): “Unexpected tautomeric equilibria of the carbanion-enamine intermediate in pyruvate oxidase highlight unrecognized chemical versatility of thiamin.” *Proc Natl Acad Sci U S A* 109 (27), pp. 10867–10872.

Mitschke, L.; Parthier, C.; Schröder-Tittmann, K.; Coy, J.; Lüdtke, S.; Tittmann, K. (2010): “The crystal structure of human transketolase and new insights into its mode of action.” *The Journal of Biological Chemistry* 285 (41) (41), pp. 31559–31570.

Monod, J.; Wyman, J.; Changeux, J.-P. (1965): “On the nature of allosteric transitions: A plausible model.” *Journal of Molecular Biology* 12 (1), pp. 88–118.

Müller, M.; Sprenger, G. A.; Pohl, M. (2013): “CC bond formation using ThDP-dependent lyases.” *Curr Opin Chem Biol* 17 (2), pp. 261–270.

Muller, Y. A.; Schulz, G. E. (1993): “Structure of the thiamine- and flavin-dependent enzyme pyruvate oxidase.” *Science* 259 (5097) (5097), pp. 965–967.

Muller, Y. A.; Lindqvist, Y.; Furey, W.; Schulz, G. E.; Jordan, F.; Schneider, G. (1993): “A thiamin diphosphate binding fold revealed by comparison of the crystal structures of transketolase, pyruvate oxidase and pyruvate decarboxylase.” *Structure* 1 (2), pp. 95–103.

Nemeria, N. S.; Arjunan, P.; Chandrasekhar, K.; Mossad, M.; Tittmann, K.; Furey, W.; Jordan, F. (2010): “Communication between thiamin cofactors in the Escherichia colipyruvate dehydrogenase complex E1 component active centers: Evidence for a "direct pathway" between the 4-aminopyrimidine N1 atoms.” *Journal of Biological Chemistry* 285 (15), pp. 11197–11209.

Nemeria, N. S.; Shome, B.; DeColli, A. A.; Heflin, K.; Begley, T. P.; Meyers, C. F.; Jordan, F. (2016): "Competence of thiamin diphosphate-dependent enzymes with 2'-methoxythiamin diphosphate derived from bacimethrin, a naturally occurring thiamin anti-vitamin." *Biochemistry* 55 (7) (7), pp. 1135–1148.

Nemeria, N. S.; Chakraborty, S.; Balakrishnan, A.; Jordan, F. (2009): "Reaction mechanisms of thiamin diphosphate enzymes: defining states of ionization and tautomerization of the cofactor at individual steps." *FEBS Journal* 276 (9), pp. 2432–3446.

Nemeria, N.; Korotchkina, L.; McLeish, M. J.; Kenyon, G. L.; Patel, M. S.; Jordan, F. (2007): "Elucidation of the Chemistry of Enzyme-Bound Thiamin Diphosphate Prior to Substrate Binding: Defining Internal Equilibria among Tautomeric and Ionization States † ." *Biochemistry* 46 (37), pp. 10739–10744.

Nemeria, N.; Binshtein, E.; Patel, H.; Balakrishnan, A.; Vered, I.; Shaanan, B.; Barak, Z.; Chipman, D.; Jordan, F. (2012): "Glyoxylate carboligase: a unique thiamin diphosphate-dependent enzyme that can cycle between the 4'-aminopyrimidinium and 1',4'-iminopyrimidine tautomeric forms in the absence of the conserved glutamate." *Biochemistry* 51 (40), pp. 7940–7952.

Nemeria, N.; Baykal, A.; Joseph, E.; Zhang, S.; Yan, Y.; Furey, W.; Jordan, F. (2004): "Tetrahedral intermediates in thiamin diphosphate-dependent decarboxylations exist as a 1',4'-imino tautomeric form of the coenzyme, unlike the michaelis complex or the free coenzyme." *Biochemistry* 43 (21), pp. 6565–6575.

Neufeld, E. J.; Fleming, J. C.; Tartaglini, E.; Steinkamp, M. P. (2001): "Thiamine-responsive megaloblastic anemia syndrome: a disorder of high-affinity thiamine transport." *Blood Cells Mol Dis* 27 (1), pp. 135–138.

Neumann, P.; Tittmann, K. (2014): "Marvels of enzyme catalysis at true atomic resolution: distortions, bond elongations, hidden flips, protonation states and atom identities." *Current Opinion in Structural Biology* 29, pp. 122–133.

Nghiêm, H. O.; Bettendorff, L.; Changeux, J. P. (2000): "Specific phosphorylation of Torpedo 43K rapsyn by endogenous kinase(s) with thiamine triphosphate as the phosphate donor." *FASEB J* 14 (3), pp. 543–554.

Nikkola, M.; Lindqvist, Y.; Schneider, G. (1994): “Refined structure of transketolase from Saccharomyces cerevisiae at 2.0 A resolution.” *J Mol Biol* 238 (3), pp. 387–404.

Nishimura, T; Tanaka, N (1963): “Biological studies on bacimehtrin, a pyrmidine antibiotic, and monazomycin.” *The Journal of Antibiotics* 16, pp. 179–181.

Nishino, H. (1972): “Biogenesis of cocarboxylase in Escherichia coli. Partial purification and some properties of thiamine monophosphate kinase.” *J Biochem* 72 (5), pp. 1093–1100.

Nosaka, K.; Kaneko, Y.; Nishimura, H.; Iwashima, A. (1993): “Isolation and characterization of a thiamin pyrophosphokinase gene, THI80, from Saccharomyces cerevisiae.” *J Biol Chem* 268 (23), pp. 17440–17447.

Oda, Y; Yamazaki, T; Nagayama, K; Kanaya, S; Kuroda, Y; Nakamura, H (1994): “Individual ionization constants of all the carboxyl groups in ribonuclease HI from Escherichia coli determined by NMR.” *Biochemistry* 33 (17) (17), pp. 5275–5284.

Pang, S. S.; Duggleby, R. G.; Guddat, L. W. (2002): “Crystal structure of yeast acetohydroxyacid synthase: a target for herbicidal inhibitors.” *Journal of Molecular Biology* 317 (2) (2), pp. 249–262.

Paulikat, M. (2014): “Theoretical investigations of electronic excitation spectra in ThDP-dependent enzymes.” MA thesis. Georg-August-University Göttingen.

Pierce, J.; Serianni, A. S.; Barker, R. (1985): “Anomerization of furanose sugars and sugar phosphates.” *J. Am. Chem. Soc.* 107 (8), pp. 2448–2456.

Pinitglang, S.; Watts, A. B.; Patel, M.; Reid, J. D.; Noble, M. A.; Gul, S.; Bokth, A.; Naeem, A.; Patel, H.; Thomas, E. W.; Sreedharan, S. K.; Verma, C.; Brocklehurst, K. (1997): “A classical enzyme active center motif lacks catalytic competence until modulated electrostatically †.” *Biochemistry* 36 (33), pp. 9968–9982.

Pletcher, J.; Sax, M.; Sengupta, S.; Chu, J.; Yoo, C. S. (1972): “The crystal and molecular structure of thiamine chloride monohydrate.” *Acta Crystallogr Sect B* 28 (10), pp. 2928–2935.

Reddick, J. J.; Saha, S.; Lee, J. ming; Melnick, J. S.; Perkins, J.; Begley, T. P. (2001): "The mechanism of action of bacimethrin, a naturally occurring thiamin antimetabolite." *Bioorganic & Medicinal Chemistry Letters* 11 (17), pp. 2245–2248.

Schellenberger, A. (1967): "Structure and Mechanism of Action of the Active Center of Yeast Pyruvate Decarboxylase." *Angewandte Chemie International Edition in English* 6 (12), pp. 1024–1035.

Schellenberger, A. (1990): "Die Funktion der 4*ı*-Aminopyrimidin-Komponente im Katalysemechanismus von Thiaminpyrophosphat-Enzymen aus heutiger Sicht." *Chemische Berichte* 123 (7), pp. 1489–1494.

Schellenberger, A.; Hübner, G. (1966): "Über die Trennung der Phosphorsäureester von Thiamin und seinen Analogen durch Gradientenelution." *Hoppe-Seyler's Zeitschrift für physiologische Chemie* 343 (Jahresband), pp. 189–192.

Schellenberger, A.; Winter, K. (1960): "Untersuchungen zur Funktion der Aminogruppe in der Cocarboxylase, I. Zur cocarboxylatischen Wirkung von N-Methyl-thiaminpyrophosphat." *Hoppe-Seyler's Zeitschrift für physiologische Chemie* 322 (Jahresband), pp. 164–172.

Schellenberger, A.; Müller, V.; Winter, K.; Hübner, G. (1966a): "Zur Theorie der Cocarboxylasewirkung, II. Ableitung und Begründung eines Zweizentrenmechanismus der Thiaminpyrophosphatwirkung aus Modellversuchen und enzymatischen Messungen." *Hoppe-Seyler's Zeitschrift für physiologische Chemie* 344 (Jahresband), pp. 244–260.

Schellenberger, A.; Winter, K.; Hübner, G.; Schwaiberger, R.; Helbig, D.; Schumacher, S.; Thieme, R.; Bouillon, G.; Rädler, K.-P. (1966b): "Zur Theorie der Thiaminpyrophosphat-Wirkung, III. Rekombinations- und Funktionskinetik der Hefe-Pyruvat-Decarboxylase." *Hoppe-Seyler's Zeitschrift für physiologische Chemie* 346 (Jahresband), pp. 123–147.

Schellenberger, A.; Wendler, K.; Creutzburg, P.; Gerhard (1967): "Zur Theorie der Thiaminpyrophosphat-Wirkung, V. Die Funktion der beiden Pyrimidin-N-Atome." *Hoppe-Seyler's Zeitschrift für physiologische Chemie* 348 (Jahresband), pp. 501–505.

Schenk, G; Layfield, R; Candy, J. M.; Duggleby, R. G.; Nixon, P. F. (1997): "Molecular evolutionary analysis of the thiamine-diphosphate-dependent enzyme, transketolase." *Journal of molecular evolution* 44 (5), pp. 552–572.

Schröder-Tittmann, K.; Meyer, D.; Arens, J.; Wechsler, C.; Tietzel, M.; Golbik, R.; Tittmann, K. (2013): "Alternating sites reactivity Is a common feature of thiamin diphosphate-dependent enzymes as evidenced by isothermal titration calorimetry studies of substrate binding." *Biochemistry* 52 (15), pp. 2505–2507.

Schüttelkopf, A. W.; van Aalten, D. M. F. (2004): "PRODRG: a tool for high-throughput crystallography of protein-ligand complexes." *Acta Crystallogr D Biol Crystallogr* 60 (8), pp. 1355–1363.

Seebach, D. (1979): "Methods of Reactivity Umpolung." *Angewandte Chemie International Edition in English* 18 (4), pp. 239–258.

Sevostyanova, I.; Solovjeva, O.; Selivanov, V.; Kochetov, G. (2009): "Half-of-the-sites reactivity of transketolase from Saccharomyces cerevisiae." *Biochemical and Biophysical Research Communications* 379 (4), pp. 851–854.

Shaanan, B.; Chipman, D. M. (2009): "Reaction mechanisms of thiamin diphosphate enzymes: new insights into the role of a conserved glutamate residue." *FEBS J* 276 (9), pp. 2447–2453.

Siu, V. M.; Ratko, S.; Prasad, A. N.; Prasad, C.; Rupar, C. A. (2010): "Amish microcephaly: Long-term survival and biochemical characterization." *Am J Med Genet A* 152 (7), pp. 1747–1751.

Smeets, E.; Muller, H.; Wael, J. D. (1971): "A NADH-dependent transketolase assay in erythrocyte hemolysates." *Clinica Chimica Acta* 33 (2), pp. 379–386.

Sprenger, G. A.; Schörken, U.; Sprenger, G.; Sahm, H. (1995): "Transketolase A of Escherichia coli K12. Purification and properties of the enzyme from recombinant strains." *Eur. J. Biochem.* 230 (2), pp. 525–532.

Steinbach, A. K.; Fraas, S.; Harder, J.; Tabbert, A.; Brinkmann, H.; Meyer, A.; Ermler, U.; Kroneck, P. M. H. (2011): "Cyclohexane-1,2-Dione Hydrolase from Denitrifying

Azoarcus sp. Strain 22Lin, a Novel Member of the Thiamine Diphosphate Enzyme Family." *Journal of Bacteriology* 193 (23), pp. 6760–6769.

Steinbach, A.; Fraas, S.; Harder, J.; Warkentin, E.; Kroneck, P. M. H.; Ermler, U. (2012): "Crystal structure of a ring-cleaving cyclohexane-1,2-dione hydrolase, a novel member of the thiamine diphosphate enzyme family." *FEBS J* 279 (7), pp. 1209–1219.

Steinmetz, A.; Vyazmensky, M.; Meyer, D.; Barak, Z. E.; Golbik, R.; Chipman, D. M.; Tittmann, K. (2010): "Valine 375 and phenylalanine 109 confer affinity and specificity for pyruvate as donor substrate in acetohydroxy acid synthase isozyme II from Escherichia coli." *Biochemistry* 49 (25) (25), pp. 5188–5199.

Stites, W. E.; Gittis, A. G.; Lattman, E. E.; Shortle, D. (1991): "In a staphylococcal nuclease mutant the side-chain of a lysine replacing valine 66 is fully buried in the hydrophobic core." *Journal of Molecular Biology* 221 (1), pp. 7–14.

Studier, F. W. (2005): "Protein production by auto-induction in high-density shaking cultures." *Protein Expression and Purification* 41 (1), pp. 207–234.

Sun, L.-H.; Liang, Z.-Q.; Jia, W.-Q.; Ye, S. (2013): "Enantioselective N-Heterocyclic Carbene Catalyzed Aza-Benzoin Reaction of Enals with Activated Ketimines." *Angewandte Chemie International Edition* 52 (22), pp. 5803–5806.

Takaki, K. (1906): "On the preservation of health among the personnel of the Japanese navy and army. Lecture II: The methods for investigating the cause of beri-beri." *Lancet* 1, pp. 1451–1455.

Tanaka, F; Tanaka, N; Yonehara, H; Umezawa, H (1962): "Studies on Bacimethrin, a new antibiotic from *B. megaterium*. I. Preparations and its properties." *J Antibiotics, Ser A.* 15, pp. 191–196.

Tittmann, K.; Proske, D.; Spinka, M.; Ghisla, S.; Rudolph, R.; Hubner, G.; Kern, G. (1998): "Activation of thiamin diphosphate and FAD in the phosphatedependent pyruvate oxidase fromLactobacillus plantarum." *Journal of Biological Chemistry* 273 (21), pp. 12929–12934.

Tittmann, K; Golbik, R; Ghisla, S; Hübner, G (2000): “Mechanism of elementary catalytic steps of pyruvate oxidase from Lactobacillus plantarum.” *Biochemistry* 39 (35) (35), pp. 10747–10754.

Tittmann, K. (2014): “Sweet siblings with different faces: The mechanisms of FBP and F6P aldolase, transaldolase, transketolase and phosphoketolase revisited in light of recent structural data.” *Bioorganic Chemistry* 57, pp. 263–280.

Tittmann, K.; Golbik, R.; Uhlemann, K.; Khailova, L.; Schneider, G.; Patel, M.; Jordan, F.; Chipman, D. M.; Duggleby, R. G.; Hübner, G. (2003): “NMR analysis of covalent intermediates in thiamin diphosphate enzymes.” *Biochemistry* 42 (26) (26), pp. 7885–7891.

Tittmann, K.; Wille, G.; Golbik, R.; Weidner, A.; Ghisla, S.; Hübner, G. (2005): “Radical phosphate transfer mechanism for the thiamin diphosphate- and FAD-dependent pyruvate oxidase from Lactobacillus plantarum. Kinetic coupling of intercofactor electron transfer with phosphate transfer to acetyl-thiamin diphosphate via a transient FAD semiquinone/hydroxyethyl-ThDP radical pair.” *Biochemistry* 44 (40) (40), pp. 13291–13303.

Tsolas, O.; Joris, L. (1975): “Transaldolase.” *Methods Enzymol* 42, pp. 290–297.

Ugai, T.; Tanaka, S.; Dokawa, S. (1943): “Thiamine catalysis of the bezoine condensation.” *J. Pharm. Soc.Jpn.*

Vogel, C.; Pleiss, J. (2014): “The modular structure of ThDP-dependent enzymes.” *Proteins* 82 (10), pp. 2523–2537.

Vogt, A. D.; Di Cera, E. (2013): “Conformational selection is a dominant mechanism of ligand binding.” *Biochemistry* 52 (34), pp. 5723–5729.

– (2012): “Conformational selection or induced fit? A critical appraisal of the kinetic mechanism.” *Biochemistry* 51 (30), pp. 5894–5902.

Vorderman, A. (1897): *Onderzoek naar het verband tusschen den aard der rijstvoeding in de gevangenissen op Java en Madoera en het voorkomen van beri-beri onder de geinterneerden.* Batavia: Jav. Boekh. & Drukkerij.

Washabaugh, M. W.; Jencks, W. P. (1988): “Thiazolium C(2)-proton exchange: structure-reactivity correlations and the pKa of thiamin C(2)-H revisited.” *Biochemistry* 27 (14), pp. 5044–5053.

Wechsler, C.; Meyer, D.; Loschonsky, S.; Funk, L.-M.; Neumann, P.; Ficner, R.; Brodhun, F.; Müller, M.; Tittmann, K. (2015): “Tuning and switching enantioselectivity of asymmetric carboligation in an enzyme through mutational analysis of a single hot spot.” *Chembiochem* 16 (18), pp. 2580–2584.

Westphal, R.; Vogel, C.; Schmitz, C.; Pleiss, J.; Müller, M.; Pohl, M.; Rother, D. (2014): “A tailor-made chimeric thiamine diphosphate dependent enzyme for the direct asymmetric synthesis of (S)-benzoins.” *Angew Chem Int Ed Engl* 53 (35), pp. 9376–9379.

Wikner, C; Meshalkina, L; Nilsson, U; Nikkola, M; Lindqvist, Y; Sundström, M; Schneider, G (1994): “Analysis of an invariant cofactor-protein interaction in thiamin diphosphate-dependent enzymes by site-directed mutagenesis. Glutamic acid 418 in transketolase is essential for catalysis.” *The Journal of Biological Chemistry* 269 (51) (51), pp. 32144–32150.

Wikner, C.; Meshalkina, L.; Nilsson, U.; Backstrom, S.; Lindqvist, Y.; Schneider, G. (1995): “His103 in Yeast Transketolase is Required for Substrate Recognition and Catalysis.” *European Journal of Biochemistry* 233 (3), pp. 750–755.

Wikner, C.; Nilsson, U.; Meshalkina, L.; Udekwu, C.; Lindqvist, Y.; Schneider, G. (1997): “Identification of Catalytically Important Residues in Yeast Transketolase † .” *Biochemistry* 36 (50), pp. 15643–15649.

Wille, G.; Meyer, D.; Steinmetz, A.; Hinze, E.; Golbik, R.; Tittmann, K. (2006): “The catalytic cycle of a thiamin diphosphate enzyme examined by cryocrystallography.” *Nature Chemical Biology* 2 (6) (6), pp. 324–328.

Williams, R.; Cline, J. (1936): “Synthesis of Vitamin B1.” *J. Am. Chem. Soc.* 58 (8), 1504–1505.

Zilles, J. L.; Croal, L. R.; Downs, D. M. (2000): “Action of the thiamine antagonist bacimethrin on thiamine biosynthesis.” *Journal of Bacteriology* 182 (19) (19), pp. 5606–5610.

Curriculum Vitae

Fabian Nikolaus Rabe von Pappenheim

Georg-August-University Göttingen
Department of Molecular Enzymology
Julia-Lermontowa-Weg 3
37077 Göttingen, Germany

Phone: +49 152 37243317
e-mail: fpappen@gwdg.de

Date of Birth:	26.02.1988
Place of Birth:	Stuttgart, Germany
Nationality:	German

Education

09/1994 – 06/1998	Primary School, Bonn-Holzlar
09/1998 – 02/2007	Gymnasium Marianum, Warburg
10/2007 – 03/2008	B.Sc. Chemistry, Georg-August-University Göttingen
10/2008 – 09/2011	B.Sc. Biology, Georg-August-University Göttingen Bachelor's Thesis: Studies on the E2LipII domain of the human pyruvate dehydrogenase complex, Department of Molecular Enzymology
10/2011 – 12/2013	M.Sc. Microbiology and Biochemistry, Georg-August-University Göttingen Master's Thesis: Structural and kinetic investigations of variants of the dihydrolipoyl dehydrogenase E3 related to phosphine resistance, Department of Molecular Enzymology
01/2014 – 05/2017	GGNB doctoral program Biomolecules: Structure – Function – Dynamics, Georg-August-University Göttingen, Department of Molecular Enzymology

Scientific Contribution

Presentations	Biannual meetings of the DFG research group 1296 "Diversity of asymmetric thiamine catalysis"
Poster	Inhibition of transketolase by the natural thiamine analogue methoxythiamine